NPS-IJWA-01-016

YELLOW SEA MINE HUNTING USING THE NAVY'S CASS/GRAB MODEL

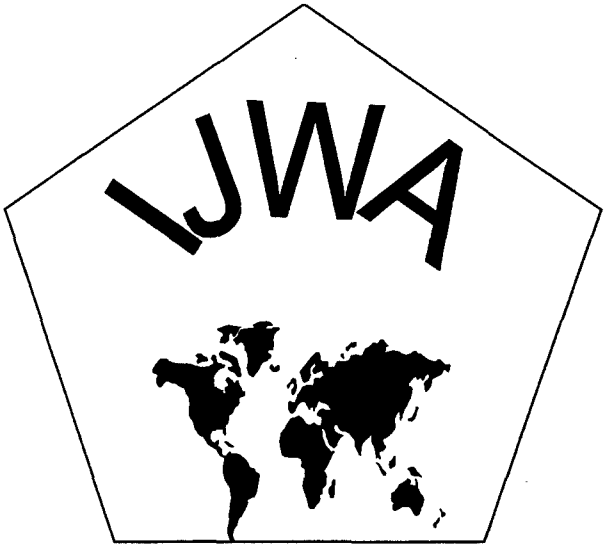

Peter C. Chu
Carlos J. Cintron
Steven D. Haeger
Dan N. Fox
Ruth E. Keenan

The Institute for Joint Warfare Analysis
Naval Postgraduate School
Monterey, California

NPS-IJWA-01-016

YELLOW SEA MINE HUNTING USING THE NAVY'S CASS/GRAB MODEL

Peter C. Chu
Carlos J. Cintron
Steven D. Haeger
Dan N. Fox
Ruth E. Keenan

INSTITUTE FOR JOINT WARFARE ANALYSIS
NAVAL POSTGRADUATE SCHOOL
Monterey, California

Rear Admiral David R. Ellison
Superintendent

Richard Elster
Provost

This report was prepared for and funded by:

Naval Oceanographic Office

This report was prepared by:

Peter C Chu, Carlos J. Cintron, Steven D. Haeger, Dan N. Fox, Ruth E. Keenan

Institute for Joint Warfare Analysis, Naval Postgraduate School

Reviewed by

GORDON SCHACHER
Director
Institute for Joint Warfare Analysis

Released by:

DAVID W. NETZER
Associate Provost and
Dean of Research

REPORT DOCUMENTATION PAGE

Form Approved
OMB No. 0704-0188

1. AGENCY USE ONLY *(Leave blank)*	2. REPORT DATE	3. REPORT TYPE AND DATES COVERED
	May 2001	IJWA Thesis Work

4. TITLE AND SUBTITLE
Yellow Sea Mine Hunting Using the Navy's CASS/GRAB Model

5. FUNDING NUMBERS

6. AUTHOR(S)
Peter C. Chu, Carlos J. Cintron, Steven D. Haeger, Dan N. Fox, Ruth E. Keenan

7. PERFORMING ORGANIZATION NAME(S) AND ADDRESS(ES)
Naval Postgraduate School, Monterey, CA 93943-5000

8. PERFORMING ORGANIZATION REPORT NUMBER
NPS-IJWA-01- 016

9. SPONSORING / MONITORING AGENCY NAME(S) AND ADDRESS(ES)
NAVOCEANO, Stennis Space Center, MS 39522-5001

10. SPONSORING / MONITORING AGENCY REPORT NUMBER

11. SUPPLEMENTARY NOTES
The views expressed in this report are those of the author and do not reflect the official policy or position of the Department of Defense or the U.S. Government.

12a. DISTRIBUTION / AVAILABILITY STATEMENT
Approved for public release; distribution is unlimited.

12b. DISTRIBUTION CODE

13. ABSTRACT *(maximum 200 words)*

The purpose of this work is to determine the necessity of a near real time ocean modeling capability such as the Naval Oceanographic Office's (NAVOCEANO) Modular Ocean Data Assimilation System (MODAS) model in shallow water (such as the Yellow Sea) mine hunting applications using the Navy's Comprehensive Acoustic Simulation System/Gaussian Ray Bundle (CASS/GRAB) model. Sound speed profiles inputted into the CASS/GRAB were calculated from observational (MOODS) and climatological (GDEM) data sets for different seasons and regions of four different bottom types (sand, gravel, mud, and rock). The CASS/GRAB model outputs were compared to the outputs from corresponding MODAS data sets. The results of the comparisons demonstrated in many cases a significant acoustic difference between the alternate profiles. These results demonstrated that there is a need for a predictive modeling capability such as MODAS to address the Mine Warfare (MIW) needs in the Yellow Sea region. There were some weaknesses detected in the profiles the MODAS model produces in the Yellow Sea, which must be resolved before it can reliably address the MIW needs in that region.

14. SUBJECT TERMS
Modeling and Simulation, Meteorology and Oceanography, Acoustic Mine Hunting, CASS/GRAB Model, Reverberation, Detection

15. NUMBER OF PAGES
262

16. PRICE CODE

17. SECURITY CLASSIFICATION OF REPORT	18. SECURITY CLASSIFICATION OF THIS PAGE	19. SECURITY CLASSIFI- CATION OF ABSTRACT	20. LIMITATION OF ABSTRACT
Unclassified	Unclassified	Unclassified	UL

NSN 7540-01-280-5500

Standard Form 298 (Rev. 2-89)
Pescribed by ANSI Std. 239-18
298-102

ACKNOWLEDGEMENTS

The work that lead to the results reported here was a partnership effort among the Naval Postgraduate School (NPS) Institute for Joint Warfare Analysis, the Naval Oceanographic Office (NAVOCEANO), Naval Research Laboratory, and the Naval Undersea Warfare Center Division Newport. Also involved were other organizations that provided personnel and equipment, too numerous to mention. We wish to acknowledge the following individuals who were responsible for making this research possible: LCDR Jim Berdeguez at the Chief of Naval Operations (N752); William and Steve Lingsch at NAVOCEANO, and Professor Gordon Schacher at NPS Institute of Joint Warfare Analysis. Special thanks are given to Chenwu Fan at NPS for computational assistance.

ABSTRACT

The purpose of this work is to determine the necessity of a near real time ocean modeling capability such as the Naval Oceanographic Office's (NAVOCEANO) Modular Ocean Data Assimilation System (MODAS) model in shallow water (such as the Yellow Sea) mine hunting applications using the Navy's Comprehensive Acoustic Simulation System/Gaussian Ray Bundle (CASS/GRAB) model. Sound speed profiles inputted into the CASS/GRAB were calculated from observational (MOODS) and climatological (GDEM) data sets for different seasons and regions of four different bottom types (sand, gravel, mud, and rock). The CASS/GRAB model outputs were compared to the outputs from corresponding MODAS data sets. The results of the comparisons demonstrated in many cases a significant acoustic difference between the alternate profiles. These results demonstrated that there is a need for a predictive modeling capability such as MODAS to address the Mine Warfare (MIW) needs in the Yellow Sea region. There were some weaknesses detected in the profiles the MODAS model produces in the Yellow Sea, which must be resolved before it can reliably address the MIW needs in that region.

THIS PAGE INTENTIONALLY LEFT BLANK

TABLE OF CONTENTS

LIST OF FIGURES

THIS PAGE INTENTIONALLY LEFT BLANK

LIST OF TABLES

THIS PAGE INTENTIONALLY LEFT BLANK

TABLE OF SYMBOLS

$\beta_{v,0}$	=	The factor that depends only on the source and is chosen so that the energy within a geometric-acoustic ray tube equals the energy within a Gaussian ray bundle
p_r	=	Horizontal sound speed slowness
r	=	Range from acoustic source
σ_v	=	Effective standard deviation of the Gaussian width
Γ_v	=	Losses due to volume attenuation and boundary interactions
Ψ_v	=	Amplitude of the power in the Gaussian ray bundle
z	=	Target depth
z_v	=	The depth along the v^{th} test ray at range r
Δz	=	Change in ray depth at constant range due to a change in source angle

THIS PAGE INTENTIONALLY LEFT BLANK

I. INTRODUCTION

During the "Cold War" the United States Navy focused most of its research and development efforts on weapon systems, sensors, and counter measures that were extremely effective in destroying and countering the Soviet Navy in "blue water" (deep water regions beginning at the 100 m mark and greater) conflicts. After the Cold War the United States did not realize how unprepared its forces were to operate in the "littoral" (shallow waters defined as beginning at the 100 meter mark and below) until its was forced to gradually increase its operations in the Persian Gulf, since the Gulf War. Unfortunately, the U.S. Navy suffered three major ship casualties as a result of mines before significant funding went into the research and development for weapon systems, sensors, and countermeasures that are effective in the littoral.

The sensors on ships and weapons torpedoes during the Cold War were designed for the acoustically range independent environments characteristic of "Blue Water" regions. These sensors are highly capable of long-range detections in deep waters but are virtually blind even at short-range scenarios. These sensors are not designed for the acoustically range dependent environment of the littoral. The source of interfering noise for acoustic sensors in the littoral is reverberation from the sea surface and sea bottom.

The major threats in the littoral are diesel submarines and sea mines. The combination of improvements in noise reducing technology and the development of Air Independent Propulsion (AIP) technology have made diesel submarines very difficult to detect in both the littoral and blue waters. After a weapon platform has detected its

targets, the sensors on torpedoes designed for blue water operations are not designed to acquire a target in a reverberation-crippling environment.

Even though sea mines are not as sophisticated a weapons system as torpedoes, they have been number one cause of U.S. Naval casualties since the end of World War II. Sea mines are a relatively cheap weapons system that can be easily obtained by any nation in mass quantities. In addition, Sea mines do not require an expensive and sophisticated weapons platform for deployment; they can be easily deployed by small watercraft. There are several types of mines, which are classified by their mode of activation and their placement in the water column. The simplest of sea mines are floating contact mines. These mines are usually detected visually and cleared by minesweepers and Explosive Ordnance Disposal (EOD) units. A more complex type of mines are influence mines. These mines have different mechanisms for activation, such as magnetic and acoustic actuators. Influence mines are much more difficult to counter since they are either tethered to the sea bottom at various depths or lie on the sea bottom. Since these types of mines are situated below the sea surface, mine hunting sonars are required for detection. The problems that are related to sonar detection of a target in the littoral are compounded when the target is a sea mine due to the low target strengths of Sea mines. The low target strengths of sea mines require the use of sensors with frequencies higher than those sonars used for submarine detection. Bottom mines create a much more difficult detection problem for the mine hunter. Operators of mine hunting systems must perform the timely process of classifying all objects that closely fit the dimensions of a Bottom mine and later evaluate these objects in closer detail with higher resolution sensors.

In recent years, the U.S. Navy has focused much of its research and development efforts in designing high frequency sensors and corresponding acoustic models to overcome the threat in the littoral. The Comprehensive Acoustic Simulation System (CASS) using the Gaussian Ray Bundle (GRAB) model is an acoustic model approved by the U.S. Navy to predict the performance of active ocean acoustic systems that operate in the 600 Hz to 100 kHz frequency range. Developed in 1993 by the Naval Undersea Warfare Center Division Newport, this model is capable of modeling all the components of passive and bistatic signal excess in range-dependent environments. The CASS/GRAB has successfully modeled torpedo acoustic performance in shallow water experiments off the coast of Southern California and Cape Cod, and is currently being developed to simulate mine warfare systems performance in the fleet (Aidala et al. 1998).

The CASS/GRAB model is valuable tool for the AN/SQQ-32 mine hunting detection and classification sonar. The performance of this model, as in all models, is determined by the accuracy of its inputs such as sea surface conditions, bathymetry, bottom type, and sound speed profiles.

The AN/SQQ-32 (Figure 1) is a variable depth mine hunting detection and classification sonar for the Avenger (MCM-1) and Osprey (MHC-51) Surface Mine Countermeasures (SMCM) ships. The AN/SQQ-32's main components are a multi-channel detection sonar assembly and near-photographic resolution classification sonar assembly. The system has multiple operating frequencies and obtains acoustic data from two independent acoustic search and classification arrays that maximize volumetric coverage. Its multiple-ping processor enables it to detect mine-like objects in the high reverberation environment of the littoral. Additionally, its multiple operating frequency

capability allows it to operate in both deep and shallow waters. The lower operating frequencies allow the system to detect mine-like objects at longer ranges in shallow waters. The classification sonar system's near-photograph resolution and the systems computer aided target classification system decreases the time required for mine searching operations by reducing false target reporting.

Figure 1. The AN/SQQ-32 Mine Hunting Sonar System (From Raytheon Electronic Systems Naval & Maritime Integrated Systems 2000).

NAVOCEANO constructs various environmental databases for Mine Warfare (MIW) applications; these databases are used by the MIW Environmental Decision

Library (MEDAL). One of these databases is the "Provinced" (user derived) profiles. This climatological database consists of spatial provinces that define an average of several alternate temperature, salinity, and sound profiles for a shallow water region on a monthly basis. Provinced profiles are derived from the MOODS database using the Naval Interactive Data Analysis System (NIDAS) software. It has been found that the Generalized Digital Environmental Model (GDEM) climatology (consisting of an average profile at grid point) is often inadequate to define the vertical features of shallow water profiles for MIW applications. Also, due to the high temporal variability in shallow water, the average profile seldom occurs, thus a better depiction is to include "alternate profiles" which can occur as often as the average. NAVOCEANO has developed the Modular Ocean Data Assimilation System (MODAS) model to meet these needs.

To determine if the MODAS model meets the MIW needs in shallow water regions, a comparison with historical observational (MOODS) and climatological (GDEM) profiles in an acoustic model is required. If there is a significant acoustic difference of CASS/GRAB outputs between using MOODS and MODAS or using GDEM and MODAS, then there is a need for a predictive modeling capability such as MODAS. If there is no significant difference, then MODAS is not required to address the MIW needs in these regions and the NAVOCEANO province profile products derived from MOODS are sufficient.

In this thesis, an input file that simulates the parameters of the AN/SQQ-32 mine hunting sonar was used to generate acoustic data. The input file was created by Ruth E.

Keenan of the Science Applications International Corporation and was created replacing any sensitive parameters of the AN/SQQ-32 sonar with generalized sonar parameters.

The outline of this thesis is as follows: A description of the Yellow Sea geological and oceanographic environments is given in Chapter II. A depiction of the oceanographic data sets used for the study and the Navy's Interactive Data Analysis System (NIDAS) are given in Chapters III and IV. The CASS/GRAB model is described in Chapter V. Seasonal variability of acoustic transmission and the severe weather effects on the acoustic transmission are investigated in Chapters VI and VII. The sensitivity study on the hydrographic data input (MOODS, GDEM, and MODAS) is given in Chapter VIII. The comparison is given during four seasons and four regions of different bottom types (rock, gravel, sand, and mud). The uncertainty propagation from the hydrographic input data into the CASS/GRAB model out put is discussed in Chapter IX. In Chapter X, the conclusions are presented.

II. ENVIRONMENT OF THE YELLOW SEA

A. GEOLOGY AND STRUCTURE

The Yellow Sea is a semi-enclosed basin situated between China and the Korean peninsula with the Bohai Sea to the northwest and the East China Sea to the south. The Yellow Sea is a large shallow water basin covering an area of approximately 295,000 km^2. The water depth over most of the area is less than 50 m (Figure 2). Four major fresh water run-offs flow into the Yellow Sea: the Yangtze River to the southwest, the Yellow River and Liao River to the north, and the Han River to the east (Chu et al. 1997a).

Due to large tidal ranges and heavy sedimentation from river outflows, most of the coasts surrounding the Yellow Sea contain numerous shoals and troughs extending from the shores. The bottom sediment types are finer along the coast of China and much coarser along the shelf and the coast of the Korean peninsula. The bottom sediment of the central and western regions of the Yellow Sea consists primarily of mud and the eastern region is primarily sand. The mud sedimentation in the central and northwestern regions of the Yellow Sea is due to the runoff from the great rivers of China (Shepard 1973).

Four regions with different bottom types were selected for the acoustic model runs in this study (Figure 3). The first region consists of a Rock Bottom type and is located in the north-central Yellow Sea at 37°-37.5° N, 123°-123.8° E. The second region consists of a Gravel Bottom type and is located in the northern Yellow Sea at 38.4°-39° N, 122°-123° E. The third region consists of a Sand Bottom type and is located in the southeastern Yellow Sea at 35.5°-36.5° N, 124.5°-126.2° E. The fourth region consists of

a Mud Bottom type and is located in the south-central Yellow Sea at 35°-36.5° N, 123°-124.5° E. The bottom sediment composition parameters are listed in Table 1.

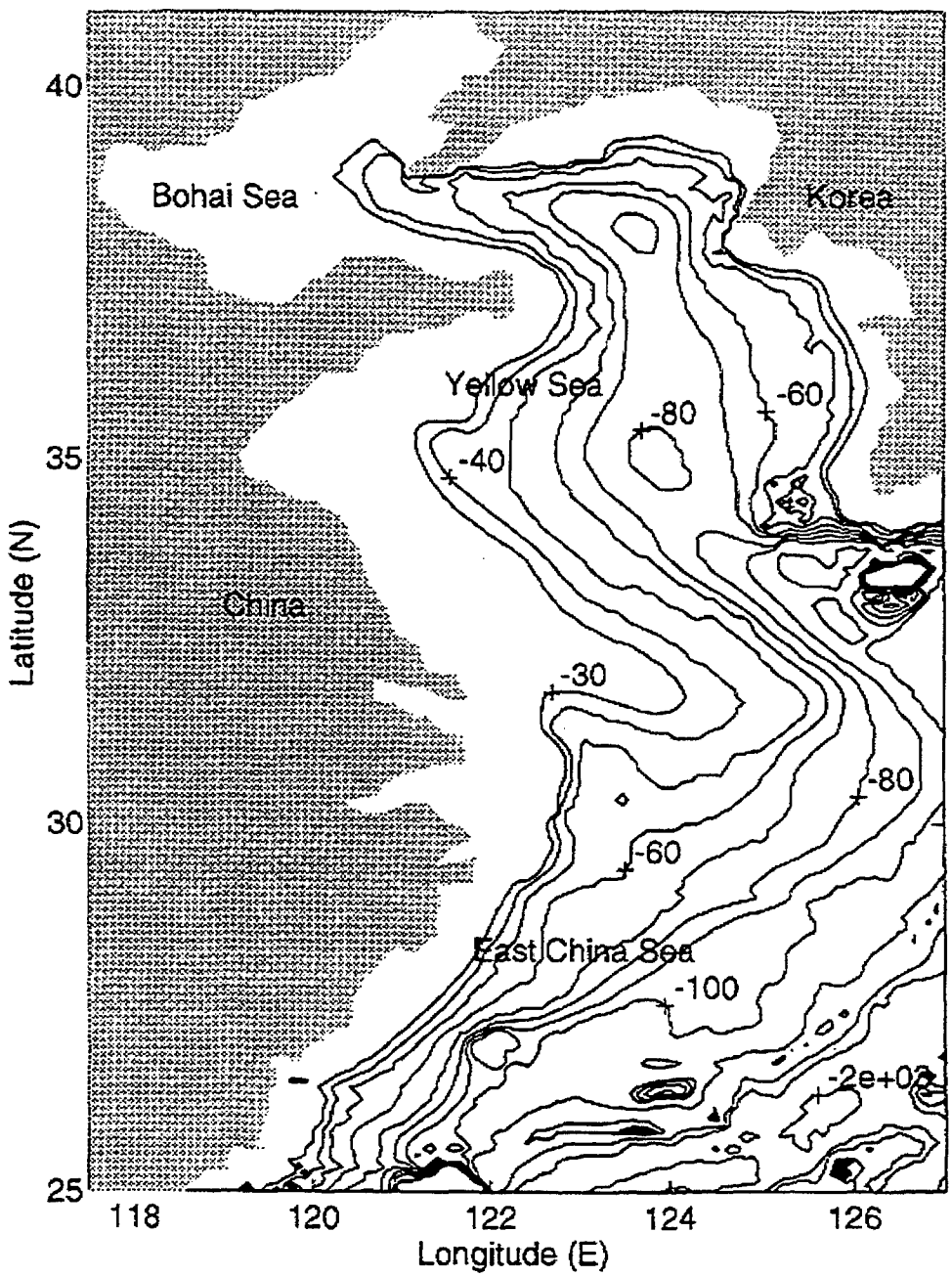

Figure 2. Bottom Topography of the Yellow Sea and the surrounding regions. The data was obtained from the U.S. Naval Oceanographic Office DBDB5 world bathymetry database. Depths are in meters. (From Chu et al. 1997a).

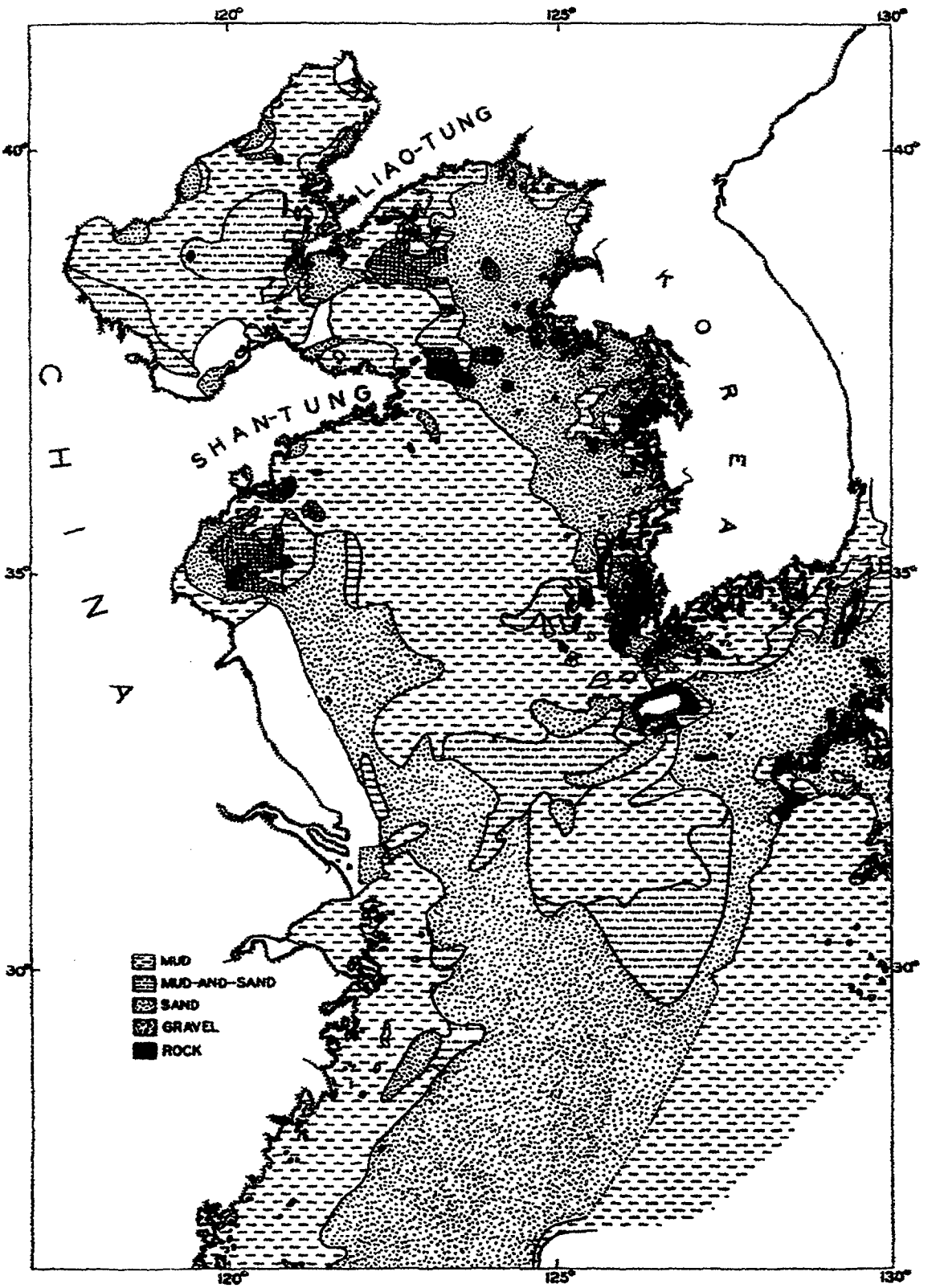

Figure 3. Yellow Sea Bottom sediment chart (From Ninno and Emery 1961).

Bottom Sediment Composition	Bulk Grain Size Index	Long (32 Char) Name	Density gm/cm^3	Sound Speed Ratio	Wave Number Ratio
BOULDER	-9	Rough Rock	2.5	2.5	0.0137
ROCK	-7	Rock	2.5	2.5	0.0137
GRAVEL	-3	Gravel, Cobble or Pebble	2.5	1.8	0.0137
	-1	Sandy Gravel	2.492	1.337	0.01705
	-0.5	Very Coarse Sand	2.401	1.3067	0.01667
	0.0	Muddy Sandy Gravel	2.314	1.2778	0.01630
	0.5	Coarse Sand	2.231	1.2503	0.01638
	1.0	Gravelly Muddy Sand	2.151	1.2241	0.01645
SAND	1.5	Sand or Medium Sand	1.845	1.1782	0.01624
	2.0	Muddy Gravel	1.615	1.1396	0.01610
	2.5	Silty Sand or Fine Sand	1.451	1.1073	0.01602
	3.0	Muddy Sand	1.339	1.0800	0.01728
	3.5	Very Fine Sand	1.268	1.0568	0.01875
	4.0	Clayey Sand	1.224	1.0364	0.02019
	4.5	Coarse Silt	1.195	1.0179	0.02158
	5.0	Sandy Silt	1.169	0.9999	0.01261
	5.5	Medium Silt	1.149	0.9885	0.00676
SILT	6.0	Silt	1.149	0.9873	0.00386
	6.5	Fine Silt	1.148	0.9861	0.00306
MUD	7.0	Sandy Clay	1.147	0.9849	0.00242
	7.5	Very Fine Silt	1.147	0.9837	0.00194
	8.0	Silty Clay	1.146	0.9824	0.00163
CLAY	9.0	Clay	1.145	0.9800	0.00148
	10.0		1.145	0.9800	0.00148

Table 1. APL/UW TR9407 Geo-acoustic parameters associated with bulk grain size index used by the CASS/GRAB model. Sand is the default value for CASS/GRAB (From NAVOCEANO 1999).

B. OCEANOGRAPHY

The four seasons in the Yellow Sea are defined as follows: the winter months run from January through March; the spring months run from April through June; the summer months run from July through September; and the fall months run from October through December. The Siberian high-pressure system during the winter monsoon season brings very cold northwest winds through the Yellow Sea region. During this period, the jet stream is located south of the Yellow Sea and the polar front is located north of the Philippines. At the beginning of the winter season the mean wind speed is 6 m/s and the sea air temperature (SAT) falls in the range of 0° to 8° C, whereas the sea

surface temperature (SST) is usually 2° to 6° C warmer causing the Yellow Sea to lose heat to the atmosphere during this time period. The winter monsoon winds peak with a maximum of 35 m/s in the central Yellow Sea, and 28 m/s mean through out the entire region (Chu et al. 1997a). These winds cause the formation of a southward sea level gradient that force bottom water to flow northward. These cold/strong winter monsoon winds cause mechanical forcing due to the strong wind stress and thermal forcing resulting from the upward buoyancy flux at the air-ocean interface caused by the cold SAT. The combined action of the mechanical and thermal forcing causes the mixed layer to drop to its deepest point during the winter season.

The transition into the spring season begins in late March when air temperatures are an average of 5° C warmer than the previous month due to a rapid weakening of the Siberian high that progress through out the months of March and April. By the end of the first month of spring, the atmospheric polar front has transited northward into Korea followed by warm and humid air masses into the Yellow Sea region. This transition brings about an average increase in the SST of 10° C during the spring. Spring in the Yellow Sea is also characterized by highly variable winds, cloud cover, and precipitation due to a numerous number of front driven events transiting through the region (Chu et al. 1997a).

The transition into the summer season begins in late May and early June where an atmospheric low-pressure system, generated north of the Yellow Sea, called the Manchurian Low moves west over Manchuria in late June. The movement of this low-pressure system sets up circulation of the southwest monsoon in the Yellow Sea during the summer months. During this period, the jet stream is located south of Korea and the

polar front is located south of the Japanese Islands of Kyushu and Shikoku. In July, the atmospheric low-pressure system in the north, in conjunction with an atmospheric high-pressure system located in the southeast called the Bonin High, generates warm and humid southerly winds over the Yellow Sea region. The warm air from these southerly winds increases the SAT over the Yellow Sea during the summer months to a range of 24° to 26° C, approximately 1.5° to 2° C warmer than the SST. Although there is a high weather activity in the Yellow Sea during the summer monsoon season, the mean wind speed throughout the region only ranges from 3 to 4 m/s. During the summer months, there is also a stronger downward net radiation and this effect, combined with the warmer air, causes a downward heat flux that reduces the depth of the mixed layer (Chu et al. 1997a, b). The summer season is also usually characterized by Tropical Cyclones that transit through the region, moving in a northwest direction from the East China Sea into the southern Yellow Sea and into China. Occasionally, a tropical cyclone will transit in a northerly direction from the East China Sea and throughout the Yellow Sea.

October marks the beginning of the fall season in the Yellow Sea. In October, the warm southerly winds of the summer monsoon begin to subside in the region and the SAT and SST begin to gradually transition to those of the winter season.

The two main characteristic temperature profiles of the Yellow Sea are during the winter and the summer months. In the winter months, the temperature profiles throughout the region are characterized as isothermal (Figure 4a). In the summer months, the temperature profiles throughout the region are characterized by a multi-layer profile consisting of a mixed layer, a thermocline, and a deep layer (Figure 4b).

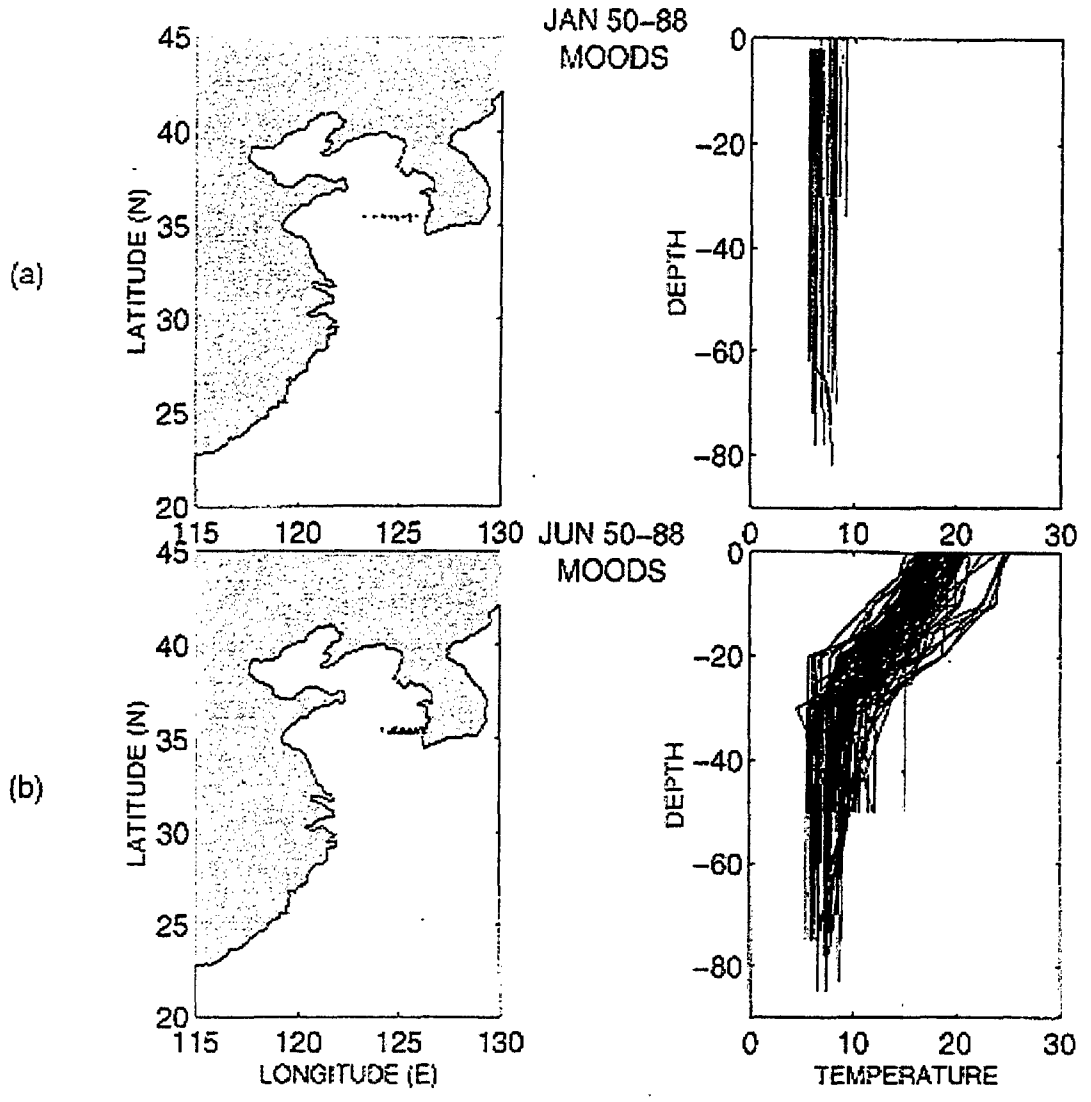

Figure 4. Eastern Yellow Sea (around 36 N) temperature profiles during 1950-1988; (a) January and (b) June. Solid dots show the location of the observation stations (From Chu et al. 1997b).

THIS PAGE INTENTIONALLY LEFT BLANK

III. OCEANOGRAPHIC DATA SETS

A. MASTER OCEANOGRAPHIC OBSERVATIONAL DATA SET (MOODS)

Master Oceanographic Observation Data Set (MOODS) is the observational database of the Navy and contains all available oceanographic profile data. MOODS currently contains over 5.8 million observations worldwide dating back to 1920 (NAVOCEANO 2000). MOODS is a collection of ocean data observed worldwide consisting of temperature-only profiles, temperature and salinity profiles, sound speed profiles, and surface temperature data. The biggest limitation of MOODS is its irregular distribution over time and space. Since observational data is collected from numerous sources during times of opportunity, the locations and times these observations are made vary greatly. Thus, the density of observations made in common shipping lanes is much greater than those made outside of the shipping lanes. In the case of the Yellow Sea, there are a very limited number of observations made off the coast of China. In addition, the number of observations are much more sparse during the fall and winter months as compared with the spring and summer months. Another limitation is the high variability of the data's vertical resolution and quality due to the numerous types of instruments used for sampling as well as the level of expertise of the sampler.

Due to the numerous sources and the tremendous quantity of samples that are incorporated into MOODS by NAVOCEANO, the data must be systematically evaluated to remove erroneous profiles. The errors usually contained in MOODS are profiles with observations obviously misplaced by location or season, duplicate profiles, and profiles with large peaks (temperatures higher than 35° C and lower than –2° C do not match the characteristics of surrounding profiles) (Chu et al. 1997b). The Naval Interactive Data

Analysis System (NIDAS) computer software was used to simplify the task of removing erroneous profiles and creating MOODS data sets for evaluation by the CASS/GRAB model.

B. GENERALIZED DIGITAL ENVIRONMENT MODEL (GDEM)

The Generalized Digital Environmental Model (GDEM) is climatology data that has been generated by the Naval Oceanographic Office since 1975. Climatological data is data that has been obtained from taking the mean of data of temperature and salinity profiles from a period of many decades. GDEM is created from all available sources of temperature and salinity profile data available globally, with MOODS being the primary input. Before incorporating MOODS into GDEM, erroneous profiles are removed as described earlier.

GDEM is gridded data in the form of a four dimensional digital model (latitude, longitude, depth, and time). The gridded data is generated in three resolutions; 30', 20', and 10' latitude-longitude grids and 3, 6, and 12-month time intervals. The Global GDEM data set, which covers much of the globe, is generated with a 30' resolution. Regions that are operationally important to the United States Navy are generated with higher horizontal resolutions of 20' and 10'. These regions predominantly consist of shallow water regions like the Mediterranean, the Yellow Sea, and the Persian Gulf (Figure 3). NAVOCEANO has combined all these different types of resolution GDEM into a single database called GDEM V (GDEM Variable resolution) to allow for the highest resolution and most updated GDEM data sets to be available to the fleet.

The higher 10-minute horizontal resolution GDEM also contains a higher vertical resolution. This GDEM is created using a separate process based more on water mass

called the Shallow Water Data Models (SWDMs) that produces the Shallow Water Data Base (SWDB) climatology. In addition, GDEM does not extend beyond 100 meters in depth whereas SWDMs extends out to 50 meters. For shallow water depths (< 200 m), the SWDB climatology is used and in depths greater than 500 m, Global GDEM is used. The complete 10-minute horizontal resolution GDEM climatology is formed by blending Global GDEM and the SWDB with a weighted average between 200 and 500 m. This GDEM is blended into adjacent GDEM of 20 and 30-minute resolution to produce a seamless transition of gridded data (NAVOCEANO 2000).

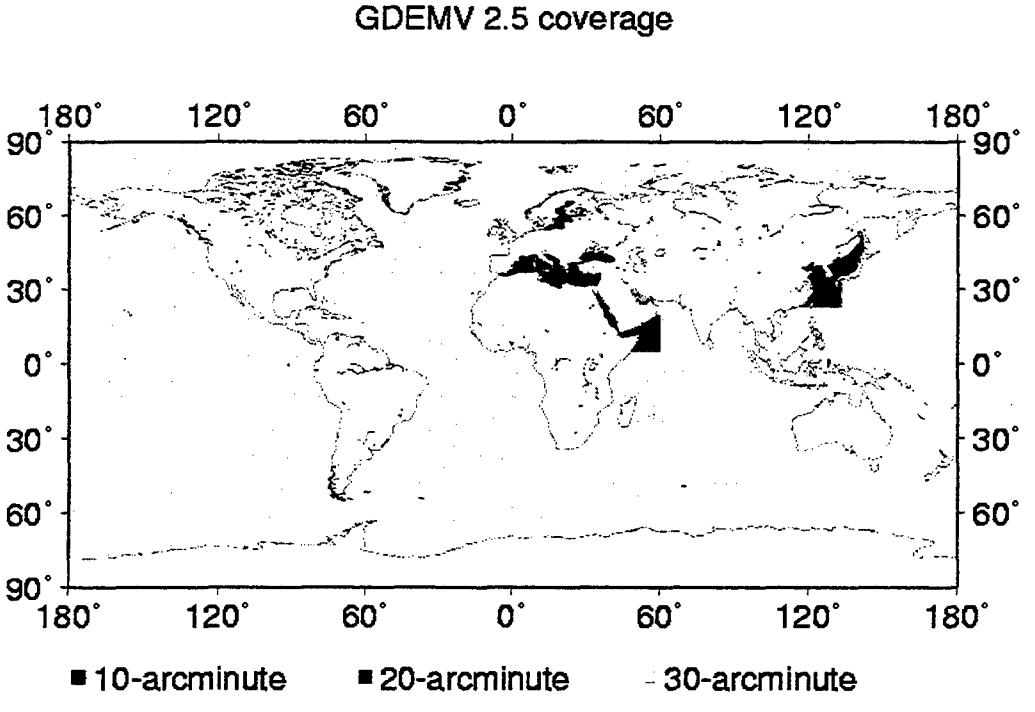

Figure 5. GDEM Coverage and Horizontal Resolutions (From NAVOCEANO 2000).

The gridded GDEM data is created by fitting each MOODS profile to a determined set of analytical curves that represent the mean vertical distributions of temperature and salinity for grid squares. These analytical curves are generated by

averaging the coefficients of the mathematical expressions for the curves found for individual profiles. There are different set of analytical curves that correspond to shallow, mid-depth and deep-depths regions. Each of the corresponding sets of analytical curves is chosen to minimize the number of parameters required to generate a smooth mean profile over the range. Discontinuities in the profiles' vertical gradients are prevented by choosing conditions that match through the depth range transitions. This process results in a climatological data set that is both horizontally and vertically continuous. In addition, temperature and salinity profiles are generated separately to allow the data to be checked for stable densities and to enable the utilization of the large database from expendable bathythermographs (XBT) observations (Teague et al. 1990).

C. MODULAR OCEAN DATA ASSIMILATION SYSTEM (MODAS)

MODAS, recently developed at the Naval Research Laboratory (NRL), uses a modular approach to generate three-dimensional gridded fields of temperature and salinity. Its data assimilation capabilities may be applied to a wide range of input data, including randomly located in-situ, satellite, and climatological data. Available measurements from any or all of these sources are incorporated into a three-dimensional, smoothly gridded output field of temperature and salinity.

MODAS' primary outputs are temperature and salinity fields that may be used to calculate three-dimensional sound speed fields. The sound speed field, in turn, may be used to drive acoustic performance prediction scenarios, including simulations, tactical decision aids, and other capabilities. Other derived fields, which may be generated and examined by the user, include two-dimensional and three-dimensional quantities such as geostrophic currents, mixed layer depths, sonic layer depth, deep sound channel axis

depth, depth excess, and critical depth. These are employed in a wide variety of naval applications and TDAs.

The most current version of MODAS in use is MODAS 2.1, (which has so far and will continued to be referred as MODAS in this paper) a second generation MODAS. The first generation MODAS was MODAS 1.0 which was accepted in the Navy's OAML in November 1995. MODAS 1.0 was initially designed to perform deep-water analyses that produced outputs that supported deep-water anti-submarine warfare operations. However, MODAS 1.0 was constrained by depth because its climatological data was the original NAVOCEANO GDEM, which did not extend beyond depths of less than 100 meters. The capabilities of MODAS 1.0 were increased when GDEM was initially augmented with SWDB, but at the time, SWDB was limited to the northern hemisphere. The Levitus global database, which has less horizontal resolution than GDEM, was used as a second source for the first guess field in MODAS 1.0, but its horizontal resolution was not sufficient for an accurate application in MODAS 1.0. In addition to a lack of vertical resolution, GDEM and Levitus lacked some of the statistical descriptors that made them inadequate for the optimum interpolation analysis of observations like XBT profiles and satellite Multi-Channel Sea Surface Temperature Sensor (MCSSTS) data.

Second generation MODAS (MODAS 2.0) was created to overcome the limitations of MODAS 1.0. One of the major implementations was the development of MODAS internal ocean climatology (Static MODAS climatology) for both deep and shallow-depths. Static MODAS climatology is produced using MOODS as in GDEM but with some improvements. Static MODAS climatology covers the ocean globally to a minimum depth of 5 meters and has variable-horizontal resolution from 7.5-minute to 60-

minute resolution. Static MODAS climatology also contains important statistical descriptors required for optimum analysis of observations that include bi-monthly means of temperature, coefficients for calculation of salinity from temperature, standard deviations of temperature and salinity, and coefficients for several models relating temperature and mixed layer depth to surface temperature and steric height anomaly. In addition, in MODAS 1.0 some of the algorithms for processing and for performing interpolations designed for speed and efficiency in deep waters with the cost of making some weak assumptions about the topography. This shortcut method extended all observational profiles to a common depth, even if the depth was well below the ocean bottom depth, by splicing onto climatology. The error introduced using this shortcut method is amplified when this method is applied to shallow water regions. MODAS 2.0 does not use this shortcut method; instead it performs optimum interpolation analysis for each depth above the ocean bottom separately. The optimum interpolation algorithms used in MODAS 2.0 increases speed of the analysis by using a method commonly used in meteorological systems called the "volume' technique. The capability to use satellite altimetry was another function implemented into MODAS 2.0. Using optimum interpolation algorithms, these SSHs are gridded and used with gridded SST and climatological algorithms and databases to produce three-dimensional temperature and salinity grids (Fox et al. 2000).

MODAS 2.0 was updated to version 2.1 with changes implemented to correct specific problems identified during several fleet exercises. One of the major implementations was the redevelopment of the global database to incorporate higher

resolutions in near shore regions to produce outputs that are more realistic (Fox et al. 2000).

MODAS has two modes of usage; Static MODAS and Dynamic MODAS. As discussed earlier, Static MODAS climatology is an internal climatology used as MODAS' first guess field. The other mode is referred to as Dynamic MODAS climatology, in which MODAS combines locally observed and remote sensed ocean data with climatological information to produce a near real time gridded three-dimensional analysis field of the ocean temperature and salinity structure as an output. Grids of MODAS climatological statistics range from 30-minute resolution in the open ocean to 15-minute resolution in shallow waters and 7.5-minute resolution near the coasts in shallow water regions.

The MODAS model operates in the following manner; the MODAS two-dimensional SST field uses the analysis from previous days field as the first guess, while the MODAS' two-dimensional SSH field uses a large-scale weighted average of 35 days of altimeter data as a first guess. The deviations calculated from the first guess field and the new observations are interpolated to produce a field of deviations from the first guess. Next, a final two-dimensional analysis is calculated by adding the field of deviations from the first guess to the first guess field. When the model performs an optimum interpolation for the first time it uses the Static MODAS climatology for the SST first guess field and zero for the SSH first guess field. Every data after the first optimum interpolation it uses previous day's first guess field for SST and a large-scale weighted average is used for SSH. Synthetic profiles are generated at each location based on the last observation made at that location. If the remotely obtained SST and SSH for a

location do not differ from the climatological data for that location, then climatology is used for that profile. Likewise, if the remotely obtained SST and SSH for a location differ from the climatological data for that location then the deviation at each depth are estimated. Adding these estimated deviations to the climatology produces the synthetic temperature profile. Finally, the synthetic temperature profile is used to produce a synthetic salinity profile by using the climatological temperature and salinity relationship at that location (Fox et al. 2000a).

In shallow water regions, it was found that generally the altimetry is not accurate enough to use, due to additional problems with orbit error and other corrections that increased the error level near land. NAVOCEANO's initial solution was to produce a file that was a highly smoothed version of the bathymetry with specified parameters to use in controlling the use of the altimetry. This solution turned out to be insufficient, based on comparisons to all the MOODS profiles that have been acquired since January 1, 1993, so a simple graphic was produced that NAVOCEANO can use to determine when to turn on or off altimetry.

Studies have shown that MODAS performs well when observational SSH (i.e. data from XBTs) is used and when the 'raw' altimeter data (the data right under a track before it's been turned into a complete grid of data) is used. In water depths less than 150 meters, altimetry is turned off and the synthetics are based solely on the SST grid. Deeper than 400 meters, the synthetics are computed using both SST and SSH. In between those two depths, two synthetics are produced, one using SST only and one using SST plus SSH. Then those two estimates of the synthetics are averaged together using weights based on the water depth. At 150 meters, the 'temperature-only-synthetic'

is weighted 1.0 and the 'SST + SSH synthetic' is weighted 0.0. At 500 meters, the 'SST only' synthetic gets a 0.0 weight and the 'SST + SSH' synthetic gets a 1.0 weight. At 325 meters (the midpoint between 150 and 400 meters), the two synthetics are each weighted 0.5 each. So there is the linearly tapered weighting that estimates the synthetic based on the 'SST synthetic' and the 'SST + SSH synthetic' (Fox, Personnel Communication).

In the Yellow Sea, the MODAS model is operated in the degraded mode of SST and MODAS climatology only mode. The correction of altimetry for use in shallow water regions will be the best improvement to MODAS so far.

THIS PAGE INTENTIONALLY LEFT BLANK

IV. NAVAL INTERACTIVE DATA ANALYSIS SYSTEM (NIDAS)

A. MODEL DESCRIPTION

The NIDAS software provides NAVOCEANO with an interactive capability for several types of oceanographic, metrological, and satellite defined data to create three-dimensional gridded fields of temperature, salinity, and sound speed profiles constructed from a combination of provinced data and gridded data. NAVOCEANO uses NIDAS to construct the environmental database called Provinced Profiles, which is used by MEDAL. Province Profiles is a climatological database derived from the MOODS database that consists of spatial provinces that define an average and several alternate temperature, salinity, and sound speed profiles for a shallow water region on a monthly basis (Mississippi State Center of Air Sea Technology 1997).

The original NIDAS software is a UNIX based software requiring the use of graphics license, thus its use was limited to facilities with UNIX systems that had the proper graphic license. In an effort to expand and facilitate the use of the NIDAS software, a JAVA based version of NIDAS was created for Windows NT operating systems in August of 2000. This version was NIDAS 5.1 developed by Clifton Abbot at Mississippi State Center of Air Sea Technology, Stennis Space Center. NIDAS 5.1a was used in this thesis and the release of version 51.b is expected sometime this year. NIDAS 5.1b will fix some of the bugs contained in the earlier versions and will have increased capabilities, such as a printing function.

B. CREATING AND COMPARING REGIONAL AND SEASONAL MODAS, MOODS, AND GDEM DATA SETS USING NIDAS

All data sets used in this thesis are unclassified. The unclassified MODAS data sets used were obtained from Mr. Dan Fox of NAVOCEANO via a public ftp site. The MODAS data sets were obtained in a NIDAS compatible binary format called "Master format'. The MOODS and GDEM data sets were also obtained from NAVOCEANO on CD-ROM. The MOODS and GDEM data sets were not in the Master format and were converted into the Master format using a FORTRAN code.

The NIDAS software allows all desired data sets for a predefined project area to be displayed all at once by overlaying the various profiles in different colors in the same analysis window. The user can select to view plots of salinity versus depth, temperature versus depth, sound speed versus depth, etc., for all the profiles in a data set in the analysis window. The analysis window allows the user to view all the data available from a data set for a project area as points on a two-dimensional geographical map. This function is especially useful in analyzing MOODS data sets since it is non-gridded observational data, thus was the limiting factor of the three data sets in selecting regions of different bottom types. The two-dimensional geographical map in the analysis was used to help select regions with sufficient MOODS observational profiles for comparison with the MODAS data sets.

The analysis window in NIDAS also has a function known as the "polygon function" that allows the user to select a region within the two-dimensional geographical map of the project area for analysis by drawing a polygon around the desired region. After a polygon has been created for a region, the profiles for that region are

automatically highlighted for analysis in all of the plots in the analysis window. The user can then choose to view and edit the data for all the profiles in the polygon to create a user defined data set. This created data set can then be saved as an export file in three different formats, "Master", "CASTAR", and "Text", for use with oceanographic and acoustic models.

In this study, the polygon function was used to visually analyze and create data sets of different regions that were defined by bottom type. The three data sets were overlaid in the analysis window using different colors and their salinity, temperature, and sound speed profiles were visually analyzed for each month at the four different regions selected for this study. The data sets for MODAS, MOODS, and GDEM for the four different months (February, May, August, and November, which represent mid-season for the four seasons) and for the selected regions were created using the polygon function.

The results of all the visual comparisons made for the MODAS, MOODS, and GDEM profiles for all four seasons were for the most part similar. This comes to no surprise since the MODAS climatology data and GDEM are derived directly from MOODS. The main differences were that the MODAS and GDEM profiles had smooth transitions, while MOODS had sharp transitions from the mixed layers to the thermocline and from the thermocline to the sub layer. This tended to weaken the gradient of the thermocline and surface ducts when they were present. The differences in transitions are due to the higher vertical resolutions contained in both MODAS AND GDEM and the averaging involved in the development of the MODAS climatology and GDEM from the MOODS observations. Another difference was found in the temperature and speed

profiles during the winter mainly between MODAS and MOODS. The difference is evident near the bottom: Many MODAS profiles in February show the increase of temperature with depth (downward positive gradient), however, all the MOODS profiles (observational) show the isothermal pattern. The profiles with such a difference were most found in the shelf of the southern Yellow Sea and northern East China Sea. This location falls in the southern portion of the mud region used in this study. This difference may be due to a lack of observational data in that region when the MODAS climatology was created, but it cannot be determined with certainty without a study of the MODAS climatology which was not available during this study. During the winter months, the near bottom positive gradient was also present in some of the GDEM profiles but the gradients were not as strong as those found in MODAS. In addition, the near bottom gradients were not isolated to just one region; they were also found in the other regions used in this study.

The data sets for MODAS and GDEM were created using the polygon function without editing. The MOODS data sets were also created using the polygon function but were edited to remove erroneous profiles as described earlier. All the data sets were saved as export files in the "CASTAR" format. The CASTAR format was chosen because most of the data for each profile can viewed as text and this format is easier to manipulate with MATLAB to create input files for the CASS/GRAB model.

V. COMPREHENSIVE ACOUSTIC SIMULATION SYSTEM/ GAUSSIAN RAY BUNDLE (CASS/GRAB)

A. MODEL DESCRIPTION

CASS/GRAB is an active and passive range dependent propagation, reverberation, and signal excess acoustic model that has been accepted as the Navy's standard model. The GRAB model's main function is to calculate eigenrays in range-dependent environments in the frequency band 600 Hz to 100 kHz and to use the eigenrays to calculate propagation loss. The CASS model is the range dependent improvement of the Generic Sonar model (GSM). CASS performs range independent monostatic and bistatic active signal excess calculations. The CASS model incorporates the GRAB eigenray model as a subset (Figure 4). CASS uses a driver that calls the GRAB eigenray model to compute eigenrays and propagation loss (Keenan 1998).

In the GRAB model, the travel time, source angle, target angle, and phase of the ray bundles are equal to those values for the classic ray path. The main difference between the GRAB model and a classic ray path is that the amplitude of the Gaussian ray bundles is global, affecting all depths to some degree, whereas classic ray path amplitudes are local. GRAB calculates amplitude globally by distributing the amplitudes according to the Gaussian equation

$$\Psi_v = \frac{\beta_{v,0}\Gamma_v^{\,2}}{\sqrt{2\pi}\,\sigma_v\, p_{r,v}\, r}\exp\left\{-0.5\left[(z-z_v)/\sigma_v\right]^2\right\},$$

where the Γ_v represents losses due to volume attenuation and boundary interaction, $\sigma_v = (0.5)(\max(\Delta z, 4\pi\lambda))$ defines the effective standard deviation of the Gaussian width, and $\beta_{v,0}$ is a factor that depends only on the source and is chosen so that the energy within a

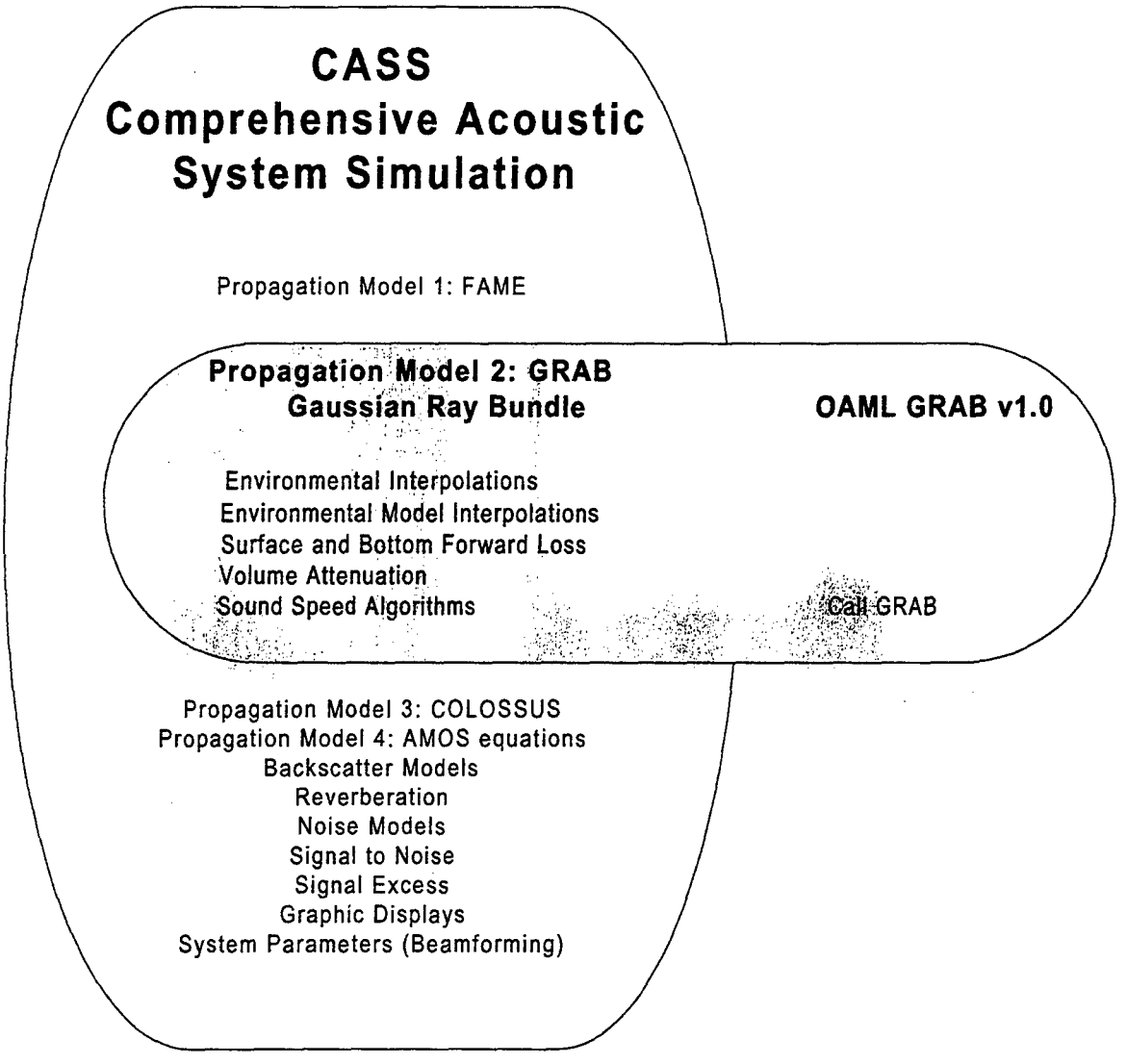

Figure 6. CASS/GRAB Overview (From Keenan et al. 1999).

geometric-acoustic ray tube equals the energy within a Gaussian ray bundle. The variable z_v is the depth along the v^{th} test ray at range r, z is the target depth, p_r is the horizontal slowness, Δz is the change in ray depth at constant range due to a change in source angle, and λ is the wavelength. The selection of the effective standard deviation σ_v is the weakest component in providing a firm theoretical basis for the GRAB model. The closer the test ray is to the target, the larger the contribution it has to the final power weighted eigenray. These test rays are called ray bundles since they distribute some

energy to each depth. GRAB classifies each ray group into a ray family. GRAB version 1.0 defines a ray family as ray groups that have a similar number of surface and bottom bounces. Under caustic conditions there will be ray bundles with surface and bottom depth differences greater than and less than zero within each ray family and GRAB computes an eigenray for each group. Thus, GRAB computes up to two weighted averaged ray groups for each ray family. GRAB does not store all the eigenrays it calculates; instead, it performs a user accessible eigenray tolerance test to determine if eigenrays are too weak to be stored in the eigenray file. GRAB then computes the random or coherent propagation loss from the eigenrays stored in the eigenray file and stores in them in separate pressure files (Aidala et al. 1998).

CASS computes range dependent reverberation for monostatic and bistatic transmitter to target and target to receiver scenarios. Reverberation is calculated in the time domain centered at the receiver. It accounts for all possible combinations of signal eigenray paths, sums them all up at a given range, and selects the peak signal to noise/ reverberation level to determine signal excess (Keenan 1998).

B. MINE WARFARE SCENARIOS

The high environmental variability and strong multi-path interactions encountered in the littoral make acoustic modeling very difficult. In these shallow water regions, accurate arrival structure information is required to model the performance of high frequency acoustic systems. Other Navy range-dependent acoustic models such as the Navy's PE (Parabolic Equation) model are inadequate because they become computationally intensive above several kilohertz. The GRAB eigenray model produces the required arrival structure needed for systems applications in the littoral zone. This

capability makes the CASS/GRAB a very effective tool for modeling the performance high frequency acoustic systems in the littoral. In addition, the CASS/GRAB model has successfully modeled torpedo reverberation data in 1994 in shallow water, range dependent environments at the NUWC Southern California (SOCAL) and Cape Cod torpedo exercise areas.

VI. SEASONAL VARIABILITY OF ACOUSTIC TRANSMISSION

A. GDEM SEASONAL VARIABILITY FOR SOUND SPEED PROFILES

The annual mean for the GDEM sound speed profiles for the four regions selected for this study were calculated and plotted against each of the monthly profiles to examine seasonal variability of the GDEM sound speed profiles. One specific location representing one sound speed profile was selected for each region.

The first location is a small region with a Rock Bottom type located in the mid-eastern Yellow Sea (Region 1). The sound speed profile for the annual mean at this location has a negative sound speed gradient from the surface to the bottom, thus having the characteristic of a thermocline that extends through the water column (Figures 7 and 8). The winter months of January through March contain sound speed profiles that are relatively isothermal with a slight positive gradient. In the first month of spring, April, the sound speed gradient begins to become negative and take the form of a thermocline very similar to the annual mean by the month of May. The sound speed gradient continues to become more negative from June to the summer month of August. Then in September, the sound speed gradient becomes less negative. In the fall month of November, a mixed layer with a surface duct is generated and by December, the sound speed profile has returned to the isothermal conditions of winter.

The second location is a small region with a Gravel Bottom type located in the northeastern Yellow Sea (Region 2). The sound speed profiles for the annual mean and for each of the 12 months closely reflect those at the first location (Figure 9). The most significant difference between the two locations is that the isothermal layer during the

winter months in Region 2 falls below 1460 m/s and the isothermal layer in Region 1 does not fall below 1465 m/s. The difference is accounted for the fact that Region 2 is located further north in the Yellow Sea.

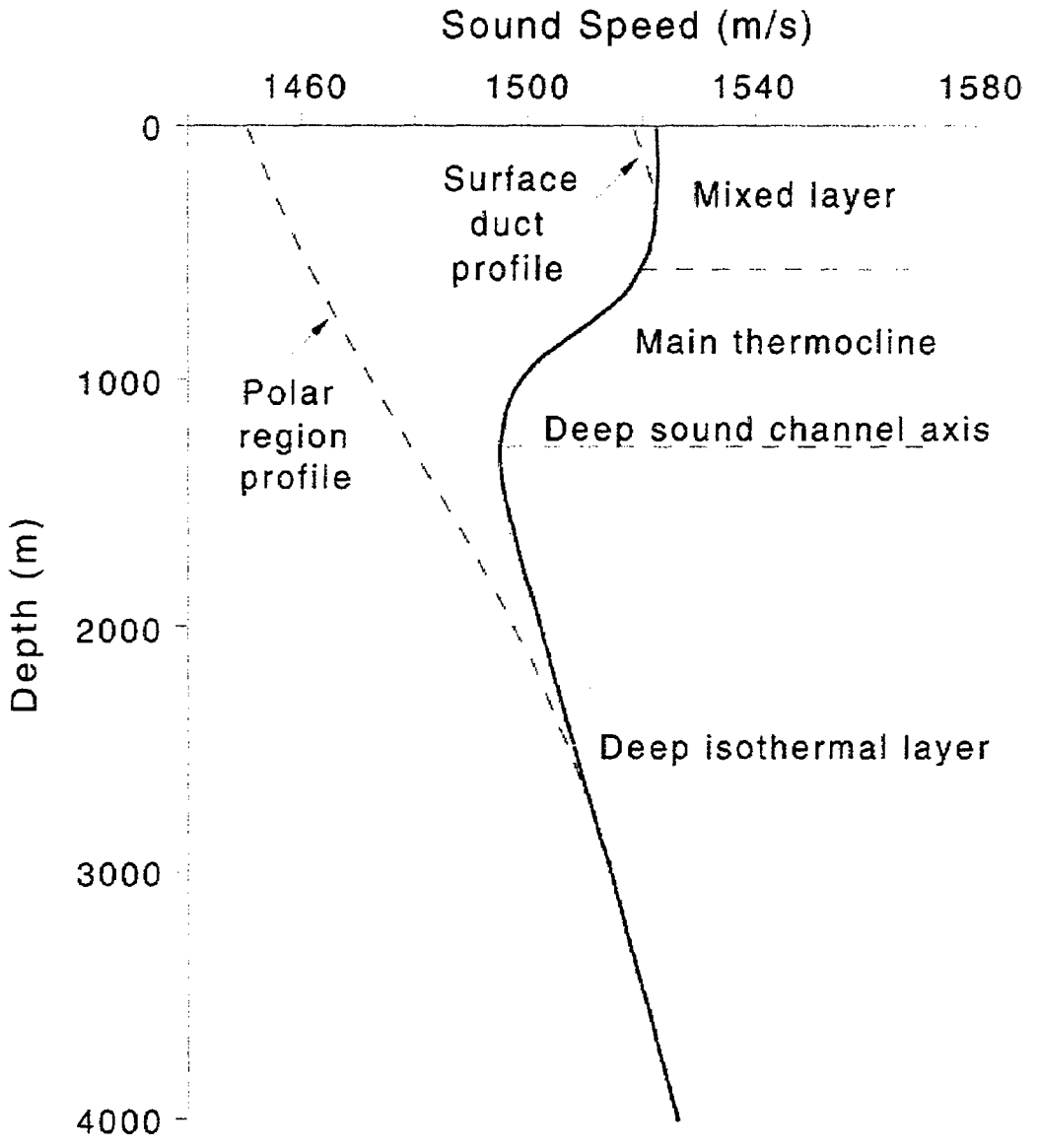

Figure 7. Generic sound speed profiles (From Jensen et al. 2000).

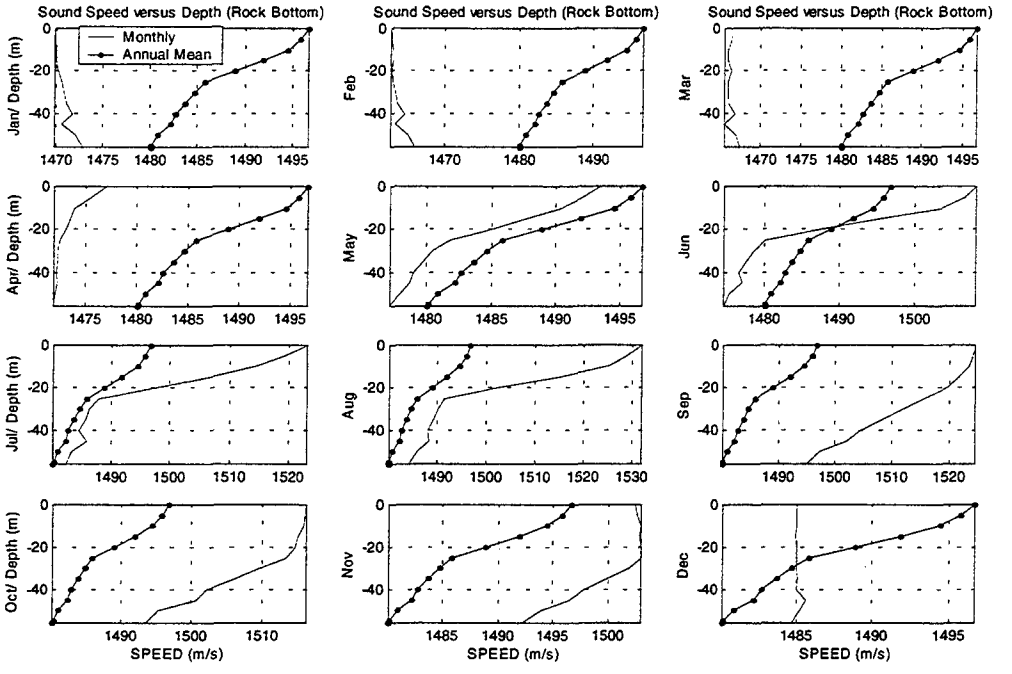

Figure 8. Monthly and annual mean sound speed comparison for Rock Bottom for all 12 months.

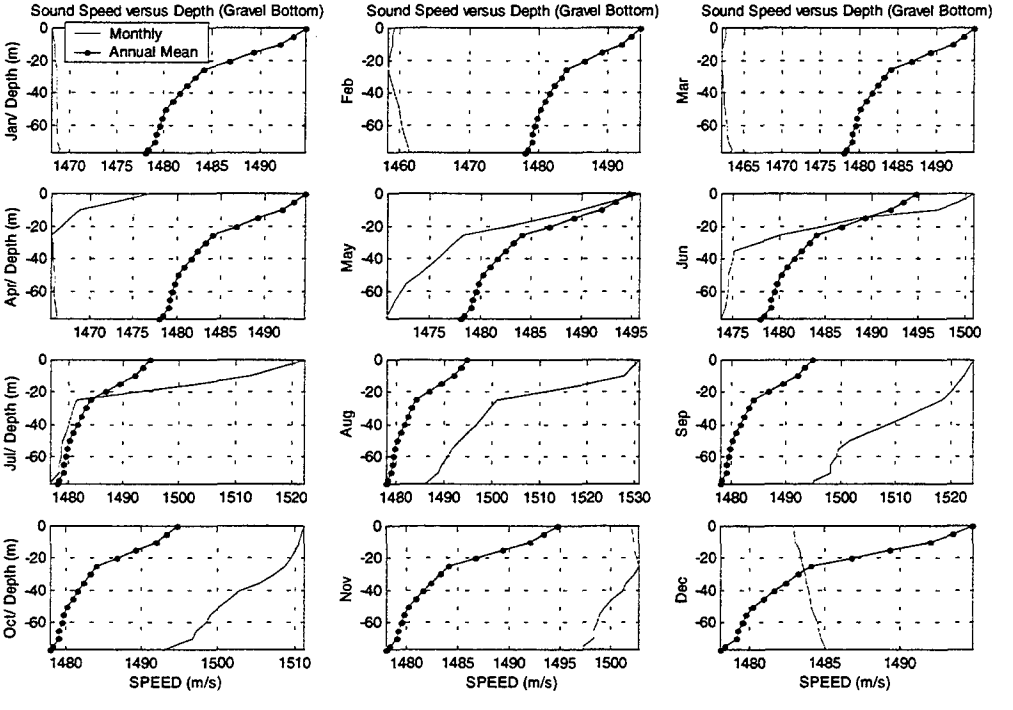

Figure 9. Monthly and annual mean sound speed comparison for Gravel Bottom for all 12 months.

The third location is a region with a Sand Bottom type, (the predominant bottom type for most of the western coast of the Korean peninsula) located in the southeastern Yellow Sea (Region 3). Again, the sound speed profiles for the annual mean and for each of the 12 months closely reflect those in Region 1 (Figure 10).

The fourth location is a region with a Mud Bottom type, (the predominant bottom type for most of the central and eastern Yellow Sea) located in the south-central Yellow Sea (Region 4). The sound speed profiles for the annual mean and the winter, spring, and summer months are very similar to those of Region 1 (Figure 11). During the fall months in this region, a mixed layer is present that extends to a depth of approximately 30 meters. A surface duct is present in the mixed layer of the November and December profiles. In addition, a deep isothermal layer is present at a depth of approximately 50 meters in the October and November profiles.

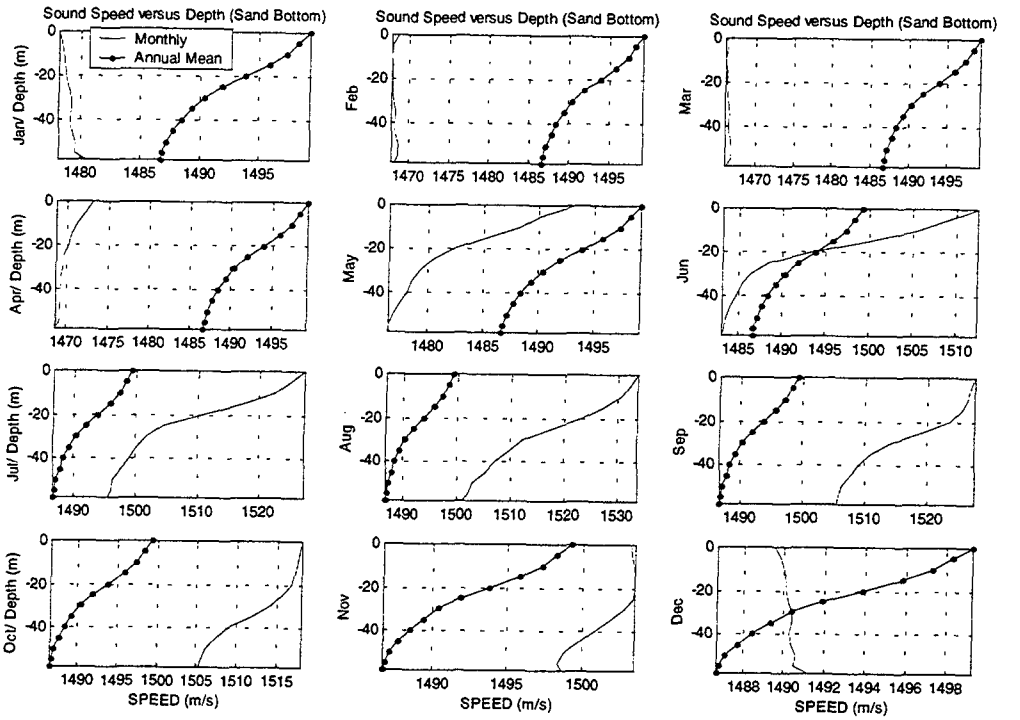

Figure 10. Monthly and Annual Mean Sound Speed comparison for Sand Bottom for all 12 months.

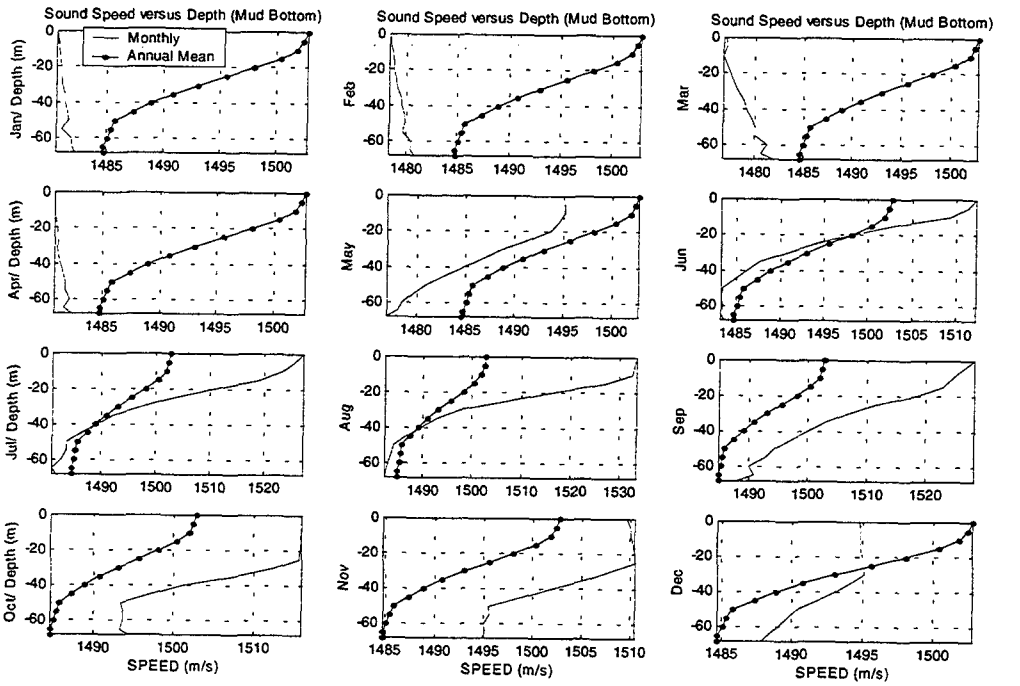

Figure 11. Monthly and Annual Mean Sound Speed comparison for Mud Bottom for all 12 months.

B. GDEM SEASONAL VARIABILITY FOR SIGNAL EXCESS

As described earlier, the environmental effects on the performance of the AN/SQQ-32 mine hunting sonar system is being simulated by the CASS/GRAB model. This system is a variable depth high frequency sonar system, which allows the user to place the sonar at various positions in the water column to optimize the detection of either Moored or Bottom mines (Figure 10). In complimenting the AN/SQQ-32 mine hunting sonar system concept, two source depths were chosen for this study. The first source depth chosen was a depth of 25 feet, which places the source at the depth of a moored mine positioned for the hull depth of a large war ship. This depth also places the source within the mixed layer or surface duct to increase detection range if either are present.

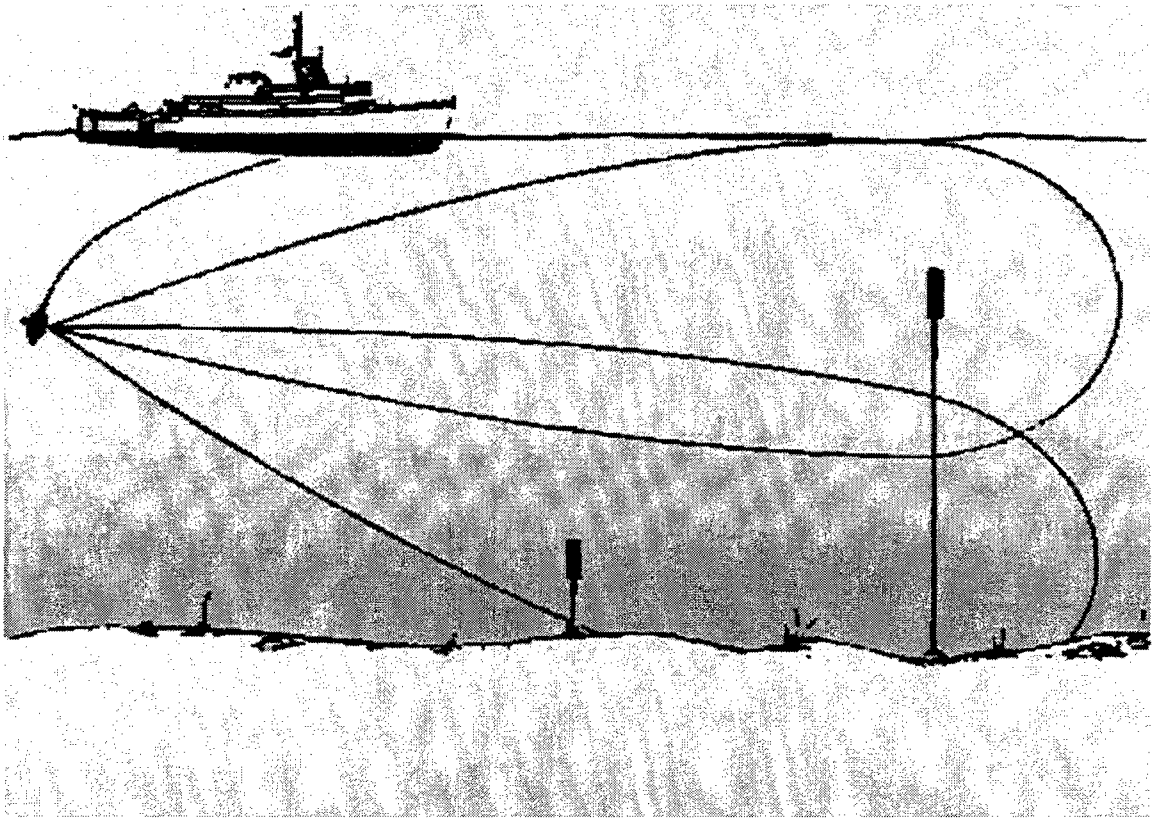

Figure 12. AN/SQQ-32 Concept.

The second source depth chosen was 125 feet for bottom depths greater than 135 feet, 75 feet for bottom depths between 135 feet and 85 feet, 50 feet for bottom depths between 85 and 55 feet, and no second source depth was chosen if the bottom depth was less than 55 feet. These depths usually place the source within or below the thermocline in order to optimize detection ranges. In addition, a moderate wind speed of 5 knots and an intermediate receiver tilt angle of 8 ° were used as inputs for all of the CASS/GRAB model runs in this study.

The maximum detection ranges were determined at both source depths for each month at the four different bottom type locations. In a range dependent environment such as the shallow waters of the Yellow Sea, the detection threshold is reverberation limited. Reverberation from a Rock Bottom is the highest of the four bottom types, followed by a Gravel Bottom, Sand Bottom, and Mud Bottom. Therefore, maximum detection ranges are very dependent on bottom type and bottom depths.

The maximum detection ranges for Region 1 were relatively short due to the high level of bottom reverberation generated by the Rock Bottom (Figure 13). The maximum detection ranges for a source depth of 25 feet and a target at a depth of 26 feet were approximately 160 yards for the months of January, February, March, and December, and were approximately 120 yards for the remaining months. The reduction in the detection ranges can be attributed to the shifting of sound propagation towards the sea bottom by the thermocline present during those months, thus causing a decrease in the sound propagating in the upper water column and an increase in reverberation from the sea bottom. There were no detections for any of the months for a target located on the

bottom due to the high level of reverberation and possibly the relatively large distance between the source and the ocean bottom (Figure 14 and 15).

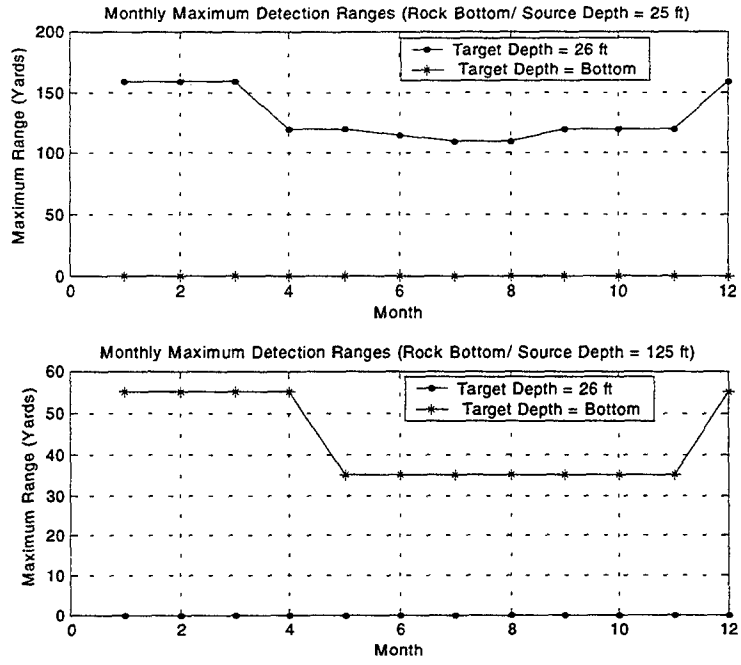

Figure 13. Monthly maximum detection ranges for a Rock Bottom at two source and target depths.

There were no detections for any of the months for a target at a depth of 26 feet and a source depth of 125 feet. This is due to placing the source further away from a target in the upper water column and placing it closer to the sea floor thus generating a higher level of bottom reverberation. The maximum detection ranges for a target on the bottom and a source depth of 125 feet were approximately 55 yards for the months of January, February, March, April, and December, and approximately 35 yards for the remaining months. The decrease in the detection ranges from May through November is due to the source situated under the main thermocline, causing the sound propagation to be trapped between the main thermocline and the bottom, thus generating a high level of reverberation from the sea floor (Figure 16-17).

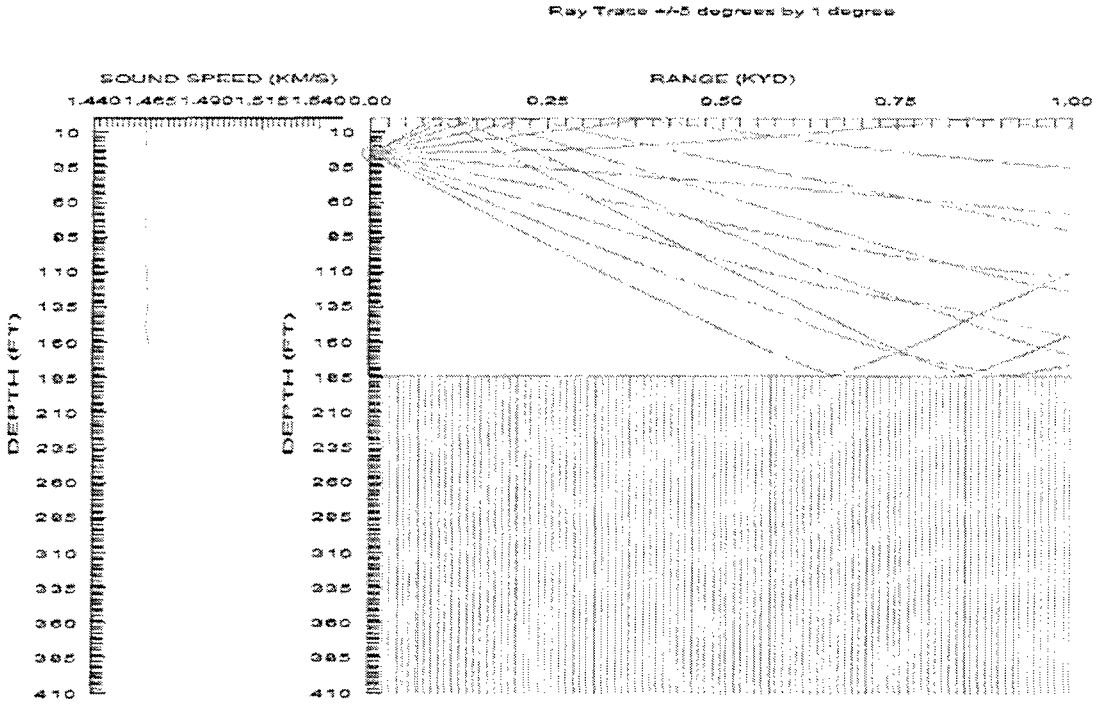

a.

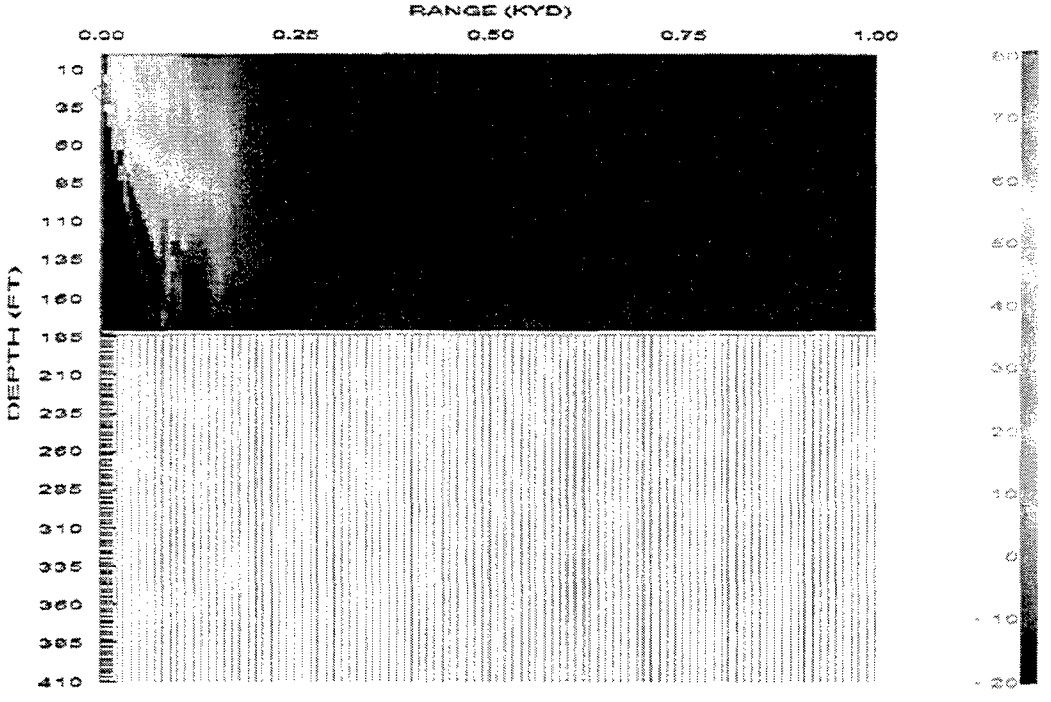

b.

Figure 14. February GDEM for a Rock Bottom at 37.5 N 123.0 E and a Source Depth = 25 ft. a. Ray Trace and b. Signal Excess Contour.

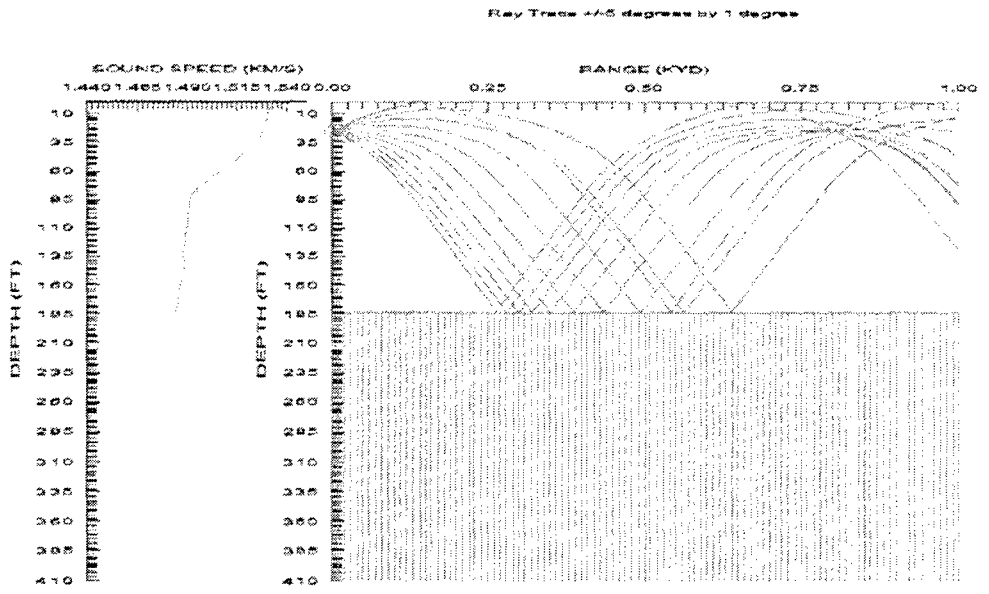

a.

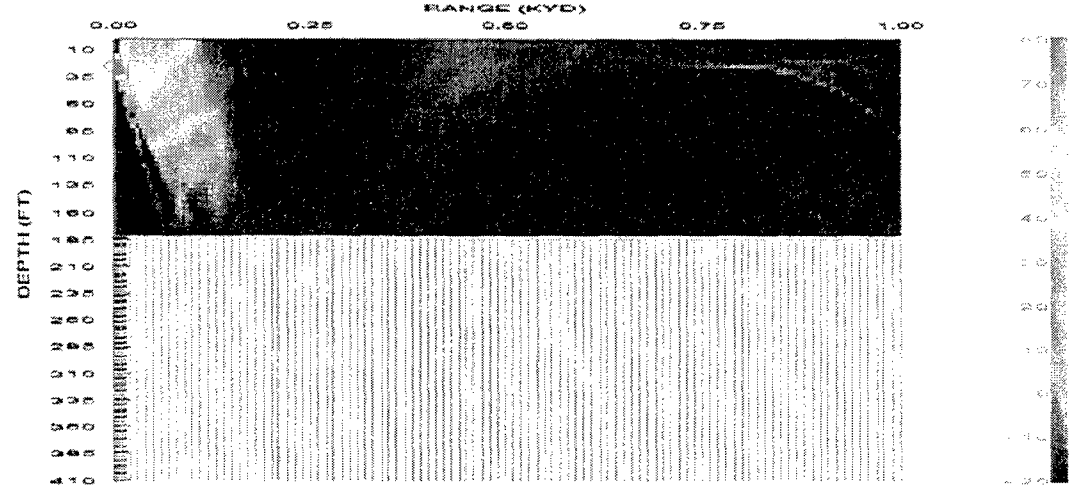

b.

Figure 15. August GDEM for a Rock Bottom at 37.5 N 123.0 E and a Source Depth = 25 ft. a. Ray Trace and b. Signal Excess Contour.

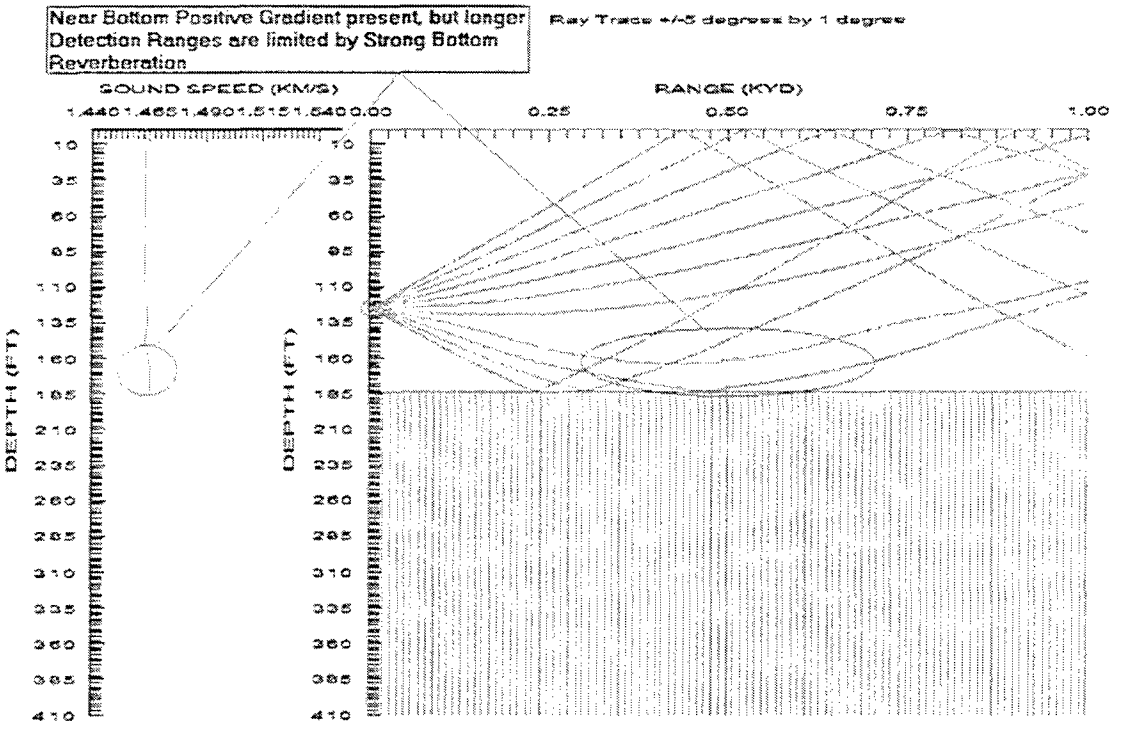

a.

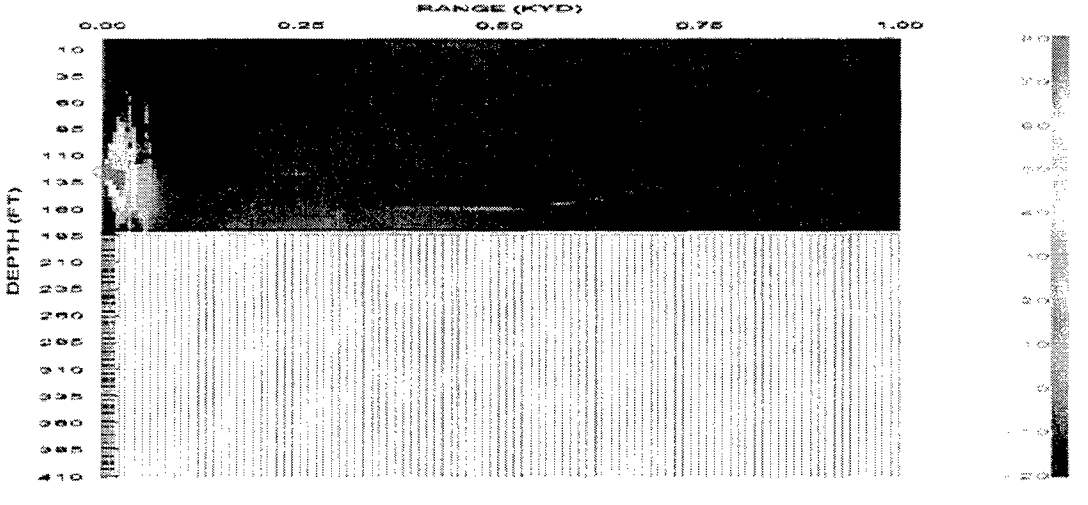

b.

Figure 16. February GDEM for a Rock Bottom at 37.5 N 123.0 E and a Source Depth = 125 ft. a. Ray Trace and b. Signal Excess Contour.

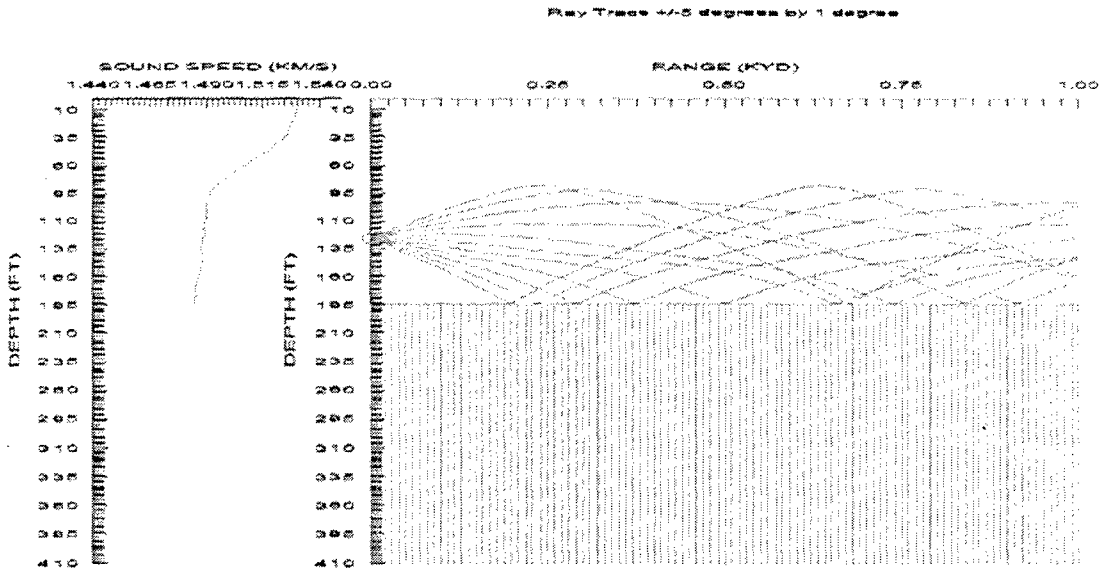

a.

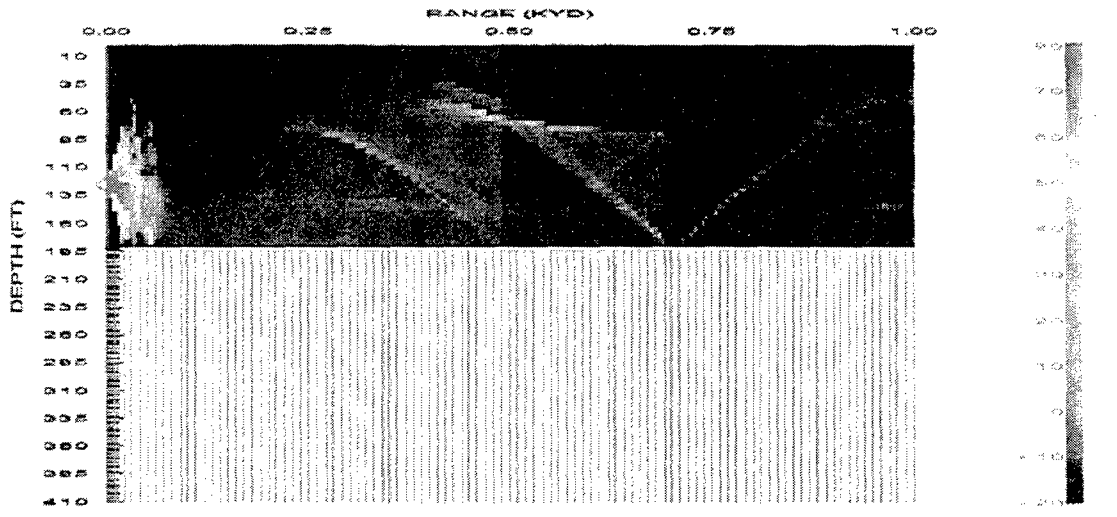

b.

Figure 17. August GDEM for a Rock Bottom at 37.5 N 123.0 E and a Source Depth = 125 ft. a. Ray Trace and b. Signal Excess Contour.

The maximum detection ranges for Region 2 were also relatively short due to the high level of bottom reverberation generated by the Gravel Bottom (Figure 20). The maximum detection ranges for a source depth of 25 feet and a target depth of 26 feet were approximately 250 yards for the months of January, February, March, October, November, and December, approximately 150 yards for the months of April, May, and June, and approximately 225 yards for the months of August and September. An interesting feature can be seen for the month of July, which has a detection range of over 1000 yards. This dramatic increase in the detection range can be attributed to the large negative gradient of the thermocline which focuses the sound propagation towards a point in the sea bottom producing a Bottom Bounce that forms a caustic at the convergence zone (Figure 18-20). As before, the decreases in detection ranges during some of the spring and summer months are attributed to the thermocline. Again, there were no detections for any of the months for a target located on the bottom due to the high level of reverberation and the relatively large distance between the source and the ocean bottom (Figure 21 and 22). The maximum detection ranges for a target at a depth of 26 feet and a source depth of 125 feet were approximately 80 yards for the months of January, February, March, and December, and approximately 120 yards for the remaining months. Again, these very small detection ranges can be contributed to the higher level of reverberation the receiver is exposed to by lowering it closer to the bottom ocean bottom. In this scenario, the increase in the detection ranges for the months of April through November may be attributed to the thermocline shifting sound propagation into the sea bottom and generating a bottom bounce, thus directing sound propagation towards the target in the upper water column. There were no detections for a target at the bottom for

source depth of 125 feet. This may be due to the water depth at this location being deeper than in Region 1 by 20 meters, thus causing the receiver to be to far away from a bottom target to detect through the strong bottom reverberation (Figure 23 and 24).

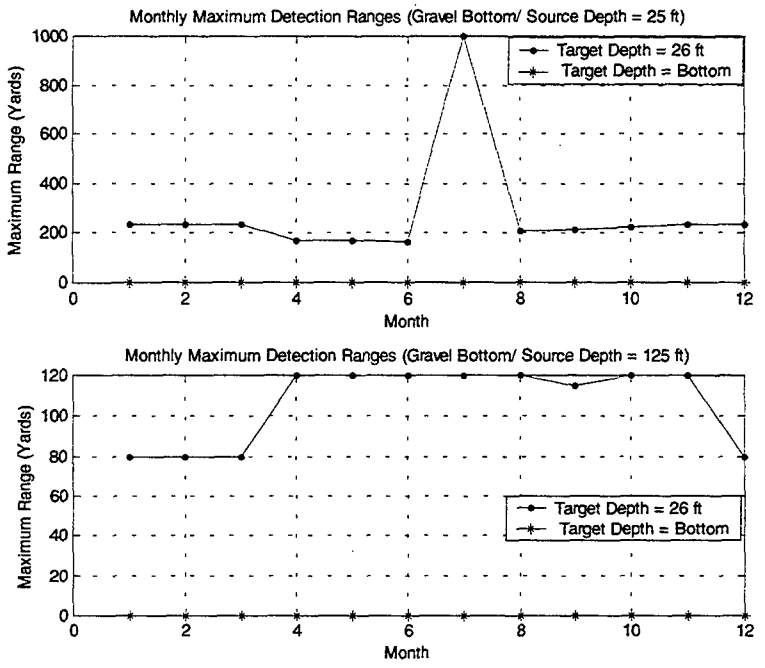

Figure 18. Monthly maximum detection ranges for a Gravel Bottom at two source depths and target depths.

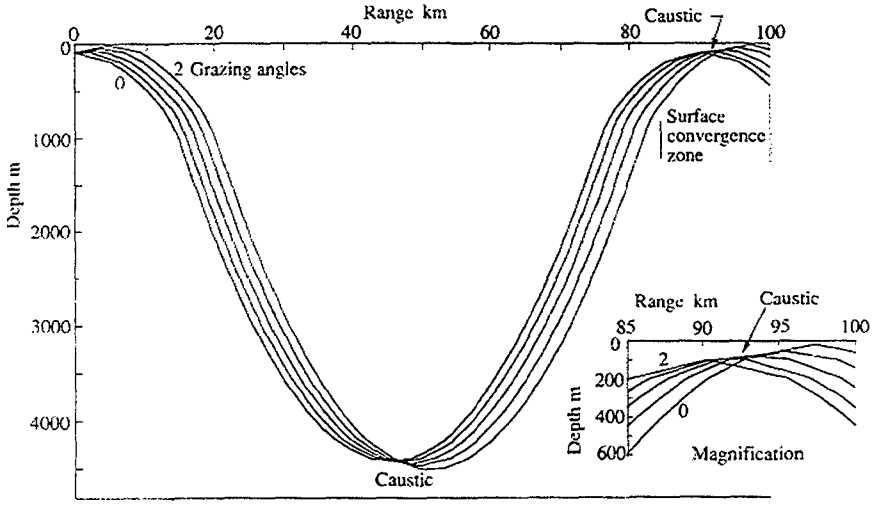

Figure 19. Convergence-zone ray paths for a source at 50 m (From Medwin 1998).

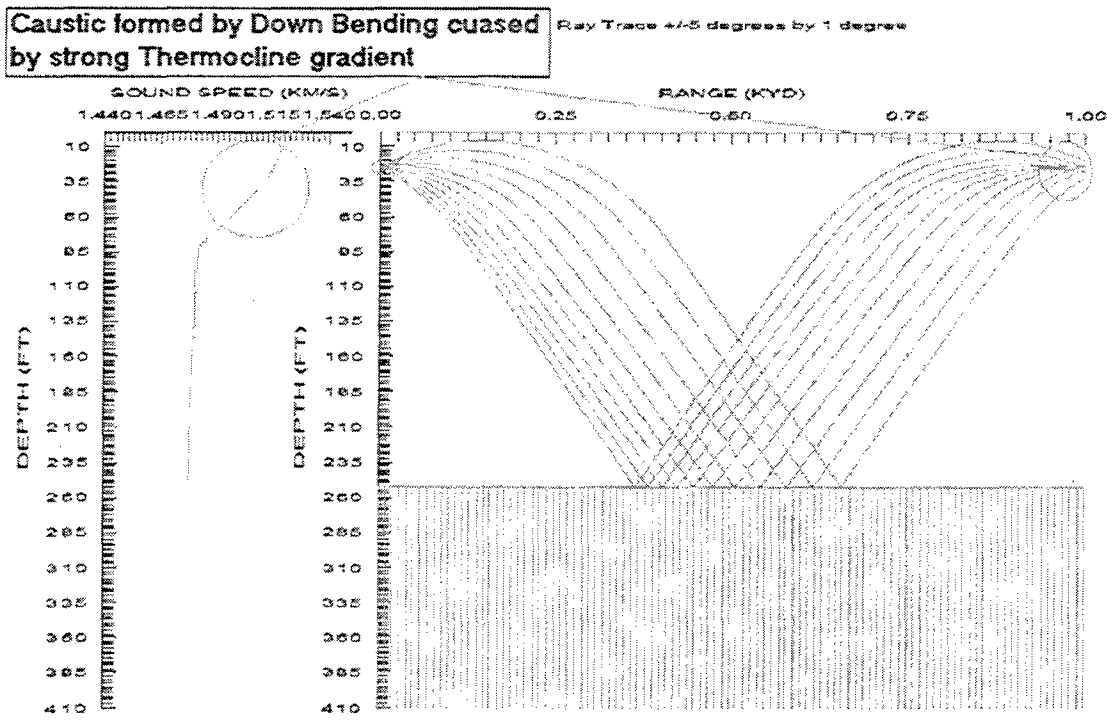

a.

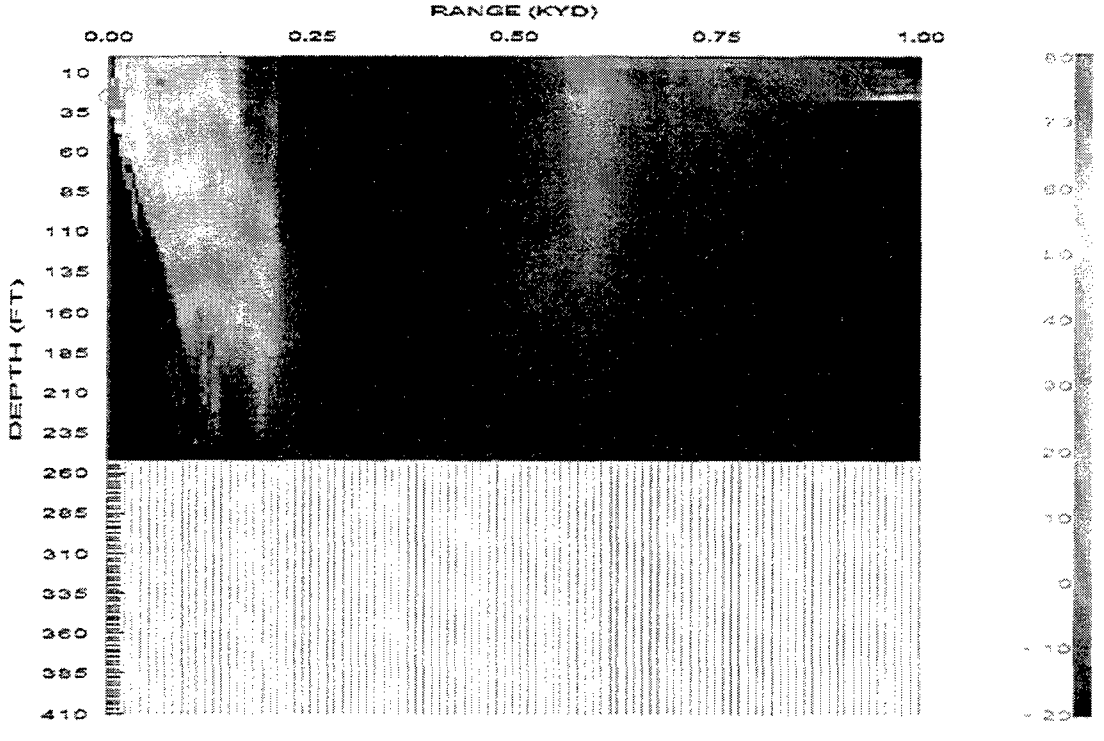

b.

Figure 20. July GDEM for a Gravel Bottom at 38.5 N 123.0 E and a Source Depth = 25 ft. a. Ray Trace and b. Signal Excess Contour.

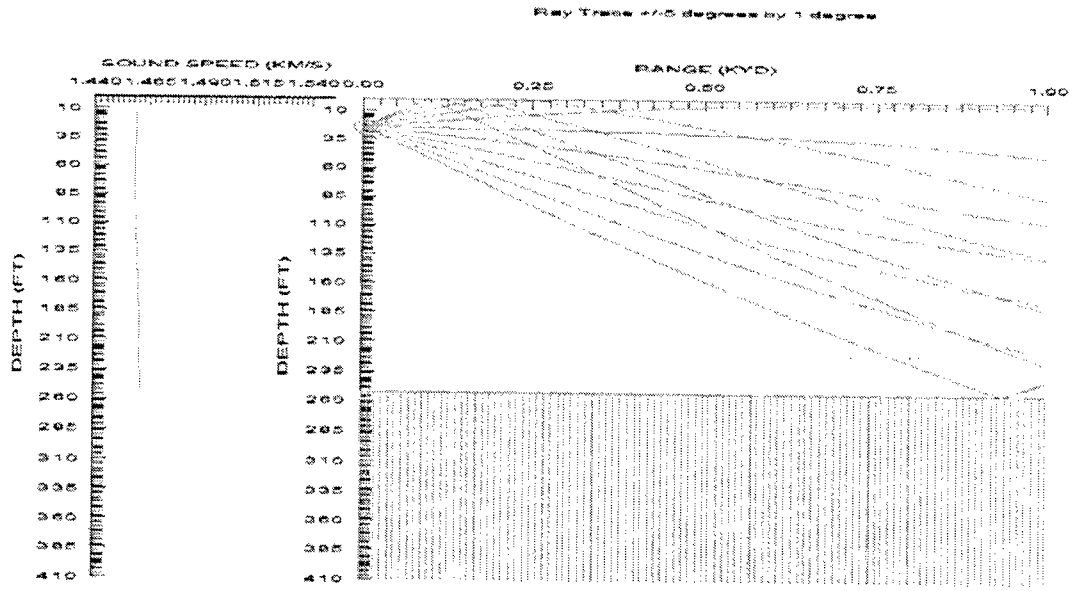

a.

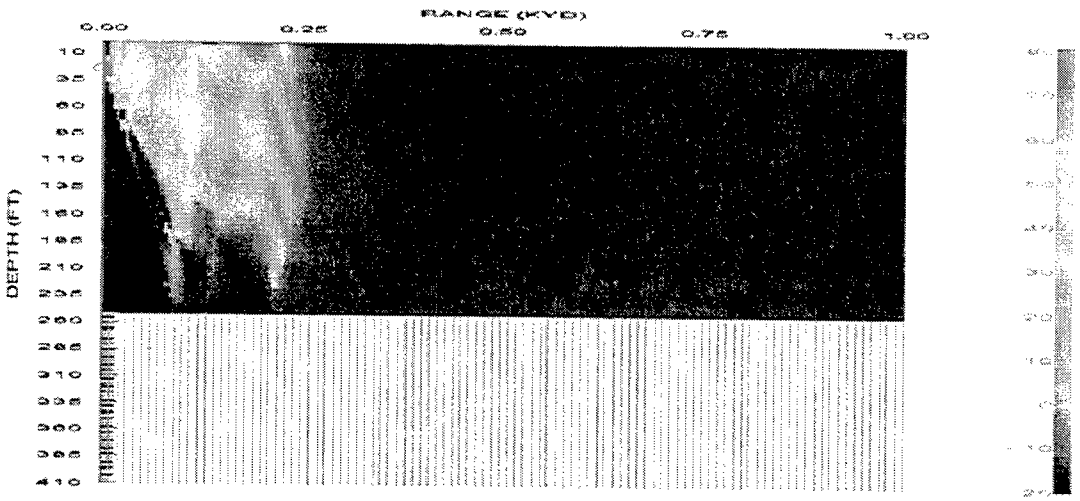

b.

Figure 21. February GDEM for a Gravel Bottom at 38.5 N 123.0 E and a Source Depth = 25 ft. a. Ray Trace and b. Signal Excess Contour.

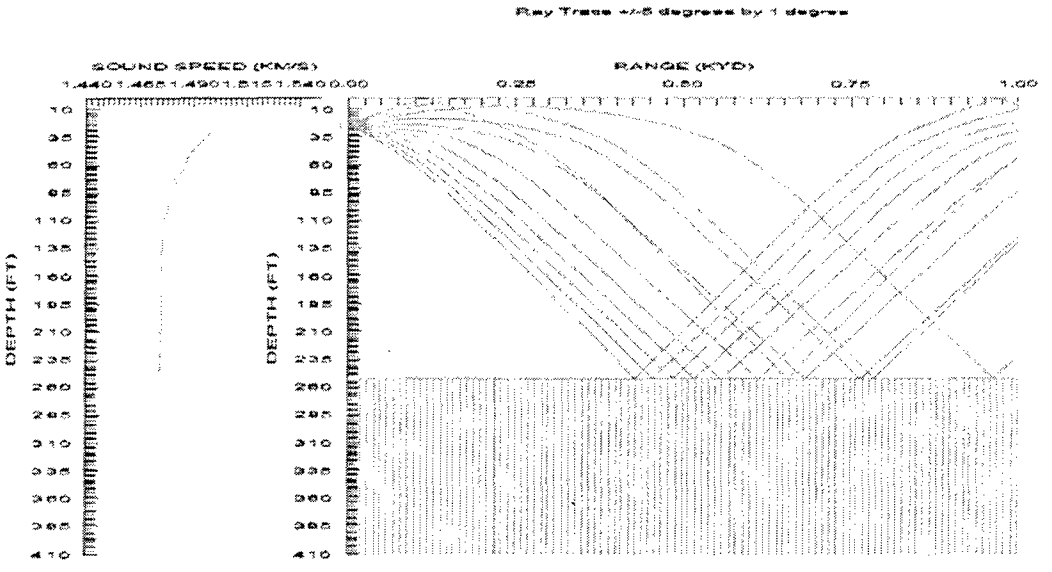

a.

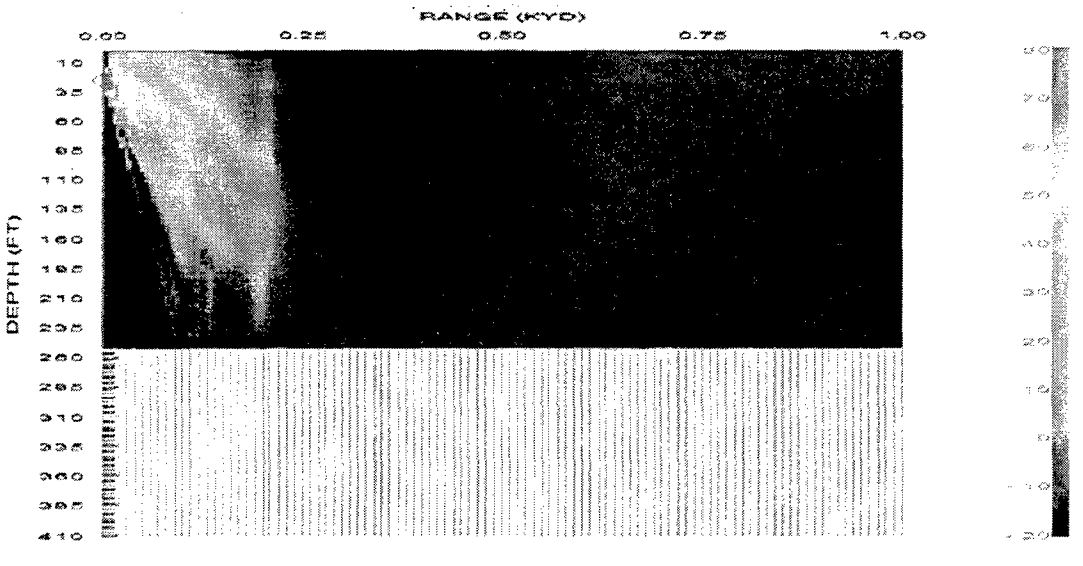

b.

Figure 22. June GDEM for a Gravel Bottom at 38.5 N 123.0 E and a Source Depth = 25 ft. a. Ray Trace and b. Signal Excess Contour.

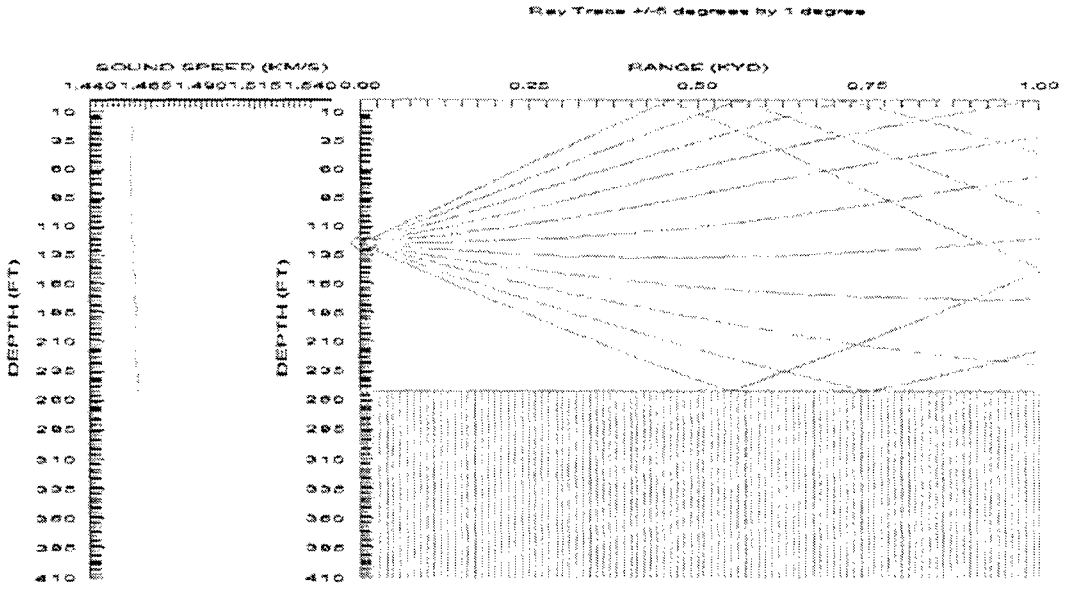

a.

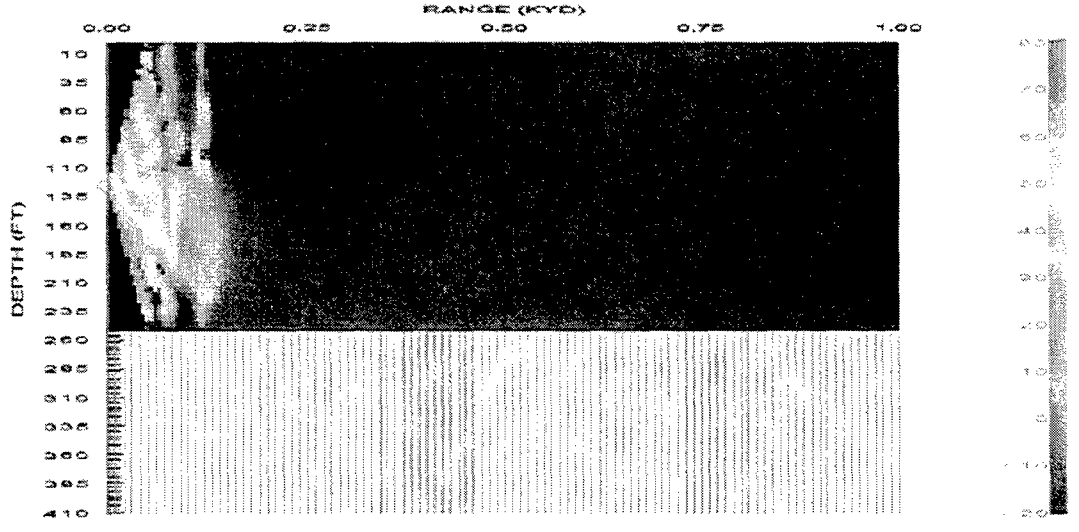

b.

Figure 23. February GDEM for a Gravel Bottom at 38.5 N 123.0 E and a Source Depth = 125 ft. a. Ray Trace and b. Signal Excess Contour.

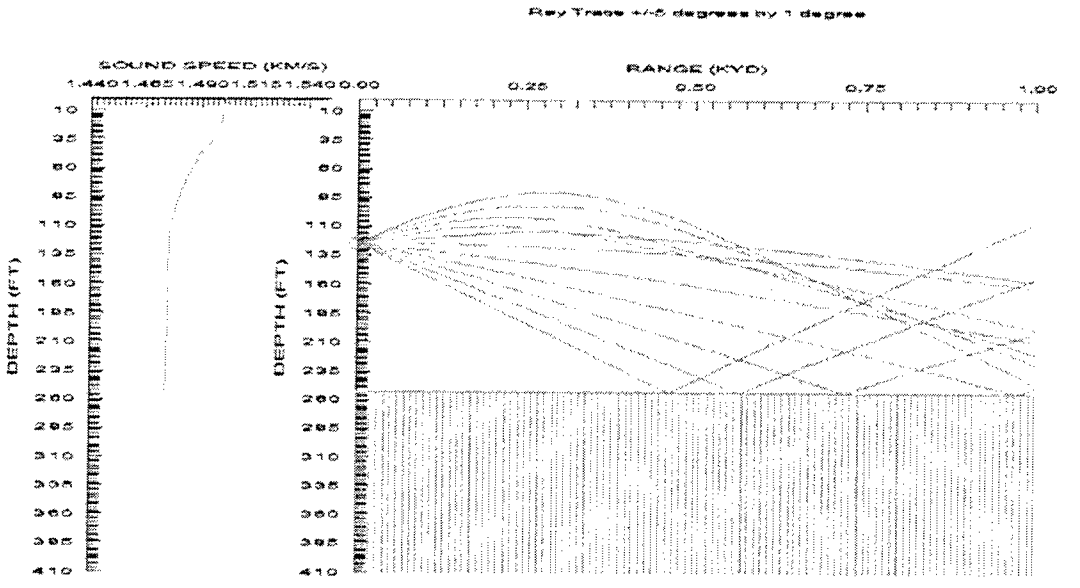

a.

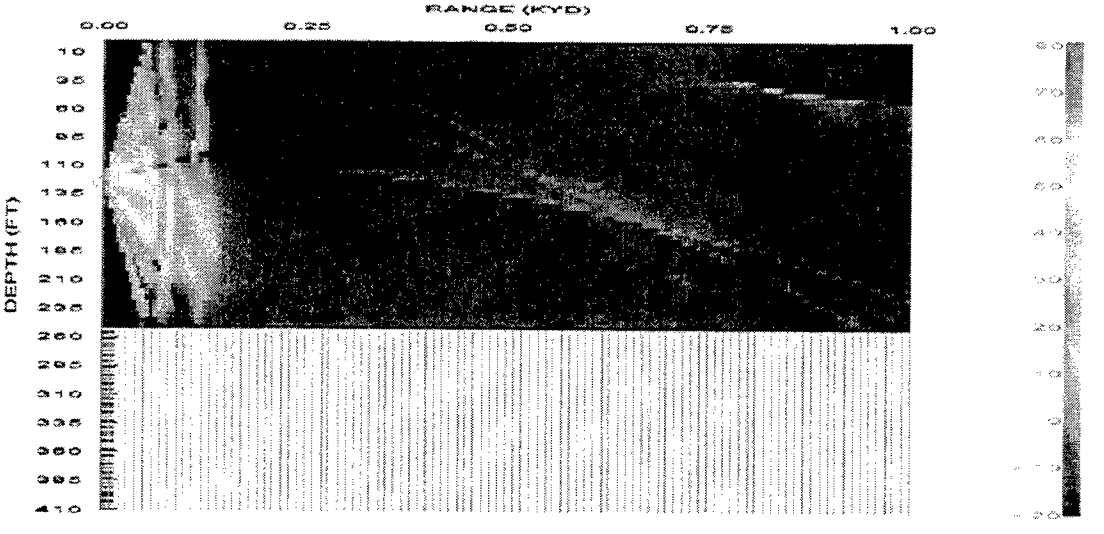

b.

Figure 24. June GDEM for a Gravel Bottom at 38.5 N 123.0 E and a Source Depth = 125 ft. a. Ray Trace and b. Signal Excess Contour.

The maximum detection ranges for Region 3 were much larger overall than the first and second regions due to the lower levels of reverberation produced by a Sand Bottom (Figure 25). The maximum detection ranges for a target at 26 feet and a source depth of 25 feet were approximately 150-175 yards for the months of January through May and August through December and over 1000 yards for the months of June and July. The strong thermocline present in the month of June and July generated a convergence zone, which contributed to the large increase in detection ranges (Figure 26). There were no detections for any of the months for a Bottom mine at this source depth due to the combined effect of bottom reverberation and the relatively large distance between the source and the sea floor (Figure 27 and 28).

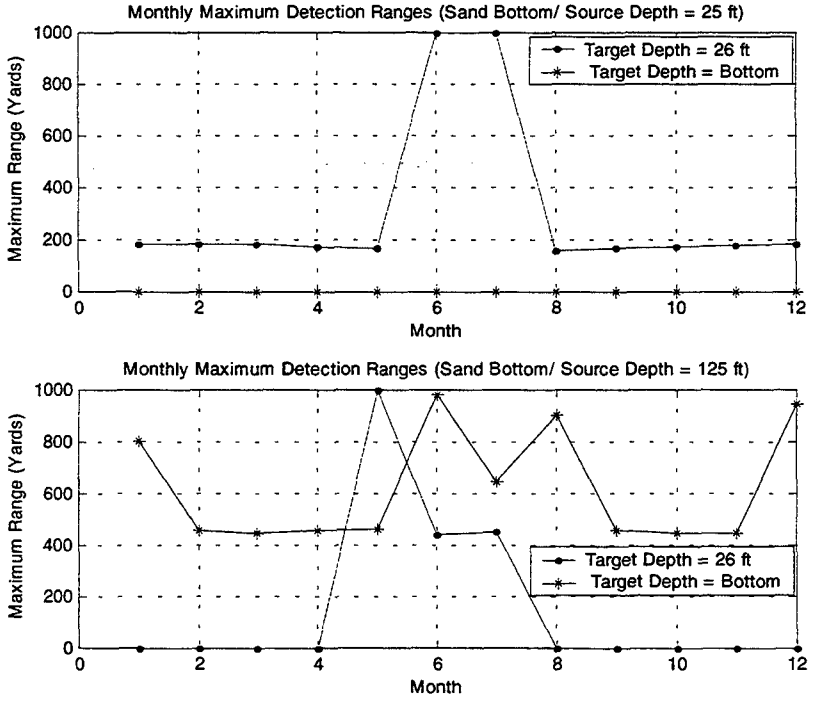

Figure 25. Monthly maximum detection ranges for a Sand Bottom at two source depths and target depths.

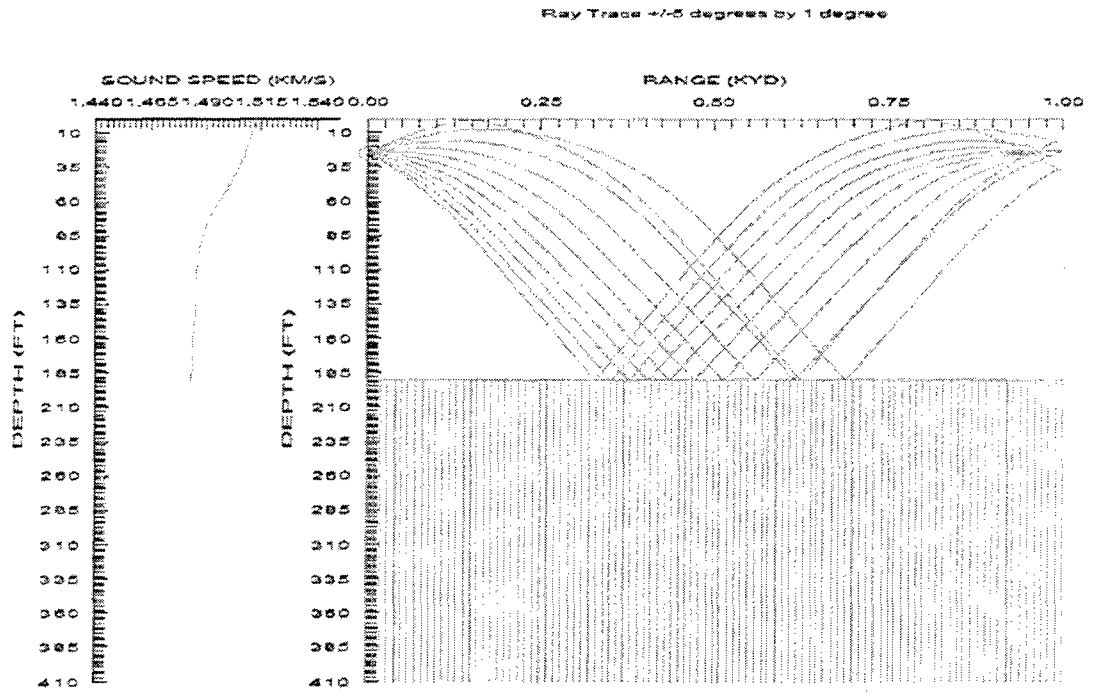

a.

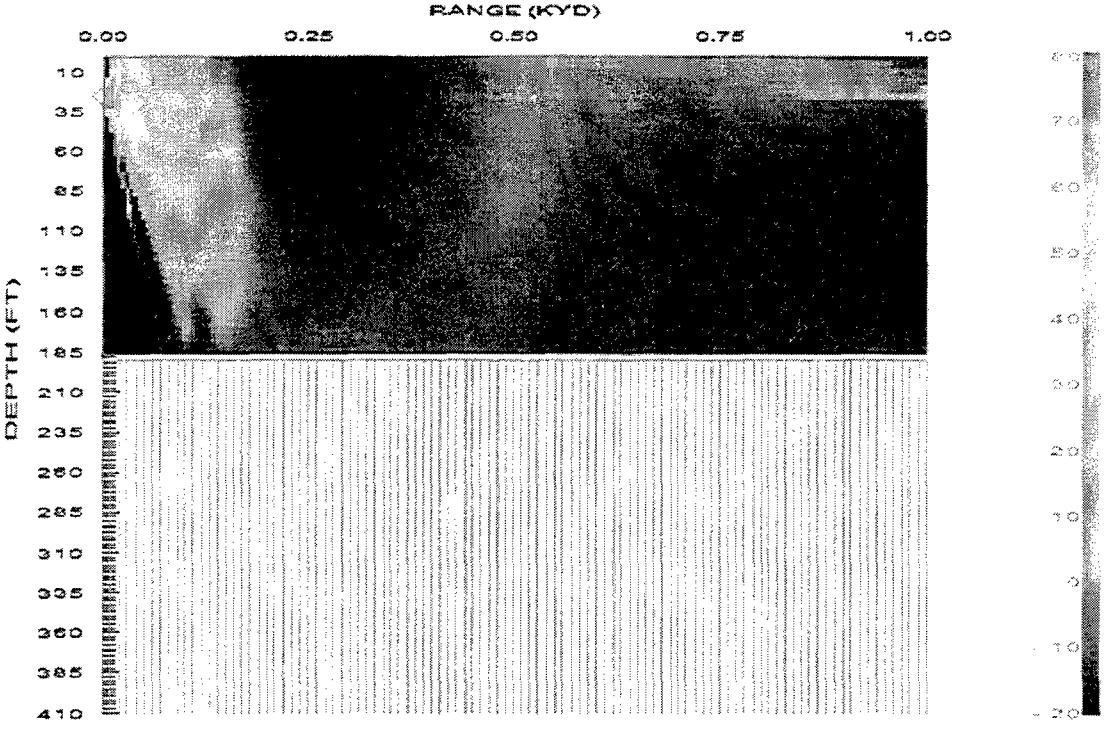

b.

Figure 26. June GDEM for a Sand Bottom at 36.0 N 125.5E and a Source Depth = 25 ft. a. Ray Trace and b. Signal Excess Contour.

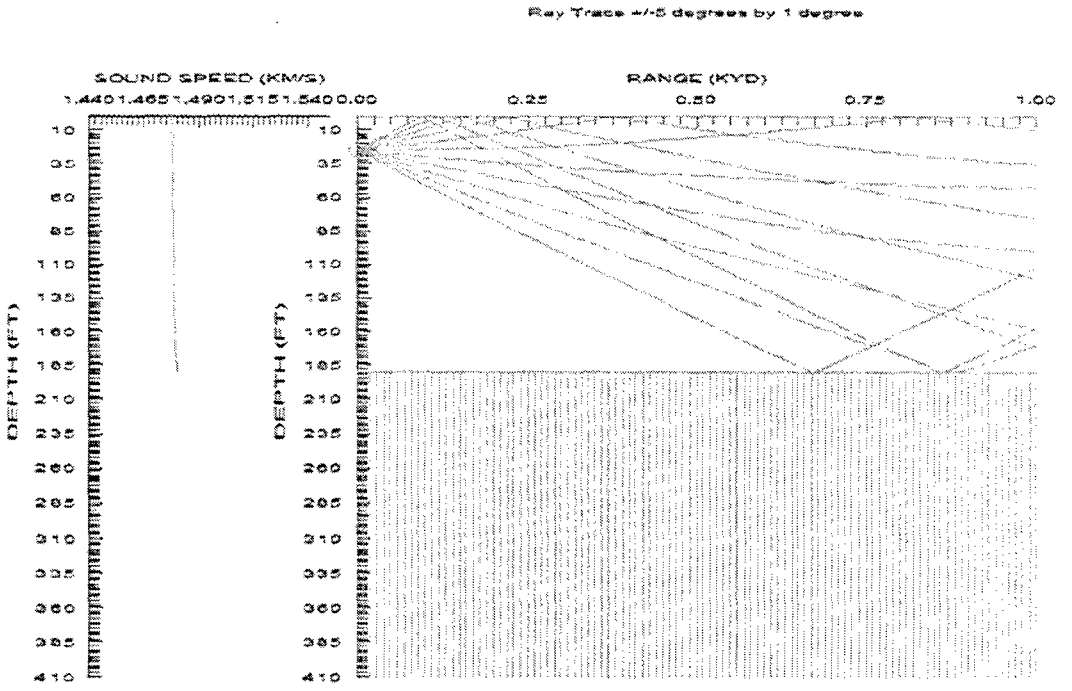

a.

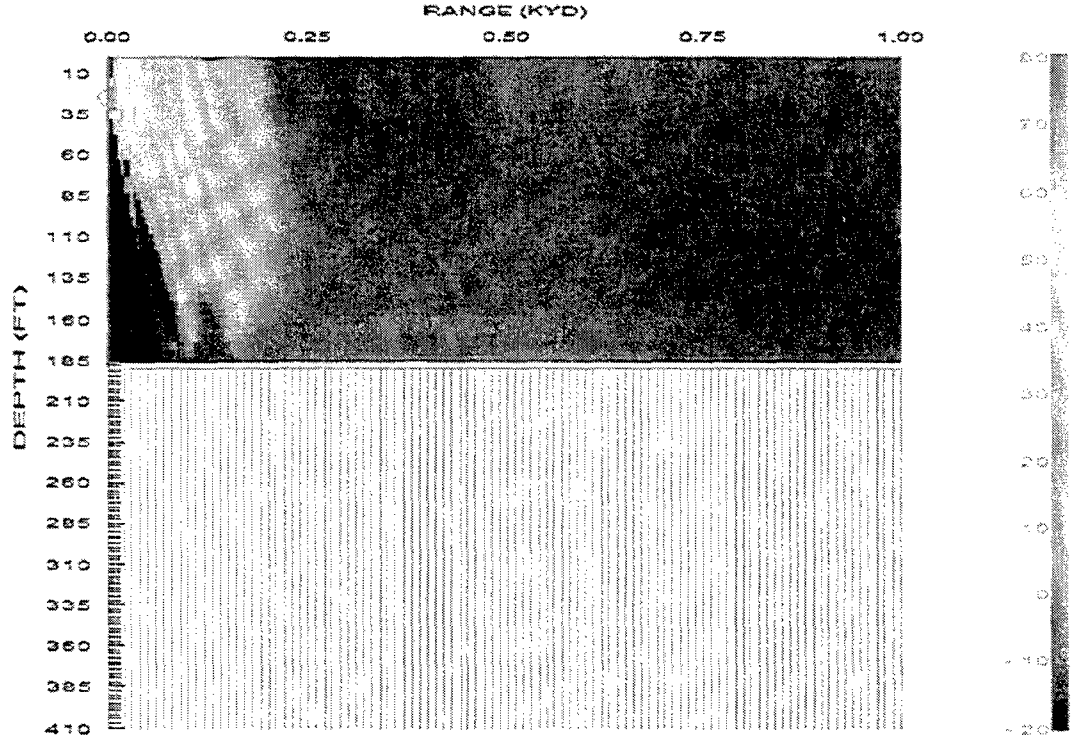

b.

Figure 27. January GDEM for a Sand Bottom at 36.0 N 125.5E and a Source Depth = 25 ft. a. Ray Trace and b. Signal Excess Contour.

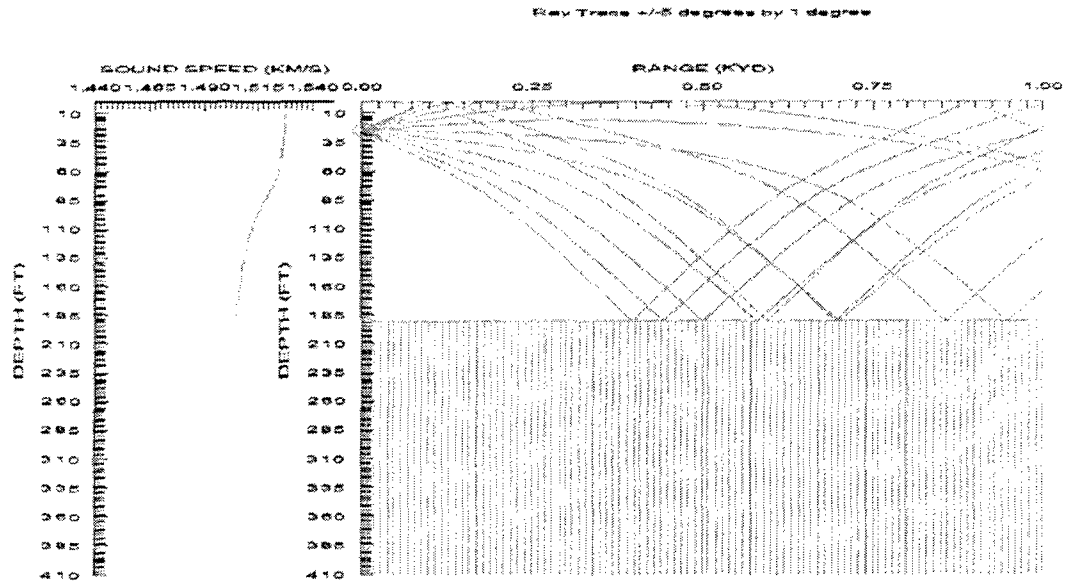

a.

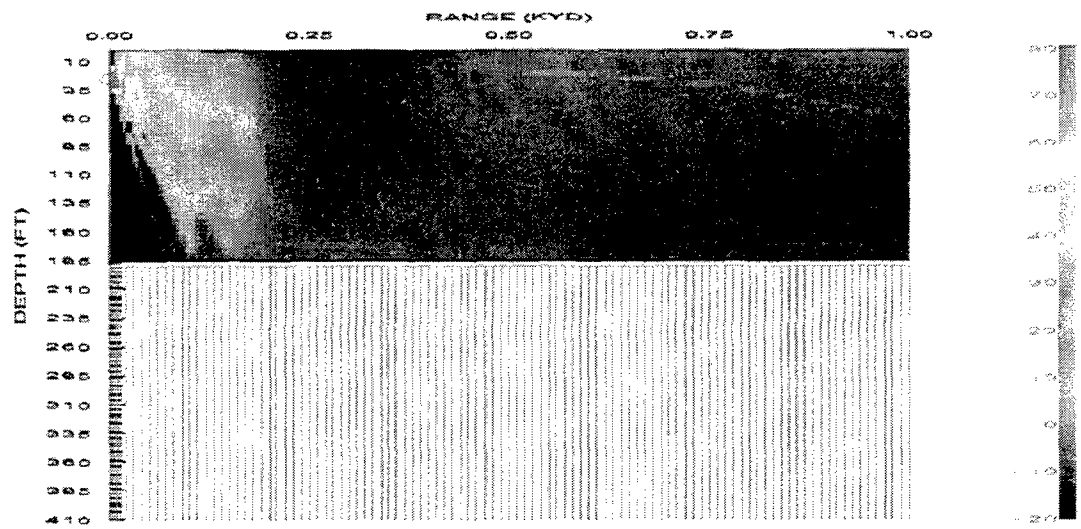

b.

Figure 28. September GDEM for a Sand Bottom at 36.0 N 125.5E and a Source Depth = 25 ft. a. Ray Trace and b. Signal Excess Contour.

The maximum detection ranges for a target at 26 feet and a source depth of 125 feet were over 1000 yards for the month of May, approximately 450 yards for June and July, and no detection for the remaining months. The large detection ranges in these cases can be contributed to the large thermocline gradient, which in turns creates caustics from down bending of sound speed propagation. The maximum detection ranges for a target at the bottom and a source depth of 125 feet were 800 yards for the month of January, approximately 450 yards for February through May and September through November, over 1000 yards for June, approximately 650 yards for July, and approximately 900 yards for August and December (Figures 29-32). The large detection ranges for a Bottom mine in January and December were due to near bottom positive gradient that caused up bending of sound propagation that just grazes the bottom thus reducing bottom reverberation and increasing detection range. The large detection ranges for June, July, and August can be attributed to the effects of a large thermocline gradient.

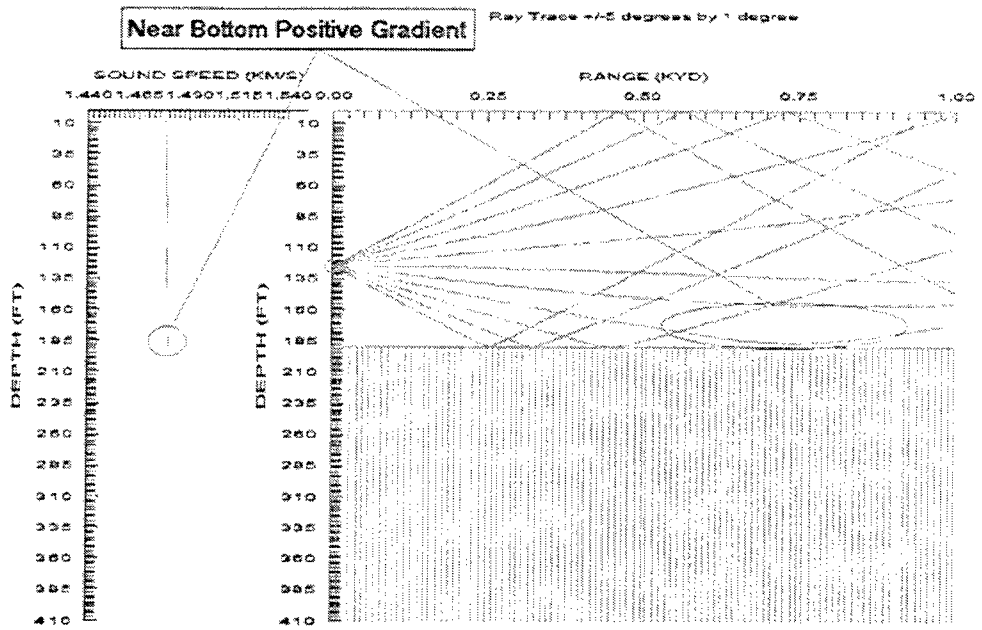

a.

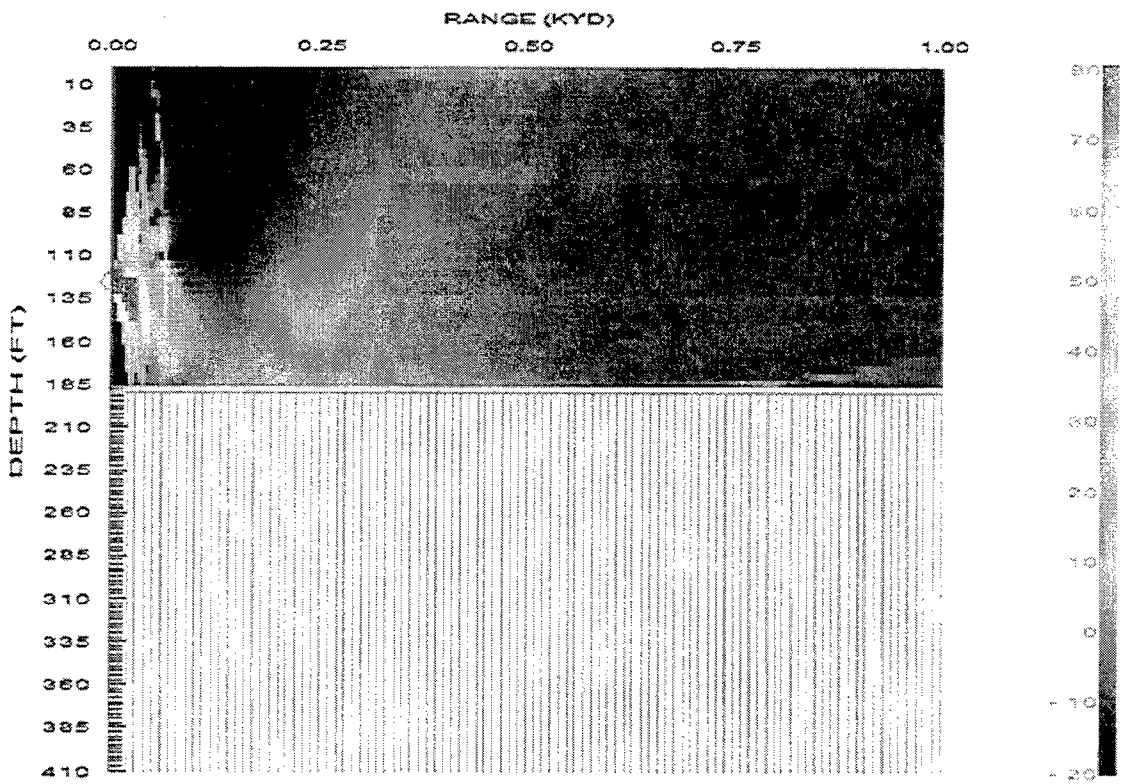

b.

Figure 29. January GDEM for a Sand Bottom at 36.0 N 125.5E and a Source Depth = 125 ft. a. Ray Trace and b. Signal Excess Contour.

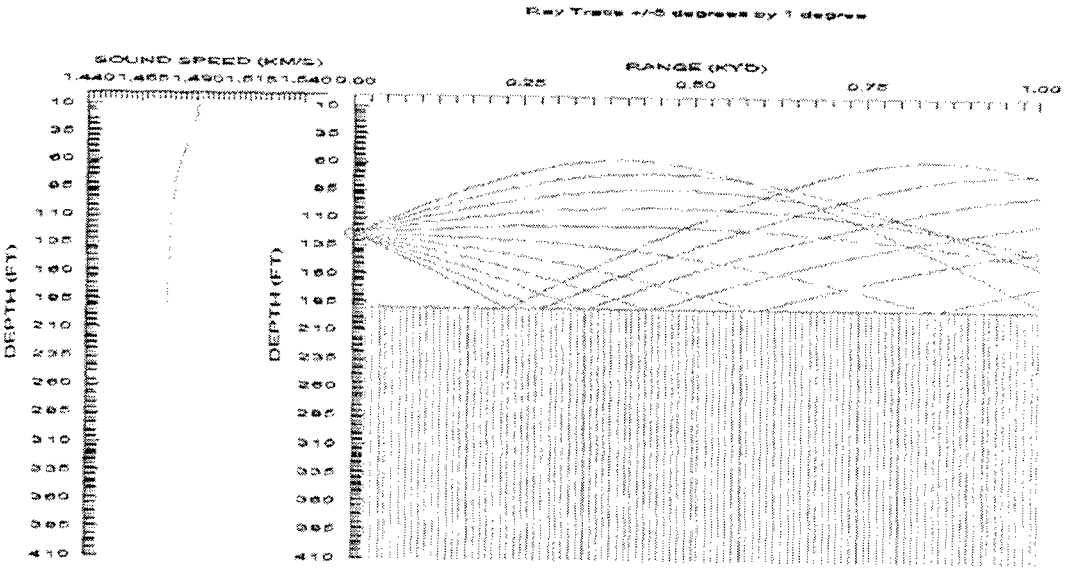

a.

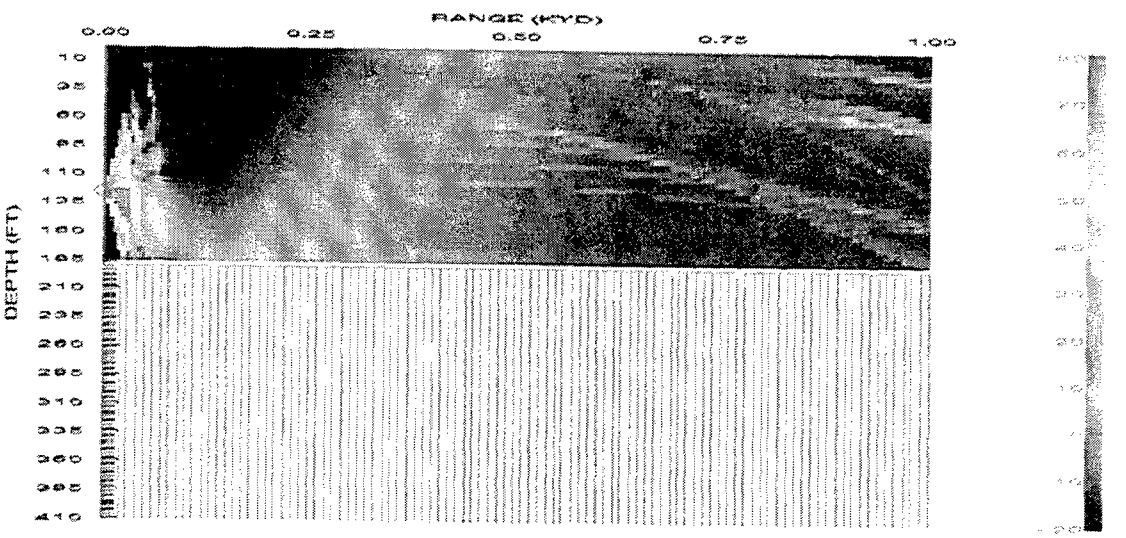

b.

Figure 30. May GDEM for a Sand Bottom at 36.0 N 125.5E and a Source Depth = 125 ft. a. Ray Trace and b. Signal Excess Contour.

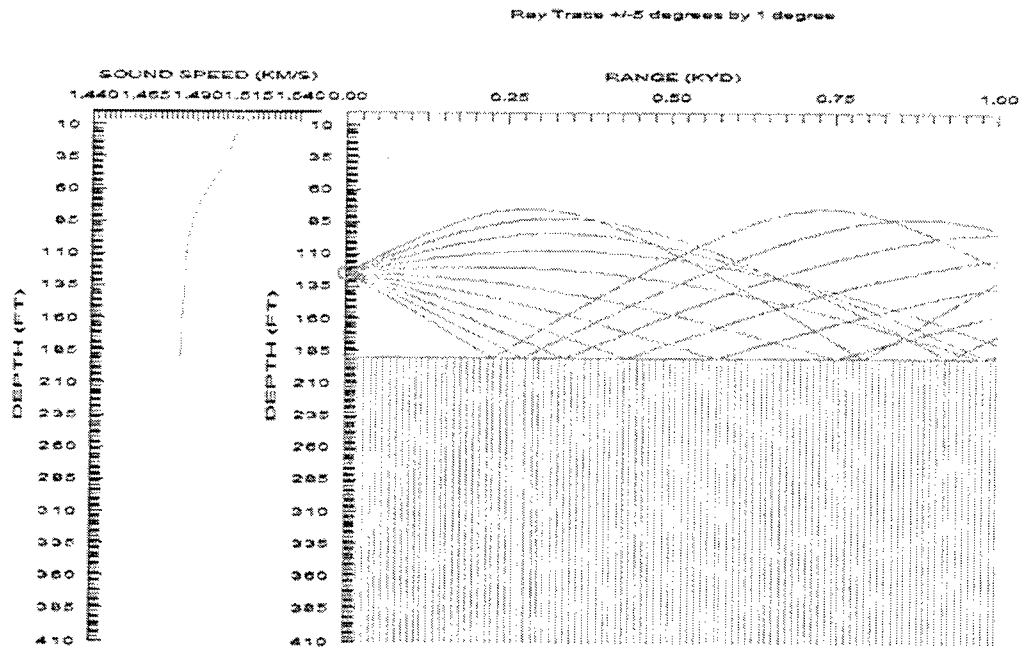

a.

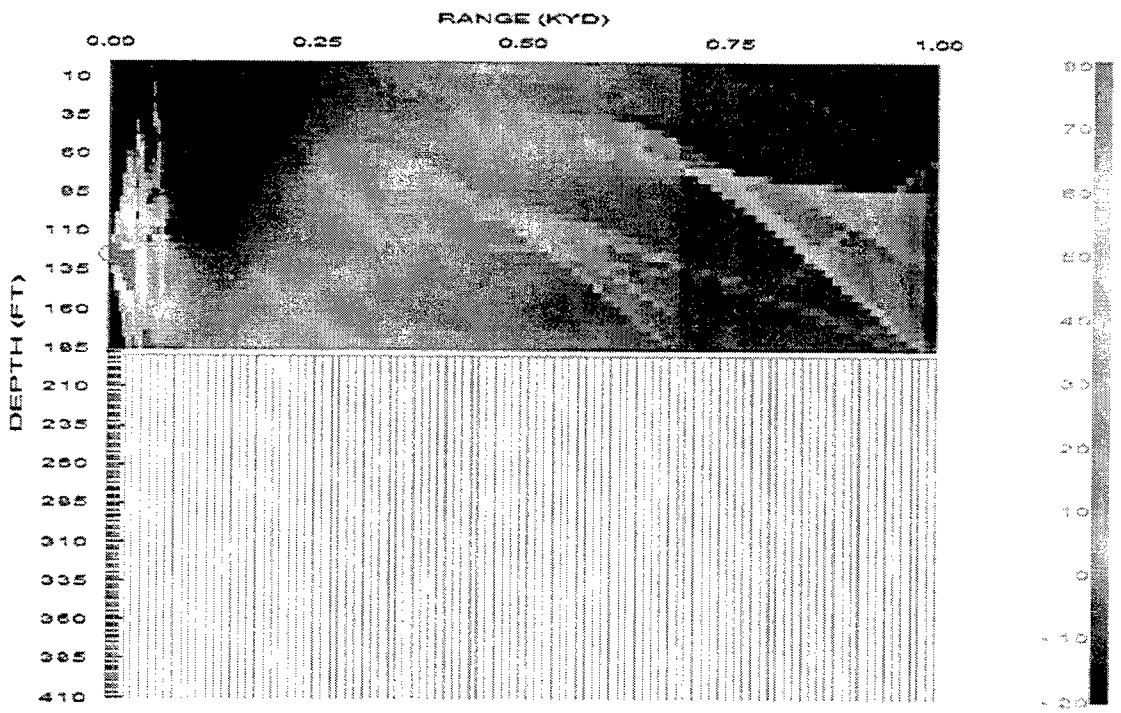

b.

Figure 31. June GDEM for a Sand Bottom at 36.0 N 125.5E and a Source Depth = 125 ft. a. Ray Trace and b. Signal Excess Contour.

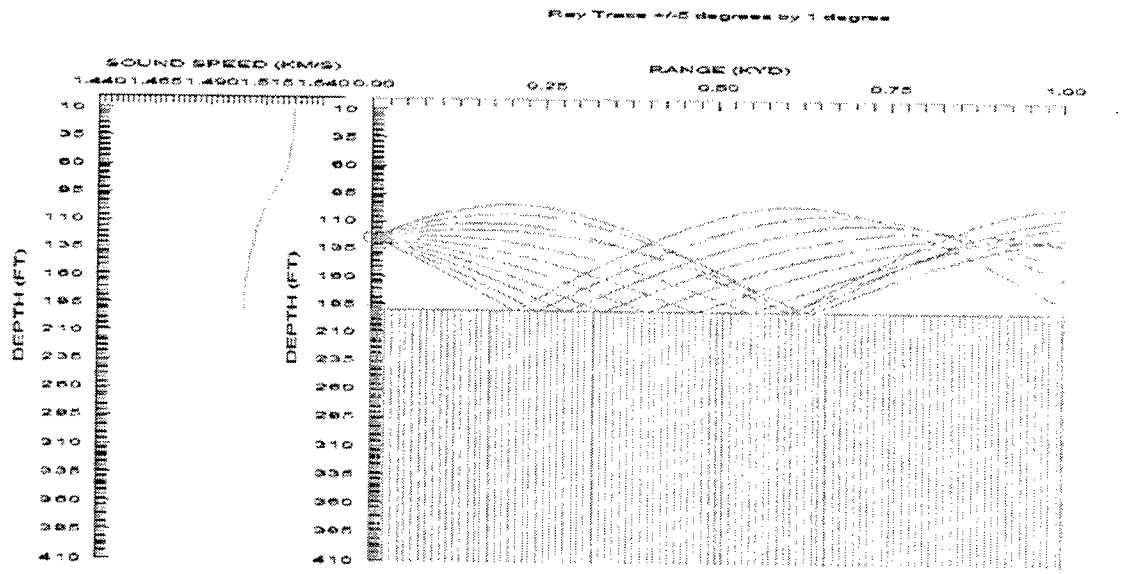

a.

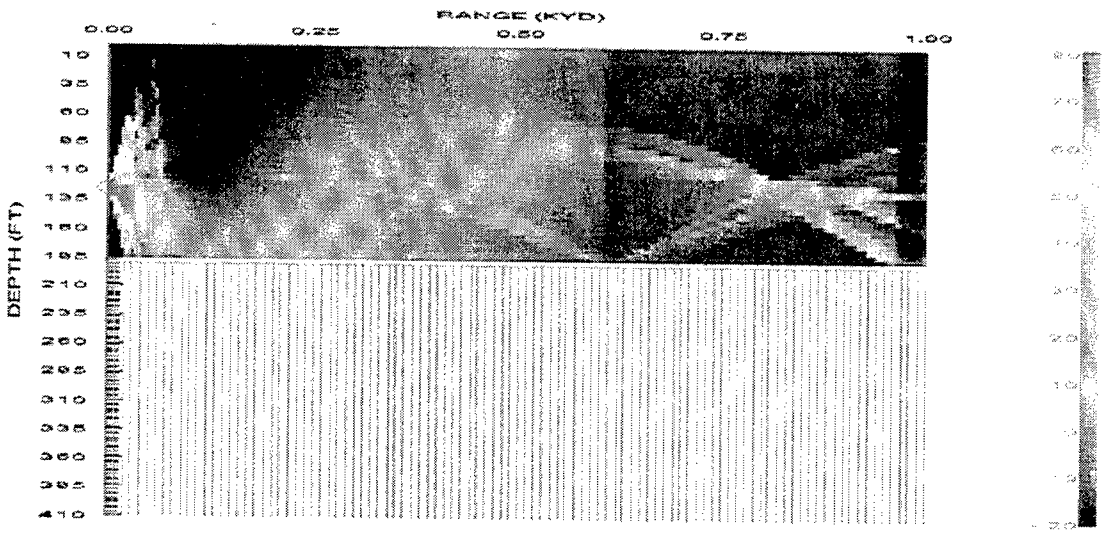

b.

Figure 32. September GDEM for a Sand Bottom at 36.0 N 125.5E and a Source Depth = 125 ft. a. Ray Trace and b. Signal Excess Contour.

The maximum detection ranges for Region 4 were also much larger overall than the first and second regions (Figure 33). The maximum detection ranges for a target at 26 feet and a source depth of 25 feet were approximately 200-225 yards for the months of January through July, September, and October, 900 yards for August, and over 1000 yards for November. The increase in Detection range was due to the caustic produced by a strong thermocline gradient. The increase in Detection range in November was produced by a Surface duct. The maximum detection range for a Bottom mine with a source depth of 25 feet was over 1000 yards for March and no detection for all other months (Figure 34-36). The increase in Detection range in March was due to a positive gradient throughout the entire sound speed profile. This produced up bending, which caused sound speed propagation to just graze the bottom, which in turn decreased bottom reverberation and increased the Detection range of Bottom mines. The months of January, February, and April also had positive gradients, but they were not strong enough to limit bottom reverberation.

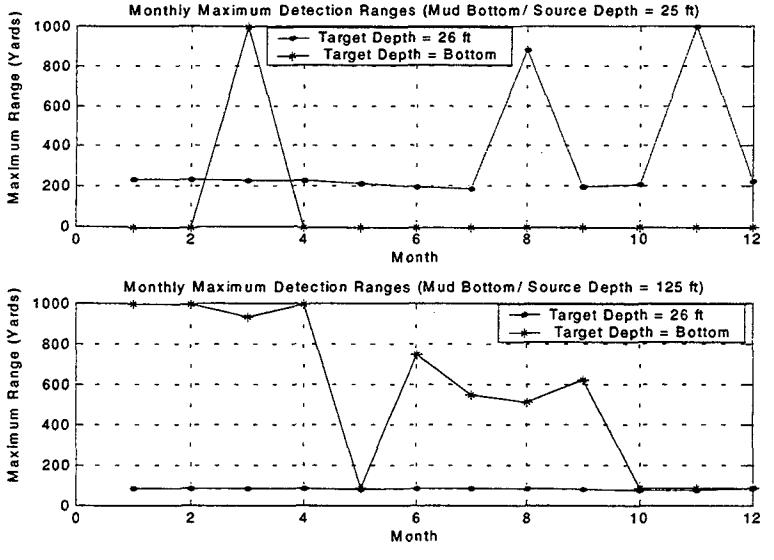

Figure 33. Monthly maximum detection ranges for a Mud Bottom at two source depths and target depths.

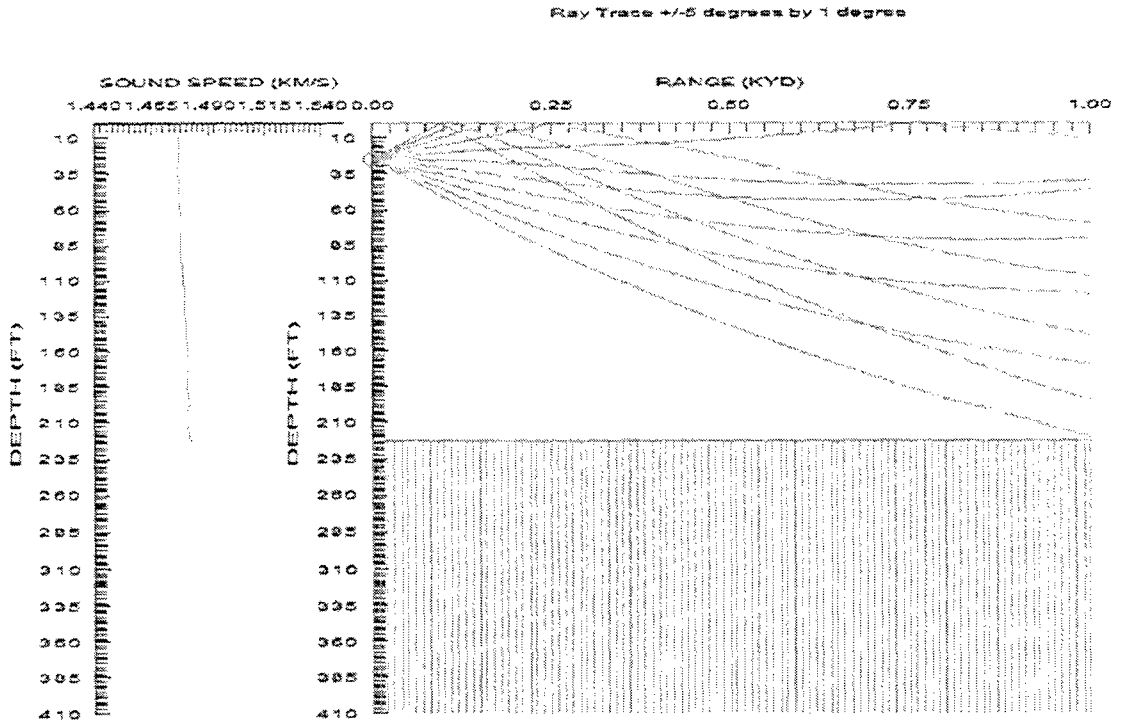

a.

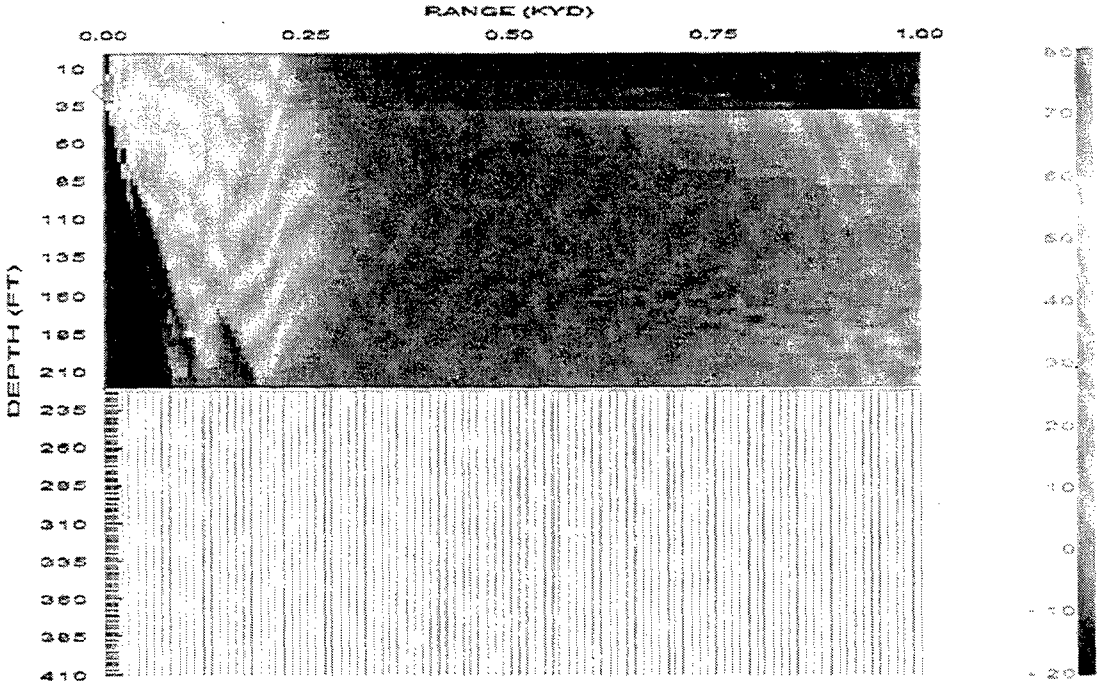

b.

Figure 34. March GDEM for a Mud Bottom at 35.5 N 123.0E and a Source Depth = 25 ft. a. Ray Trace and b. Signal Excess Contour.

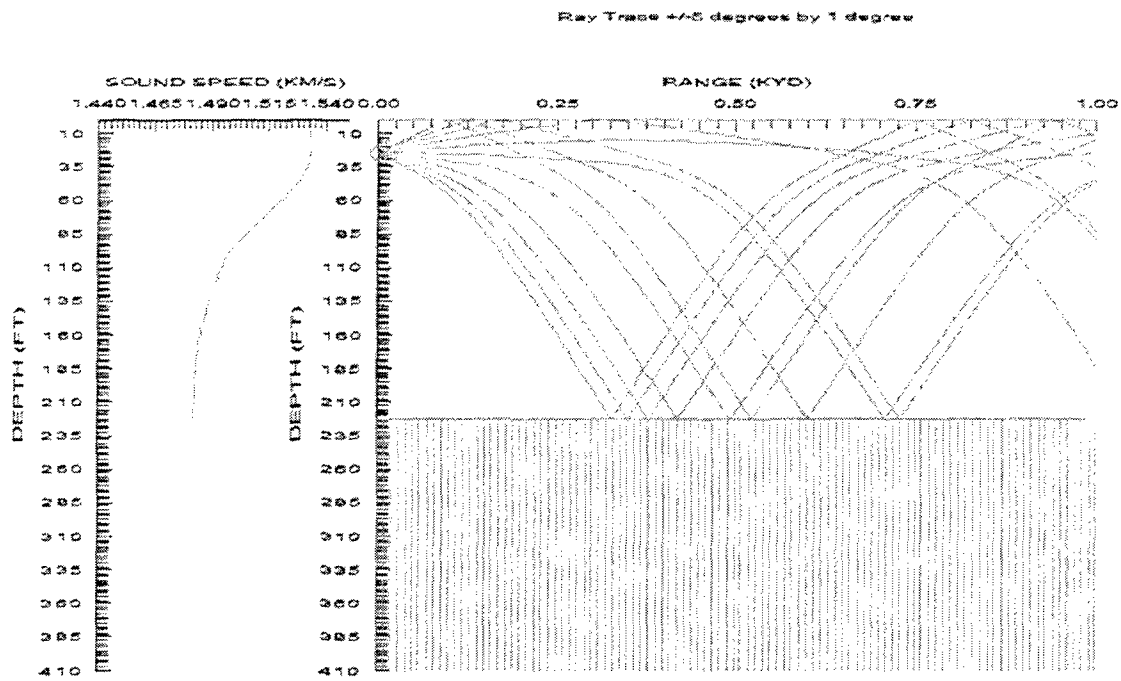

a.

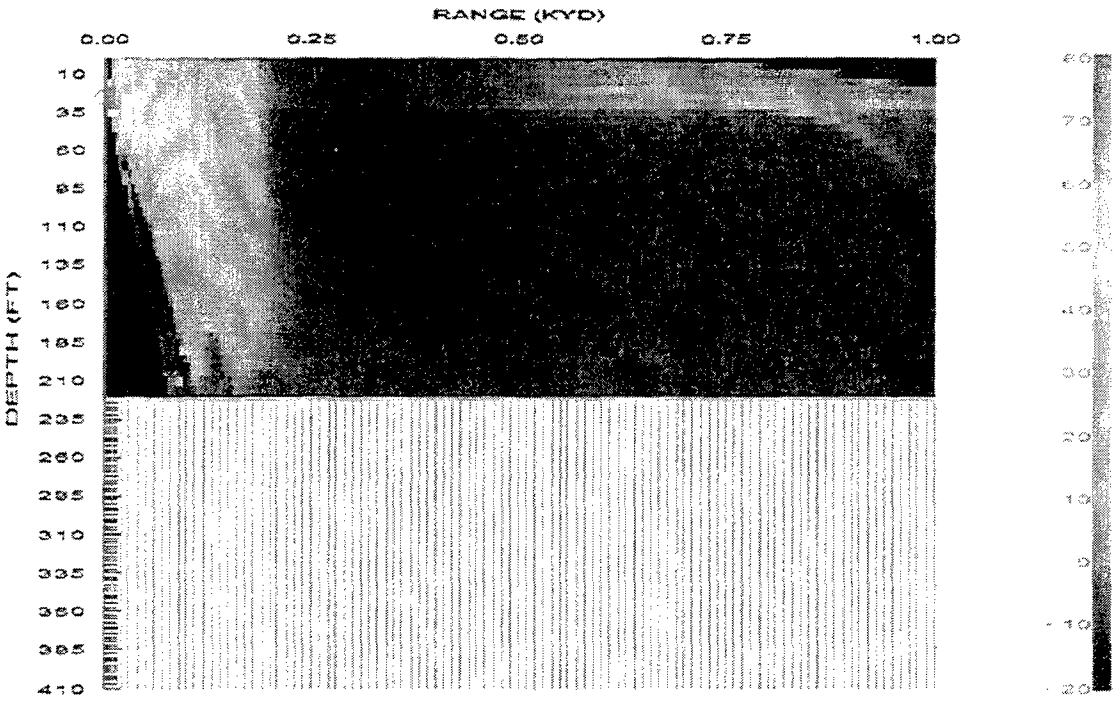

b.

Figure 35. August GDEM for a Mud Bottom at 35.5 N 123.0E and a Source Depth = 25 ft. a. Ray Trace and b. Signal Excess Contour.

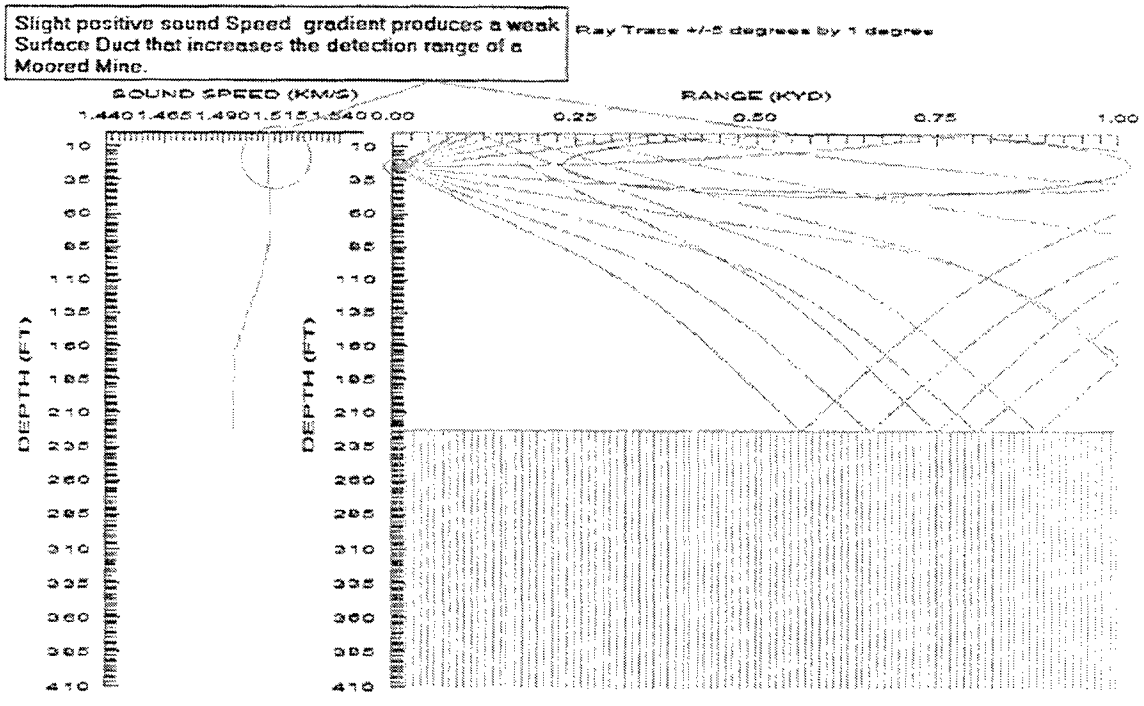

a.

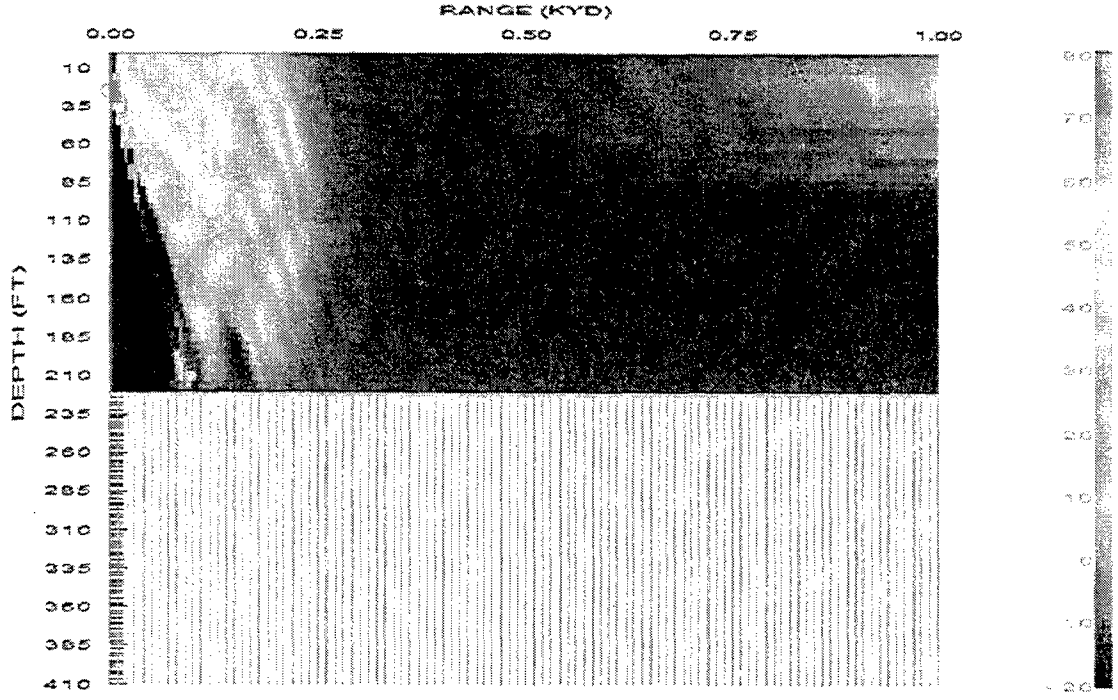

b.

Figure 36. November GDEM for a Mud Bottom at 35.5 N 123.0E and a Source Depth = 25 ft. a. Ray Trace and b. Signal Excess Contour.

The maximum detection ranges for a target at 26 feet and a source depth of 125 feet was approximately 100 yards for each month. The maximum detection ranges for a Bottom mine and a source depth of 125 feet ranged from 925 yards to over 1000 yards for the months of January through April. Detection ranges were approximately 100 yards for May, October, November, and December, and were between 550 to 750 yards for June through September (Figure 37 and 38). The increased detection ranges for the months of January through April were due to a positive gradient that was present in the structure of their sound speed profiles, which caused up bending of the sound speed propagation, resulting in a decrease in bottom reverberation, which in turn increased the detection ranges of Bottom mines. The increased detection ranges for June through September were due to effects of a strong thermocline gradient.

In this study, the seasonal variation in acoustic transmission in the Yellow Sea for all regions was mainly due to the isothermal sound speed structure of the fall and winter months and the multi-layer sound speed structure of the spring and summer months. Another factor in the variation was the presence of a surface duct in some of the profiles during the fall months. The positive near bottom gradient found in some of the profiles during the winter months may be due more to an error in the GDEM climatology than a seasonal factor. The error may be due to a lack of historical observational data in the region.

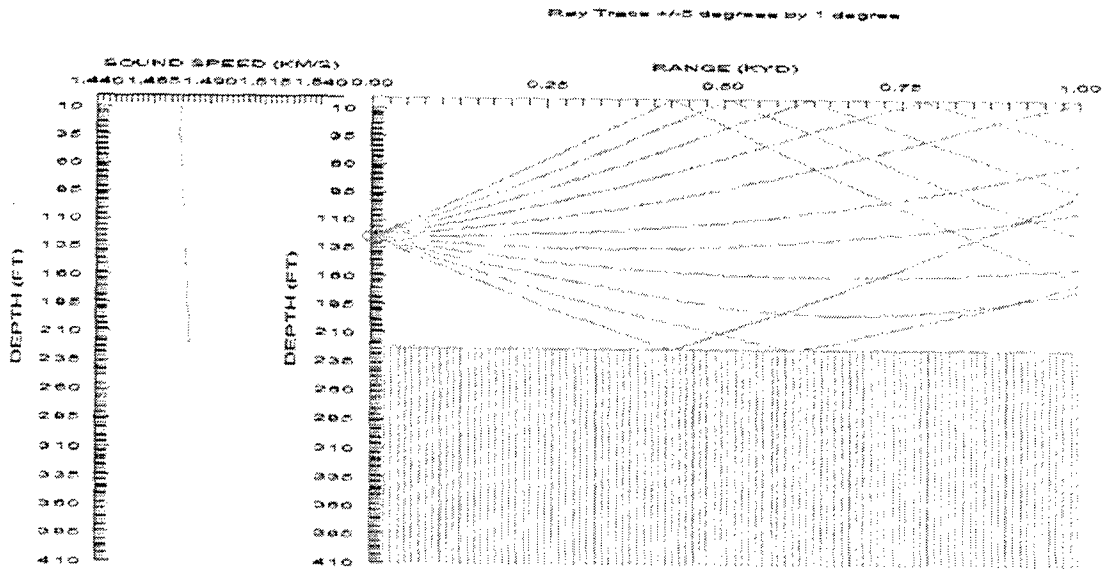

a.

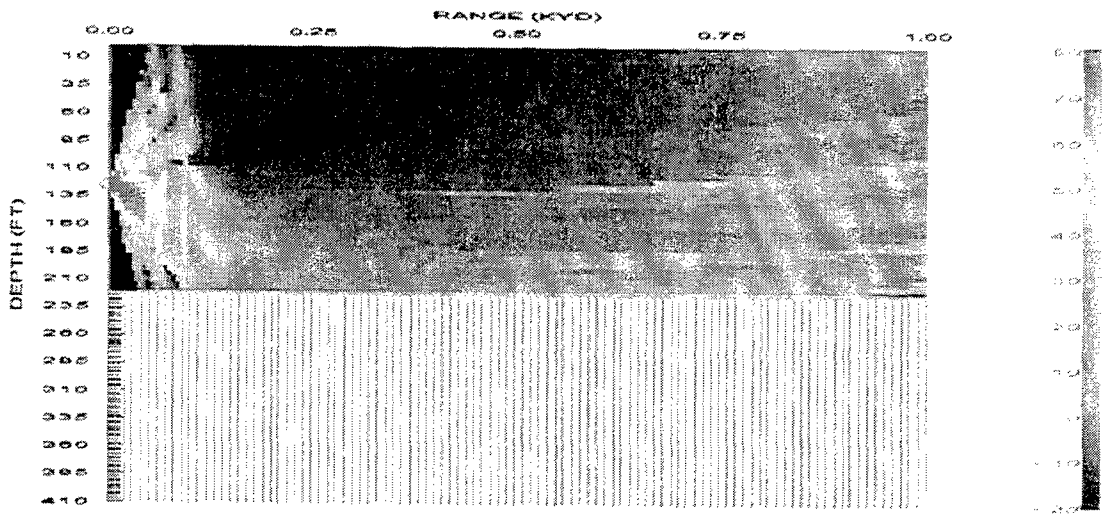

b.

Figure 37. March GDEM for a Mud Bottom at 35.5 N 123.0E and a Source Depth = 125 ft. a. Ray Trace and b. Signal Excess Contour.

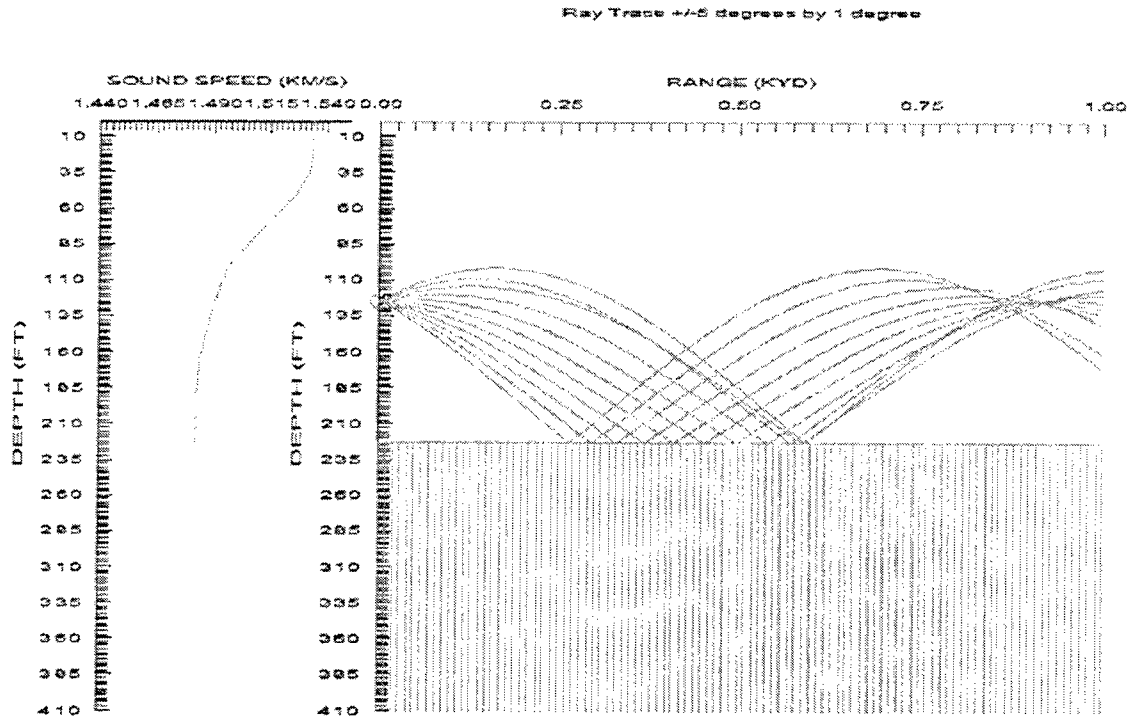

a.

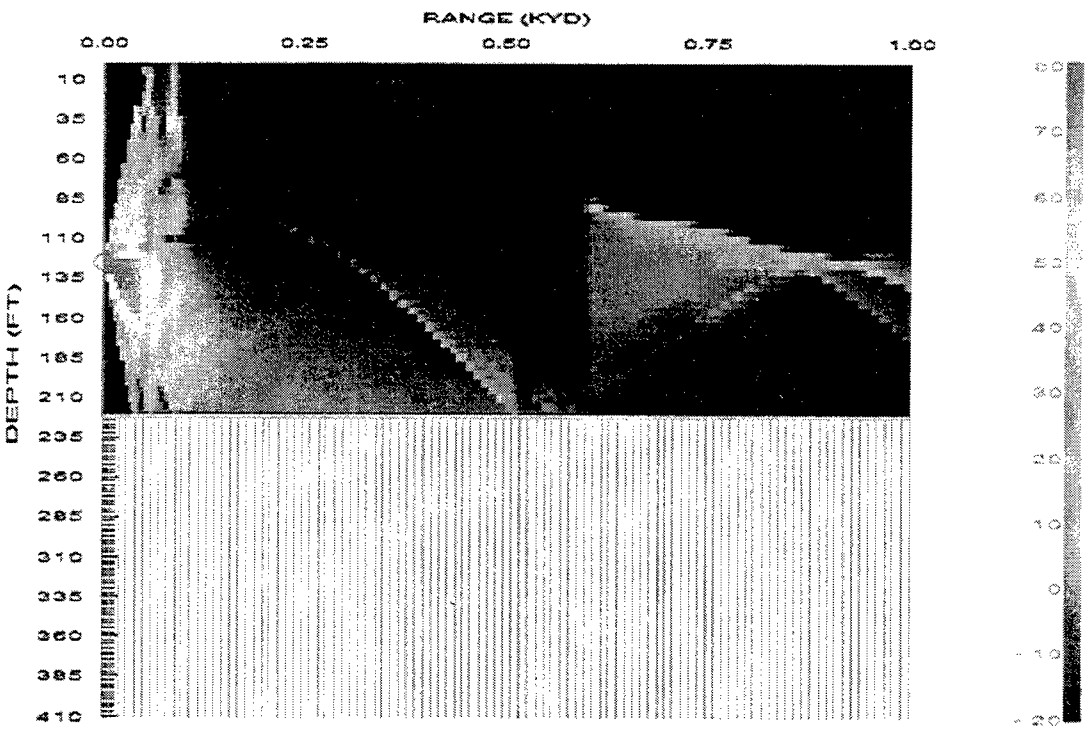

b.

Figure 38. August GDEM for a Mud Bottom at 35.5 N 123.0E and a Source Depth = 125 ft. a. Ray Trace and b. Signal Excess Contour.

THIS PAGE INTENTIONALLY LEFT BLANK

VII. ACOUSTIC TRANSMISSION UNDER SEVERE WEATHER EVENTS

A. EFFECTS ON ACOUSTIC TRANSMISSION BY A TROPICAL DEPRESSION

In this part of the study, the ability of the MODAS model to capture the environmental effects on acoustic transmission of a severe weather event transiting through the Yellow Sea was studied. The severe weather event was chosen from the 1999 and 2000 archives of the Naval Research Laboratory (NRL) Monterey Marine Meteorology Division (Code 7500) Tropical Cyclone Web Page. The tropical depression Kai-Tak (July 10 and 11, 2000) was chosen for this study because its track had the best coverage of the Yellow Sea of all the weather events in the NRL 1999 and 2000 archive (Figures 39 and 40).

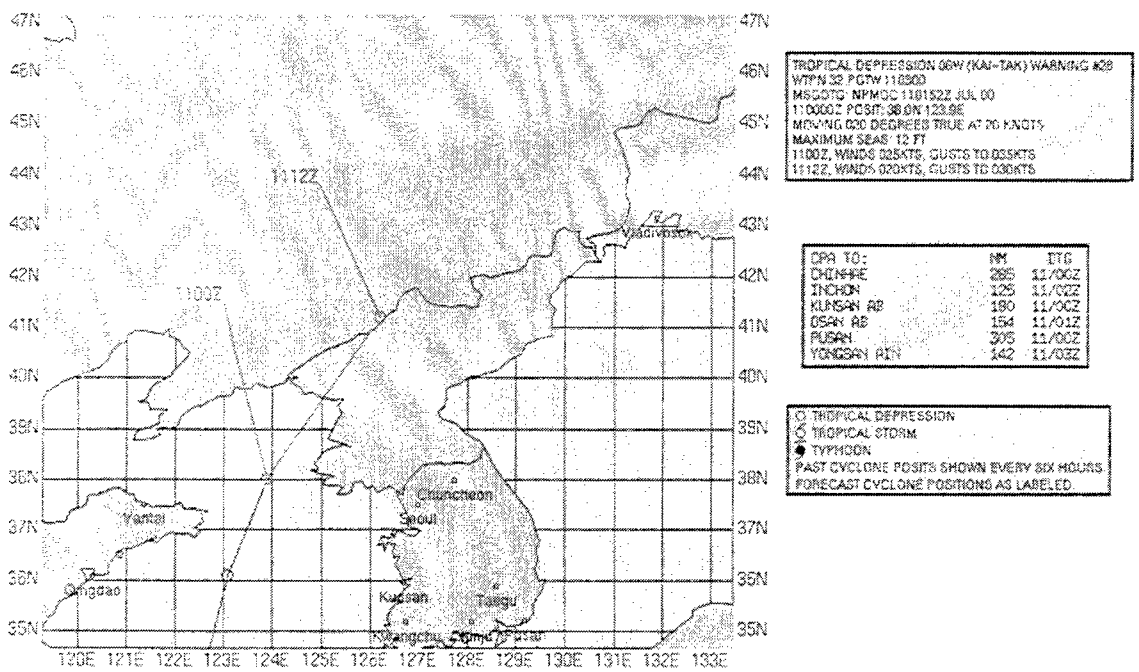

Figure 39. Track of Tropical Depression Kai-Tak over the Yellow Sea for 10-11 July 2000 (From Naval Research Laboratory 2000).

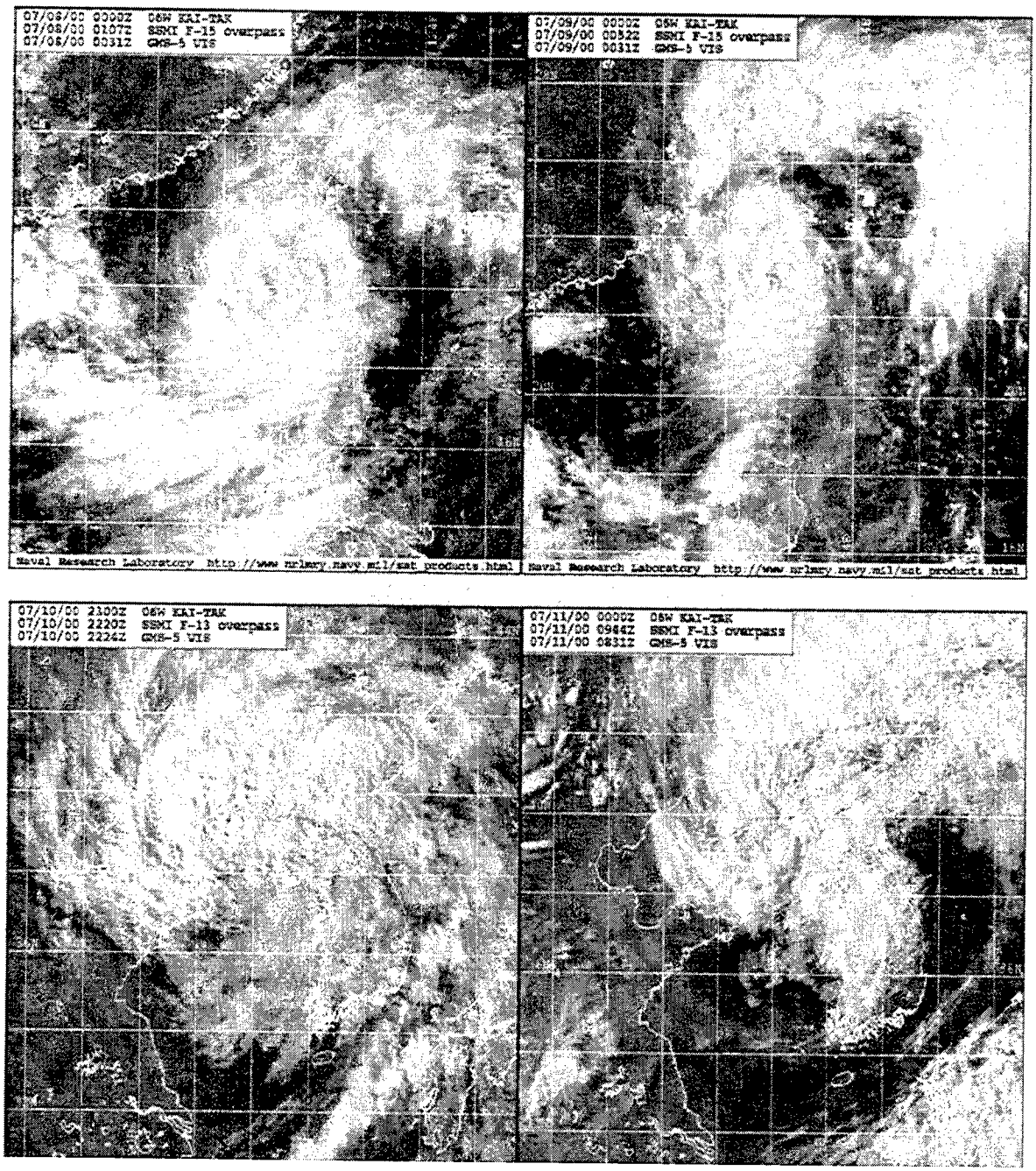

Figure 40. Satellite Images of Tropical Depression Kai-Tak for July 8-11, 2000 respectively (From Naval Research Laboratory 2000).

NIDAS was used to visually analyze the MODAS temperature, salinity, and sound speed profiles before, during, and after (July 1-15, 2000) the transit of the tropical depression through the Yellow Sea. The temperature and sound speed fields when viewed in NIDAS demonstrated very little or no differences between the days being analyzed. Since mud and sand bottom regions were the least limited by bottom reverberation, they were chosen for this part of the study. The mud region was located closet to the center of Kai-Tak track while the sand region was located to the east of the track. Four profiles for each region, for the days of July 7 (prior to event), 10 (during the event), and 15 (after the event), and at source depths of 25 feet and 125 feet were evaluated using the CASS/GRAB model. The differences in sound speed and detection ranges throughout the water column between July 10 minus July 7 and July 15 minus July 10 were plotted to study the distribution of the differences in sound speed and detection ranges (Figures 41 and 42).

The differences in the mud region ranged from 0 to 7.5 m/s for sound speed and 0 to 850 yards for detection range. The greater differences were between July 10 and 15. Location 2 (Lat 35.6 N Lon 124.0 E) and Location 4 (Lat 36.0 N Lon 124.0) were the only two of the four locations that had significant differences in detection ranges at the two target depths being analyzed in this study (26 feet and the bottom). The differences in the sand region ranged from 0 to 7.5 m/s for sound speed, and 0 to 905 yards for detection range. The greater differences again were between July 10 and 15. In the sand region, there were no significant differences in detection ranges for the two target depths at any of the four locations.

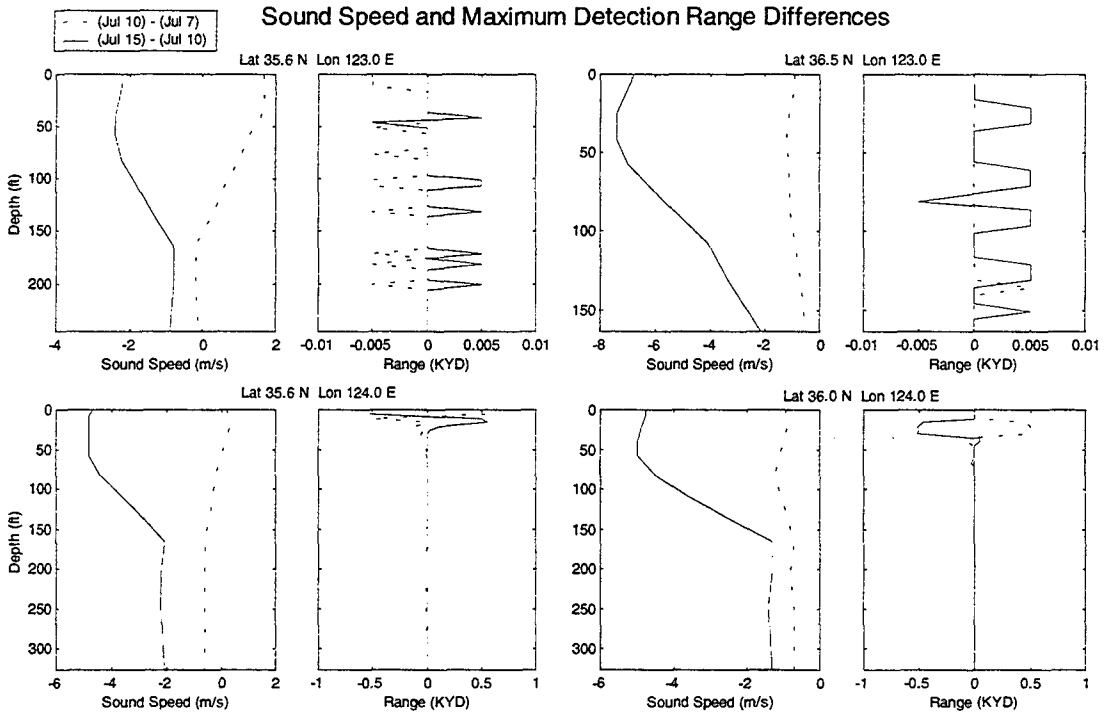

a.

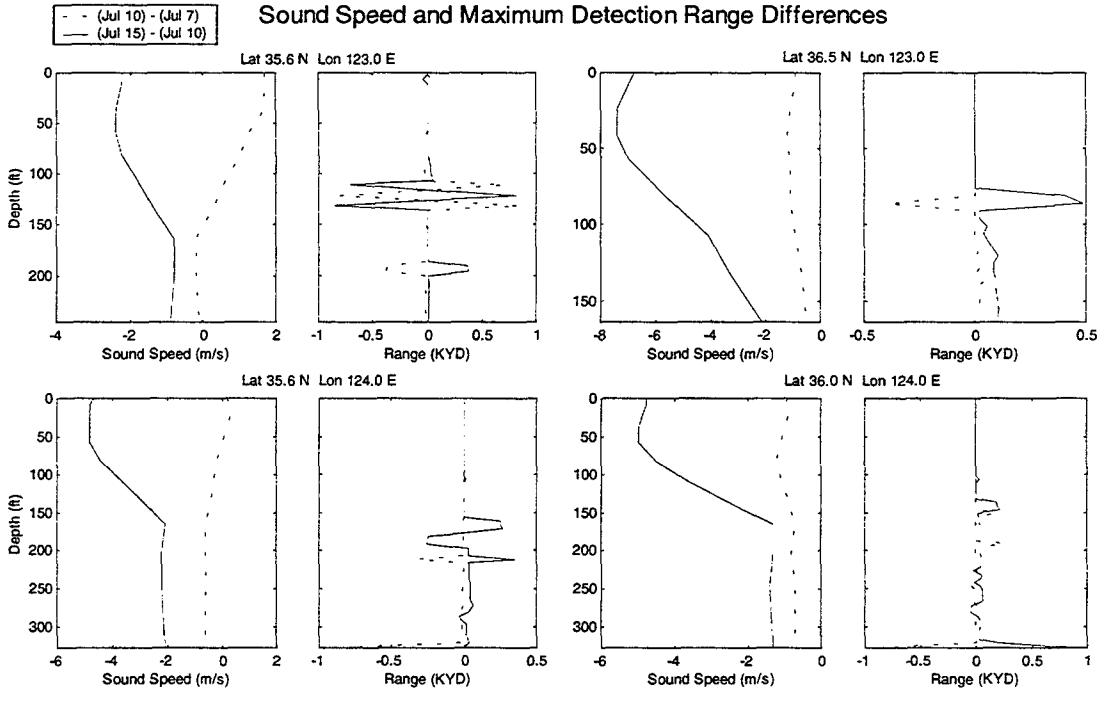

b.

Figure 41. Sound Speed and Maximum Detection Range Differences for July 10 minus July 7 and July 15 minus July 10 for a Mud Bottom region and Source Depths of a. 25 ft and b. 125 ft.

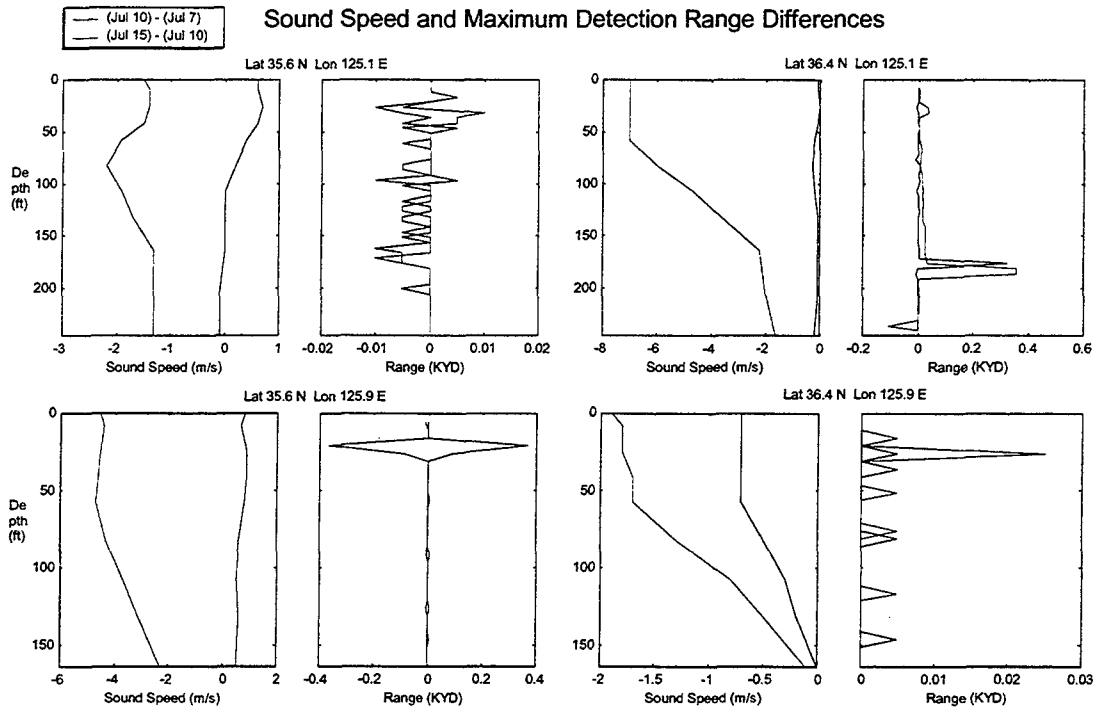

a.

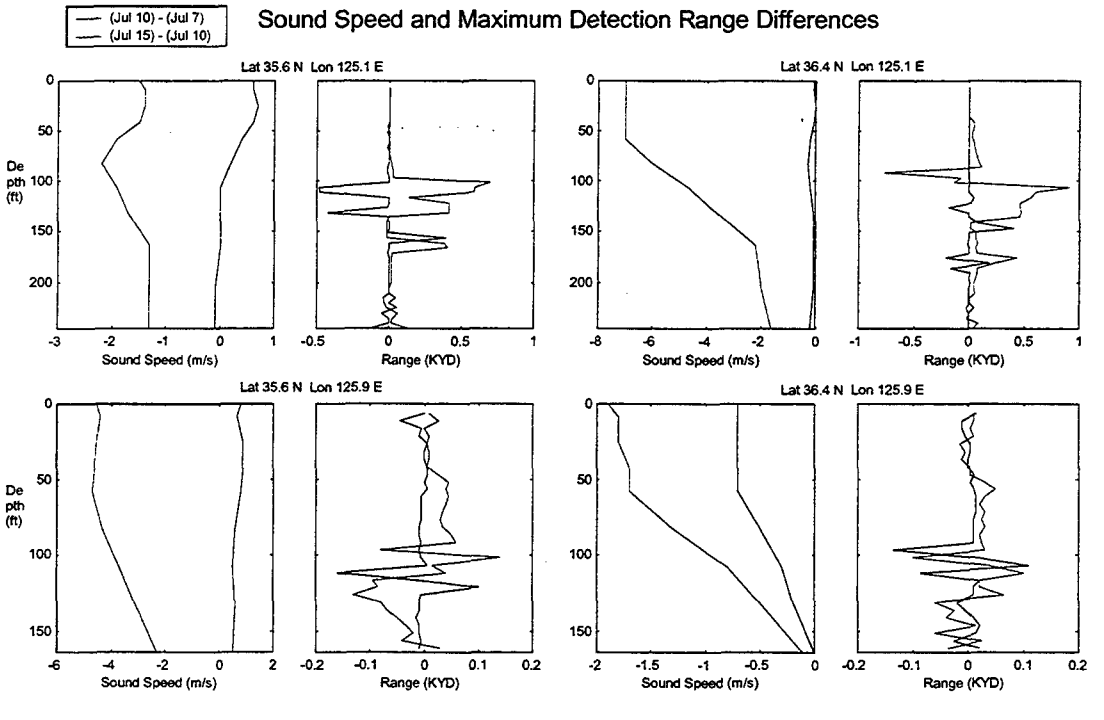

b.

Figure 42. Sound Speed and Maximum Detection Range Differences for July 10 minus July 7 and July 15 minus July 10 for a Sand Bottom region and Source Depths of a. 25 feet and b. 125 feet.

The differences between the detection ranges were analyzed to determine if there were significant acoustic differences between the profiles generated by MODAS for the three days being analyzed. A significant acoustic difference between sound speed profiles as operationally defined by NAVOCEANO is as follows: (1) If both of the detection ranges are less than 600 yards form the source and if the difference between the detection ranges is greater than 100 yards, there exists a significant acoustic difference between the two profiles, and (2) If either of the detection ranges is greater than 600 yards from the source, and if the difference between the detection ranges is greater than 200 yards, there exists a significant difference between the two profiles (Table 2).

The only significant acoustic difference observed for a source depth of 25 feet and target depth of 26 feet was at Location 4 of the mud region (Figure 43 and 44). The difference in detection ranges was 490 yards for both July 10, 2000 minus July 7, 2000, and July 10, 2000 minus July 15, 2000. The difference can be attributed to a slightly negative gradient in the mixed layer on July 10 that was not present on July 7 or July 15. This negative gradient produced stronger down bending of the sound propagation, which in turn increased the focusing of sound propagation at convergence zones. The slightly negative gradient in the mixed layer may due to the effect of the weather event and the stabilizing of the mixed layer afterwards on July 15 as the effects of the weather event weakened (Figure 45 and 46). There were no significant acoustic differences for a source depth of 25 feet and a target at the bottom for either of the regions.

There were no significant acoustic differences for a source depth of 125 feet and a target depth of 26 feet for either of the regions. The only significant acoustic difference observed for a source depth of 125 feet and a target at the bottom was at Location 4 of the

mud region (Figure 47 and 48). The significant acoustic differences in this case were 790 yards for July 10 minus July 7, and –810 yards for July 10 minus July 15. Thus, there was a decrease in detection range during the weather event. The decrease can be attributed to the slightly stronger gradient of thermocline on July 10 that causes stronger down bending, which shifts the shadow zone closer to the source thus decreasing the detection range of a bottom target.

Figures 45 and 46 were created to analyze in more detail, the effects of the tropical depression on SST and sound speed at Location 4 of the mud region. There was only a decrease of 0.4 ° C in the SST between July 7 and July 10; which may have been due to the unavailability of remote SST data due to heavy cloud coverage on July 10. The first significant decrease in SST was observed on July 11 where the SST decreased 1.7 ° C between July 7 and July 10. This may have been due to the availability of remote SST data on July 11. The SST continued to decrease until July 13 to the minimum temperature of 22.0° C, a difference of 2.50° C. Afterwards, the SST began to increase as observed on July 15 due to the weakening effects of the tropical depression in the Yellow Sea. The sound speed profiles also followed this pattern with a maximum difference of 5.2 m/s between July 7 and July 13.

Although the MODAS model captured the effects on the SST temperature by the tropical depression, a significant acoustic difference was only observed in Location 4 of the mud region. As demonstrated for the sand region in Figure 42, overall there were smaller differences in sound speeds and detection ranges as compared to the mud region in Figure 41. This is because the sand region was located further east of the tropical cyclone tracks than the mud region. The MODAS' entire temperature and sound speed

profiles were shifted to the left with a decrease in temperature. Acoustic transmission is not significantly effected by the shifting of the entire profile. The significant changes in acoustic transmission are due to a change in the gradients of the sound speed profiles that may be caused by the change in the mixed layer depth, presence of a surface duct, the gradient of the thermocline, etc. This was the case for the Location 4 in the mud region, where a slight change in the gradient of the mixed layer and the thermocline produced significant acoustic differences between the corresponding profiles. With the cold air mass and strong winds that are characteristic of a tropical depression, there should have been some occurrence of a change in the mixed layer depth and significant changes in the sound speed gradients. Since the MODAS model operates without remote SSH data in shallow water, the model may not be able to capture the effect severe weather has on the upper water column, thus under predicting the effects of severe weather events in a shallow water region.

A SIGNIFICANT ACOUSTIC DIFFERENCE IN DETECTION RANGES AS DEFINED OPERATIONALLY FOR THIS STUDY:	
POSITION OF DETECTION RANGES OF MINE RELATIVE TO SOURCE	**A SIGNIFICANT ACOUSTIC DIFFERENCE EXISTS IF:**
IF BOTH DETECTION RANGES ARE LESS THAN 600 YARDS	**Δ DETECTION RANGES >100 YARDS**
IF EITHER OF THE DETECTION RANGES ARE GREATER THAN OR EQUAL TO 600 YARDS	**Δ DETECTION RANGES >200 YARDS**

Table 2. Significant Acoustic Differences in Detection Ranges as Defined Operationally for this study.

Target Depth	**SOURCE DEPTH = 25 FT.**			
	Mud		**Sand**	
	July 10 – July 7	July 15 – July 10	July 10 – July 7	July 15 – July 10
26 ft	Lat 36.0N Lon 124.0E **490 yd (Figure 43 and 44)**	Lat 36.0N Lon 124.0E **490 yd (Figure 43 and 44)**	None	None
Bottom	None	None	None	None

a.

Target Depth	**SOURCE DEPTH = 125 FT.**			
	Mud		**Sand**	
	July 10 – July 7	July 15 – July 10	July 10 – July 7	July 15 – July 10
26 ft	None	None	None	None
Bottom	Lat 36.0N Lon 124.0E **790 yd (Figure 45 and 46)**	Lat 36.0N Lon 124.0E **810 yd (Figure 45 and 46)**	None	None

b.

Table 3. Maximum Significant Acoustic Differences in Detection Ranges between MODAS Profiles before and after a Tropical Depression for Mud and Sand Bottom regions at a. Source Depth of 25 ft, b. Source Depth of 125 ft.

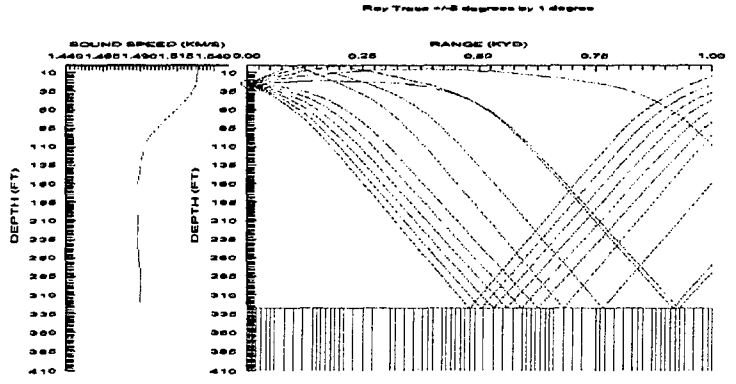

a. Maximum Detection Range for 26 ft Mine Depth = 770 yd

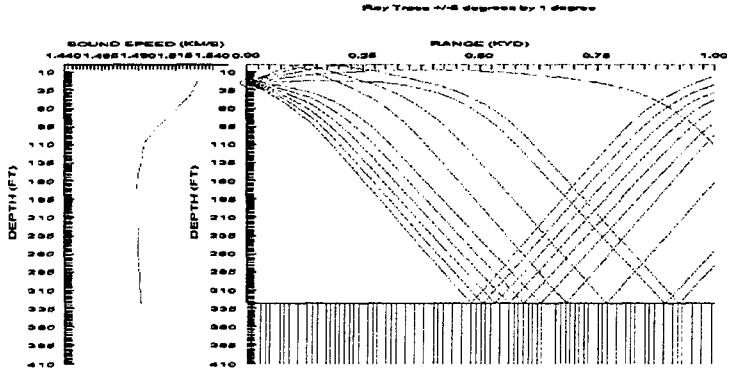

b. Maximum Detection Range (DR) for 26 ft Mine depth = 280 yd, ΔDR = 490 yd

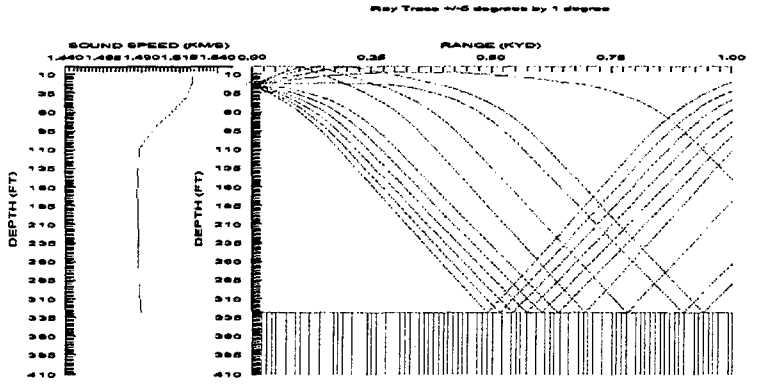

c. Maximum Detection Range (DR) for 26 ft Mine depth = 280 yd, ΔDR = 490 yd

Figure 43. Sound Speed profiles and Ray traces for Mud Bottom at 36.0 N 124.0 E and Source Depth =25 ft for a. July 10, 2000, b. July 7, 2000, c. July 15, 2000.

a. Maximum Detection Range for 26 ft Mine Depth = 770 yd

b. Maximum Detection Range (DR) for 26 ft Mine depth = 280 yd, ΔDR = 490 yd

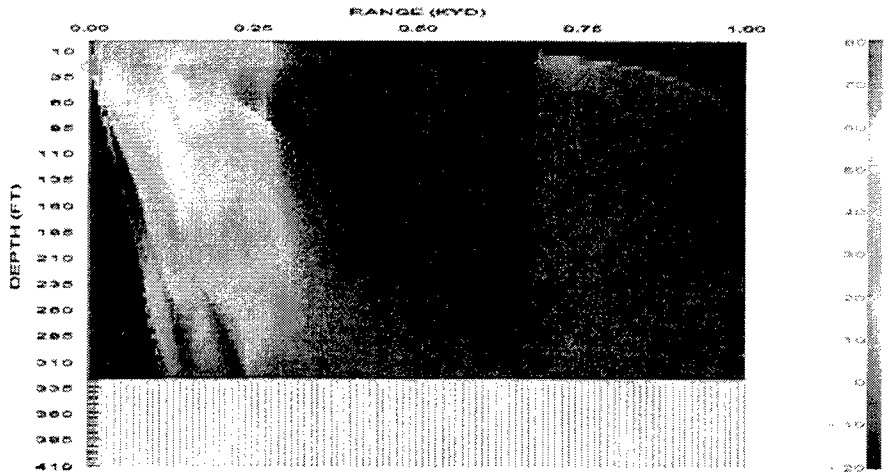

c. Maximum Detection Range (DR) for 26 ft Mine depth = 280 yd, ΔDR = 490 yd

Figure 44. Signal Excess contours for Mud Bottom at 36.0 N 124.0 E and Source Depth = 25 ft for a. July 10, 2000, b. July 7, 2000, c. July 15, 2000.

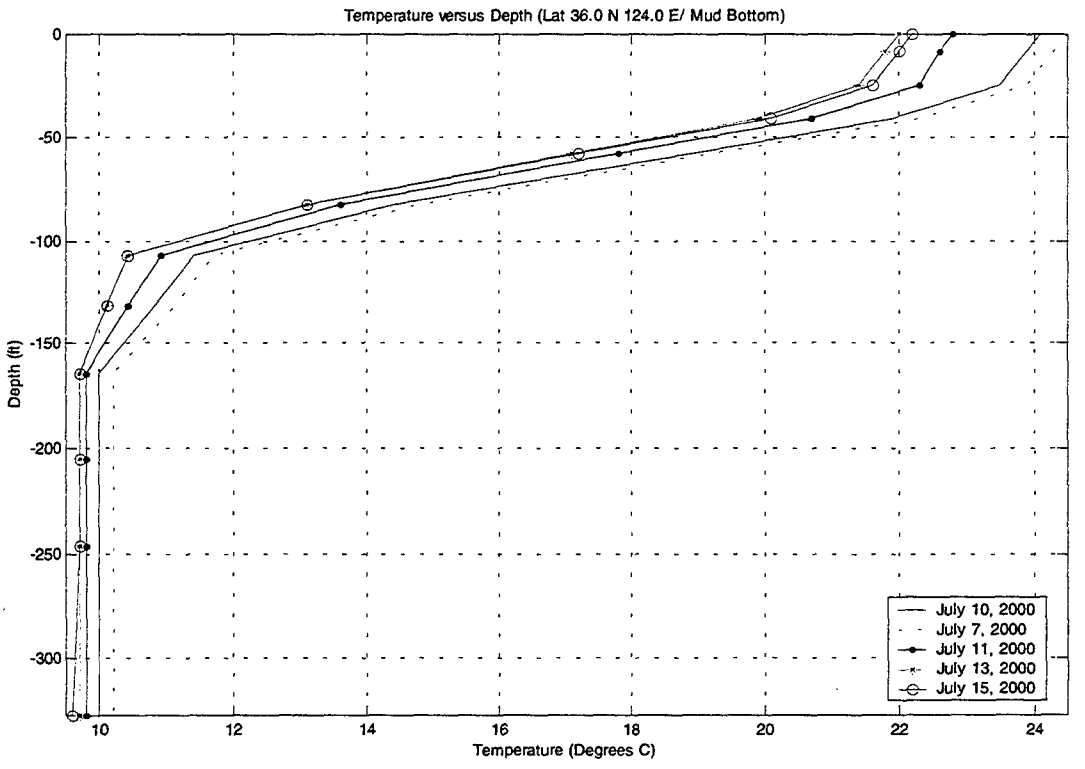

Figure 45. Temperature Profile Comparisons for July 7, 10, 11, 13, and 15.

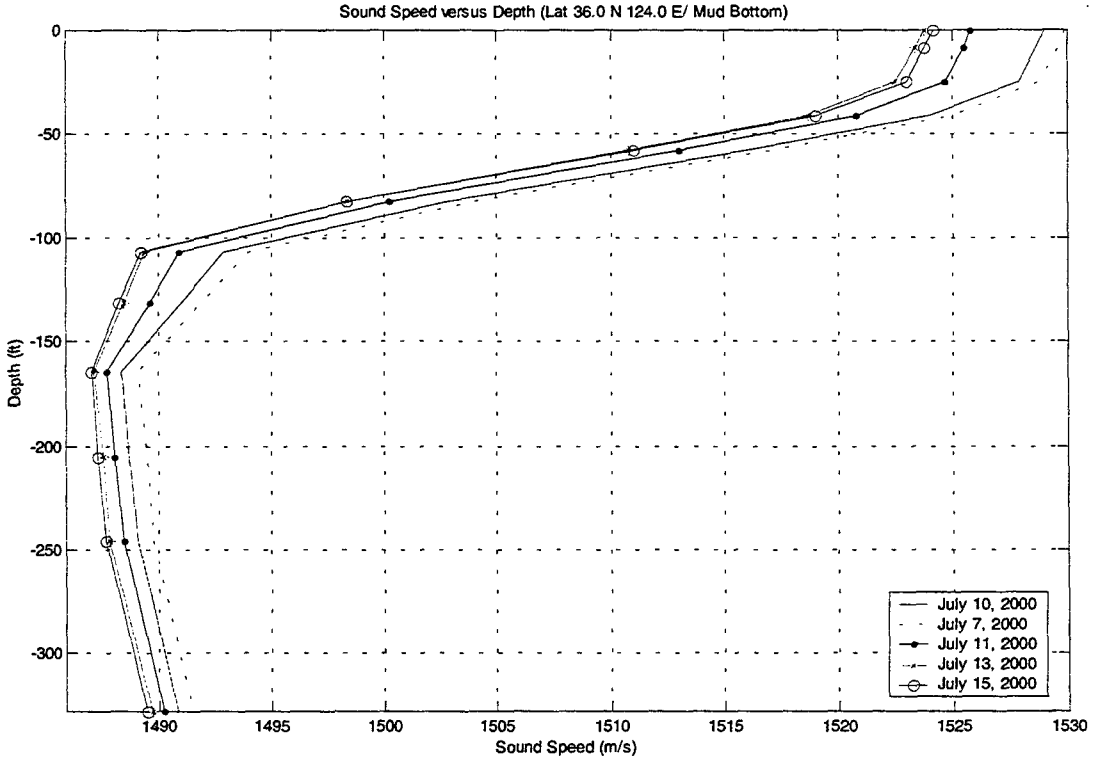

Figure 46. Sound Speed Profile Comparisons for July 7, 10, 11, 13, and 15.

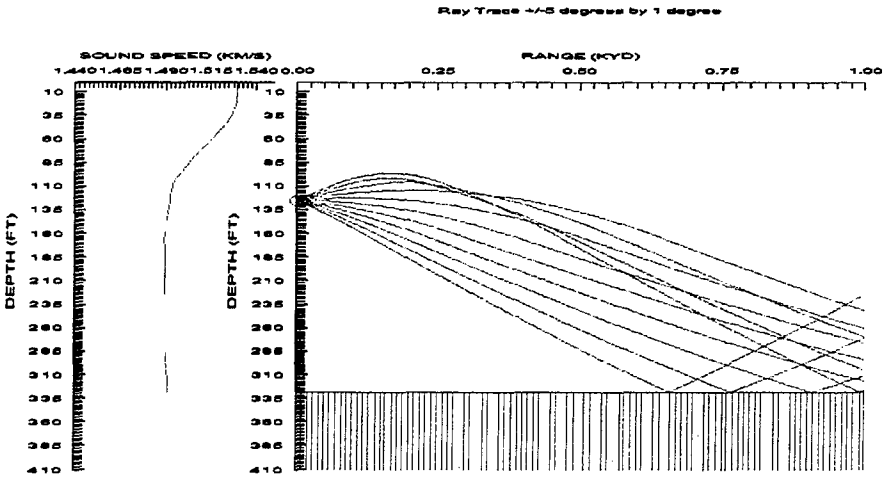

a. Maximum Detection Range for Bottom Mine = 0 yd

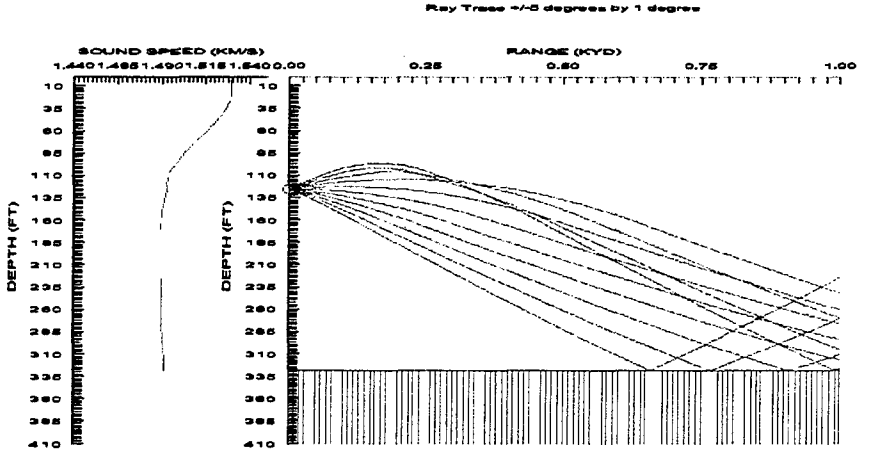

b. Maximum Detection Range (DR) for a Bottom Mine = 775 yd, ΔDR = -775 yd

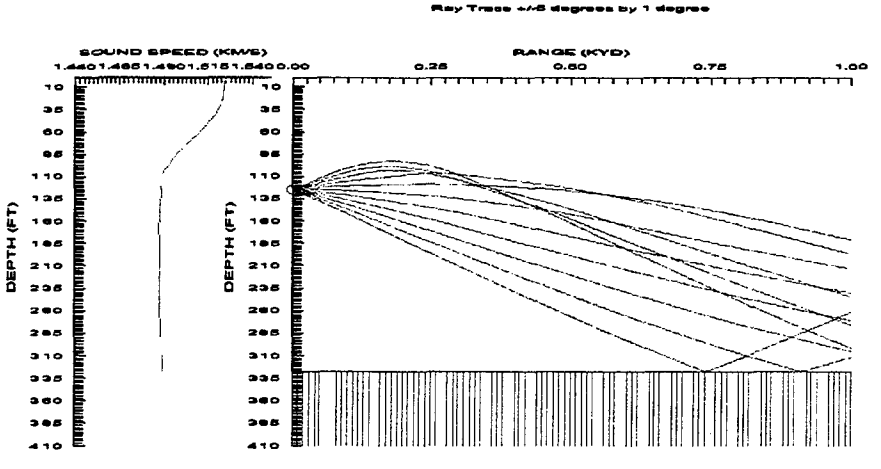

c. Maximum Detection Range (DR) for a Bottom Mine = 810 yd, ΔDR = -810 yd

Figure 47. Sound Speed profiles and Ray traces for Mud Bottom at 36.0 N 124.0 E and Source Depth = 125 ft for a. July 10, 2000, b. July 7, 2000, c. July 15, 2000.

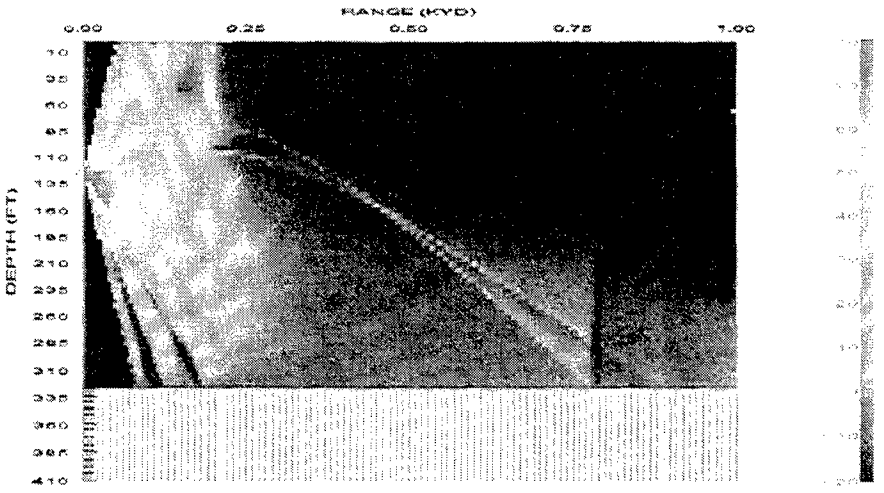

a. Maximum Detection Range for Bottom Mine = 0 yd

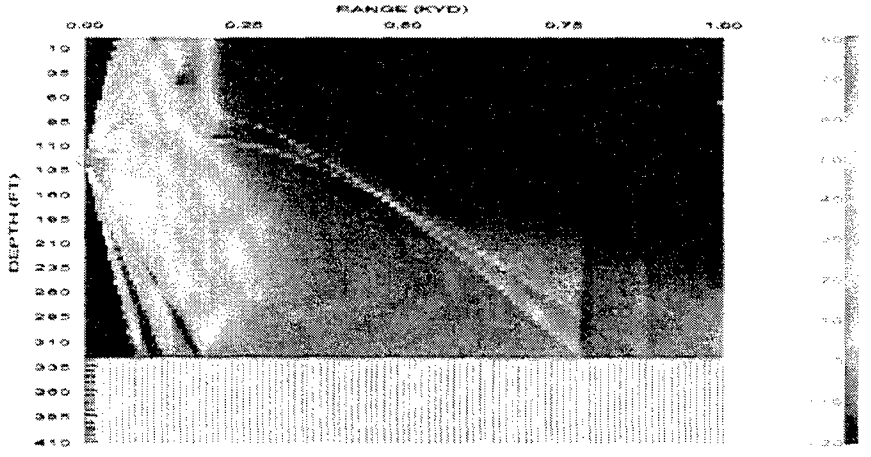

b. Maximum Detection Range (DR) for a Bottom Mine = 775 yd, ΔDR = -775 yd

c. Maximum Detection Range (DR) for a Bottom Mine = 810 yd, ΔDR = -810 yd

Figure 48. Signal Excess contours for Mud Bottom at 36.0 N 124.0 E and Source Depth =25 ft for a. July 10, 2000, b. July 15, 2000.

B. EFFECTS ON ACOUSTIC TRANSMISSION IN THE WINTER BY A STRONG COLD FRONT

In this part of the study the effects on acoustic transmission by a cold front moving through the Yellow Sea was analyzed using MODAS sound speed profiles in the CASS/GRAB model. The dates for the cold front were obtained from NAVPACMETOCCEN Yokosuka Japan Operational Support Web Site. The cold front chosen passed through the Yellow Sea on January 31, 2001 (Figure 49). The temperature, salinity, and sound speed profiles for the dates of January 28 through February 2, 2001 were first analyzed visually using NIDAS. Again, the structures of the profiles demonstrated very little to no difference between the dates being analyzed. MCSST color composite maps were obtained from NAVOCEANO Yellow Sea Oceanographic Features Analysis Color Composite web site to confirm the SSTs the MODAS profiles contained. The two MCSST color composite maps obtained for January 29 and February 2 (Figure 50) complimented the small changes in SST that were observed in the MODAS profiles.

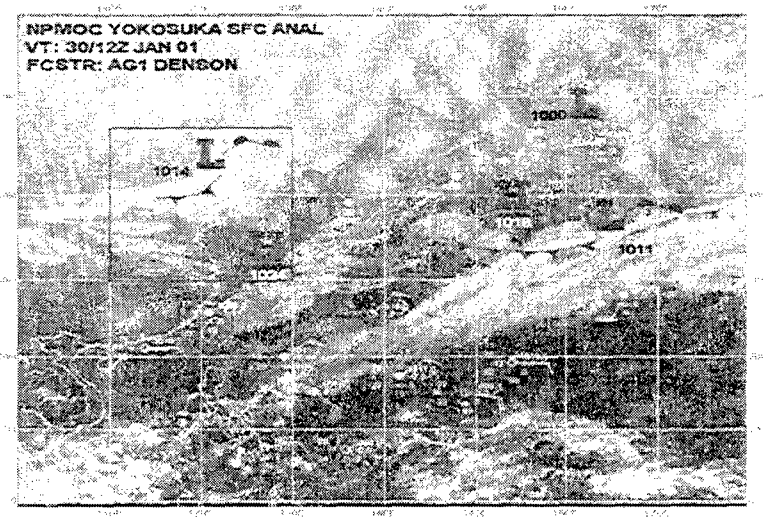

a.

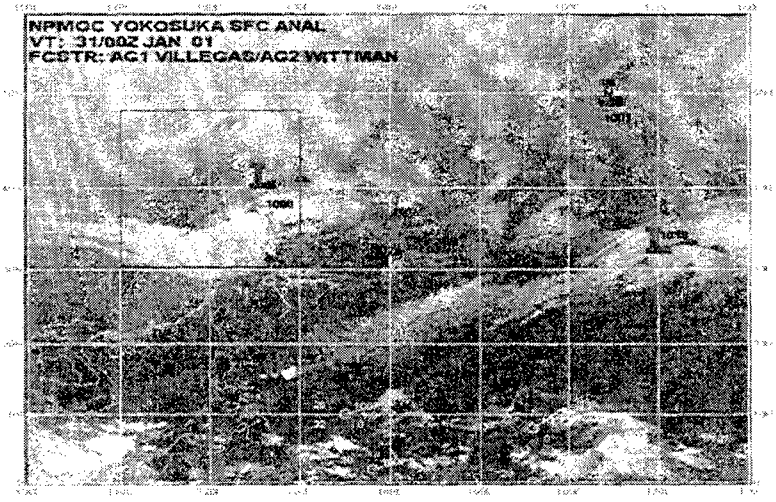

b.

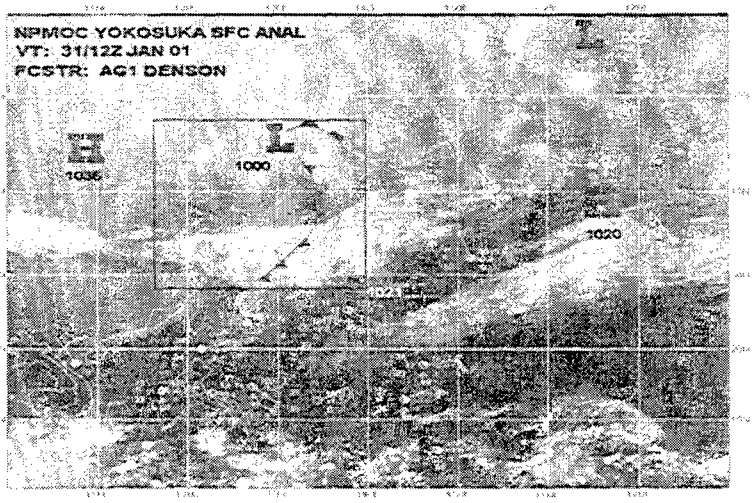

c.

Figure 49. Weather Maps of Cold Front moving through Yellow Sea: a. January 30, 2001/1200Z, b. Jan 31, 2001/0000Z, January 31/1200Z. (From Naval Meteorology and Oceanography Command 2000).

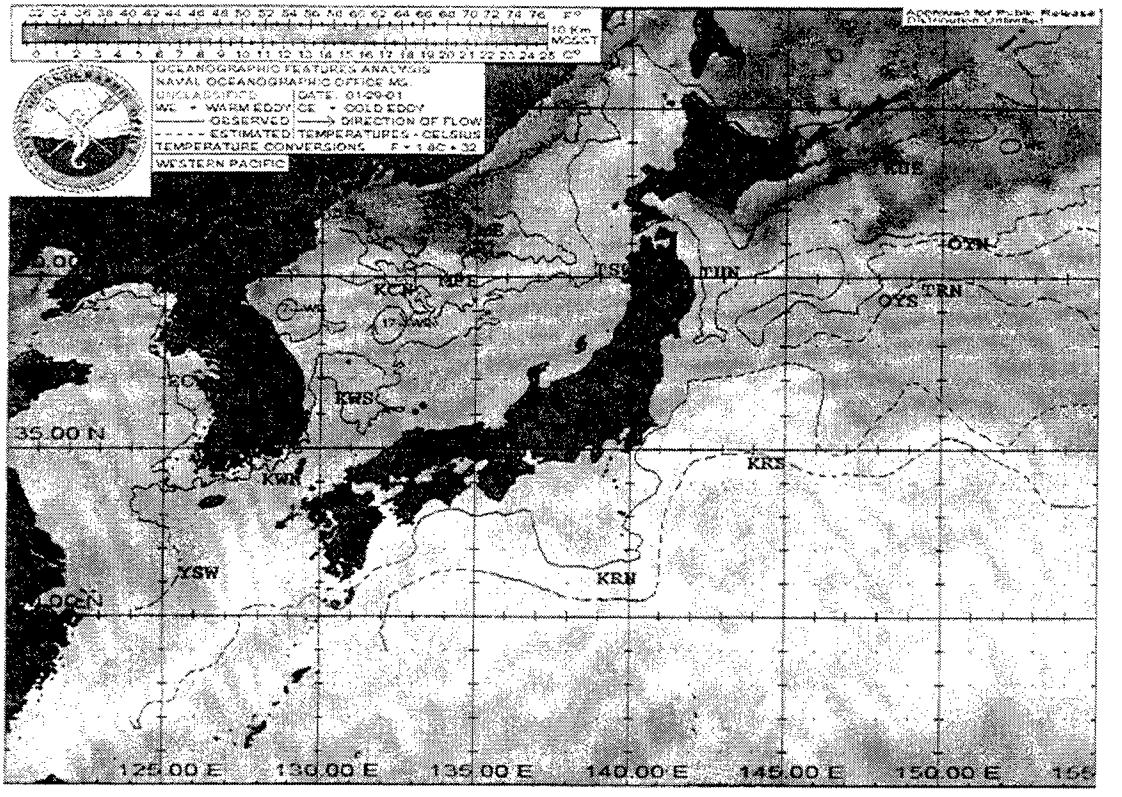

a.

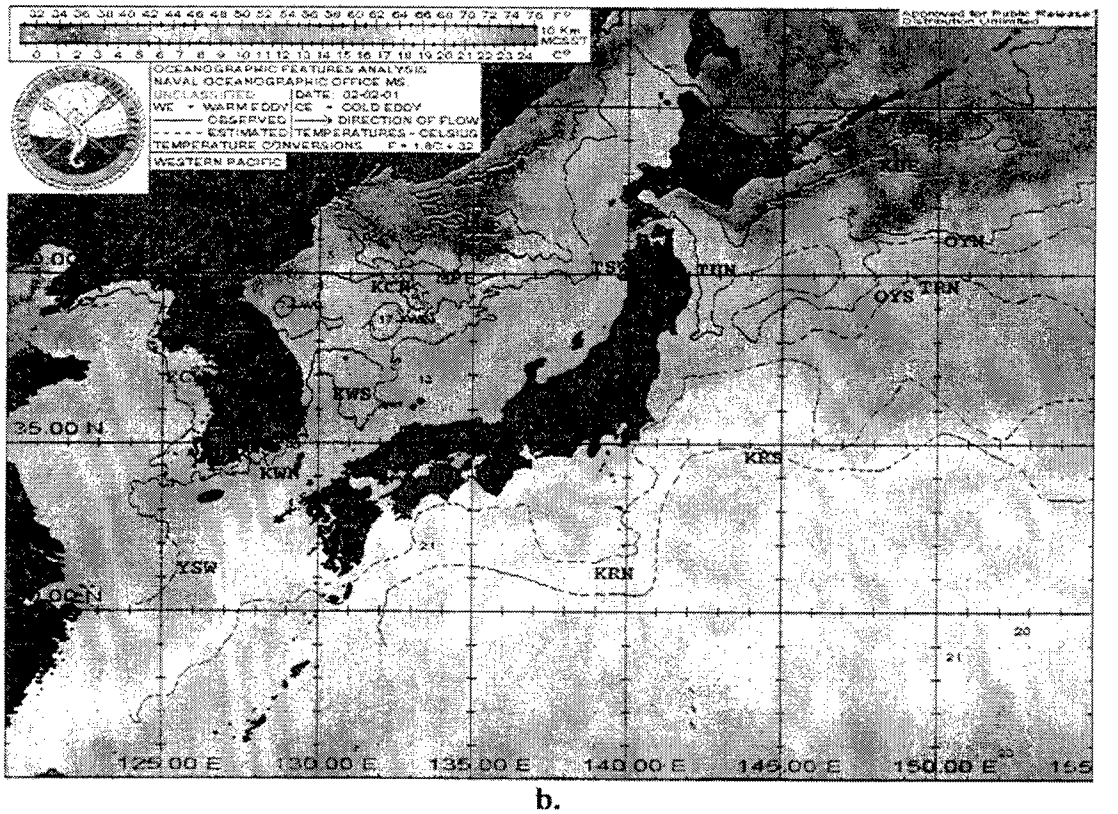

b.

Figure 50. MCSST Maps of Western Pacific before and after Yellow Sea Cold Front: a. January 29, 2001, b. February 02, 2001 (From NAVOCEANO 2001).

Mud and sand bottom regions were again chosen for this part of the study, however, at the mud region, there was a problem with near bottom positive gradients in the temperature profiles at the locations chosen earlier for the tropical depression study so profiles further north were chosen. There were no significant acoustic differences produced by the CASS/GRAB model for any of the scenarios for the profiles in either region (Table 4). There was, however, a significant acoustic difference observed for a source depth of 25 feet and target depth of 21 feet in the mud region for the sound speed profiles at latitude 36.0 N longitude 123.0 E, and latitude 37.0 N longitude 124.0 E. The detection ranges for January 29 for both profiles had detection ranges for a 21 feet target of over 1000 yards. The detection ranges for January 31 and February 2 were 160 yards at latitude 36.0 N longitude 123.0 E, and 260 yards at latitude 37.0 N longitude 124.0 E. The reason for the large difference in detection ranges on January 29 was that both locations had sound speed profiles that contained surface ducts, which were not present in the profiles of the other days. These sound speed profiles also contained deeper mixed layers than the sound speed profiles of January 31 and February 2.

Target Depth	SOURCE DEPTH = 25 FT.			
	Mud		Sand	
	January 31– January 29	January 31– February 2	January 31– January 29	January 31– February 2
26 ft	None	None	None	None
Bottom	None	None	None	None

a.

Target Depth	SOURCE DEPTH = 125 FT.			
	Mud		Sand	
	January 31– January 29	January 31– February 2	January 31– January 29	January 31– February 2
26 ft	None	None	None	None
Bottom	None	None	None	None

b.

Table 4. Maximum Significant Acoustic Differences in Detection Ranges between MODAS Profiles before and after a Cold Front for Mud and Sand Bottom regions at a. Source Depth of 25 ft, b. Source Depth of 125 ft.

In order to analyze the effects of the cold front in more detail, the plots of temperature and sound speed profiles for the days of January 29 through February 2, 2001 were generated for the mud region location at latitude 36.0 N longitude 123.0 E latitude (Figures 51 and 52). The decrease in SST during the period was 0.6° C with a temperature of 9.3 ° C on January 29 and remaining steady at 8.7 ° C for the days of January 31 through February 2. The sound speed profiles show a mixed layer with a surface duct that extends to a depth of a little over 20 ft. on January 29, but shoals to a depth of 10 ft. from January 30 through February 2. This may be due to SSH data being left out of the MODAS model, since the mixed layer would not be expected to shoal with the type of winds generated by a strong cold front. Again, the conclusion is that MODAS may have under predicted the effects of a weather event because SSH data was absent from the model.

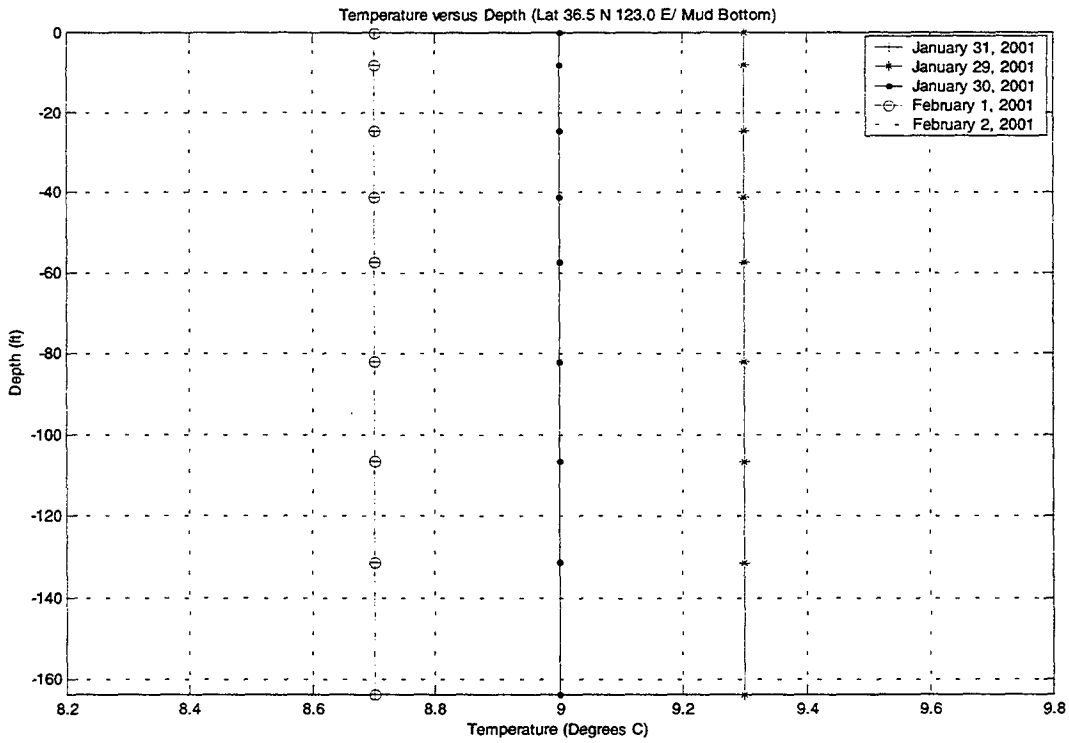

Figure 51. Temperature Profile Comparisons for January 29 through February 2.

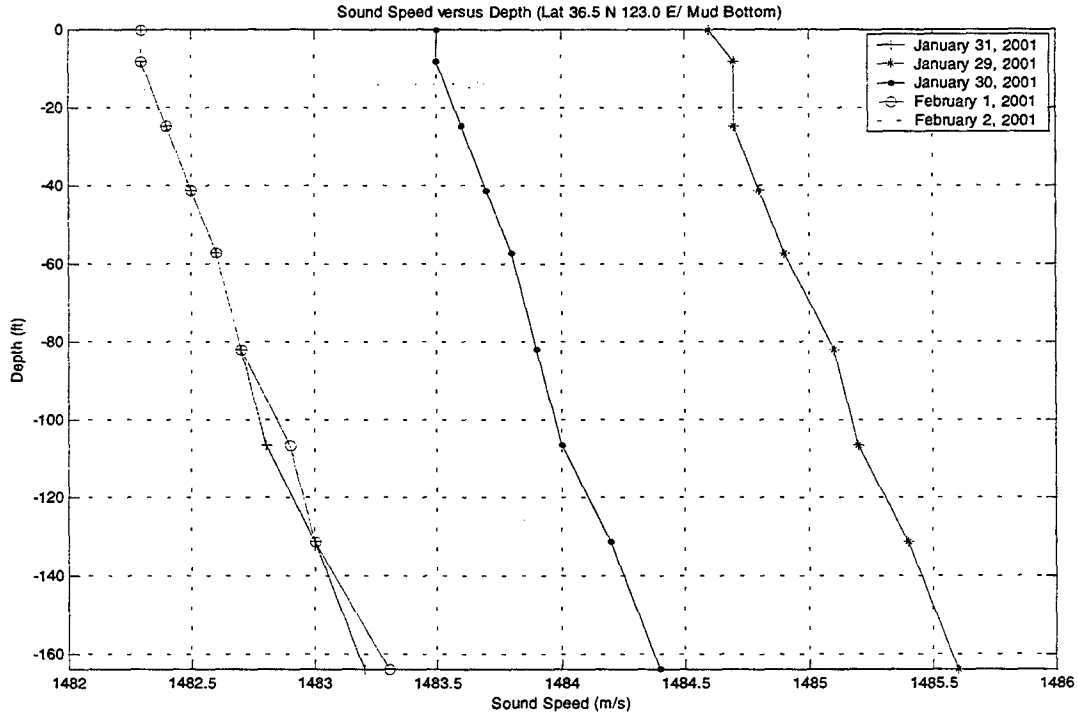

Figure 52. Sound Speed Profile Comparisons for January 29 through February 2.

VIII. SENSITIVITY STUDIES ON HYDROGRAPHIC INPUT DATA

A. COMPARISON BETWEEN MODAS AND MOODS

In this part of the study, corresponding pairs of CASS/GRAB MODAS and MOODS outputs for different scenarios were examined to determine if the two different hydrographic data sets produced detection ranges with significant acoustic differences. As described earlier, data sets for MODAS and MOODS were created using NIDAS. The data set pairs that were created were for four regions of mud, sand, gravel, and rock bottom type region and for the four seasons of winter (February), spring (MAY), summer (August), and fall (November). MODAS data sets for 1999 and 2000 were created for comparison with MOODS in this study. The bottom depths for all of the corresponding data set pairs were made equal using an interpolation code in MATLAB. These data set pairs were entered into the CASS/GRAB model for source depths of 25 feet and, depending on water depths, 50, 75 or 125 feet as described earlier in the seasonal variability chapter. Maximum detection range data for a 26 feet and a bottom target were obtained from CASS/GRAB signal excess calculations. The absolute difference in these detection ranges for each of the corresponding pairs of data sets for each scenario was calculated. The maximum difference in detection ranges that had a significant acoustic difference for each scenario was entered into Tables 5 and 6.

The scenario that generated the largest number of significant acoustic differences was a source depth of 25 feet and a target depth of 26 feet, for all four seasons in the mud and sand regions. The scenario that generated the least number of significant acoustic differences was a source depth of 25 feet and a bottom target, for all four seasons and for all four regions. Overall, the most significant acoustic differences were for the mud and

Target Depth = 26 ft	SOURCE DEPTH = 25 FT.				
	Month	Mud		Sand	
		1999	2000	1999	2000
	February	Lt 35.0N Ln 123.5E **760 yd**	Lt 35.0N Ln 123.5E **760 yd**	Lt 35.9N Ln 125.8E **840 yd**	Lt 35.9N Ln 125.8E **840 yd**
	May	Lt 35.0N Ln 123.0E **795 yd**	Lt 35.0N Ln 123.0E **780 yd**	Lt 35.9N Ln 126.0E **795 yd**	Lt 35.9N Ln 126.0E **810 yd**
	August	Lt 35.9N Ln 124.4E **545 yd**	Lt 35.9N Ln 124.4E **535 yd**	Lt 35.9N Ln 124.8E **820 yd**	Lt 35.9N Ln 124.8E **815 yd**
	November	Lt 36.5N Ln 123.0E **840 yd**	Lt 36.5N Ln 123.0E **840 yd**	Lt 35.9N Ln 125.8E **765 yd**	Lt 35.9N Ln 125.8E **765 yd**

Target Depth = Bottom	SOURCE DEPTH = 25 FT.				
	Month	Mud		Sand	
		1999	2000	1999	2000
	February	Lt 35.0N Ln 123.5E **900 yd**	Lt 35.0N Ln 123.5E **890 yd**	None	None
	May	None	None	None	None
	August	None	None	None	None
	November	None	None	None	None

Target Depth = 26 ft	SOURCE DEPTH = 50/ 75/ 125 FT.				
	Month	Mud		Sand	
		1999	2000	1999	2000
	February	Lt 35.0N Ln 123.5E **495 yd**	Lt 35.0N Ln 123.5E **510 yd**	None	None
	May	Lt 36.3N Ln 125.0E **620 yd**	Lt 36.3N Ln 125.0E **620 yd**	NA	NA
	August	None	None	Lt 35.9N Ln 124.6E **545 yd**	Lt 35.9N Ln 124.6E **545 yd**
	November	Lt 35.0N Ln 123.0E **445 yd**	Lt 35.0N Ln 123.0E **445 yd**	Lt 36.0N Ln 124.8E **495 yd**	Lt 36.0N Ln 124.8E **495 yd**

Target Depth = Bottom	SOURCE DEPTH = 50/ 75/ 125 FT.				
	Month	Mud		Sand	
		1999	2000	1999	2000
	February	Lt 36.4N Ln 124.4E **1000 yd**	Lt 36.4N Ln 124.4E **1000 yd**	None	None
	May	Lt 36.3N Ln 125.0E **225 yd**	Lt 36.3N Ln 125.0E **315 yd**	NA	NA
	August	None	None	Lt 35.9N Ln 125.8E **265 yd**	Lt 35.9N Ln 125.8E **225 yd**
	November	None	None	Lt 35.9N Ln 124.6E **205 yd**	Lt 35.9N Ln 124.6E **205 yd**

Table 5. Maximum Differences in Detection Ranges with a Significant Acoustic Difference: for MODAS versus MOODS for Mud and Sand Bottoms.

Target Depth = 26 ft	SOURCE DEPTH = 25 FT.				
	Month	Gravel		Rock	
		1999	2000	1999	2000
	February	None	None	None	None
	May	Lt 38.9N Ln 122.5E **800 yd**	Lt 38.9N Ln 122.5E **800 yd**	None	None
	August	None	None	None	None
	November	None	None	None	None

Target Depth = Bottom	SOURCE DEPTH = 25 FT.				
	Month	Gravel		Rock	
		1999	2000	1999	2000
	February	None	None	None	None
	May	None	None	None	None
	August	None	None	None	None
	November	None	None	None	None

Target Depth = 26 ft	SOURCE DEPTH = 50/ 75/ 125 FT.				
	Month	Gravel		Rock	
		1999	2000	1999	2000
	February	None	None	None	None
	May	None	None	None	None
	August	None	None	Lt 37.4N Ln 123.1E **210 yd**	Lt 37.4N Ln 123.1E **210 yd**
	November	None	None	None	None

Target Depth = Bottom	SOURCE DEPTH = 50/ 75/ 125 FT.				
	Month	Gravel		Rock	
		1999	2000	1999	2000
	February	None	None	None	None
	May	Lt 39.0N Ln 122.8E **655 yd**	Lt 39.0N Ln 122.8E **655 yd**	Lt 37.5N Ln 123.0E **190 yd**	Lt 37.5N Ln 123.0E **185 y**
	August	Lt 38.9N Ln 122.2E **425 yd**	None	None	None
	November	Lt 38.4N Ln 122.1E **220 yd**	Lt 38.4N Ln 122.1E **225 yd**	Lt 37.5N Ln 123.4E **960 yd**	Lt 37.5N Ln 123.4E **960 yd**

Table 6. Maximum Differences in Detection Ranges with a Significant Acoustic Difference for MODAS versus MOODS for Gravel and Rock Bottoms.

sand regions. In the gravel and rock regions, acoustic transmission was so limited by bottom reverberation, that only one scenario (Source Depth = 50/75/125 ft and a bottom target) generated a significant number of significant acoustic differences.

The oceanographic differences between differences between MODAS and MOODS varied between the colder fall and winter months and the warmer spring and summer months. The differences that occurred during the fall and winter months were due to surface ducts, and differences in thermocline gradients and differences in mixed layer depths. The differences that occurred during the spring and summer months were due to differences in thermocline gradients, differences in mixed layer depths, and the presence of a sub-layer.

In the fall and winter months, the differences due to surface ducts were that the MOODS profiles contained surface ducts and the MODAS profiles did not, or the MOODS profiles contained stronger surface ducts than the MODAS profiles. The differences resulting from the differences in the thermocline gradients were that in all the cases, the MOODS profiles gradients were always greater than the gradients in the MODAS profiles. The differences resulting from the differences in the mixed layer depths were that in all cases, the MOODS profiles contained mixed layer depths that were deeper than those of the MODAS profiles. In most cases, the weaker surface ducts, the weaker thermoclines, and the shallower mixed layer, may be due to the effects of averaging historical observational data in creating the MODAS climatological data. Without the input of SSH data into the MODAS model the characteristics of the surface ducts, thermocline, and mixed layer are possibly the same as the MODAS climatology. It must be noted that this possible problem cannot be determined with certainty to be a

problem with the MODAS climatology without studying the actual MODAS climatology. The MODAS climatological data was not available for this study.

One of the differences observed was a near bottom positive gradient that was sometimes present in the isothermal structure of both of the MODAS temperature and sound speed profiles during the winter months in the mud region. This near bottom positive gradient was not observed in the any of the MOODS profiles that were used in this study. This type of profile structure is very unlikely because a water column structure containing a large cold-water layer above a small layer of warm water would be very unstable. The absence of this structure in the MOODS profiles and the very unstable nature of the profile structure indicates that this structure is due to a discrepancy in the MODAS climatology during the winter months in the mud region. The discrepancy is most likely a result to a lack of observational data in the region during the winter months. The region where this problem existed was along a shelf in the southern Yellow Sea near the northern East China Sea this region consisted of approximately 15 % of the Yellow Sea.

In the spring and summer months, the differences due to the differences in the thermocline gradients were that in all the cases, the MOODS profiles gradients were always greater than the gradients in the MODAS profiles. The differences due to the differences in the mixed layer depths were that in all cases, the MOODS profiles contained mixed layer depths that were deeper than those of the MODAS profiles. The differences due to a sub-layer in the multi-layer structure of the sound speed profiles of the spring and the summer months varied in that the sub-layer was present or absent in either the MODAS or MOODS profile. In most cases, as stated previously, the weaker

thermoclines, and the shallower mixed layer may be due to the effects of averaging historical observational data in creating the MODAS climatological data. Without the input of SSH data into the MODAS model, the characteristics of the surface ducts, thermocline, and mixed layer, are possibly the same as the MODAS climatology. It must be noted that this possible problem cannot be determined with certainty to be a problem with the MODAS climatology without studying the actual MODAS climatology. The MODAS climatological data was not available for this study.

Tables 8 through 15 were created to facilitate for the reader the description of the oceanographic differences between the MODAS and the MOODS profiles of Tables 5 and 6 and their effects on the acoustic model. The ray traces with detection ranges for each of the corresponding MODAS and MOODS profiles of Tables 5 and 6 can be found in Appendix A.

MODAS versus MOODS	
February /Mud Bottom	
1. Oceanographic Difference between MODAS and MOODS	Differences were due to a near Bottom positive gradient in the MODAS profile that was not present in the MOODS profile.
2. How this affected the Acoustic Model	This near Bottom positive gradient produced up bending near the bottom. When the Source was at hull depth, both moored and Bottom mines detection ranges were over predicted. When the Source was at 125 ft, moored mines detection ranges were over predicted and Bottom mines detection ranges were under predicted.
3. Prevalence of Problems, if any, in the Yellow Sea or North East China Sea	This may be a problem in the MODAS climatology. The problem was present in approximately 15 % of the MODAS profiles in the Yellow Sea.

a.

MODAS versus MOODS	
May/ Mud Bottom	
1. Oceanographic Difference between MODAS and MOODS	1. At a source depth of 25 ft., the difference was due to the presence of a mixed layer in the MOODS profile that was not present in the MODAS profiles. 2. At a source depth of 125 ft., the difference was due to a presence of sub-layer in the MODAS profile that was not present in the MOODS profile.
2. How this affected the Acoustic Model	1. The mixed layer in the MOODS profile produced allowed sound propagation above the thermocline, thus increasing the detection range of a moored mine. The thermoclines in both types of data sets were too weak to produce significant caustics. 2. The sub-layer in the MODAS profile trapped sound propagation under the thermocline, thus decreasing the detection ranges for moored mines and increasing the detection ranges of bottom mines.
3. Prevalence of Problems, if any, in the Yellow Sea or the North East China Sea	1. Possible problem since the mixed layers in most of the MODAS profiles were always shallower than the MOODS profiles were. 2. Not a prevalent problem.

b.

Table 7. Description of Significant Acoustic Differences in Detection Ranges between MODAS and MOODS Profiles in a Mud Bottom region in a. February, and b. May.

MODAS versus MOODS	
August/ Mud Bottom	
1. Oceanographic Difference between MODAS and MOODS	At a source depth of 25 ft., the difference was due to the MOODS profile having a much deeper mixed layer depth.
2. How this affected the Acoustic Model	The negative gradient in the deeper mixed layer of the MOODS profile where the source was located produced less down bending than the negative gradient of the thermoclines of the MODAS profiles, thus forming weaker caustics and decreasing the detection range of moored mines.
3. Prevalence of Problems, if any, in the Yellow Sea or the North East China Sea	Possible problem since the mixed layers in most of the MODAS profiles were always shallower than the MOODS profiles were.

a.

MODAS versus MOODS	
November/ Mud Bottom	
1. Oceanographic Difference between MODAS and MOODS	1. The first difference was due to a surface duct that was present in the MOODS profile and not in the MODAS profile when source depth was at 25 ft. 2. When the source depth was at 125 ft., the difference was due to a weaker thermocline gradient in the MODAS profile.
2. How this affected the Acoustic Model	1. The surface ducts trapped sound propagation in a subsurface layer that produced greater detection ranges for moored mines. 2. The source depth was within the thermocline; the weaker thermocline gradients produced by MODAS caused less down bending of sound propagation. This produced weaker caustics due to less focusing of sound propagation, which in turn causes an under prediction of moored mines.
3. Prevalence of Problems, if any, in the Yellow Sea or the North East China Sea	1. When there was a surface duct in both profiles, it was much stronger in the MOODS profile for most cases. The weaker surface ducts found in the MODAS profiles cannot be determined to be a problem without performing a study of the MODAS climatology. 2. The weaker MODAS thermocline gradients were observed in almost all of the MODAS profiles used in this study.

b.

Table 8. Description of Significant Acoustic Differences in Detection Ranges between MODAS and MOODS Profiles in a Mud Bottom region in a. August, and b. November.

MODAS versus MOODS	
February/ Sand Bottom	
1. Oceanographic Difference between MODAS and MOODS	The difference was due to a surface duct that was present in the MOODS profile and not in the MODAS profile when source depth was at 25 ft.
2. How this affected the Acoustic Model	The surface duct trapped sound propagation in a subsurface layer that produced greater detection ranges for moored mines.
3. Prevalence of Problems, if any, in the Yellow Sea or the North East China Sea	When there was a surface duct in both profiles, it was much stronger in the MOODS profile for most cases.

a.

MODAS versus MOODS	
May/ Sand Bottom	
1. Oceanographic Difference between MODAS and MOODS	At a source depth of 25 ft., the difference was due to a presence of sub-layer in the MOODS profile that was not present in the MODAS profiles.
2. How this affected the Acoustic Model	The sub-layer weakened the effect of thermocline gradient, which caused less down bending of sound propagation. This produced weaker caustics due to less focusing of sound propagation, which in turn causes an under prediction of moored mines.
3. Prevalence of Problems, if any, in the Yellow Sea or the North East China Sea	Not a prevalent problem.

b.

Table 9. Description of Significant Acoustic Differences in Detection Ranges between MODAS and MOODS Profiles in a Sand Bottom region in a. February, and b. May.

MODAS versus MOODS	
August/ Sand Bottom	
1. Oceanographic Difference between MODAS and MOODS	1. At a source depth of 25 ft., the difference was due to the MODAS profiles having a much shallower mixed layer depth and a negative gradient within the mixed layer of the MOODS profile. 2. At a source depth of 125 ft., the first difference was due to a presence of sub-layer in the MODAS profiles that was not present in the MOODS profile. 3. At a source depth of 125 ft., the second difference was due the source being located within a sub-layer that was present in the MOODS profiles but was not present in the MODAS profile.
2. How this affected the Acoustic Model	1. The negative gradient in the deeper mixed layer of the MOODS profile where the source was located produced less down bending than the stronger negative gradient of the thermoclines of the MODAS profiles. 2. Although the source was located above the sub-layer, it weakened the effect of thermocline gradient, which caused less down bending of sound propagation. This produced weaker caustics due to less focusing of sound propagation, which in turn caused an under prediction of moored mines. 3. The sub-layer trapped all sound propagation under the thermocline, thus making sound propagation very limited by bottom reverberation.
3. Prevalence of Problems, if any, in the Yellow Sea or the North East China Sea	1. Possible problem since the mixed layers in most of the MODAS profiles were usually shallower than the MOODS profiles were. 2. Not a prevalent problem. 3. Not a prevalent problem.

Table 10. Description of Significant Acoustic Differences in Detection Ranges between MODAS and MOODS Profiles in a Sand Bottom region in August.

MODAS versus MOODS	
November/ Sand Bottom	
1. Oceanographic Difference between MODAS and MOODS	1. When source depth was at 25 ft., the difference was due to a stronger surface duct that was present in the MOODS profile 2. When the source depth was at 125 ft., the first difference was due to a weaker thermocline gradient in the MODAS profile. 3. When the source depth was at 125 ft., the second difference was due to the MOODS profile having a much deeper mixed layer depth.
2. How this affected the Acoustic Model	1. The stronger surface duct in the MOODS profile more effectively trapped sound propagation in a subsurface layer, thus producing greater detection ranges for moored mines. 2. The source depth was within the thermocline; the weaker thermocline gradients produced by MODAS caused less down bending of sound propagation. This produced weaker caustics due to less focusing of sound propagation, which in turn caused an under prediction of moored mines. 3. The negative gradient in the deeper mixed layer of the MOODS profile where the source was located produced less down bending than the negative gradient of the thermoclines of the MODAS profiles, thus forming weaker caustics and decreasing the detection range of a bottom mine.
3. Prevalence of Problems, if any, in the Yellow Sea or the North East China Sea	1. When there was a surface duct in both profiles, it was much stronger in the MOODS profile for most cases. The weaker surface ducts found in the MODAS profiles cannot be determined to be a problem without performing a study of the MODAS climatology. 2. The weaker MODAS thermocline gradients were observed in almost all of the MODAS profiles used in this study. 3. Possible problem since the mixed layers in most of the MODAS profiles were always shallower than the MOODS profiles were.

Table 11. Description of Significant Acoustic Differences in Detection Ranges between MODAS and MOODS Profiles in a Sand Bottom region in November.

MODAS versus MOODS	
February/ Gravel Bottom	
1. Oceanographic Difference between MODAS and MOODS	None
2. How this affected the Acoustic Model	NA
3. Prevalence of Problems, if any, in the Yellow Sea or the North East China Sea	NA

a.

MODAS versus MOODS	
May/ Gravel Bottom	
1. Oceanographic Difference between MODAS and MOODS	When the source depth was at 25 ft. and 75 ft., the difference was due to a weaker thermocline gradient in the MODAS profile.
2. How this affected the Acoustic Model	The source depth was within the thermocline; the weaker thermocline gradients produced by MODAS caused less down bending of sound propagation. This produced weaker caustics due to less focusing of sound propagation, which in turn causes a decreased detection ranges of both moored and bottom mines.
3. Prevalence of Problems, if any, in the Yellow Sea or the North East China Sea	The weaker MODAS thermocline gradients were observed in almost all of the MODAS profiles used in this study.

b.

Table 12. Description of Significant Acoustic Differences in Detection Ranges between MODAS and MOODS Profiles in a Gravel Bottom region in a. February, and b. May.

MODAS versus MOODS	
August/ Gravel Bottom	
1. Oceanographic Difference between MODAS and MOODS	For a source depth of 50 ft., the difference was due to a thermocline that was present in the MODAS profiles and an isothermal structure of the MOODS profile.
2. How this affected the Acoustic Model	The source was located within the thermocline, and the negative gradient of the thermocline caused down bending of sound propagation, which produced caustics that increased the detection range of bottom mines.
3. Prevalence of Problems, if any, in the Yellow Sea or the North East China Sea	Not a prevalent problem.

a.

MODAS versus MOODS	
November/ Gravel Bottom	
1. Oceanographic Difference between MODAS and MOODS	For a source depth of 125 ft., the difference was due to a thermocline that was present in the GDEM profiles and an isothermal structure of the MODAS profiles.
2. How this affected the Acoustic Model	In this scenario, the source was very close to the bottom. The down bending caused by the thermocline in the GDEM profile caused sound propagation to become very limited by bottom reverberation, thus decreasing the detection range of a bottom mine.
3. Prevalence of Problems, if any, in the Yellow Sea or the North East China Sea	Not a prevalent problem.

b.

Table 13. Description of Significant Acoustic Differences in Detection Ranges between MODAS and MOODS Profiles in a Gravel Bottom region in a. August, and b. November.

MODAS versus MOODS	
February/ Rock Bottom	
1. Oceanographic Difference between MODAS and MOODS	None
2. How this affected the Acoustic Model	NA
3. Prevalence of Problems, if any, in the Yellow Sea or the North East China Sea	NA

a.

MODAS versus MOODS	
May for Rock Bottom Type	
1. Oceanographic Difference between MODAS and MOODS	For a source depth of 125 ft., the difference was due to a stronger thermocline in the GDEM profile.
2. How this affected the Acoustic Model	In this scenario, the source was very close to the bottom. The down bending caused by the thermocline in the GDEM profile caused sound propagation to become very limited by bottom reverberation, thus decreasing the detection range of a bottom mine.
3. Prevalence of Problems, if any, in the Yellow Sea or the North East China Sea	Not a prevalent problem.

b.

Table 14. Description of Significant Acoustic Differences in Detection Ranges between MODAS and MOODS Profiles in a Rock Bottom region in a. February, and b. May.

MODAS versus MOODS	
August/ Rock Bottom	
1. Oceanographic Difference between MODAS and MOODS	For a source depth of 125 ft., the difference was due to a sub-layer that was present in the MOODS profile and not in the MODAS profiles.
2. How this affected the Acoustic Model	The source was in the sub-layer for the MOODS profile and in the thermocline for the MODAS profiles. In this scenario, the source was very close to the bottom. The down bending caused by thermocline in the MODAS profiles caused sound propagation to become very limited by bottom reverberation, thus decreasing the detection range of a bottom mine.
3. Prevalence of Problems, if any, in the Yellow Sea or the North East China Sea	Not a prevalent problem.

a.

MODAS versus MOODS	
November/ Rock Bottom	
1. Oceanographic Difference between MODAS and MOODS	For a source depth of 125 ft., the difference was due to a weaker thermocline gradient in the MODAS profiles.
2. How this affected the Acoustic Model	The source depth was within the thermocline; the weaker thermocline gradients produced by MODAS caused less down bending of sound propagation. This produced weaker caustics due to less focusing of sound propagation, which in turn causes a decreased detection ranges of both moored and bottom mines.
3. Prevalence of Problems, if any, in the Yellow Sea or the North East China Sea	The weaker MODAS thermocline gradients were observed in almost all of the MODAS profiles used in this study.

b.

Table 15. Description of Significant Acoustic Differences in Detection Ranges between MODAS and MOODS Profiles in a Rock Bottom region in a. August, and b. November.

B. COMPARISON BETWEEN MODAS AND GDEM

In this part of the study, corresponding pairs of CASS/GRAB MODAS and GDEM outputs for different scenarios were examined to determine if the two different hydrographic data sets produced detection ranges with significant acoustic differences. As described earlier, data sets for MODAS and GDEM were created using NIDAS. The data set pairs that were created were for four bottom type regions of mud, sand, gravel, and rock, and for the four seasons of winter (February), spring (MAY), summer (August), and fall (November). The bottom depths for all of the corresponding data set pairs were made equal using an interpolation code in MATLAB. These data set pairs were entered into the CASS/GRAB model for source depths of 25 feet and, depending on water depths, 50, 75 or 125 feet as described earlier in the seasonal variability chapter. Maximum detection range data for a source depth of 26 feet and a bottom target were obtained from CASS/GRAB signal excess calculations. The absolute difference in these detection ranges for each of the corresponding pairs of data sets for each scenario was calculated. The maximum difference in detection ranges that had a significant acoustic difference for each scenario was entered into Tables 7 and 8.

The scenario that generated the largest number of significant acoustic differences was a source depth of 25 feet and a target depth of 26 feet for all four seasons in the mud region. The scenario that generated the least number of significant acoustic differences was a source depth of 25 feet and a bottom target for all four seasons in the sand, gravel, and rock regions. Overall, most the significant acoustic differences were for the mud and sand regions. In the gravel and rock regions, acoustic transmission was so limited by

bottom reverberation, that only one scenario (Source Depth = 50/75/125 ft and a bottom target) generated a significant number of significant acoustic differences.

Target Depth = 26 ft	SOURCE DEPTH = 25 FT.				
	Month	Mud		Sand	
		1999	2000	1999	2000
	February	Lt 35.0N Ln 123.5E **755 yd**	Lt 35.0N Ln 123.5E **755 yd**	None	None
	May	Lt 35.0N Ln 123.0E **795 yd**	Lt 35.0N Ln 123.0E **780 yd**	Lt 35.9N Ln 125.2E **860 yd**	Lt 35.9N Ln 125.2E **860 yd**
	August	Lt 35.9N Ln 124.4E **545 yd**	Lt 35.9N Ln 124.4E **535 yd**	Lt 35.9N Ln 124.8E **390 yd**	Lt 35.9N Ln 124.8E **385 yd**
	November	Lt 36.5N Ln 123.0E **840 yd**	Lt 36.5N Ln 123.0E **840 yd**	None	None

Target Depth = Bottom	SOURCE DEPTH = 25 FT.				
	Month	Mud		Sand	
		1999	2000	1999	2000
	February	Lt 35.0N Ln 123.5E **900 yd**	Lt 35.0N Ln 123.5E **890 yd**	None	None
	May	Lt 36.3N Ln 125.0E **655 yd**	Lt 36.3N Ln 125.0E **655 yd**	None	None
	August	None	None	None	None
	November	None	None	None	None

Target Depth = 26 ft	SOURCE DEPTH = 50/ 75/ 125 FT.				
	Month	Mud		Sand	
		1999	2000	1999	2000
	February	Lt 35.0N Ln 123.5E **495 yd**	Lt 35.0N Ln 123.5E **510 yd**	None	None
	May	None	None	NA	NA
	August	None	None	Lt 35.9N Ln 124.6E **525 yd**	Lt 35.9N Ln 124.6E **525 yd**
	November	Lt 36.5N Ln 123.0E **525 yd**	Lt 36.5N Ln 123.0E **510 yd**	None	Lt 35.9N Ln 124.6E **535 yd**

Target Depth = Bottom	SOURCE DEPTH = 50/ 75/ 125 FT.				
	Month	Mud		Sand	
		1999	2000	1999	2000
	February	Lt 35.0N Ln 123.5E **340 yd**	Lt 35.0N Ln 123.5E **355 yd**	None	None
	May	Lt 35.0N Ln 123.5E **895 yd**	Lt 35.0N Ln 123.5E **895 yd**	NA	NA
	August	None	None	Lt 35.9N Ln 124.6E **385 yd**	Lt 35.9N Ln 124.6E **360 yd**
	November	Lt 36.5N Ln 123.0E **250 yd**	Lt 36.5N Ln 123.0E **235 yd**	None	None

Table 16. Maximum Differences in Detection Ranges with a Significant Acoustic Difference: for MODAS versus GDEM for Mud and Sand Bottoms.

Target Depth = 26 ft	SOURCE DEPTH = 25 FT.				
	Month	Gravel		Rock	
		1999	2000	1999	2000
	February	None	None	None	None
	May	None	Lt 39.0N Ln 122.8E **775 yd**	None	None
	August	Lt 38.6N Ln 122.0E **850 yd**	Lt 38.6N Ln 122.0E **850 yd**	None	None
	November	None	None	None	None

Target Depth = Bottom	SOURCE DEPTH = 25 FT.				
	Month	Gravel		Rock	
		1999	2000	1999	2000
	February	None	None	None	None
	May	None	None	None	None
	August	None	None	None	None
	November	None	None	None	None

Target Depth = 26 ft	SOURCE DEPTH = 50/ 75/ 125 FT.				
	Month	Gravel		Rock	
		1999	2000	1999	2000
	February	None	None	None	None
	May	None	None	None	None
	August	None	None	None	None
	November	None	None	None	None

Target Depth = Bottom	SOURCE DEPTH = 50/ 75/ 125 FT.				
	Month	Gravel		Rock	
		1999	2000	1999	2000
	February	None	None	None	None
	May	None	None	Lt 37.4N Ln 123.1E **190 yd**	Lt 37.4N Ln 123.1E **185 yd**
	August	Lt 38.6N Ln 122.0E **955 yd**	Lt 38.6N Ln 122.0E **955 yd**	None	None
	November	Lt 38.4N Ln 122.1E **220 yd**	Lt 38.4N Ln 122.1E **225 yd**	None	None

Table 17. Maximum Differences in Detection Ranges with a Significant Acoustic Difference: for MODAS versus GDEM for Gravel and Rock Bottoms.

The oceanographic differences between differences between MODAS and GDEM varied between the colder fall and winter months and the warmer spring and summer months. The differences that occurred during the fall and winter months were due to surface ducts, and differences in thermocline gradients, and differences in mixed layer depths. The differences that occurred during the spring and summer months were due to differences in thermocline gradients, differences in mixed layer depths, and the presence of a sub-layer.

In the fall and winter months, the differences due to surface ducts were that the GDEM profiles contained surface ducts and the MODAS profiles did not, or the GDEM profiles contained stronger surface ducts than the MODAS profiles. The differences due to the differences in the thermocline gradients were that either the MODAS or the GDEM profiles thermocline gradient was stronger than the other. The differences due to the differences in the mixed layer depths were that either the MODAS or the GDEM profiles mixed layer depths were deeper than the other. In most cases, the weaker surface ducts, the weaker thermoclines, and the shallower mixed layer, may be due to the effects of averaging historical observational data in creating the GDEM and MODAS climatological data. Without the input of SSH data into the MODAS model, the characteristics of the surface ducts, thermocline, and mixed layer are possibly the same as the MODAS climatology. Again, it must be noted that this possible problem cannot be determined with certainty to be a problem with the MODAS climatology without studying the actual MODAS climatology.

One of the differences observed was a near bottom positive gradient that was sometimes present in the isothermal structure of both of the MODAS temperature and

sound speed profiles during the winter months in the mud region. The near bottom positive gradient was also observed in many of the GDEM profiles during the winter months, although they were located through the entire Yellow Sea. As described earlier, this type of profile structure is a very unlikely because a water column structure containing a large cold-water layer above a small layer of warm water would be very unstable. The absence of this structure in the MOODS profiles, and the very unstable nature of the profile structure, indicates this structure is due to a discrepancy in GDEM and the MODAS climatology during the winter months. The discrepancy is most likely a result of a lack of observational data during the winter months in the mud region for MODAS and throughout the Yellow Sea for GDEM.

In the spring and summer months, the differences due to the differences in the thermocline gradients were that either the MODAS or the GDEM profiles thermocline gradient was stronger than the other. The differences due to the differences in the mixed layer depths were that either the MODAS or the GDEM profiles mixed layer depths were deeper than the other. In most cases, the weaker surface ducts, the weaker thermoclines, and the shallower mixed layer may be due to the effects of averaging historical observational data in creating the GDEM and MODAS climatological data. The differences due to the differences in the mixed layer depths were that in all cases, the GDEM profiles contained mixed layer depths were deeper than those of the MODAS profiles. The differences due to a sub-layer in the multi-layer structure of the sound speed profiles of the spring and the summer months varied in that the sub-layer was present or absent in either the MODAS or GDEM profile. In most cases, as stated previously, the weaker thermoclines and the shallower mixed layer may be due to the

effects of averaging historical observational data in creating the GDEM and MODAS climatological data. Without the input of SSH data into the MODAS model, the characteristics of the surface ducts, thermocline, and mixed layer are possibly the same as the MODAS climatology. Again, it must be noted that this possible problem cannot be determined with certainty to be a problem with the MODAS climatology without studying the actual MODAS climatology.

Tables 18 through 24 were created to facilitate for the reader the description of the oceanographic differences between the MODAS and the GDEM profiles of Tables 16 and 17 and their effects on the acoustic model. The ray traces with detection ranges for each of the corresponding MODAS and MOODS profiles of Tables 16 and 17 can be found in Appendix B.

In Appendix C, histograms for all the scenarios were created to show the distributions of differences in detection ranges for MODAS minus GDEM and MODAS minus GDEM throughout the water column at five feet increments. The biggest differences in detection ranges were found in spring and summer for both mud and sand regions. The smallest differences in detection ranges were during the fall and winter months for both gravel and rock regions. As mentioned earlier, sound propagation becomes very limited by bottom reverberation in regions of gravel and rock bottom types.

MODAS versus GDEM	
February /Mud Bottom	
1. Oceanographic Difference between MODAS and MOODS	Differences are due to a near Bottom positive gradient in the MODAS profile that was not present in the GDEM profile.
2. How this affected the Acoustic Model	This near Bottom positive gradient produced up bending near the bottom. When the Source was at hull depth, both moored and Bottom mines detection ranges were over predicted. When the Source was at 125 ft., moored mines detection ranges were over predicted and Bottom mines detection ranges were under predicted.
3. Prevalence of Problems, if any, in the Yellow Sea or North East China Sea	-This may be a problem in the MODAS climatology. The problem was present in approximately 15 % of the MODAS profiles in the Yellow Sea. -This problem was more prevalent in GDEM throughout the entire Yellow Sea.

a.

MODAS versus GDEM	
May/ Mud Bottom	
1. Oceanographic Difference between MODAS and MOODS	1. At a source depth of 25 ft., the difference was due to the presence of a mixed layer in the GDEM profile that was not present in the MODAS profiles 2. At source depths of 25 and 125 ft., the difference was due to a presence of sub-layer in the MODAS profile that was not present in the GDEM profile.
2. How this affected the Acoustic Model	1. The mixed layer in the GDEM profile produced allowed sound propagation above the thermocline, thus increasing the detection range of a moored mine. The thermoclines in both types of data sets were too weak to produce significant caustics. 2. At a source depth of 25 ft., the sub-layer in the MODAS profiles weakened down bending thus weakening any caustics that would increase the detection range of a bottom mine. At a source depth of 125 ft., the sub-layer in the MODAS profiles weakened down thus weakened bottom reverberation, which increased the detection range of bottom mines.
3. Prevalence of Problems, if any, in the Yellow Sea or the North East China Sea	1. Possible problem since the mixed layers in most of the MODAS profiles were always shallower than the GDEM profiles were. 2. Not a prevalent problem.

b.

Table 18. Description of Significant Acoustic Differences in Detection Ranges between MODAS and GDEM Profiles in a Mud Bottom region in a. February, b. May.

MODAS versus GDEM	
August/ Mud Bottom	
1. Oceanographic Difference between MODAS and MOODS	At a source depth of 25 ft., the difference was due to the GDEM profile having a much deeper mixed layer depth.
2. How this affected the Acoustic Model	The negative gradient in the deeper mixed layer of the GDEM profile where the source was located produced less down bending than the negative gradient of the thermoclines of the MODAS profiles, thus forming weaker caustics and decreasing the detection range of moored mines.
3. Prevalence of Problems, if any, in the Yellow Sea or the North East China Sea	Not a prevalent problem.

a.

MODAS versus GDEM	
November/ Mud Bottom	
1. Oceanographic Difference between MODAS and MOODS	1. The first difference was due to a surface duct that was present in the GDEM profile and not in the MODAS profile when source depth was at 25 ft. 2. At a source depth of 125 ft., the difference was due to a weaker thermocline gradient in the GDEM profile.
2. How this affected the Acoustic Model	1. The surface ducts trapped sound propagation in a subsurface layer that produced greater detection ranges for moored mines. 2. The source depth was within the thermocline; the weaker thermocline gradients produced by the GDEM profile caused less down bending of sound propagation. This produced weaker caustics due to less focusing of sound propagation, which in turn causes an under prediction of moored mines.
3. Prevalence of Problems, if any, in the Yellow Sea or the North East China Sea	1. When there was a surface duct in both profiles, it was much stronger in the GDEM profile for most cases. 2. The weaker thermocline gradients were observed in almost all of the GDEM and MODAS profiles used in this study.

b.

Table 19. Description of Significant Acoustic Differences in Detection Ranges between MODAS and GDEM Profiles in a Mud Bottom region in a. August, and b. November.

MODAS versus GDEM	
February/ Sand Bottom	
1. Oceanographic Difference between MODAS and GDEM	NONE
2. How this affected the Acoustic Model	NA
3. Prevalence of Problems, if any, in the Yellow Sea or the North East China Sea	NA

a.

MODAS versus GDEM	
May/ Sand Bottom	
1. Oceanographic Difference between MODAS and GDEM	At a source depth of 25 ft., the difference was due to a weaker thermocline gradient in the GDEM profile.
2. How this affected the Acoustic Model	The source depth was within the thermocline; the weaker thermocline gradients produced by the GDEM profile caused less down bending of sound propagation. These produced weaker caustics due to less focusing of sound propagation, which in turn causes a decreased in detection range for a moored mine.
3. Prevalence of Problems, if any, in the Yellow Sea or the North East China Sea	The weak thermocline gradients were observed in almost all of the GDEM and MODAS profiles used in this study.

b.

Table 20. Description of Significant Acoustic Differences in Detection Ranges between MODAS and GDEM Profiles in a Sand Bottom region in a. February, and b. May.

MODAS versus GDEM	
August/ Sand Bottom	
1. Oceanographic Difference between MODAS and MOODS	1. At a source depth of 25 ft., the difference was due to the MODAS profiles having a much shallower mixed layer depth and a negative gradient within the mixed layer of the GDEM profile. 2. At a source depth of 125 ft., the first difference was due to a presence of sub-layer in the MODAS profiles that was not present in the GDEM profile. 3. At a source depth of 125 ft., the second difference was due the source being located within a sub-layer that was present in the GDEM profiles but was not present in the MODAS profile.
2. How this affected the Acoustic Model	1. The negative gradient in the deeper mixed layer of the GDEM profile where the source was located produced less down bending than the stronger negative gradient of the thermoclines of the MODAS profiles. 2. Although the source was located above the sub-layer, it weakened the effect of thermocline gradient, which caused less down bending of sound propagation. This produced weaker caustics due to less focusing of sound propagation, which in turn caused an under prediction of moored mines. 3. The sub-layer trapped all sound propagation under the thermocline thus making sound propagation very limited by bottom reverberation.
3. Prevalence of Problems, if any, in the Yellow Sea or the North East China Sea	1. Possible problem since the mixed layers in most of the MODAS profiles were usually shallower than the GDEM profiles were. 2. Not a prevalent problem. 3. Not a prevalent problem.

a.

MODAS versus GDEM	
November/ Sand Bottom	
1. Oceanographic Difference between MODAS and GDEM	At a source depth of 125 ft., the difference was due to a weaker thermocline gradient in the MODAS profile.
2. How this affected the Acoustic Model	The source depth was within the thermocline; the weaker thermocline gradients produced by the MODAS profile caused less down bending of sound propagation. These produced weaker caustics due to less focusing of sound propagation, which in turn causes a decreased in detection range for a moored mine.
3. Prevalence of Problems, if any, in the Yellow Sea or the North East China Sea	The weaker thermocline gradients were observed in almost all of the GDEM and MODAS profiles used in this study.

b.

Table 21. Description of Significant Acoustic Differences in Detection Ranges between MODAS and GDEM Profiles in a Sand Bottom region in a. August, and b. November.

MODAS versus GDEM	
February/ Gravel Bottom	
1. Oceanographic Difference between MODAS and GDEM	None
2. How this affected the Acoustic Model	NA
3. Prevalence of Problems, if any, in the Yellow Sea or the North East China Sea	NA

a.

MODAS versus GDEM	
May/ Gravel Bottom	
1. Oceanographic Difference between MODAS and GDEM	At a source depth of 25 ft., the difference was due to a weaker thermocline gradient in the MODAS profile.
2. How this affected the Acoustic Model	The source depth was within the thermocline; the weaker thermocline gradients produced by the MODAS profile caused less down bending of sound propagation. This produced weaker caustics due to less focusing of sound propagation, which in turn causes a decreased in detection range for a moored mine.
3. Prevalence of Problems, if any, in the Yellow Sea or the North East China Sea	The weaker thermocline gradients were observed in almost all of the MODAS and GDEM profiles used in this study.

b.

Table 22. Description of Significant Acoustic Differences in Detection Ranges between MODAS and GDEM Profiles in a Gravel Bottom region in a. February, and b. May.

MODAS versus GDEM	
August/ Gravel Bottom	
1. Oceanographic Difference between MODAS and GDEM	1. At a source depth of 25 ft., the difference was due to a mixed layer that was present in the MODAS profile and not in the GDEM Profile. 2. At a source depth of 75 ft., the difference was due to a weaker thermocline gradient in the GDEM profile.
2. How this affected the Acoustic Model	1. The source depth was within the mixed layer; this caused less down bending of sound propagation. This produced weaker caustics due to less focusing of sound propagation, which in turn causes a decreased in detection range for a moored mine. 2. . In this scenario, the source was very close to the bottom. The down bending caused by stronger thermocline in the MODAS profiles caused sound propagation to become very limited by bottom reverberation, thus decreasing the detection range of a bottom mine.
3. Prevalence of Problems, if any, in the Yellow Sea or the North East China Sea	1. Not a prevalent problem. 2. The weaker thermocline gradients were observed in almost all of the GDEM and MODAS profiles used in this study.

a.

MODAS versus GDEM	
November/ Gravel Bottom	
1. Oceanographic Difference between MODAS and MOODS	At a source, depth of 125 ft., the difference was due to a thermocline that was present in the GDEM profiles and an isothermal structure of the MODAS profiles.
2. How this affected the Acoustic Model	In this scenario, the source was very close to the bottom. The down bending caused by the thermocline in the GDEM profile caused sound propagation to become very limited by bottom reverberation, thus decreasing the detection range of a bottom mine.
3. Prevalence of Problems, if any, in the Yellow Sea or the North East China Sea	Not a prevalent problem.

b.

Table 23. Description of Significant Acoustic Differences in Detection Ranges between MODAS and GDEM Profiles in a Gravel Bottom region in a. August, and b. November.

MODAS versus GDEM	
February/ Rock Bottom	
1. Oceanographic Difference between MODAS and GDEM	None
2. How this affected the Acoustic Model	NA
3. Prevalence of Problems, if any, in the Yellow Sea or the North East China Sea	NA

a.

MODAS versus GDEM	
May for Rock Bottom Type	
1. Oceanographic Difference between MODAS and MOODS	At a source depth of 125 ft., the difference was due to a stronger thermocline in the GDEM profile.
2. How this affected the Acoustic Model	In this scenario, the source was very close to the bottom. The down bending caused by the thermocline in the GDEM profile caused sound propagation to become very limited by bottom reverberation, thus decreasing the detection range of a bottom mine.
3. Prevalence of Problems, if any, in the Yellow Sea or the North East China Sea	The weaker thermocline gradients were observed in almost all of the GDEM and MODAS profiles used in this study.

b.

MODAS versus GDEM	
August/ Rock Bottom	
1. Oceanographic Difference between MODAS and GDEM	None
2. How this affected the Acoustic Model	NA
3. Prevalence of Problems, if any, in the Yellow Sea or the North East China Sea	NA

c.

MODAS versus GDEM	
November/ Rock Bottom	
1. Oceanographic Difference between MODAS and GDEM	None
2. How this affected the Acoustic Model	NA
3. Prevalence of Problems, if any, in the Yellow Sea or the North East China Sea	NA

d.

Table 24. Description of Significant Acoustic Differences in Detection Ranges between MODAS and GDEM Profiles in a Rock Bottom region in a. February, b. May, c. August, and d. November.

IX. ACOUSTIC UNCERTAINTY CAUSED BY HYDROGRAPHIC DATA UNCERTAINTY

A. GAUSSIAN-TYPE ERRORS IN SOUND SPEED DATA

In this final study, the sensitivity of the CASS/GRAM model to uncertainty by hydrographical uncertainty was analyzed. The uncertainty in the hydrographic data is in the form of small or large errors that may be present in the sound speed profiles possibly due to the accuracy of the instruments used to obtain the data, the expertise of the person obtaining the data, and in the case of MODAS, the accuracy of the algorithms in the model.

To simulate hydrographic data uncertainty, a MATLAB code was used to randomly enter a various range gaussian-type error into the MODAS sound speed profiles. The MATLAB code was written to allow the user to enter the desired size of the error to be entered into the sound speed profiles to be studied. For this study three sizes of errors, 1, 5, and 10 meters per second, were entered into the sound speed profiles and then inputted into the CASS/GRAB model. The regions selected for this study were mud and sand. The seasons chosen for this study were winter (February) and summer (August) to capture the effects of the error on the two main sound speed profile structures of the Yellow Sea.

B. CORRESPONDING ERRORS IN SIGNAL EXCESS

The CASS/GRAB model was run using the MODAS profiles with the three level of errors. The runs were performed for a source of 25 feet and 125 feet. The maximum detection ranges derived from the signal excess (SE) calculations of the model were

compared to those of the MODAS sound speed profile runs without error by taking the absolute deference of MODAS profiles without error and the corresponding MODAS profiles with error to determine if a significant acoustic difference existed. The results were that a significant acoustic difference was observed in all of the scenarios for both bottom types, with the exception of the scenarios of a 25 feet source depth and bottom target, and a 125 feet source depth and a 26 feet target depth in the mud region during the summer.

The winter scenarios for both regions had the most cases of significant acoustic differences and the largest significant acoustic differences. Histograms of all the scenarios were generated to show the distribution of the differences in detection ranges throughout the entire water column (Appendix D). The distribution of the differences in detection ranges in the histograms demonstrated that differences in detection ranges were much larger during winter than summer (Figures 53 and 54). This indicates that the isothermal structure of the winter profiles is much more susceptible to errors in sound speed.

There was no pattern of the significant acoustic differences increasing with an increased amount of gaussian-error entered into the profiles. The differences depend on where the random error is situated in the water column in relation to the position of the source. For a specific profile, if an error of 1 m/s is positioned within approximately 5 feet of the source depth and an error of 10 m/s is positioned greater than the 5 feet of the source depth, the 1 m/s error will have a much greater effect on the acoustic transmission. If the error near the source is positive, the gradient that is formed in the sound speed

Target Depth	FEBRUARY /SOURCE DEPTH = 25 FT.					
	Mud			Sand		
	Error (m/s)			Error (m/s)		
	1	5	10	1	5	10
26 ft	Lt35.4N Ln124.4E **735 yd**	Lt35.4N Ln124.4E **735 yd**	Lt35.4N Ln124.4E **735 yd**	Lt36.3N Ln125.0E **845 yd**	Lt36.3N Ln125.0E **845 yd**	Lt36.3N Ln125.0E **845 yd**
Bottom	None	Lt35.4N Ln124.4E **1000 yd**	Lt35.0N Ln123.5E **990 yd**	None	None	Lt35.9NLn124.6E **665 yd**

a.

Target Depth	FEBRUARY /SOURCE DEPTH = 125 FT.					
	Mud			Sand		
	Error (m/s)			Error (m/s)		
	1	5	10	1	5	10
26 ft	Lt35. 0N Ln123.5E **390 yd**	Lt36.4N Ln124.4E **885 yd**	Lt35.9N Ln124.4E **885 yd**	None	Lt35.9N Ln125.9E **390 yd**	Lt35.9N Ln124.6E **565 yd**
Bottom	Lt36.4N Ln124.4E **1000 yd**	Lt35.1N Ln124.3E **875 yd**	Lt35.4N Ln124.4E **1000 yd**	Lt36.4N Ln124.6E **115 yd**	Lt 5.9N Ln125.9E **320 yd**	Lt36.4N Ln124.6E **210 yd**

b.

Target Depth	AUGUST /SOURCE DEPTH = 25 FT.					
	Mud			Sand		
	Error (m/s)			Error (m/s)		
	1	5	10	1	5	10
26 ft	Lt35.4N Ln124.4E **550 yd**	Lt35.4N Ln124.4E **560 yd**	Lt35.4N Ln 24.4E **600 yd**	Lt36.4N Ln125.9E **810 yd**	Lt36.4N Ln125.9E **785 yd**	None
Bottom	None	None	None	None	Lt35.9N Ln124.6E **590 yd**	None

c.

Target Depth	AUGUST /SOURCE DEPTH = 125 FT.					
	Mud			Sand		
	Error (m/s)			Error (m/s)		
	1	5	10	1	5	10
26 ft	None	None	None	Lt36.4N Ln124.4E **530 yd**	Lt36.4N Ln124.6E **440 yd**	Lt36.4N Ln124.4E **380 yd**
Bottom	None	Lt36.4N Ln124.4E **595 yd**	None	Lt36.4N Ln124.6E **340 yd**	Lt36.4N Ln124.6E **375 yd**	Lt36.4N Ln124.6E **755 yd**

d.

Table 25. Maximum Significant Acoustic Differences in Detection Ranges for MODAS versus MODAS with Gaussian Error in Sound Speed for Mud and Sand Bottom in a. February/ Source Depth = 25 feet, b. February/ Source Depth = 125 feet, c. August / Source Depth = 25 feet, d. August/ Source Depth = 125 feet.

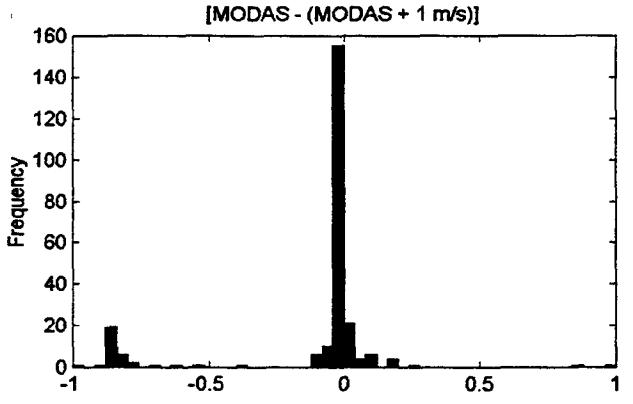

a.

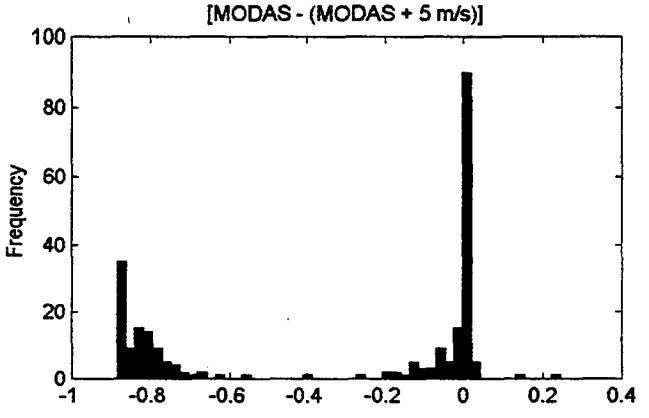

b.

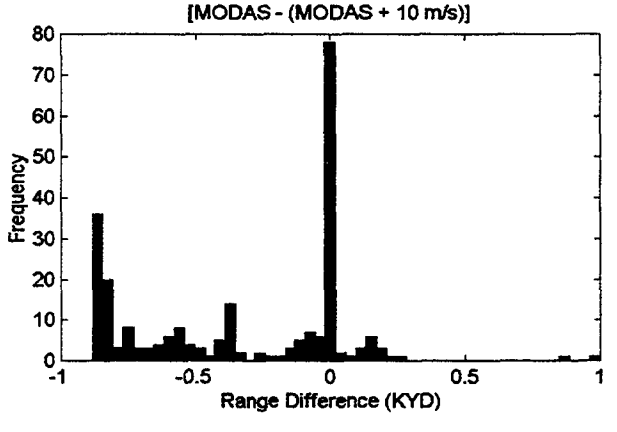

c.

Figure 53. Histograms of the Acoustic Difference Distribution throughout the Water Column for February 15, 2000, Mud Bottom and 125 ft source depth. a. MODAS minus MODAS with 1 m/s error, b. MODAS minus MODAS with 5 m/s error, c. MODAS minus MODAS with 10 m/s error.

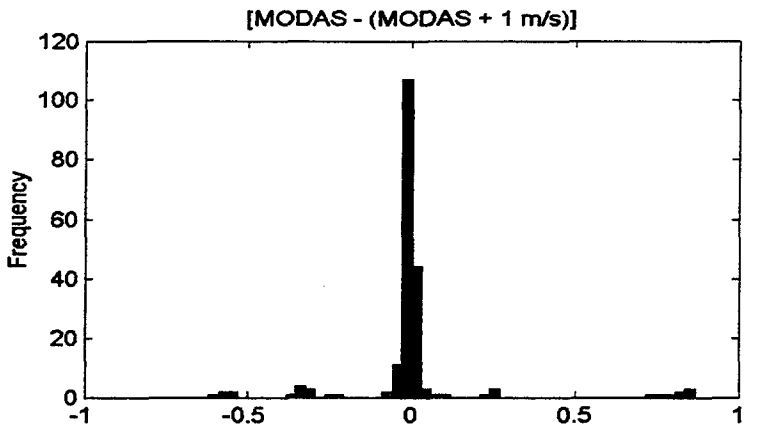

a.

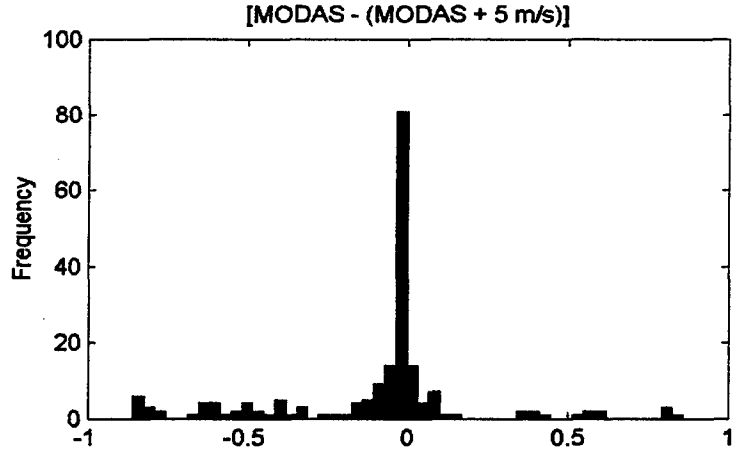

b.

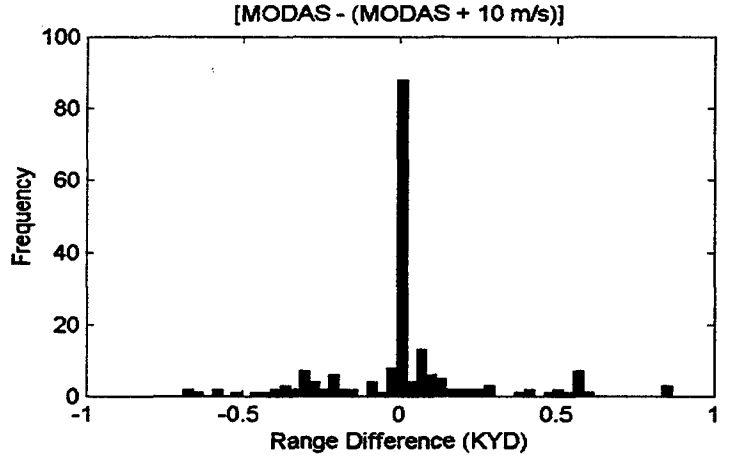

c.

Figure 54. Histograms of the Acoustic Difference Distribution throughout the Water Column for August 15, 2000, Mud Bottom and 125 ft source depth. a. MODAS minus MODAS with 1 m/s error, b. MODAS minus MODAS with 5 m/s error, c. MODAS minus MODAS with 10 m/s error.

profile will decrease detection ranges. If the error is negative, the gradient that is formed in the sound speed profile will increase detection ranges.

The results of the CASS/GRAB model with isothermal sound speed profiles demonstrated that the model was sensitive to decreases in the sound speed profile near the source depth, as small 0.1 m/s in some cases. In Table 22, a decrease in the MODAS sound speed profile of 0.2 m/s between 0 and 8.2 ft and 0.1 m/s between 24.6 and 57.4 ft created a small gradient that was not present in a corresponding MOODS sound speed profile. The CASS/GRAB model's response to this gradient was the generation of a weak sound channel (Figure 55) that was significant enough to create a large acoustic difference between the two data sets.

In order to further illustrate the sensitivity of the CASS/GRAB model to small sound speed errors near the source, +/- 1 m/s errors were manually entered into the MODAS sound speed profile of Table 22 at the source depths of 25 ft. and 125 ft. When a +1 m/s error was entered at both source depths, a shadow zone was formed in front of the source that significantly decreased the detection ranges at that depth, and when a −1m/s error was entered at both source depths, a strong sound channel formed that dramatically increased detection ranges at that depth (Figures 55-60).

In conclusion, the CASS/GRAB sensitivity to error in sound speed profiles was very dependent on the location of that error in relation to the source. In addition, CASS/GRAB is more sensitive to errors in the isothermal structure of the sound speed profiles characteristic of the winter months. This sensitivity was due to the introduction of either a positive or negative sound speed gradient by the error to a linear sound speed structure.

MODAS FEBRUARY 15, 1999, LAT 36.4 N LON 124.4 E, MUD BOTTOM

SOUND SPEED TABLE	
Depth (Feet)	M/S
0.00	1479.90
8.20	**1479.70**
24.60	**1479.80**
41.00	**1479.80**
57.40	1480.00
82.00	1480.00
106.60	1480.10
131.20	1480.30
164.00	1480.50
205.00	1480.40
246.00	1480.40

a.

MOODS FEBRUARY 23, 1970, LAT 36.4 N LON 124.4 E, MUD BOTTOM

SOUND SPEED TABLE	
Depth (M)	M/S
0.00	1468.50
32.80	**1468.70**
65.60	1468.80
98.40	1469.00
164.00	1469.40
246.00	1470.10

b.

Table 26. Comparison of MODAS and MOODS Sound Speed Tables. The small difference in Sound Speed Gradient is labeled in red. a. MODAS Sound Speed Table, b. MOODS Sound Speed Table.

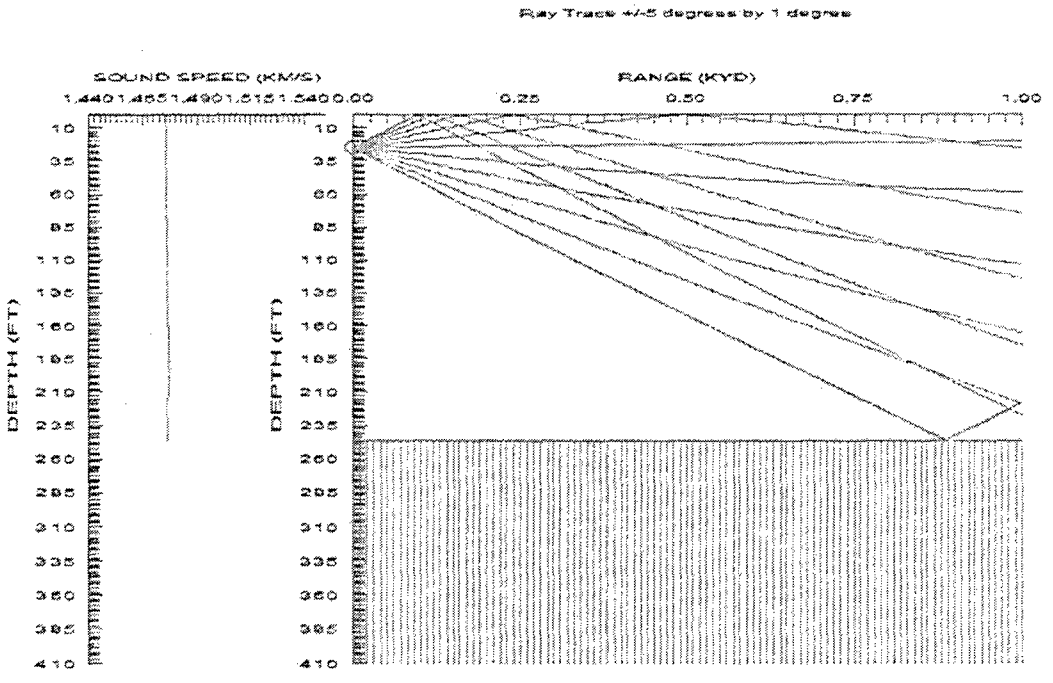

a.

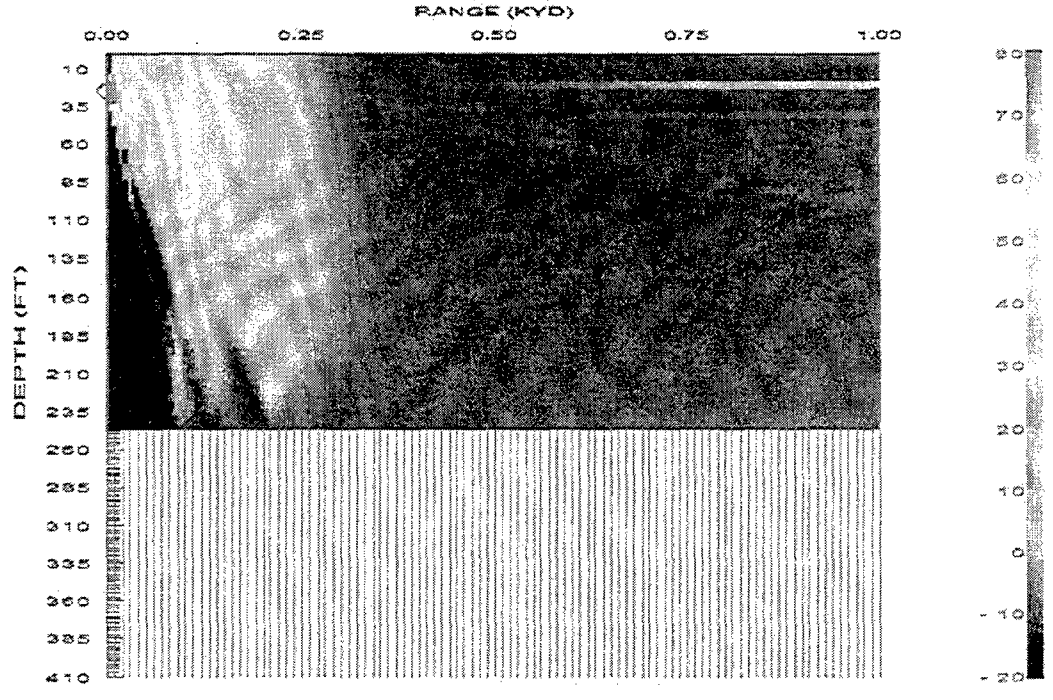

b.

Figure 55. MODAS without error for February 15, 2000, 36.4 N 124.4 E, Mud Bottom, and Source Depth =25 ft. a. Ray Trace, b. Signal Excess Contour Plot (Max Detection Range at Source Depth = 260 yd).

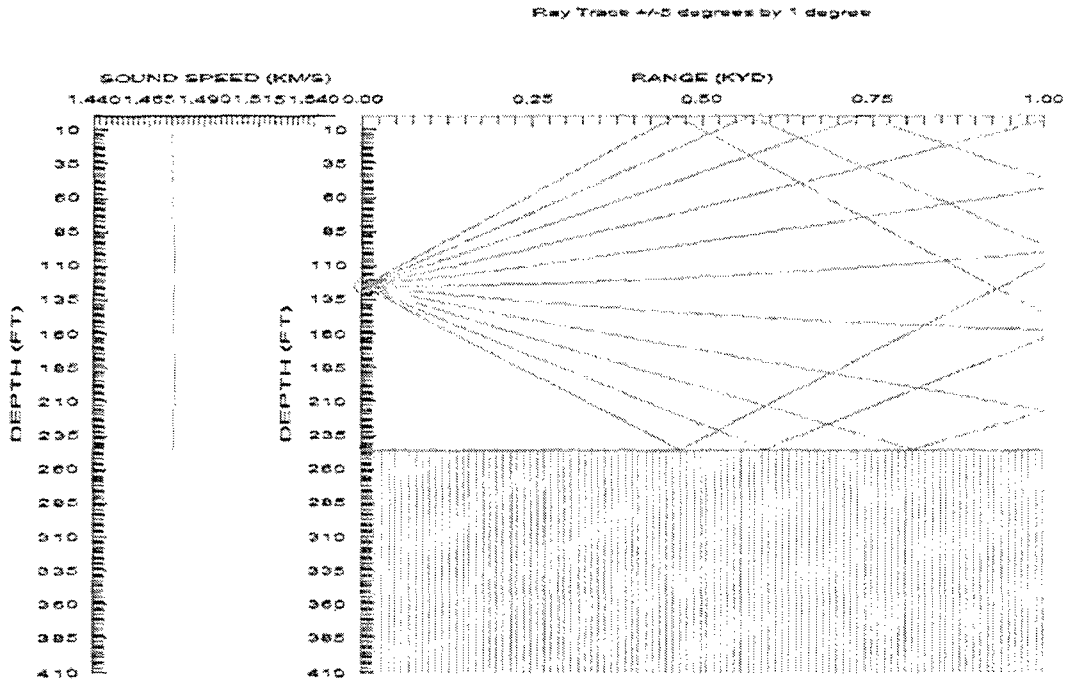

a.

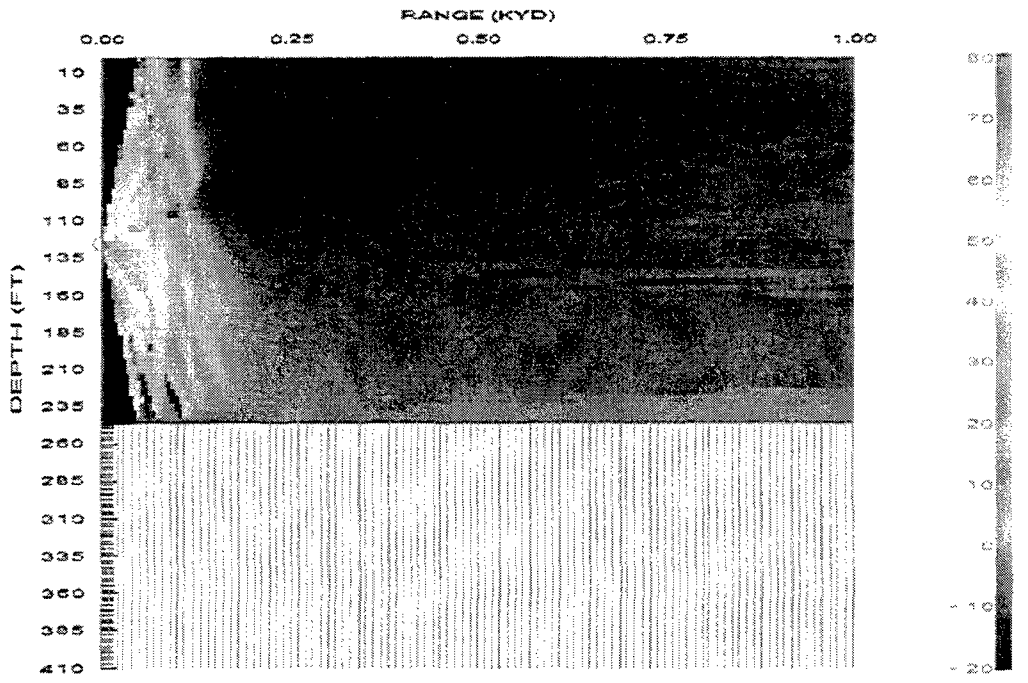

b.

Figure 56. MODAS without error for February 15, 2000, 36.4 N 124.4 E, Mud Bottom, and Source Depth =125 ft. a. Ray Trace, b. Signal Excess Contour Plot (Max Detection Range at Source Depth = 145 yd).

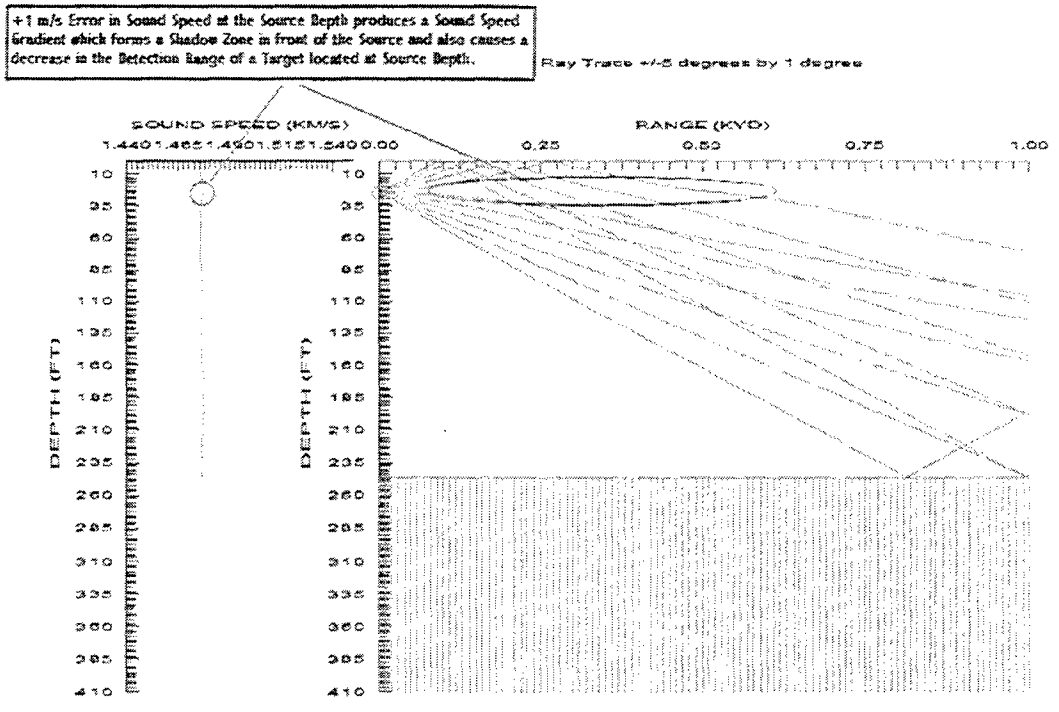

a.

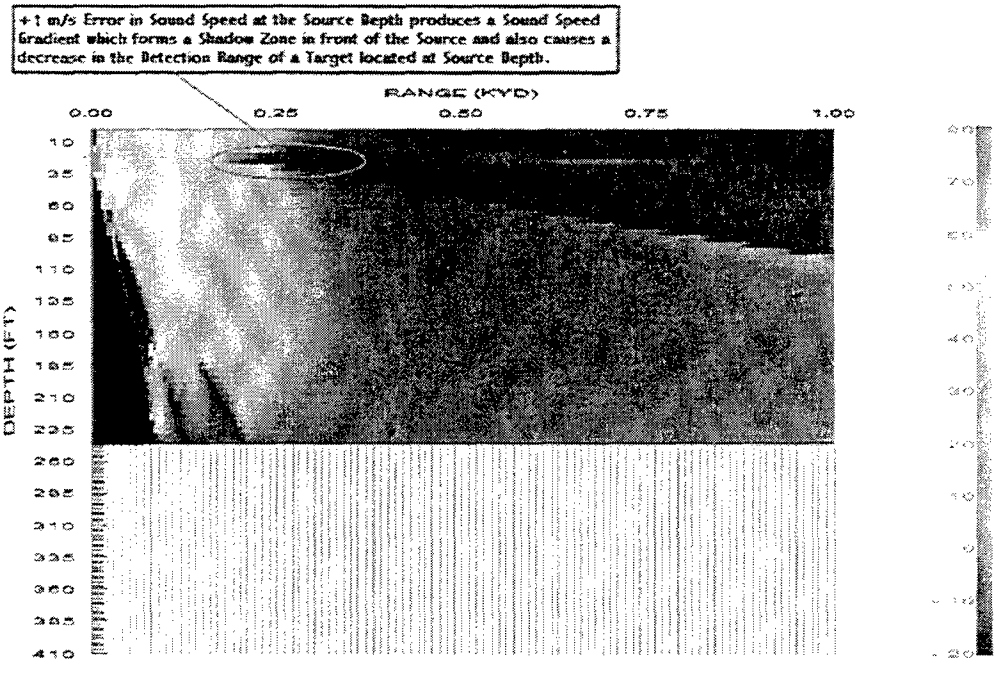

b.

Figure 57. MODAS with +1 m/s Sound Speed error at Source Depth for February 15, 2000, 36.4 N 124.4 E, Mud Bottom, and Source Depth =25 ft. a. Ray Trace. b. Signal Excess Contour Plot (Max Detection Range at Source Depth = 175 yd, Δ Max Detection Range at Source Depth = 85 yd).

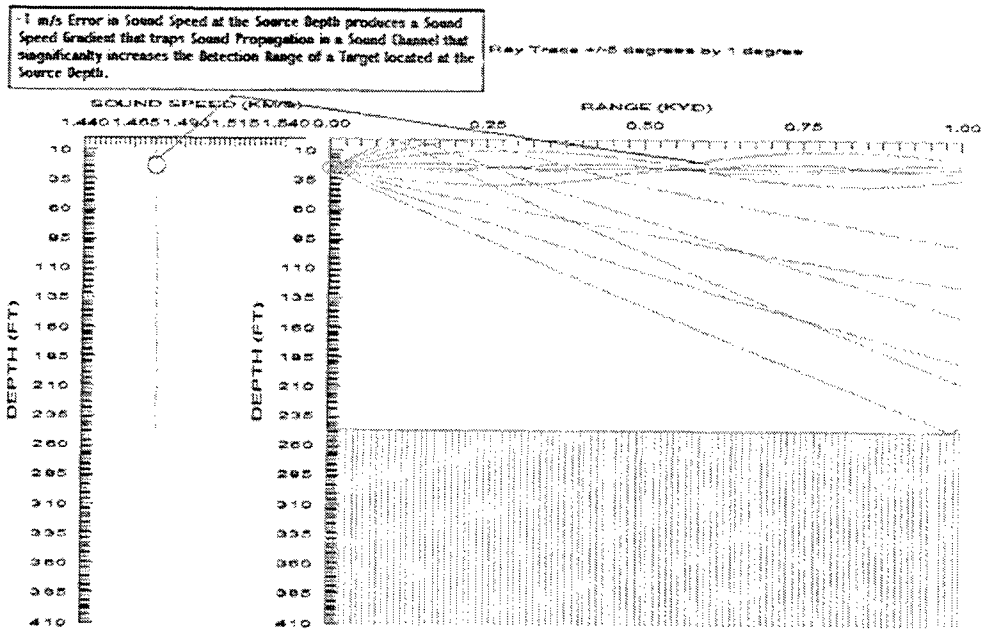

a.

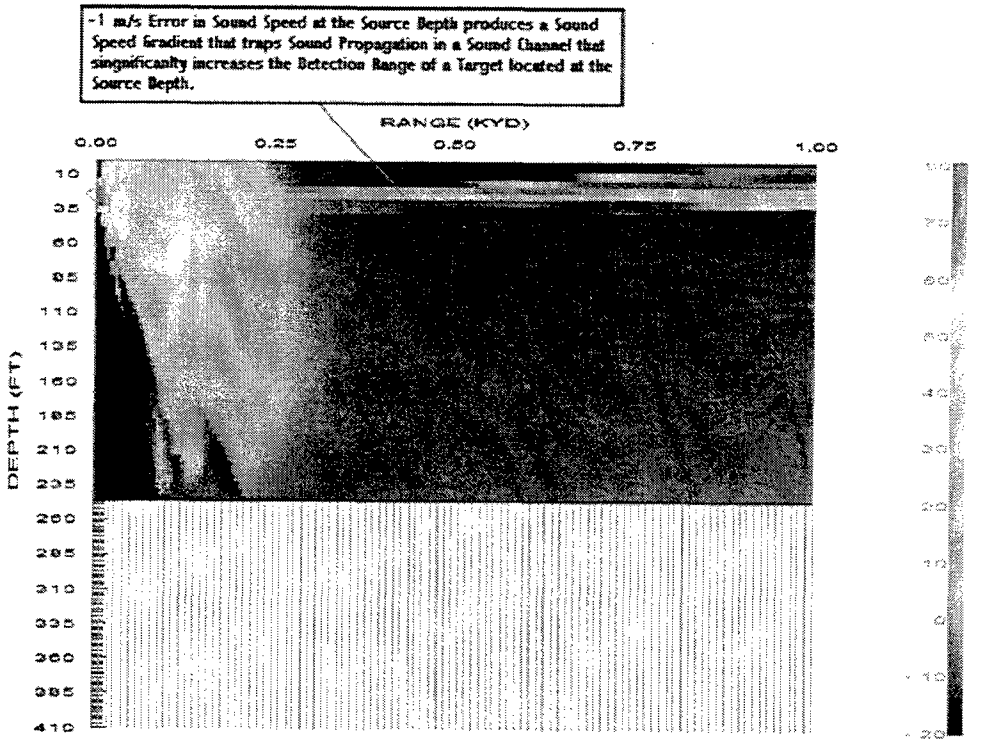

b.

Figure 58. MODAS with -1 m/s Sound Speed error at Source Depth for February 15, 2000, 36.4 N 124.4 E, Mud Bottom, and Source Depth =25 ft. a. Ray Trace, b. Signal Excess Contour Plot (Max Detection Range at Source Depth >1000 yd, Δ Max Detection Range at Source Depth >740 yd).

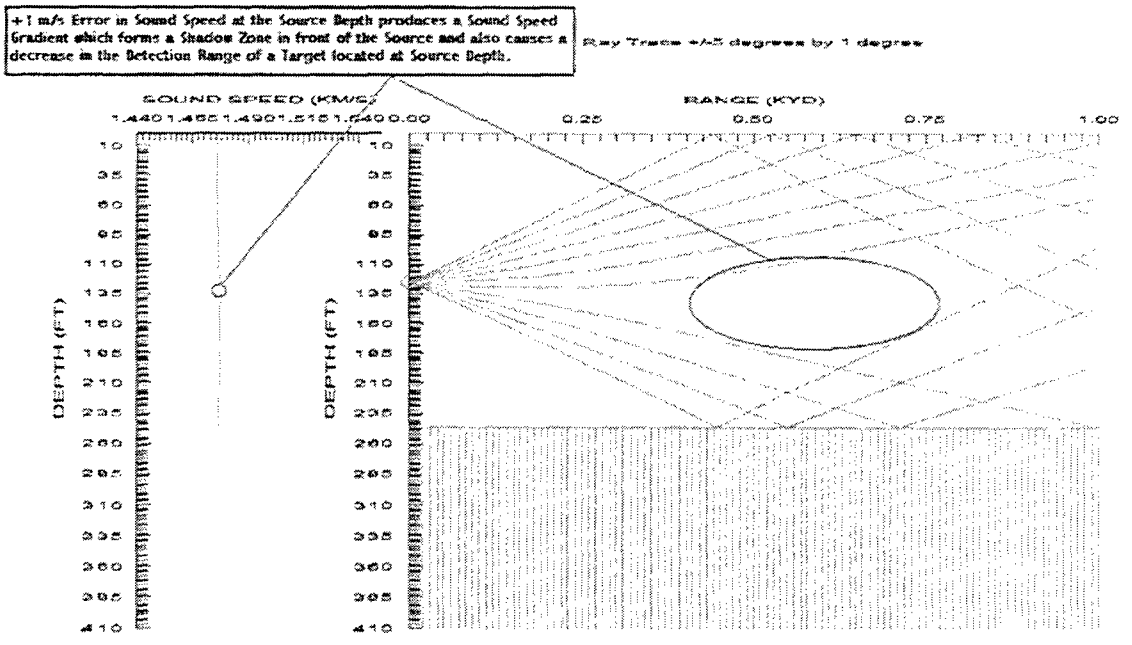

a.

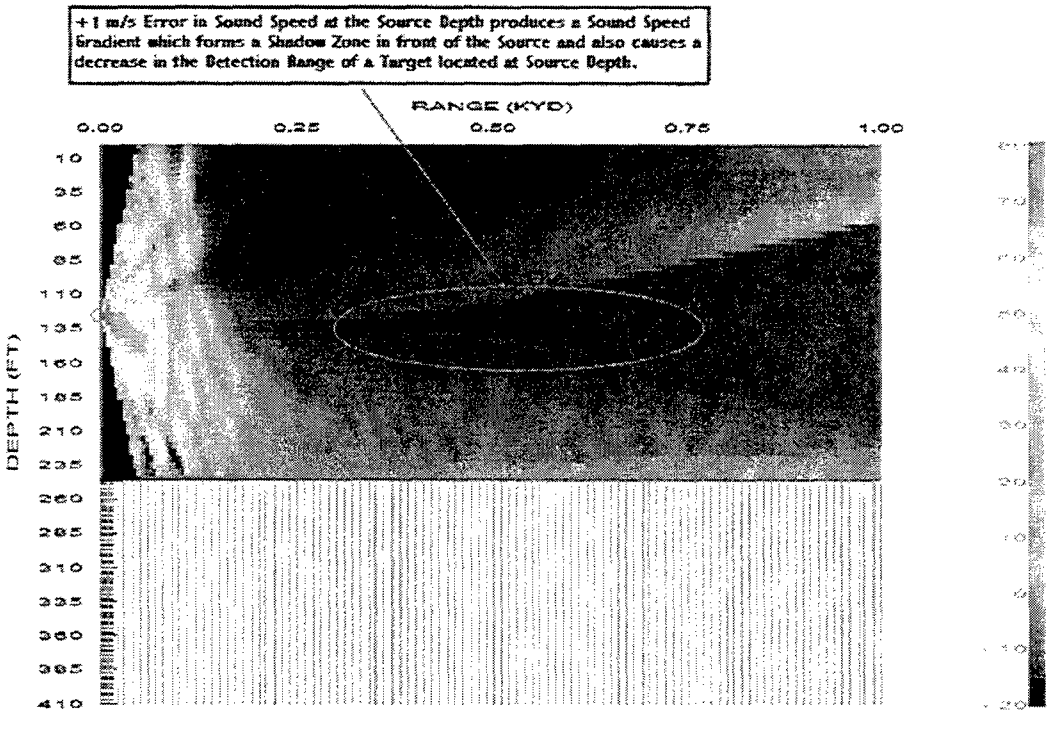

b.

Figure 59. MODAS with +1 m/s Sound Speed error at Source Depth for February 15, 2000, 36.4 N 124.4 E, Mud Bottom, and Source Depth =125 ft. a. Ray Trace, b. Signal Excess Contour Plot (Max Detection Range at Source Depth = 150 yd, Δ Max Detection Range at Source Depth = 5 yd).

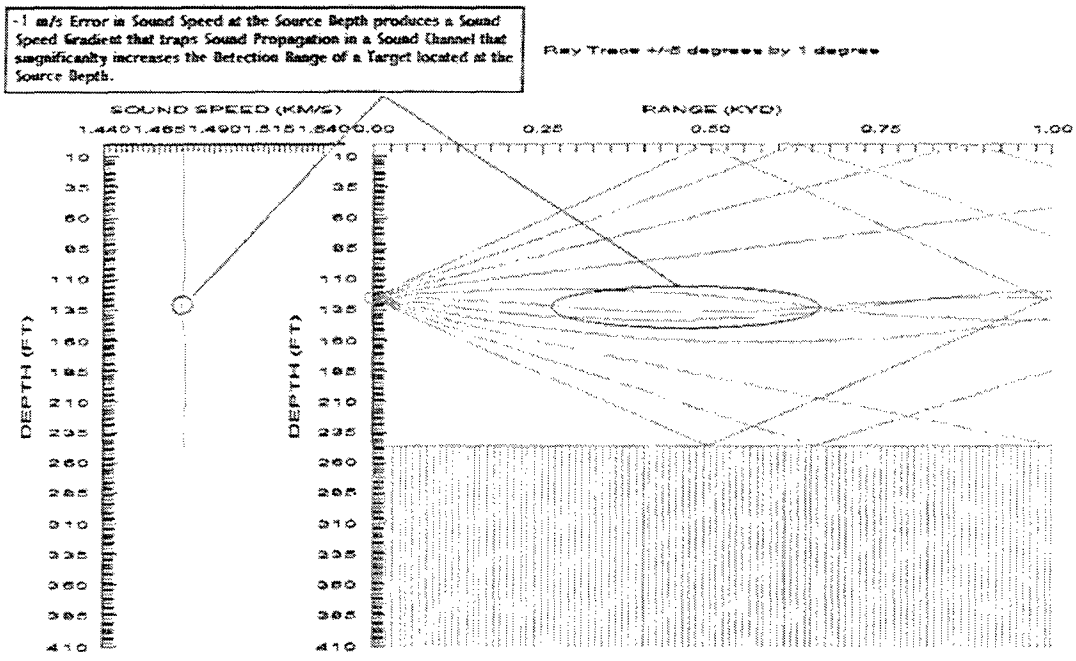

a.

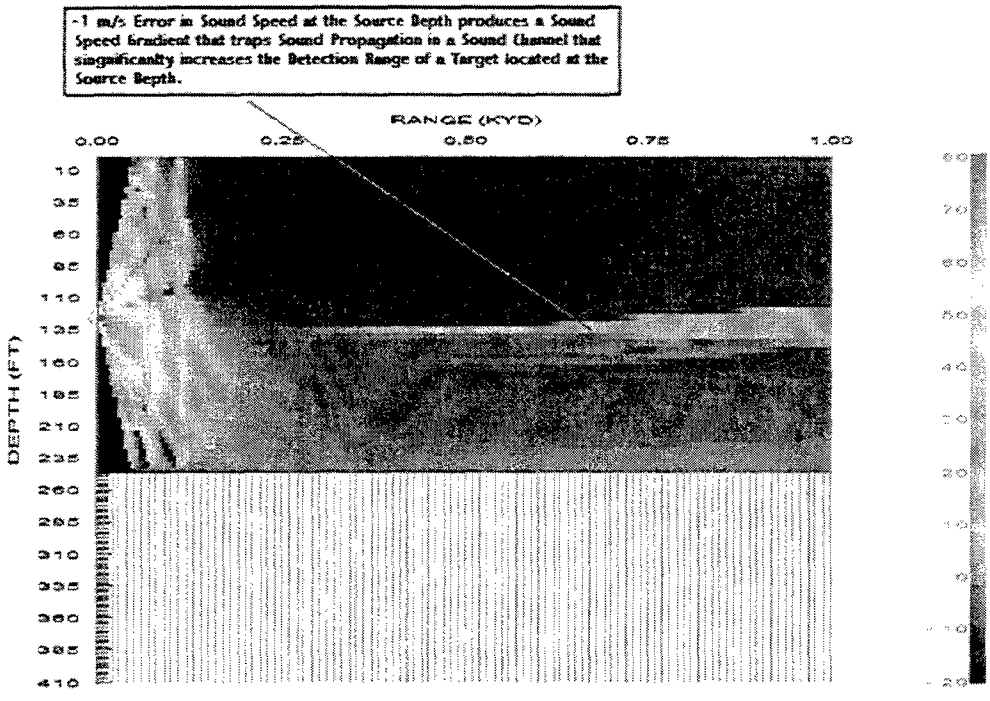

b.

Figure 60. MODAS with -1 m/s Sound Speed error at Source Depth for February 15, 2000, 36.4 N 124.4 E, Mud Bottom, and Source Depth =125 ft. a. Ray Trace, b. Signal Excess Contour Plot (Max Detection Range at Source Depth >1000 yd, Δ Max Detection Range at Source Depth >855 yd).

THIS PAGE INTENTIONALLY LEFT BLANK

X. CONCLUSION

In this study, the seasonal variation in acoustic transmission in the Yellow Sea for all regions was mainly due to the isothermal structure in the winter and a multi-layer thermal structure in the summer. The acoustic transmission in the winter is shorter due to the effect of the isothermal structure of the sound speed profile, thus detection ranges are shorter. The acoustic transmission in the summer is significantly longer due to the down bending effects of the multi-layer structure of the sound speed profiles, which produce convergence zone and caustics.

Although the MODAS model captured the effects on the SST temperature by the tropical depression in July and the cold front in January, a significant acoustic difference was only observed in one of the profiles in July and none in none of the profiles for January weather event. The entire MODAS temperature and sound speed profiles were shifted to the left with a decrease in temperature. This did not affect acoustic transmission since acoustic transmission is not significantly effected by the positive or negative shifting of the entire profile. The significant changes in acoustic transmission arise when a change in the gradients of the sound speed profiles occur, which may be caused by the change in the mixed layer depth, presence of a surface duct, the gradient of the thermocline, etc. With the cold air mass and strong winds that are characteristic of a tropical depression and to a less extent a strong cold front, there should have been some occurrences where there was change in the mixed layer depth thermocline gradient. Since the MODAS model operates without remote SSH data in shallow water, the model may not be able to capture the effects weather has on the mixed layer depth or the

thermocline gradient, which in turn cause the under prediction of the effects of weather events in a shallow water region.

When MODAS profile outputs form the CASS/GRAB model was compared with those of MOODS and GDEM there was many cases of significant acoustic difference between the two pairs of data sets especially during the spring and summer months in the regions of sand and mud bottoms. In both cases, there were cases where differences could have occurred due to weather events reflected by MODAS, but in the comparisons with MOODS, there were cases that differences may have occurred due to limitations of the MODAS climatology. Since both MODAS and the GDEM profiles both demonstrated some of the same limitations like the weakening thermocline gradients, most of the differences appeared to be weather events reflected by the MODAS model.

Since there is a significant effect to acoustic transmission by environmental factors as demonstrated by the seasonal variability and the hydrographical data set comparisons, the conclusion is that there is a need for a predictive modeling capability such as MODAS to address the MIW needs in the Yellow Sea region. Although MODAS is the best model available at this time to meet the MIW needs, the model demonstrated some limitations in the Yellow Sea. In many cases the MODAS profile did a good job in producing profiles that reflected changes in the climate, but for the reasons stated earlier it sometimes under predicted the effects of the changes in the climate. There were also problems with inaccurate profiles that related to the limitations of the MODAS climatology.

The most significant problem with the climatology that generated an acoustic difference was detected in the winter months in the southern region of the Yellow Sea.

Many of the MODAS temperature and sound speed profiles had near bottom positive gradients below an isothermal layer, which was not observed in NIDAS for any of the MOODS profiles in the Yellow Sea regions studied. This downward positive gradient in MODAS caused an under prediction in detection ranges for Bottom mines due to the up bending of sound propagation near the sea bottom. In the case of a near surface volume mine (moored mine), this up bending produced less bottom reverberation, thus causing an over prediction of the detection ranges of these mines. Since this near bottom downward positive gradient was present in both the 1999 and 2000 MODAS profiles used, the cause may be due to the sparseness of observational data along the shelf located between the southern Yellow Sea and the northern East China Sea for use in developing the MODAS climatology. Since the MODAS climatology data sets were not available for analysis during this study, this conclusion is speculation.

Another problem that was a major source of significant acoustic difference was observed in the summer months. Although MODAS profiles did capture surface ducts in the mixed layer, they were much weaker than expected, and much weaker than those observed in most of the MOODS profiles. The weaker surface duct caused an under prediction of moored mines when the source was at hull depth. In many cases, MODAS tended to weaken the thermocline gradient found in many of the MOODS profiles during the summer months. This weakening of the thermocline gradient produces less down bending of sound propagation. This in turn produces less focusing of sound propagation, which translates into the under prediction of detection ranges.

The CASS/GRAB sensitivity to error in sound speed profiles was very dependent on the location of that error in relation to the source. In addition, CASS/GRAB is more

sensitive to errors in the isothermal structure of the sound speed profiles characteristic of the winter months. This sensitivity was due to the introduction of either a positive or negative sound speed gradient by the error to a linear sound speed structure.

NAVOCEANO has been working with numerical ocean models to fix the problems with MODAS altimeter SSH data input in shallow water region. They hope to implement this SSH correction into the MODAS within the next couple of years. In addition, NAVOCEANO is developing a new MODAS climatology that will correct some of the problems in climatology that were mentioned earlier. These new improvements into the MODAS model will show a significant improvement to the models performance in shallow waters regions thus increasing the utility of the model for MIW applications in shallow water.

Suggested future work in studying the environmental effects on mine hunting in the Yellow Sea using the CASS/GRAB model are as follows: 1. Comparing the MODAS climatological profiles (Static MODAS) with the corresponding synthetic MODAS profiles (Dynamic MODAS), 2. Comparing recent XBTs with corresponding synthetic MODAS profiles, and 3. Performing various studies with Bathymetry data entered into the CASS/GRAB model.

APPENDIX A. MODAS AND MOODS RAY TRACES

Mud Bottom/ February/ 35.0 N 123.5 E/ Source Depth = 25 ft/ a. MODAS 1999, b. MODAS 2000, c. MOODS

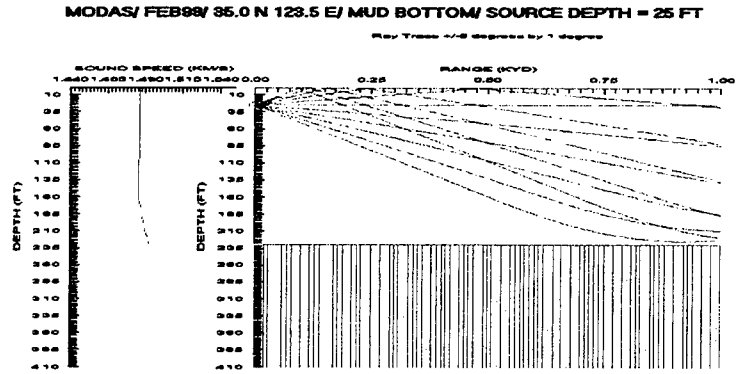

a. Maximum Detection Range (DR) for a 26 ft. Target Depth >1000 yd ΔDR >760 yd

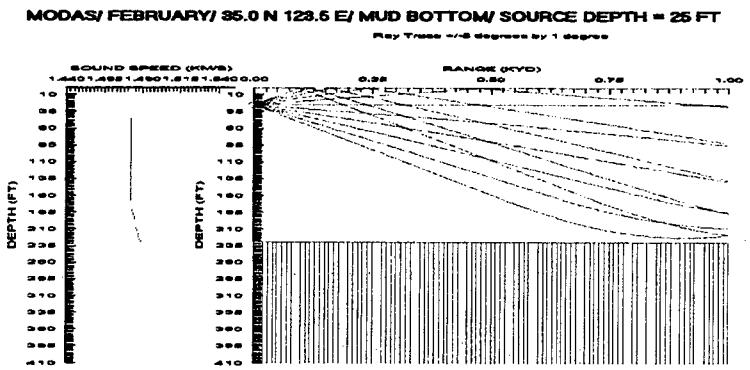

b. Maximum Detection Range for a 26 ft. Target Depth > 1000 yd ΔDR >760 yd

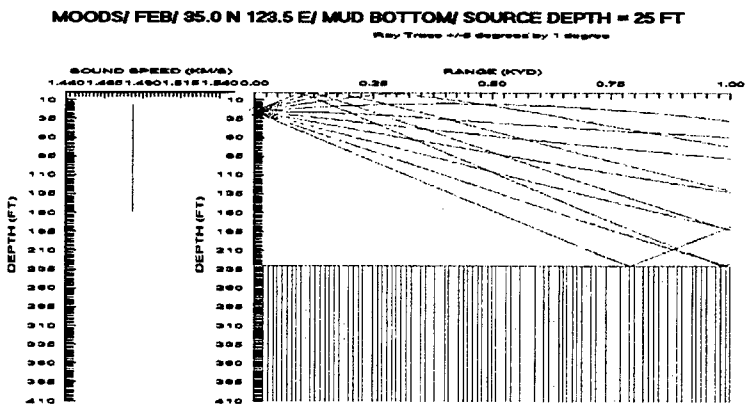

c. Maximum Detection Range for a 26 ft. Target Depth = 240 yd

Mud Bottom/ May/ 35.0 N 123.0 E/ Source Depth = 25 ft/ a. MODAS 1999, b. MODAS 2000, c. MOODS

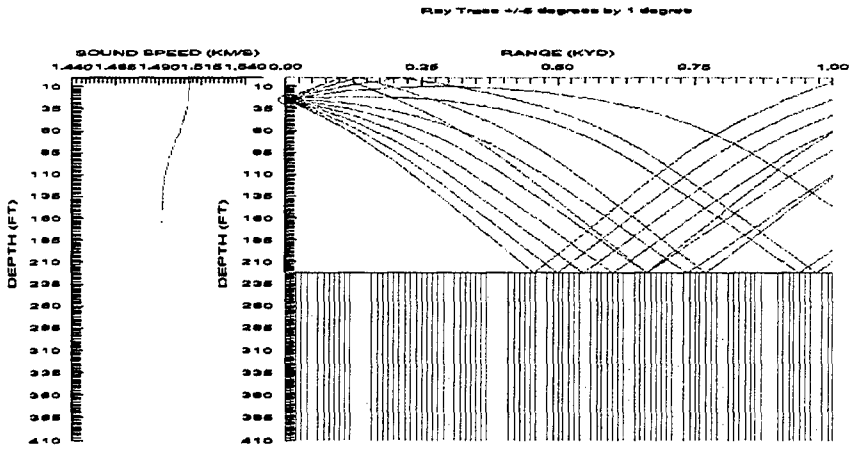

a. Maximum Detection Range (DR) for a 26 ft. Target Depth = 205 yd ΔDR >795 yd

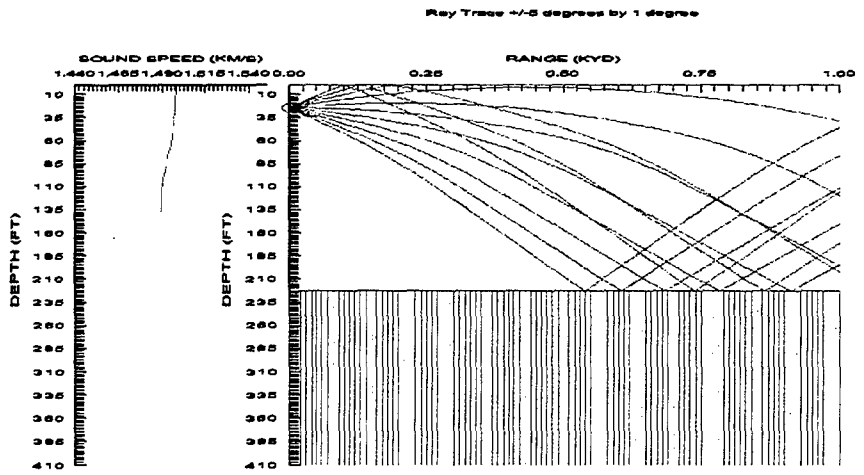

b. Maximum Detection Range (DR) for a 26 ft. Target Depth = 220 yd, ΔDR >780 yd

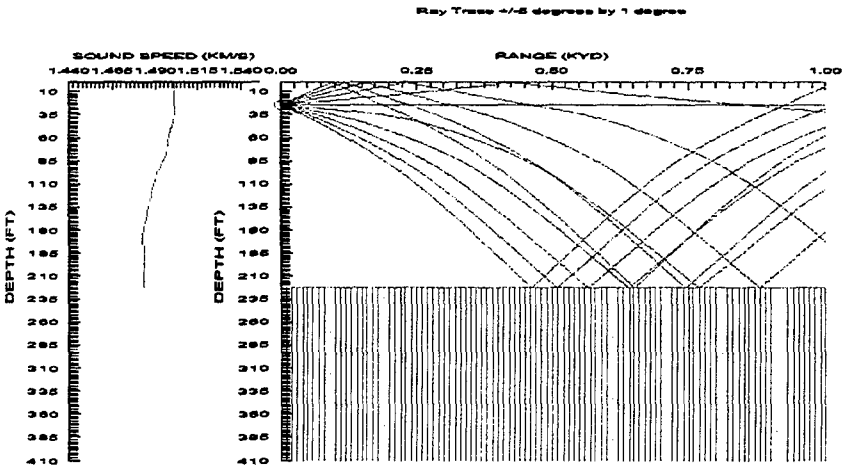

c. Maximum Detection Range (DR) for a 26 ft. Target Depth >1000 yd

Mud Bottom/ August/ 35.9 N 124.4 E/ Source Depth = 25 ft/ a. MODAS 1999, b. MODAS 2000, c. MOODS

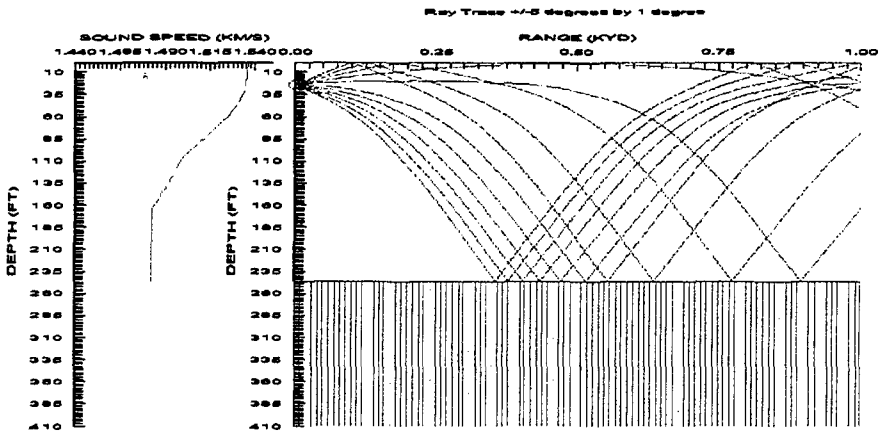

a. **Maximum Detection Range (DR) for a 26 ft. Target Depth = 765 yd, ΔDR = 545 yd**

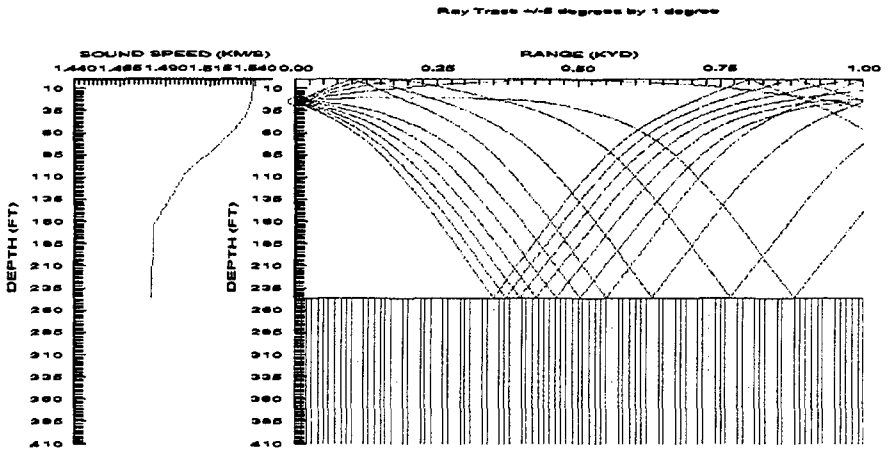

b. **Maximum Detection Range (DR) for a 26 ft. Target Depth = 755 yd, ΔDR = 535 yd**

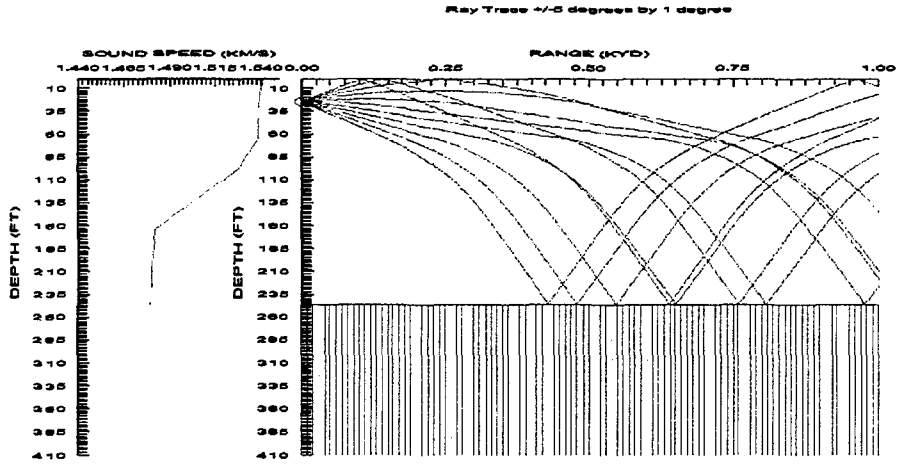

c. **Maximum Detection Range (DR) for a 26 ft. Target Depth = 220 yd**

Mud Bottom/ November/ 36.5 N 123.0 E/ Source Depth = 25 ft/ a. MODAS 1999, b. MODAS 2000, c. MOODS

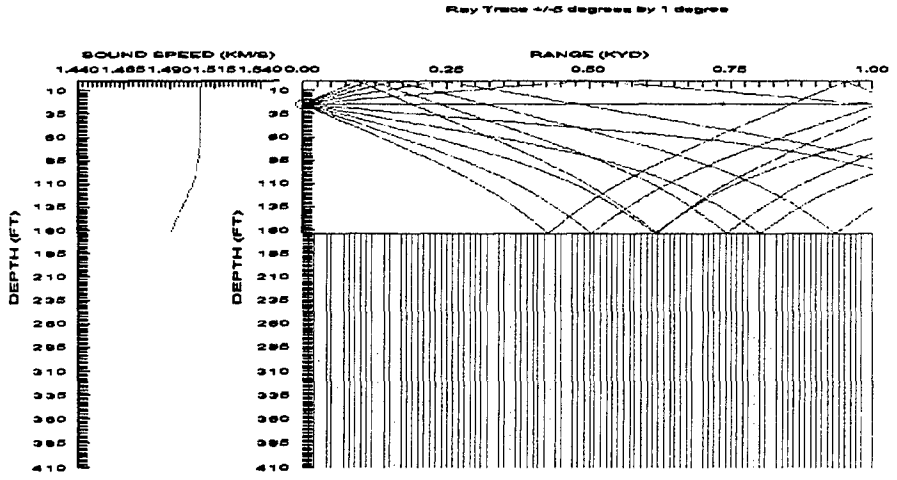

a. **Maximum Detection Range (DR) for a 26 ft. Target Depth = 160 yd, ΔDR >840 yd**

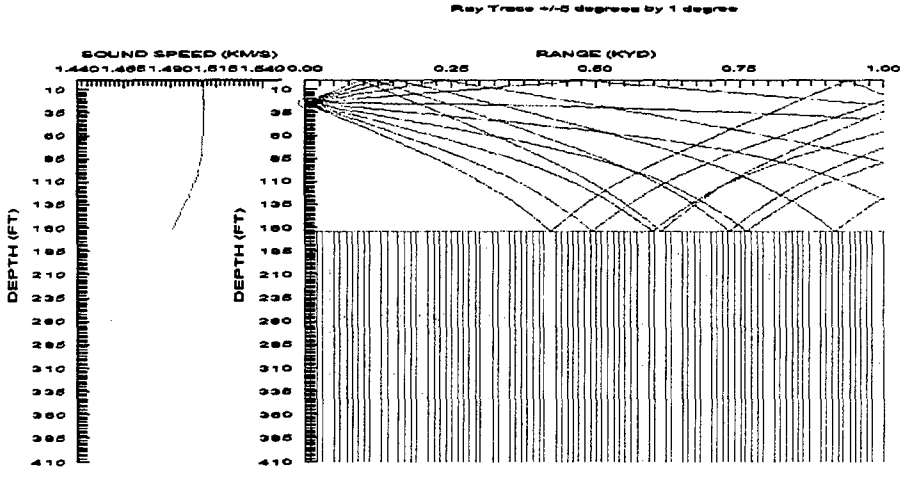

b. **Maximum Detection Range (DR) for a 26 ft. Target Depth = 160 yd, ΔDR >840 yd**

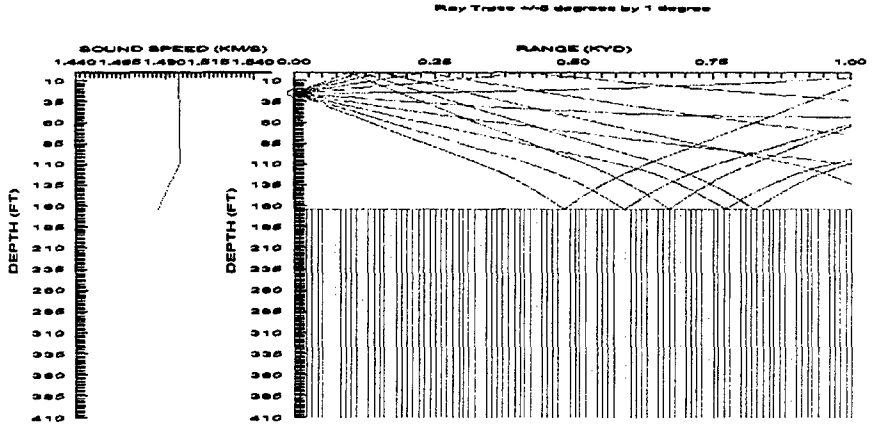

c. **Maximum Detection Range (DR) for a 26 ft. Target Depth > 1000 yd**

Sand Bottom/ February/ 35.9 N 125.8 E/ Source Depth = 25 ft/ a. MODAS 1999, b. MODAS 2000, c. MOODS

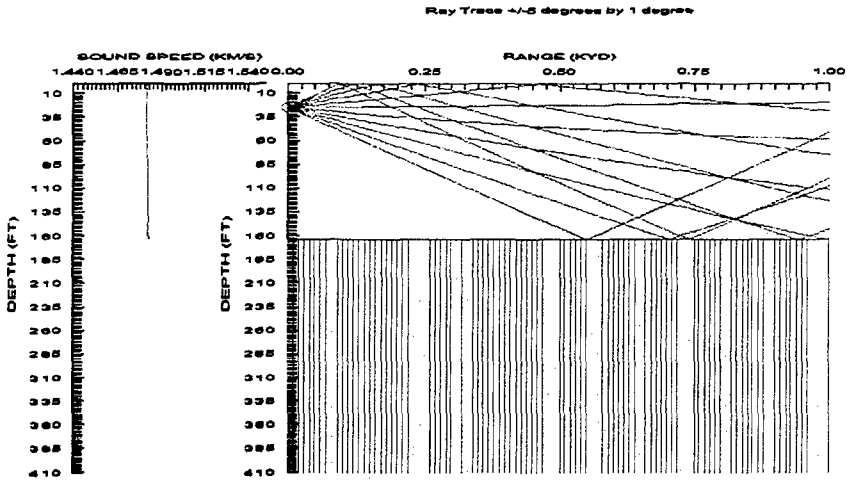

a. **Maximum Detection Range (DR) for a 26 ft. Target Depth = 155 yd, ΔDR = 840 yd**

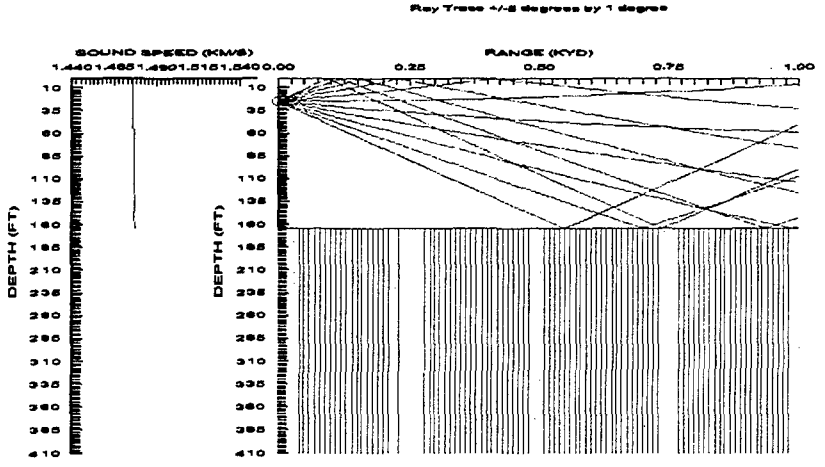

b. **Maximum Detection Range (DR) for a 26 ft. Target Depth = 155 yd, ΔDR = 840 yd**

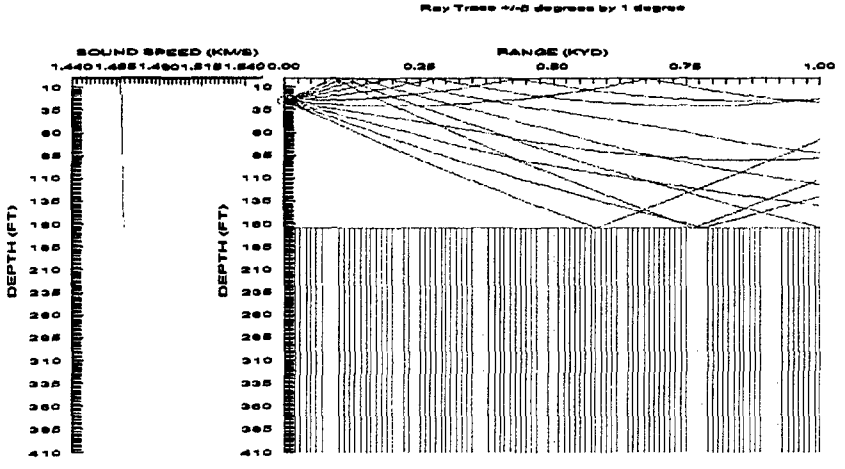

c. **Maximum Detection Range (DR) for a 26 ft. Target Depth = 995 yd**

Sand Bottom/ May/ 35.9 N 126.0 E/ Source Depth = 25 ft/ a. MODAS 1999, b. MODAS 2000, c. MOODS

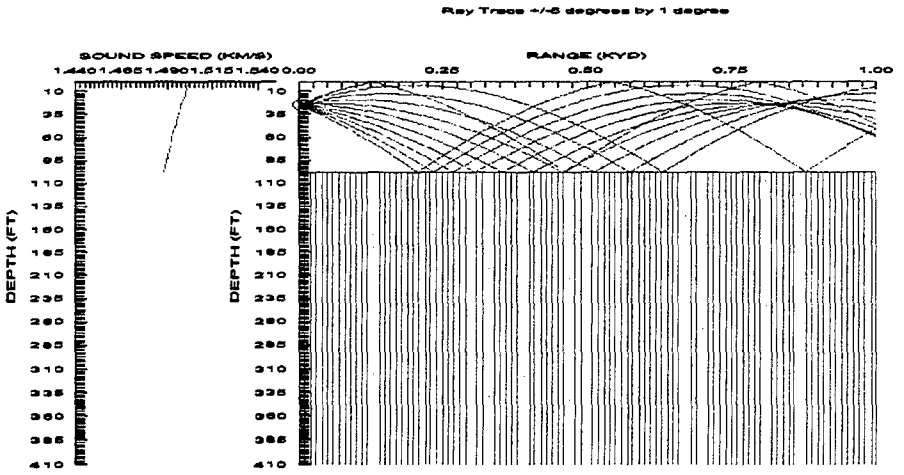

a. **Maximum Detection Range (DR) for a 26 ft. Target Depth = 880 yd, ΔDR = 795 yd**

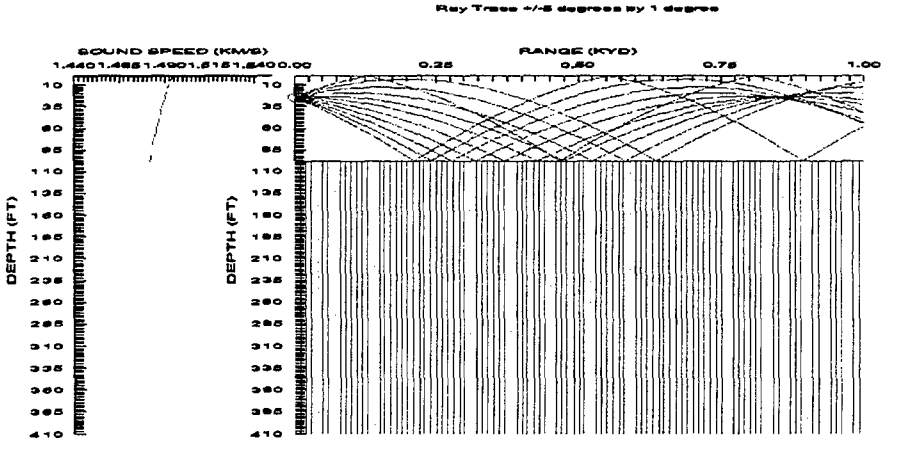

b. **Maximum Detection Range (DR) for a 26 ft. Target Depth = 895 yd, ΔDR = 810 yd**

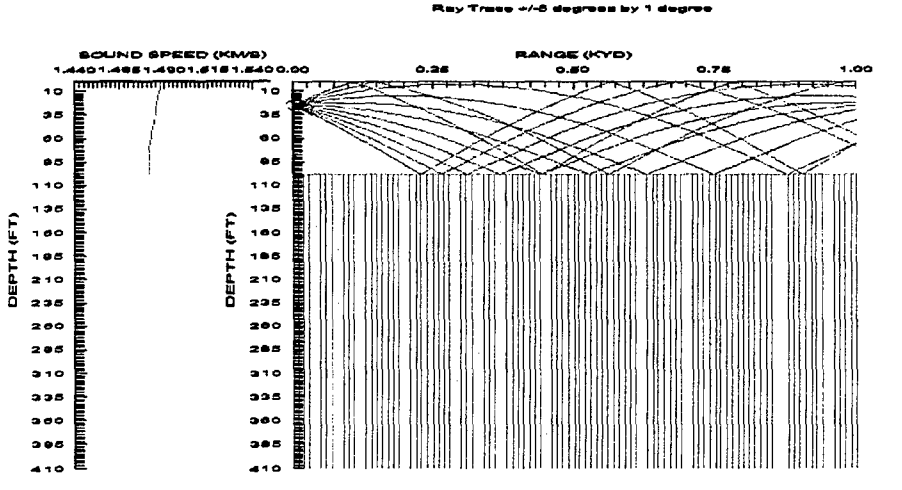

c. **Maximum Detection Range (DR) for a 26 ft. Target Depth = 85 yd**

Sand Bottom/ August/ 35.9 N 124.8 E/ Source Depth = 25 ft/ a. MODAS 1999, b. MODAS 2000, c. MOODS

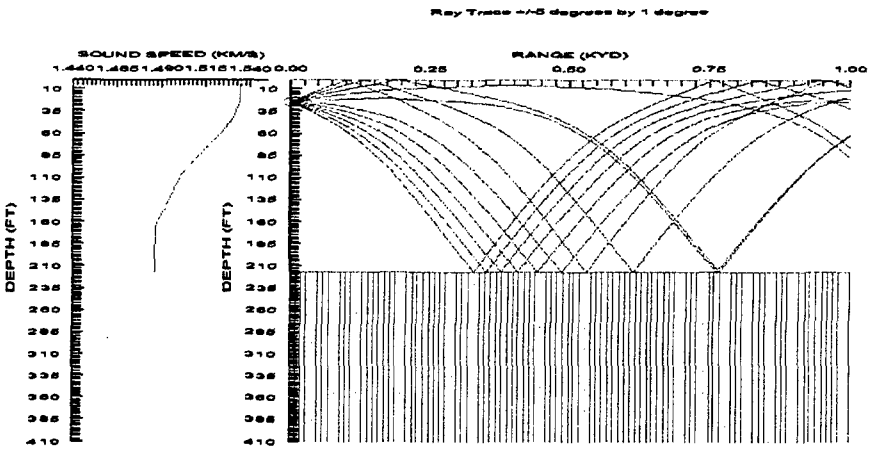

a. **Maximum Detection Range (DR) for a 26 ft. Target Depth > 1000 yd, ΔDR > 820 yd**

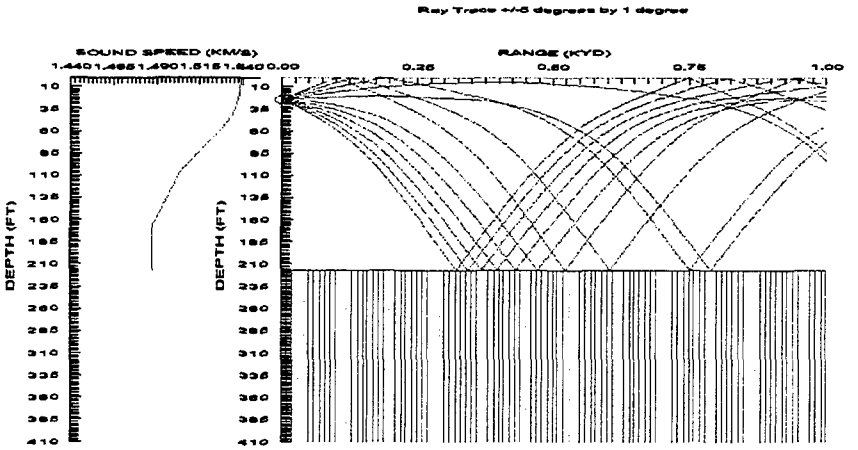

b. **Maximum Detection Range (DR) for a 26 ft. Target Depth = 995 yd, ΔDR = 815 yd**

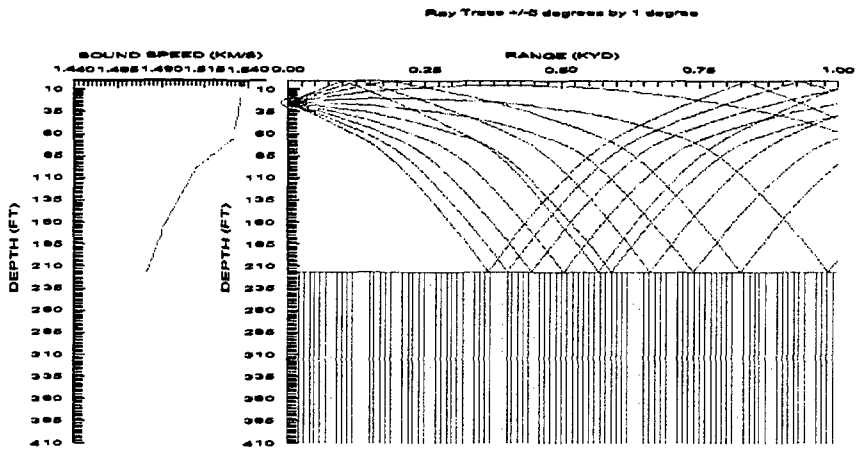

c. **Maximum Detection Range (DR) for a 26 ft. Target Depth = 180 yd**

Sand Bottom/ November/ 35.9 N 125.8 E/ Source Depth = 25 ft/ a. MODAS 1999, b. MODAS 2000, c. MOODS

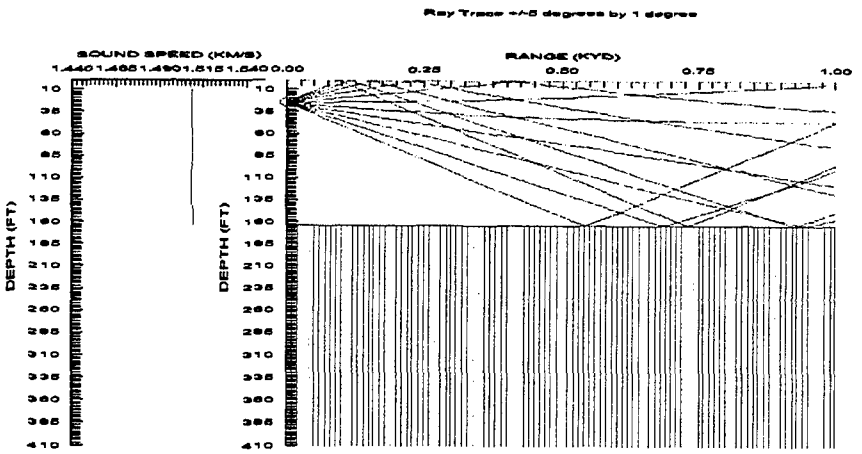

a. **Maximum Detection Range (DR) for a 26 ft. Target Depth = 155 yd, ΔDR = 765 yd**

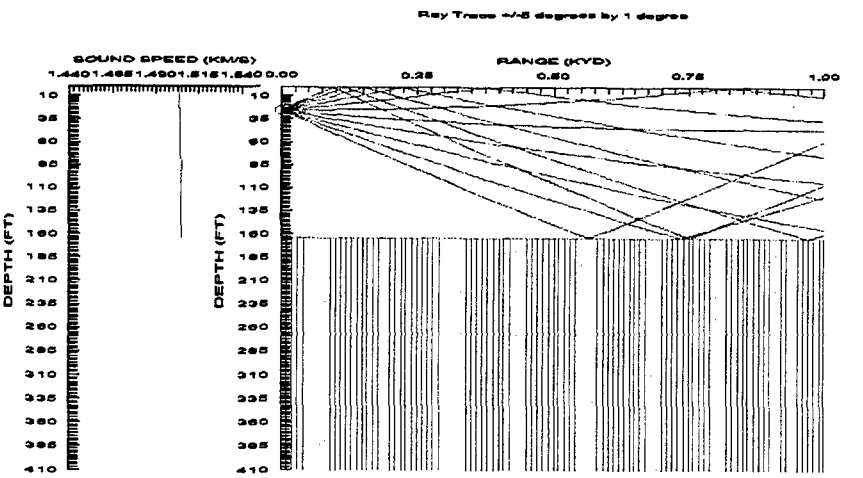

b. **Maximum Detection Range (DR) for a 26 ft. Target Depth = 155 yd, ΔDR = 765 yd**

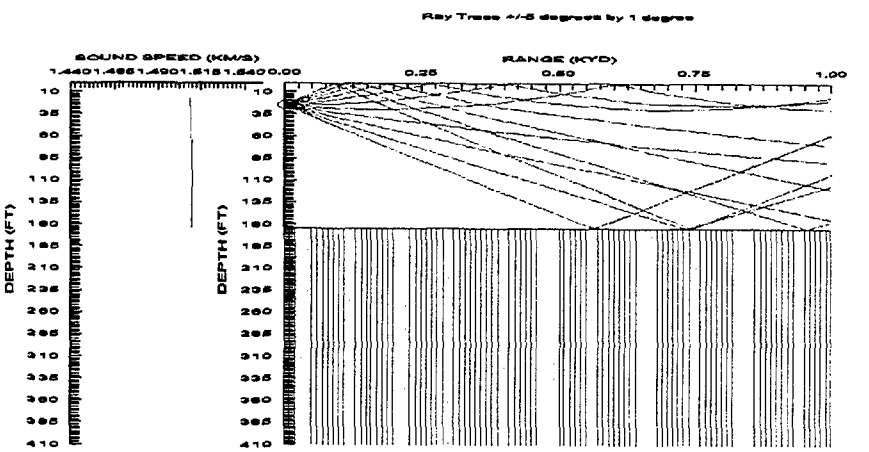

c. **Maximum Detection Range (DR) for a 26 ft. Target Depth = 920 yd**

Mud Bottom/ February/ 35.0 N 123.5 E/ Source Depth = 25 ft/ a. MODAS 1999, b. MODAS 2000, c. MOODS

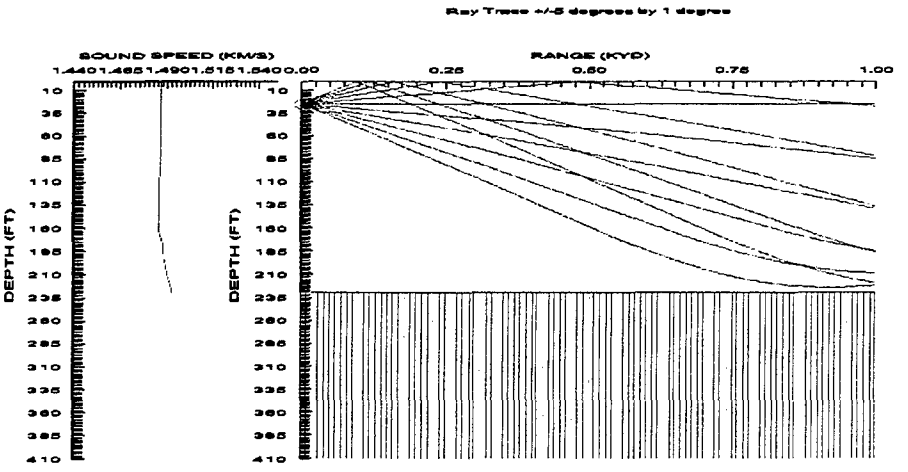

a. **Maximum Detection Range (DR) for a Bottom Target Depth > 1000 yd, ΔDR > 900 yd**

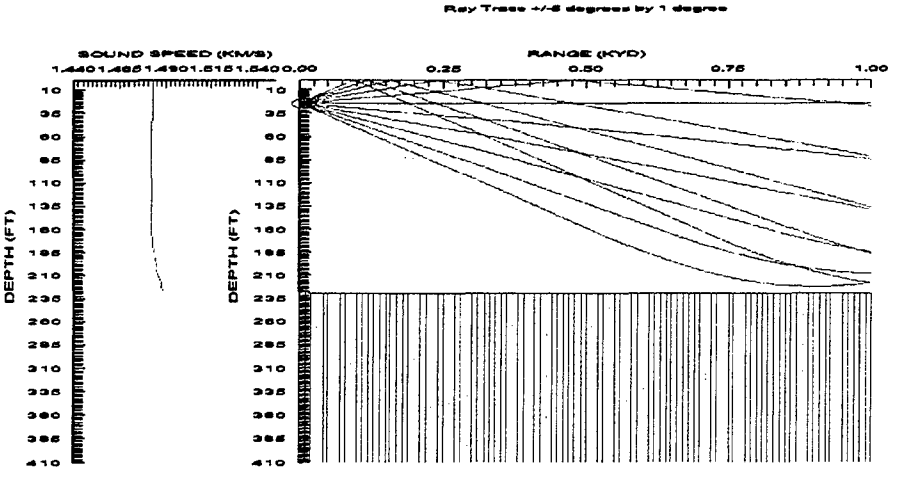

b. **Maximum Detection Range (DR) for a Bottom Target Depth = 990 yd, ΔDR = 100 yd**

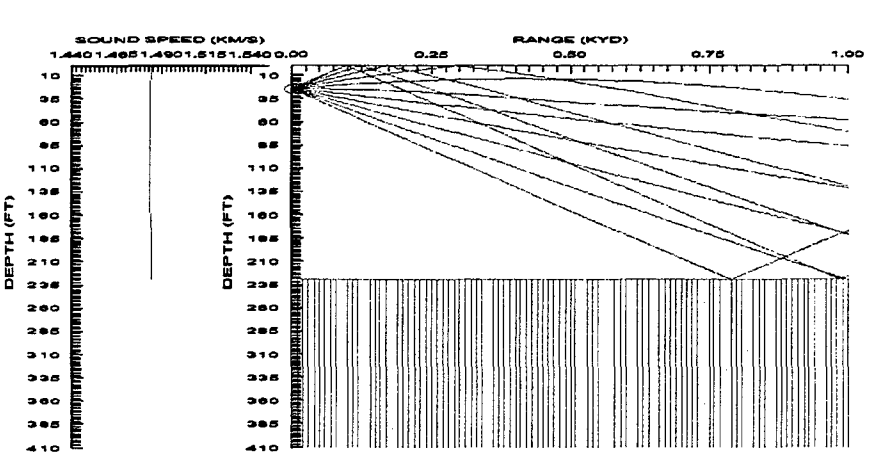

c. **Maximum Detection Range (DR) for a Bottom Target Depth = 100 yd**

Mud Bottom/ February/ 35.0 N 123.5 E/ Source Depth = 125 ft/ a. MODAS 1999, b. MODAS 2000, c. MOODS

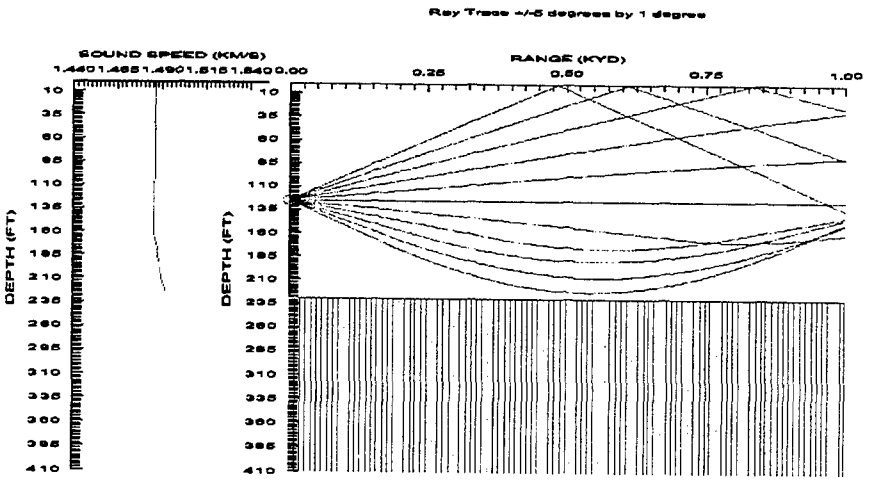

a. **Maximum Detection Range (DR) for a 26 ft. Target Depth = 595 yd, ΔDR = 495 yd**

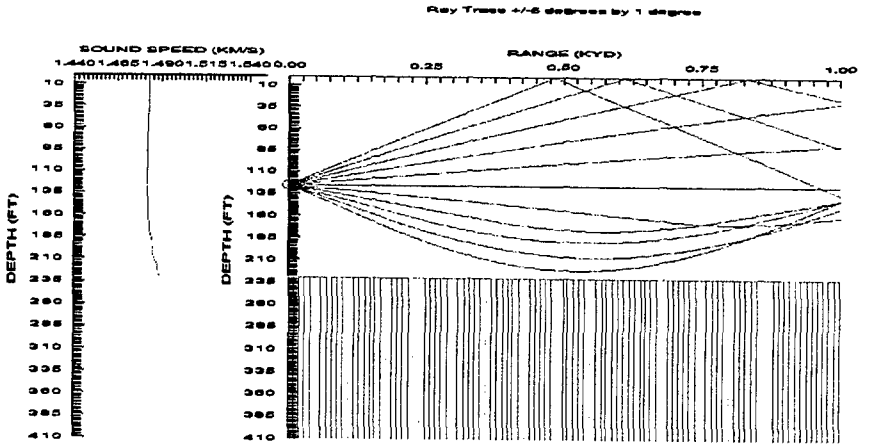

b. **Maximum Detection Range (DR) for a 26 ft. Target Depth = 610 yd, ΔDR = 510 yd**

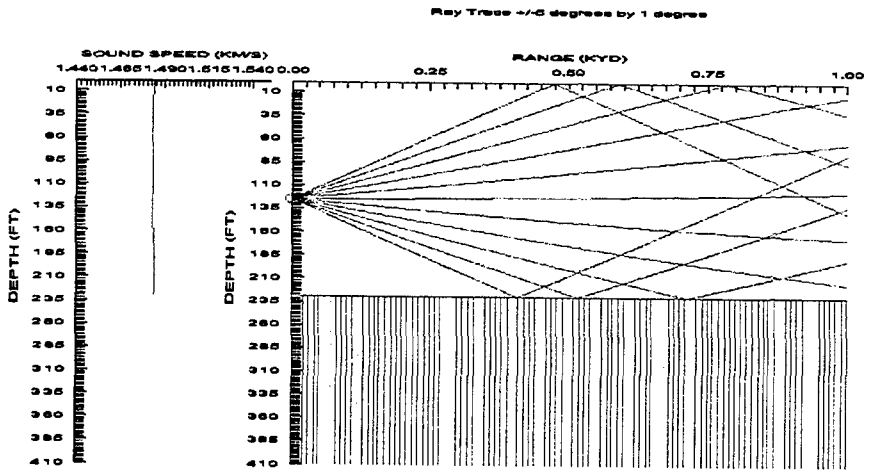

c. **Maximum Detection Range (DR) for a 26 ft. Target Depth = 100 yd**

Mud Bottom/ May/ 36.3 N 125.0 E/ Source Depth = 125 ft/ a. MODAS 1999, b. MODAS 2000, c. MOODS

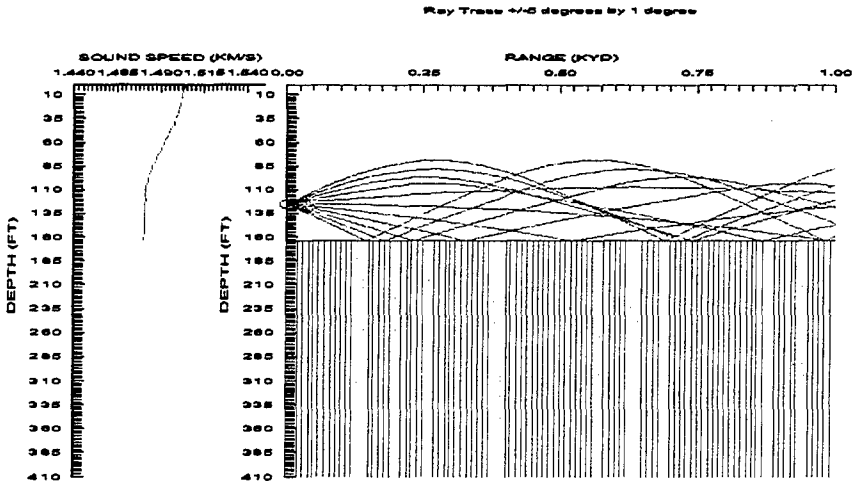

a. **Maximum Detection Range (DR) for a 26 ft. Target Depth = 0 yd, ΔDR = 620 yd**

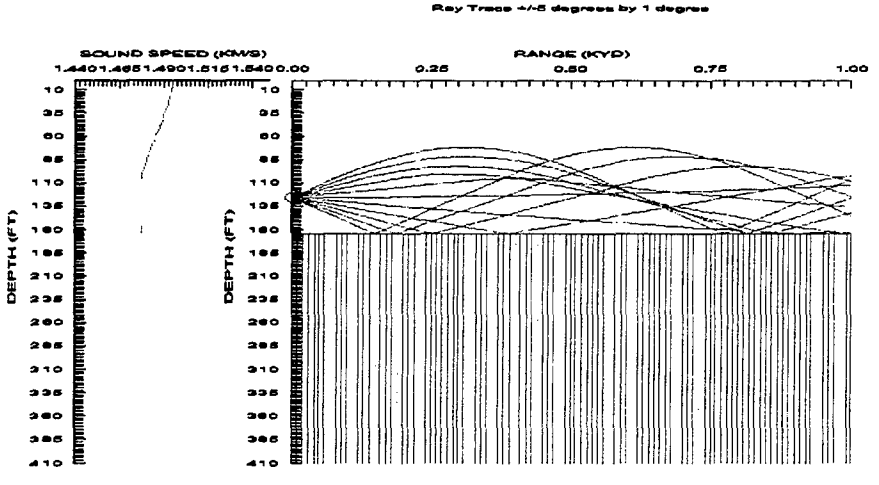

b. **Maximum Detection Range (DR) for a 26 ft. Target Depth = 0 yd, ΔDR = 620 yd**

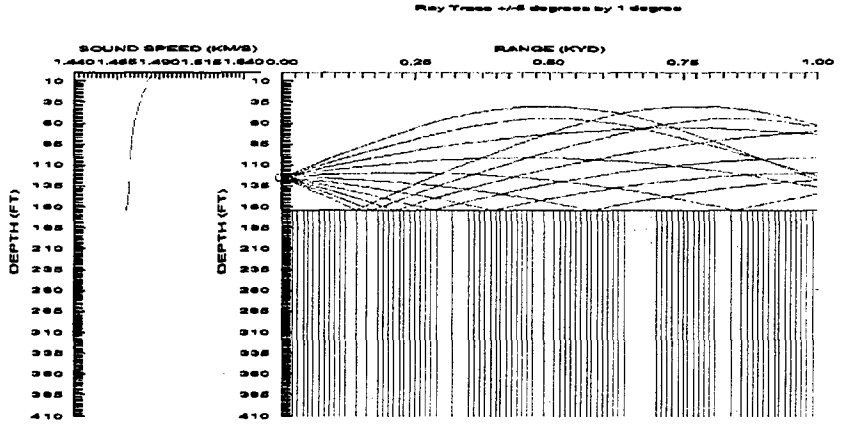

c. **Maximum Detection Range (DR) for a 26 ft. Target Depth = 620 yd**

Mud Bottom/ November/ 35.0 N 123.0 E/ Source Depth = 125 ft/ a. MODAS 1999, b. MODAS 2000, c. MOODS

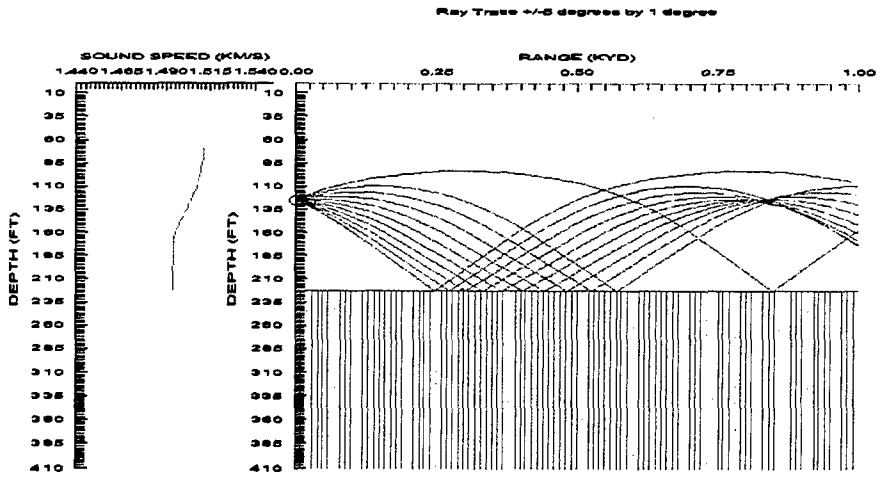

a. **Maximum Detection Range (DR) for a 26 ft. Target Depth = 85 yd, ΔDR = 445 yd**

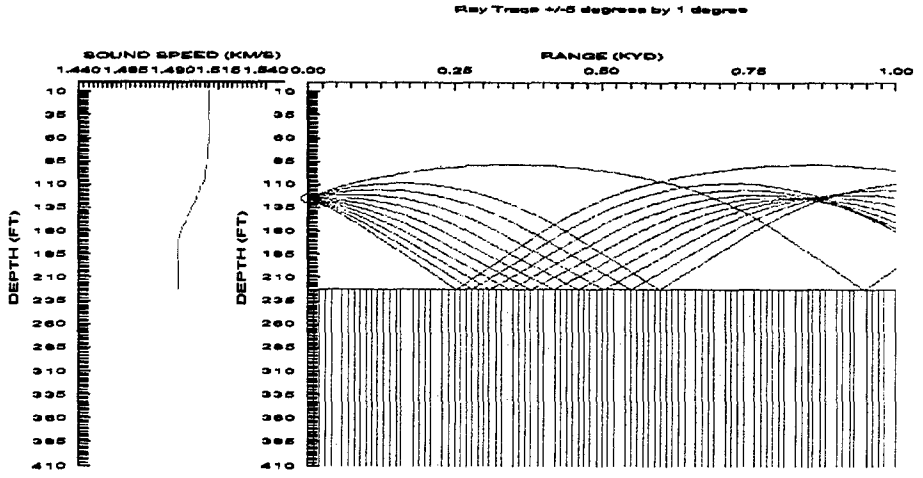

b. **Maximum Detection Range (DR) for a 26 ft. Target Depth = 85 yd, ΔDR = 445 yd**

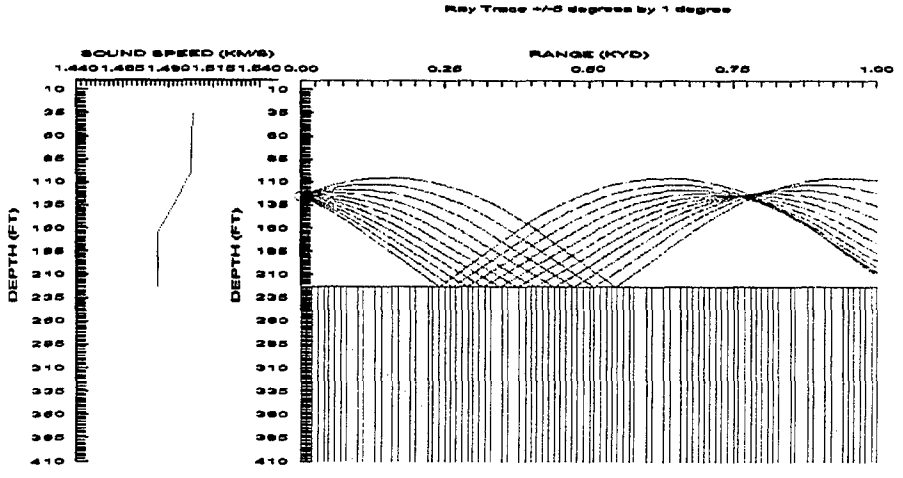

c. **Maximum Detection Range (DR) for a 26 ft. Target Depth = 530 yd**

Sand Bottom/ August/ 35.9 N 124.6 E/ Source Depth = 125 ft/ a. MODAS 1999, b. MODAS 2000, c. MOODS

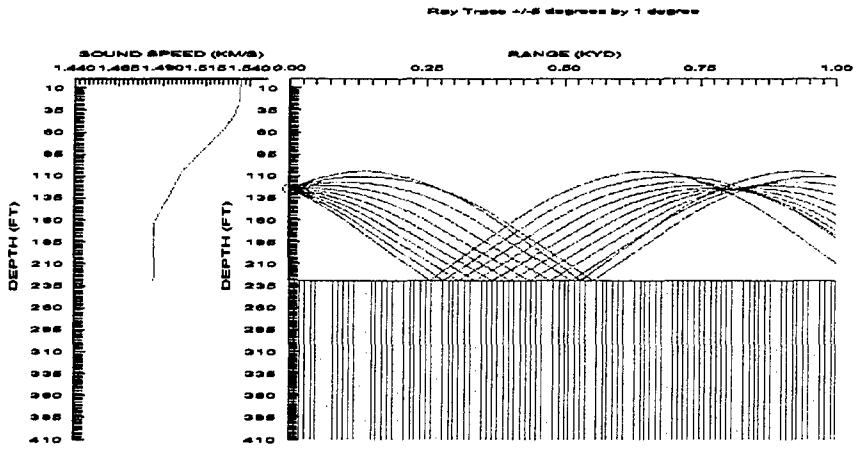

a. **Maximum Detection Range (DR) for a 26 ft. Target Depth = 90 yd, ΔDR = 545 yd**

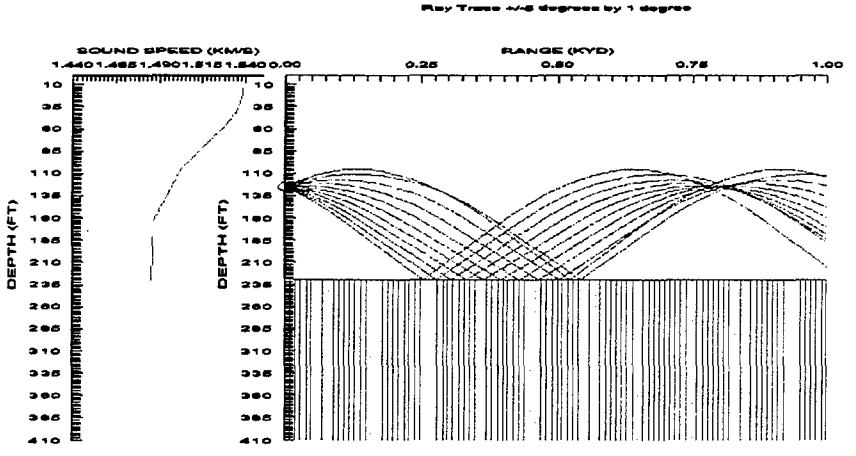

b. **Maximum Detection Range (DR) for a 26 ft. Target Depth = 90 yd, ΔDR = 545 yd**

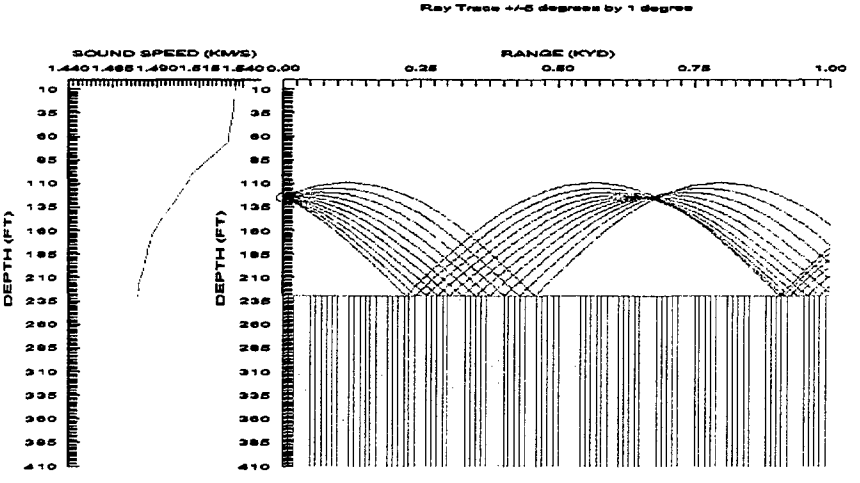

c. **Maximum Detection Range (DR) for a 26 ft. Target Depth = 635 yd**

Sand Bottom/ November/ 36.0 N 124.8 E/ Source Depth = 125 ft/ a. MODAS 1999, b. MODAS 2000, c. MOODS

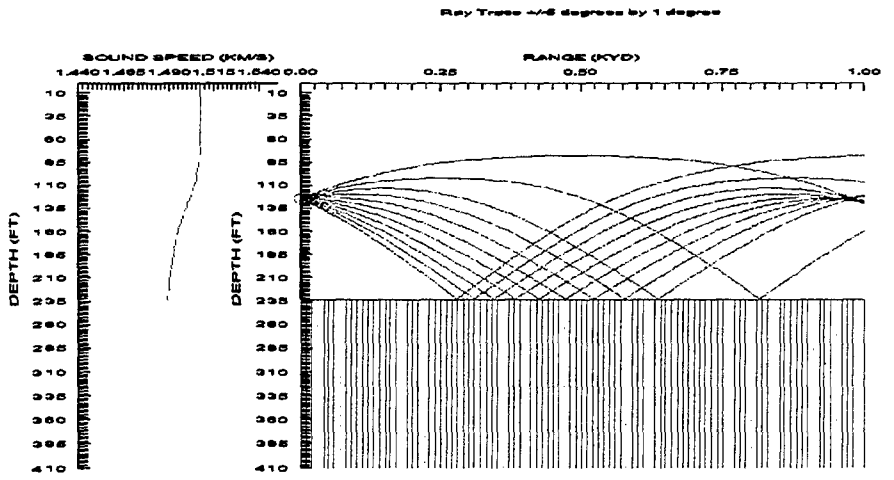

a. **Maximum Detection Range (DR) for a 26 ft. Target Depth = 95 yd, ΔDR = 495 yd**

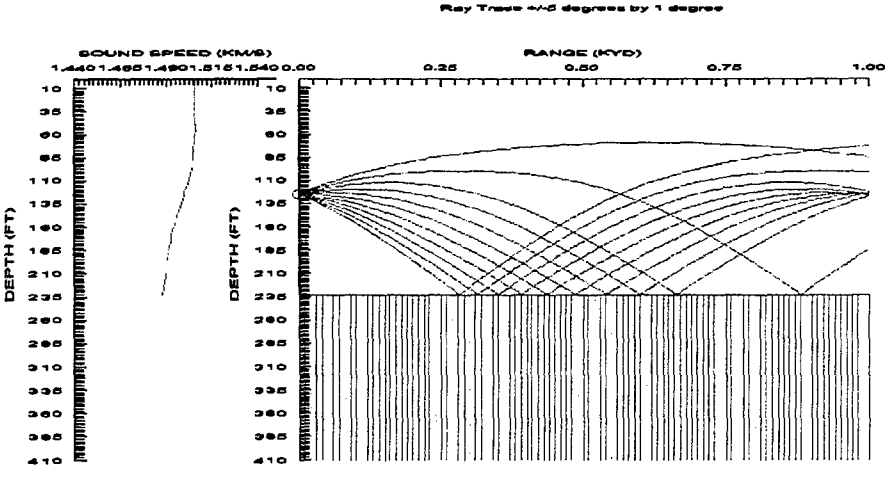

b. **Maximum Detection Range (DR) for a 26 ft. Target Depth = 95 yd, ΔDR = 495 yd**

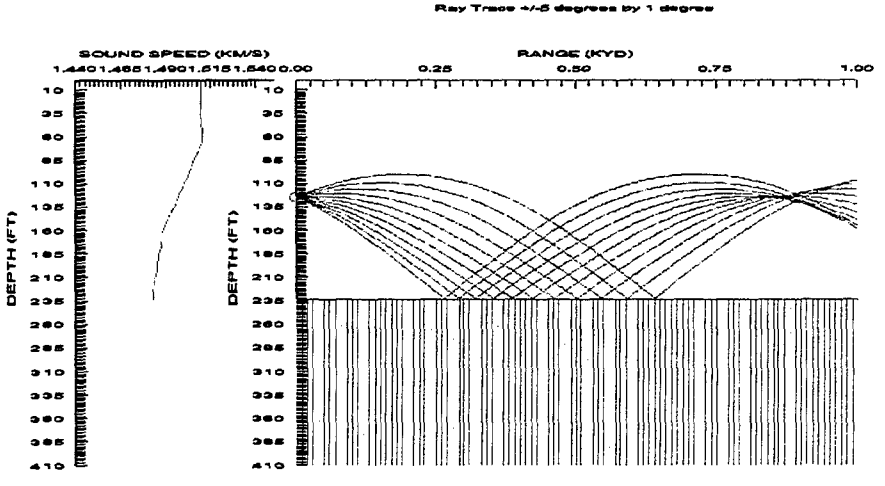

c. **Maximum Detection Range (DR) for a 26 ft. Target Depth = 590 yd**

Mud Bottom/ February/ 36.3 N 124.4 E/ Source Depth = 125 ft/ a. MODAS 1999, b. MODAS 2000, c. MOODS

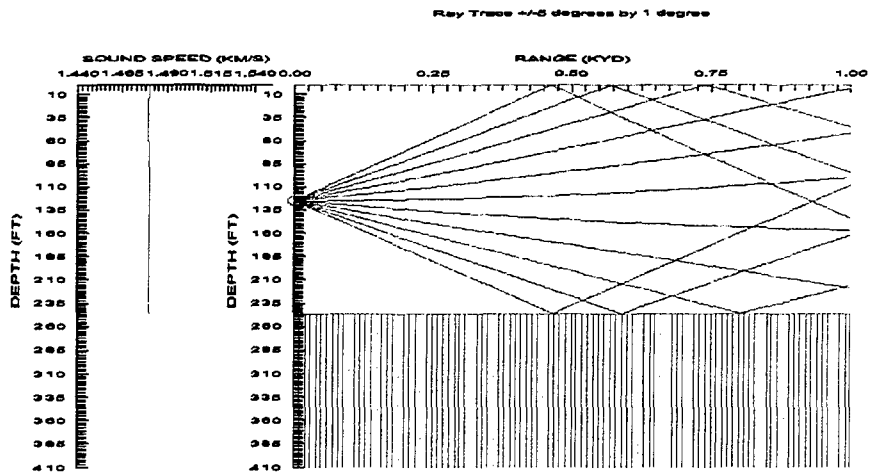

a. Maximum Detection Range (DR) for a Bottom Target Depth = 0 yd, ΔDR > 1000 yd

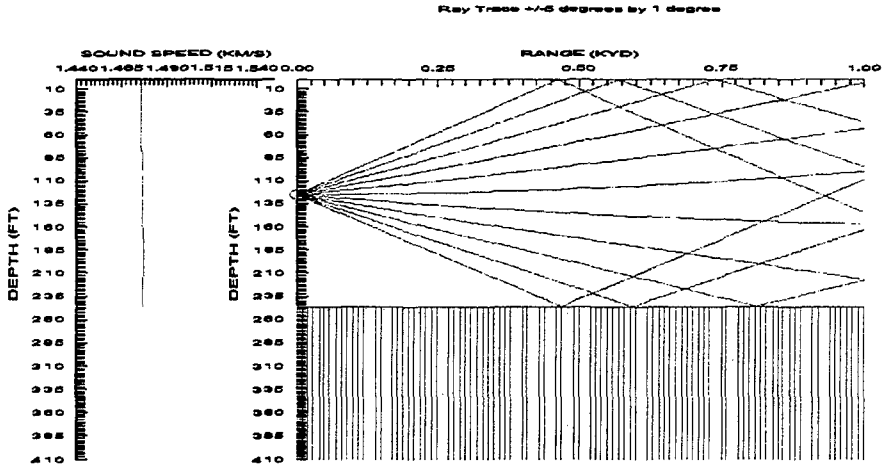

b. Maximum Detection Range (DR) for a Bottom Target Depth = 0 yd, ΔDR > 1000 yd

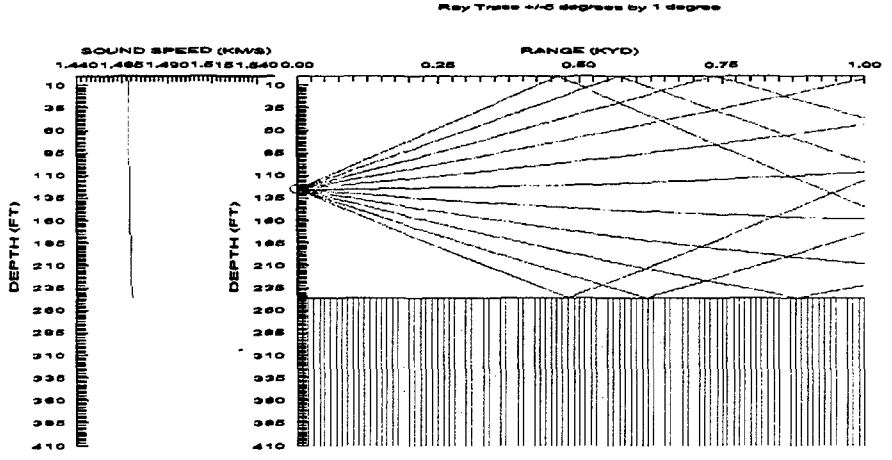

c. Maximum Detection Range (DR) for a Bottom Target Depth > 1000 yd

Mud Bottom/ May/ 36.3 N 125.0 E/ Source Depth = 125 ft/ a. MODAS 1999, b. MODAS 2000, c. MOODS

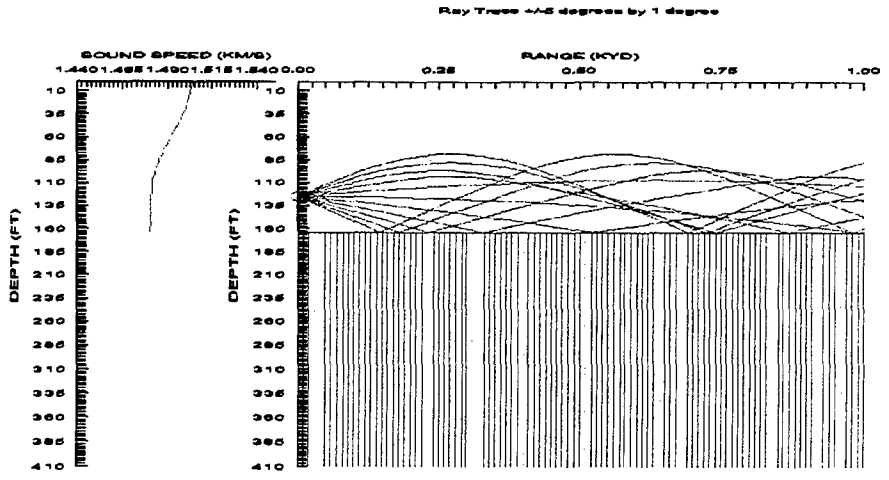

a. Maximum Detection Range (DR) for a Bottom Target Depth = 910 yd, ΔDR = 225 yd

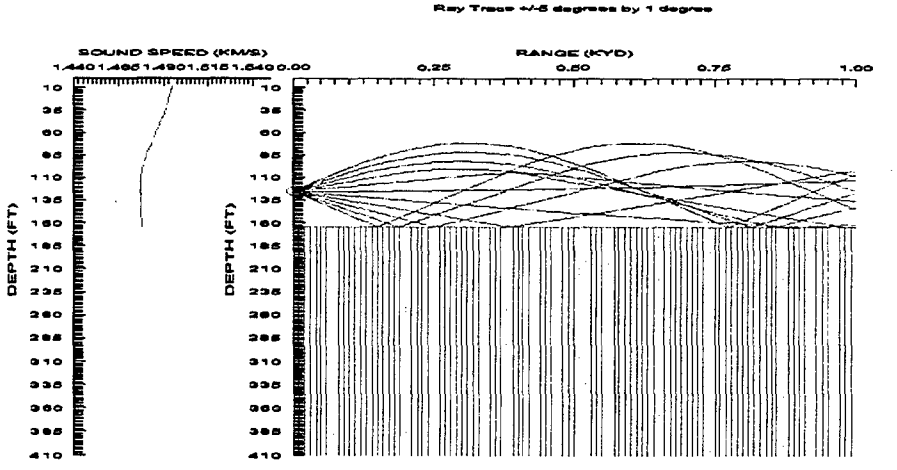

b. Maximum Detection Range (DR) for a Bottom Target Depth > 1000 yd, ΔDR > 315 yd

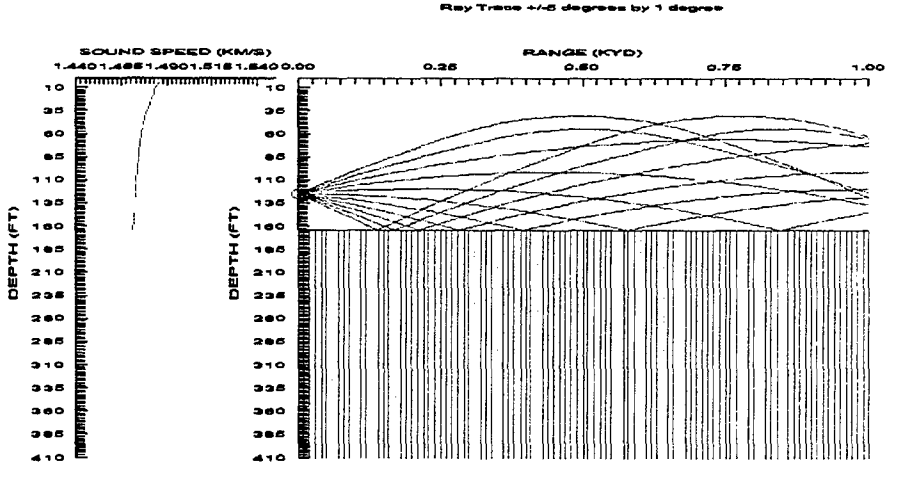

c. Maximum Detection Range (DR) for a Bottom Target Depth = 610 yd

Sand Bottom/ August/ 35.9 N 125.8 E/ Source Depth = 125 ft/ a. MODAS 1999, b. MODAS 2000, c. MOODS

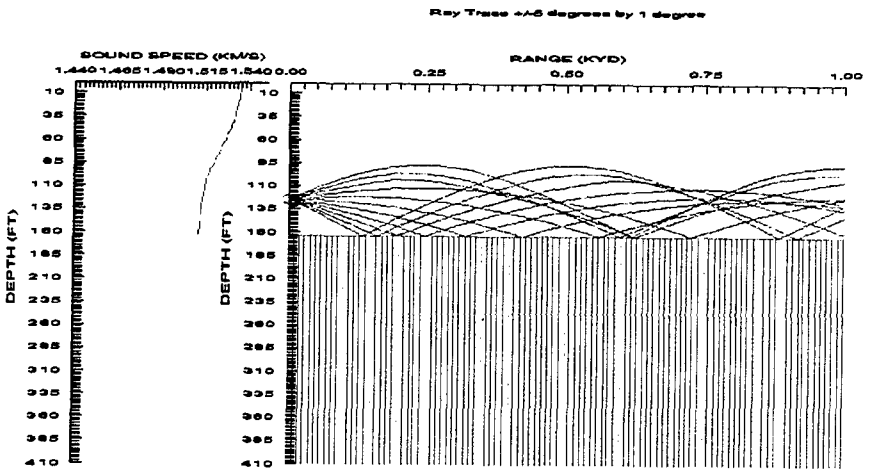

a. **Maximum Detection Range (DR) for a Bottom Target Depth = 875 yd, ΔDR = 265 yd**

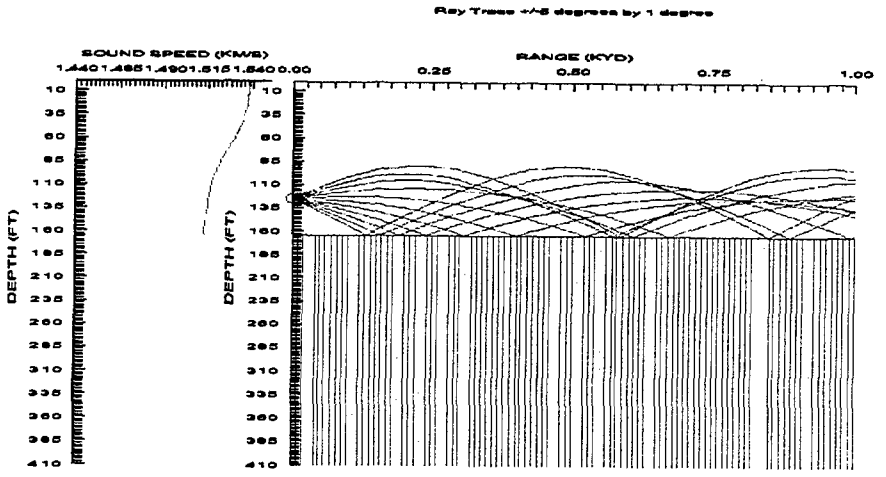

b. **Maximum Detection Range (DR) for a Bottom Target Depth = 835 yd, ΔDR = 225 yd**

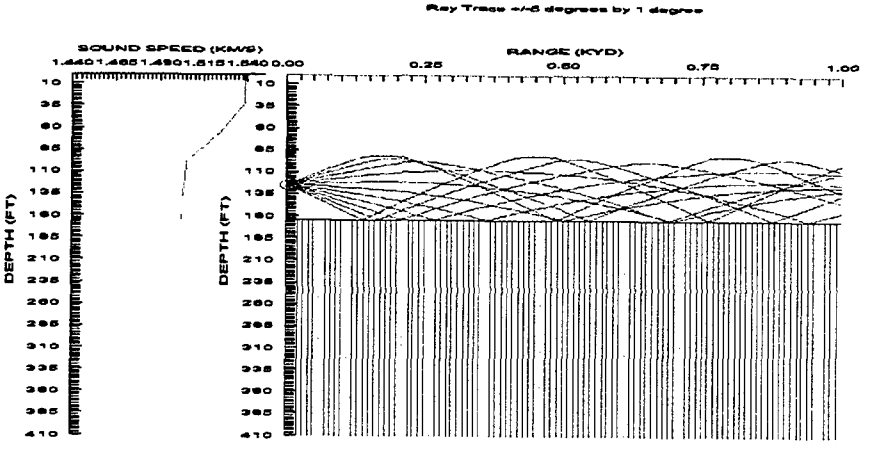

c. **Maximum Detection Range (DR) for a Bottom Target Depth = 610 yd**

Sand Bottom/ November/ 35.9 N 124.6 E/ Source Depth = 125 ft/ a. MODAS 1999, b. MODAS 2000, c. MOODS

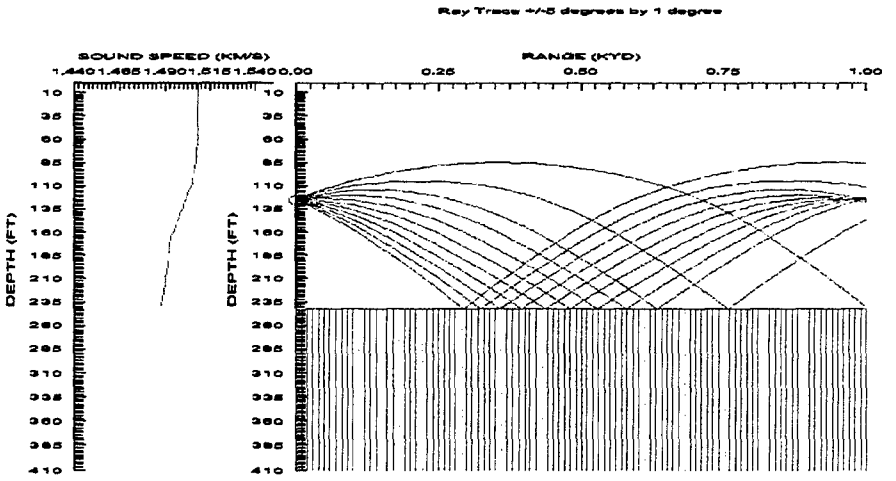

a. **Maximum Detection Range (DR) for a Bottom Target = 310 yd, ΔDR = 205 yd**

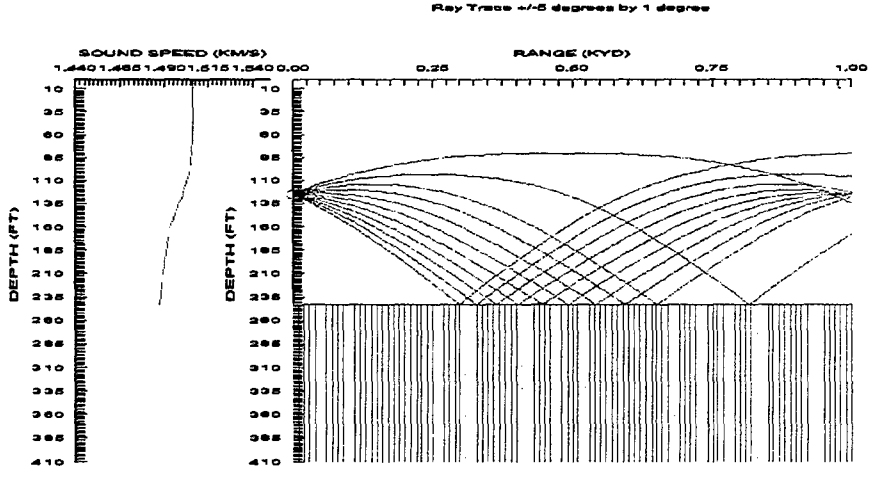

b. **Maximum Detection Range (DR) for a Bottom Target = 310 yd, ΔDR = 205 yd**

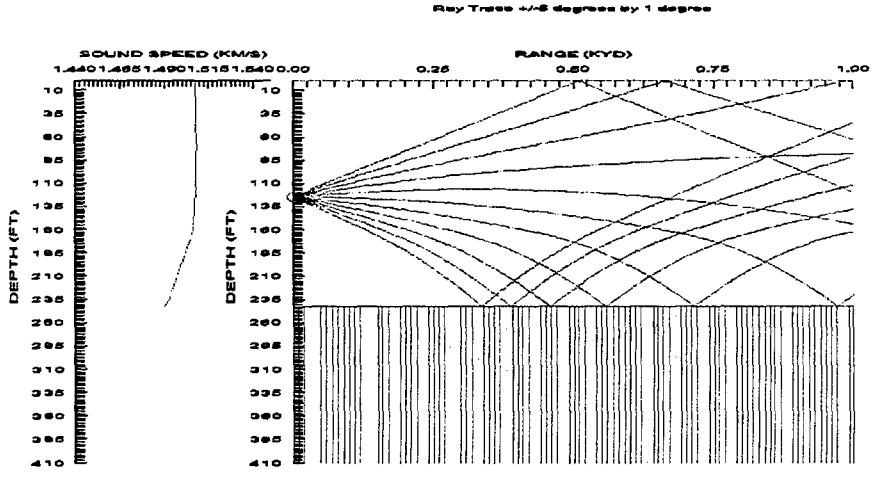

c. **Maximum Detection Range (DR) for a Bottom Target = 105 yd**

Gravel Bottom/ May/ 38.9 N 122.5 E/ Source Depth = 25 ft/ a. MODAS 1999, b. MODAS 2000, c. MOODS

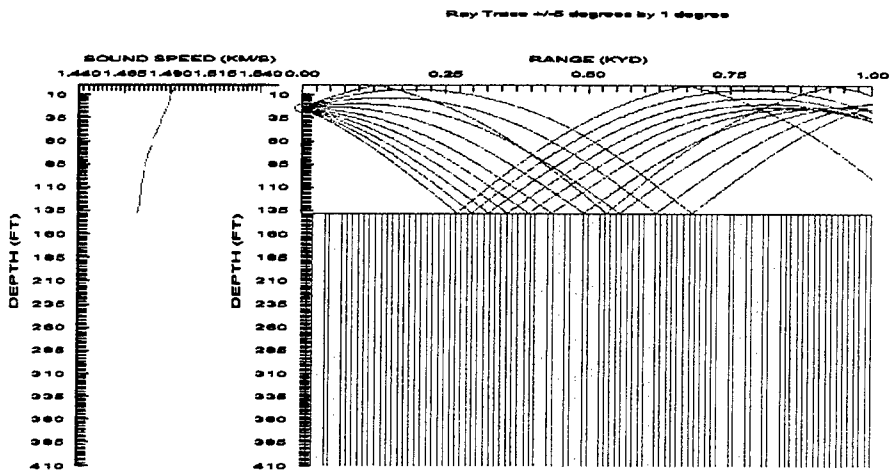

a. **Maximum Detection Range (DR) for a 26 ft. Target Depth = 90 yd, ΔDR = 800 yd**

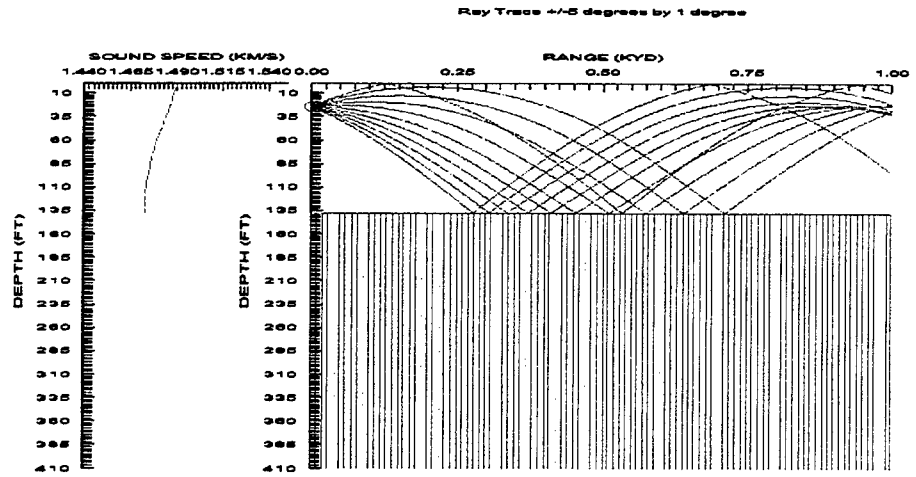

b. **Maximum Detection Range (DR) for a 26 ft. Target Depth = 90 yd, ΔDR = 800 yd**

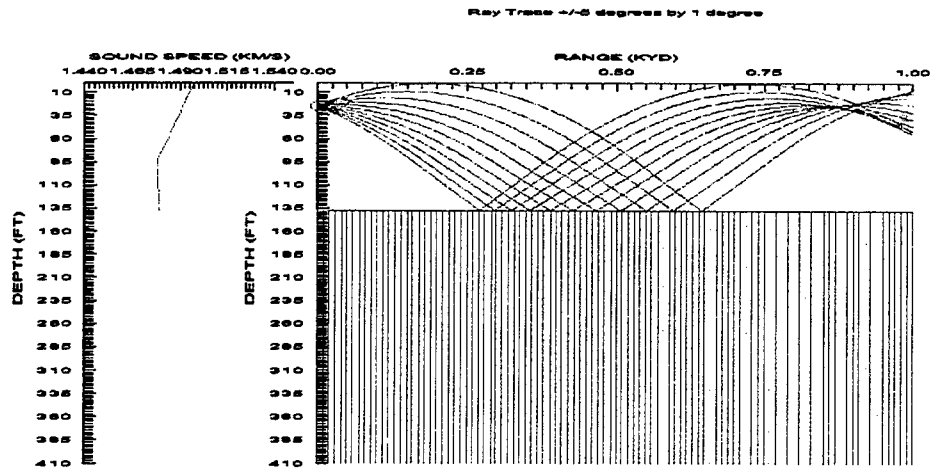

c. **Maximum Detection Range (DR) for a 26 ft. Target Depth = 890 yd**

Rock Bottom/ August/ 38.9 N 122.2 E/ Source Depth = 125 ft/ a. MODAS 1999, b. MODAS 2000, c. MOODS

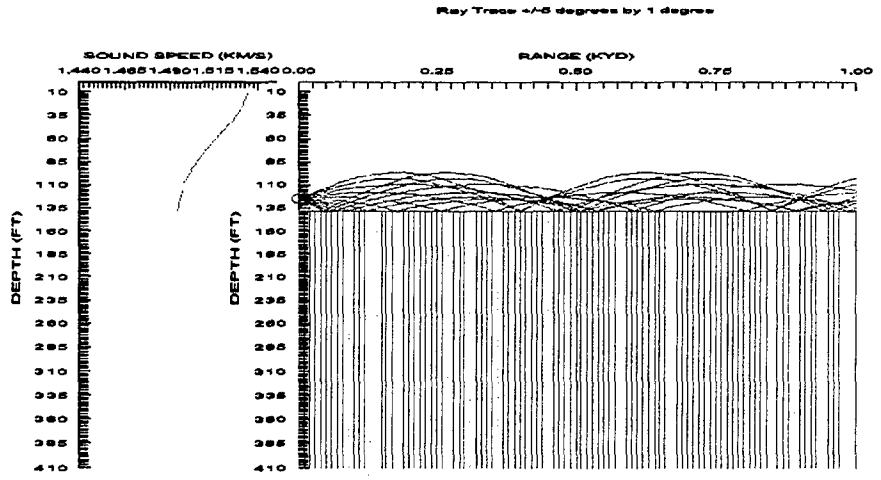

a. **Maximum Detection Range (DR) for a 26 ft. Target Depth = 0 yd, ΔDR = 210 yd**

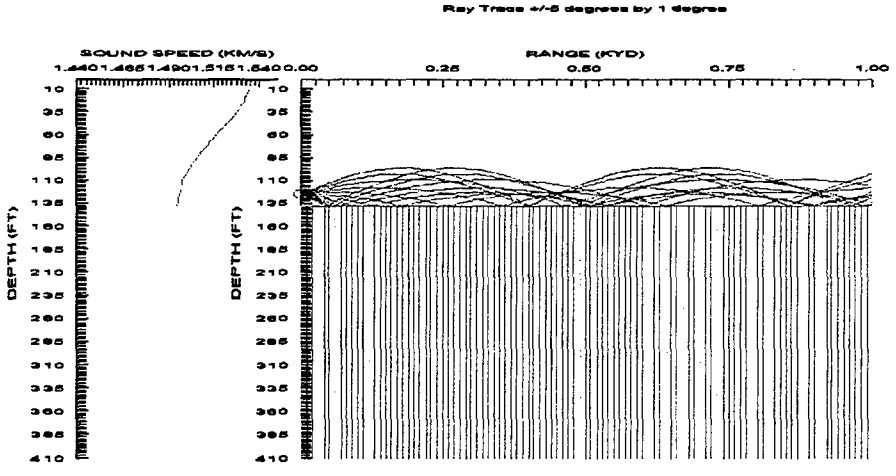

b. **Maximum Detection Range (DR) for a 26 ft. Target Depth = 0 yd, ΔDR = 210 yd**

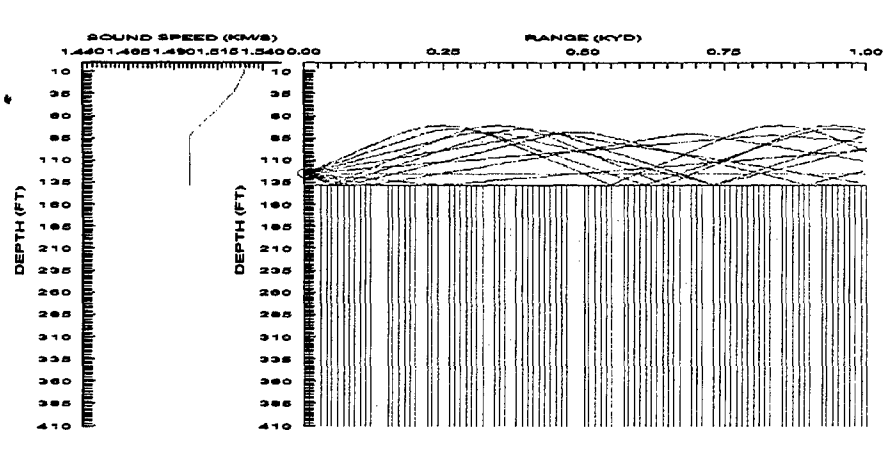

c. **Maximum Detection Range (DR) for a 26 ft. Target Depth = 210 yd**

Gravel Bottom/ May/ 39.0 N 122.8 E/ Source Depth = 75 ft/ a. MODAS 1999, b. MODAS 2000, c. MOODS

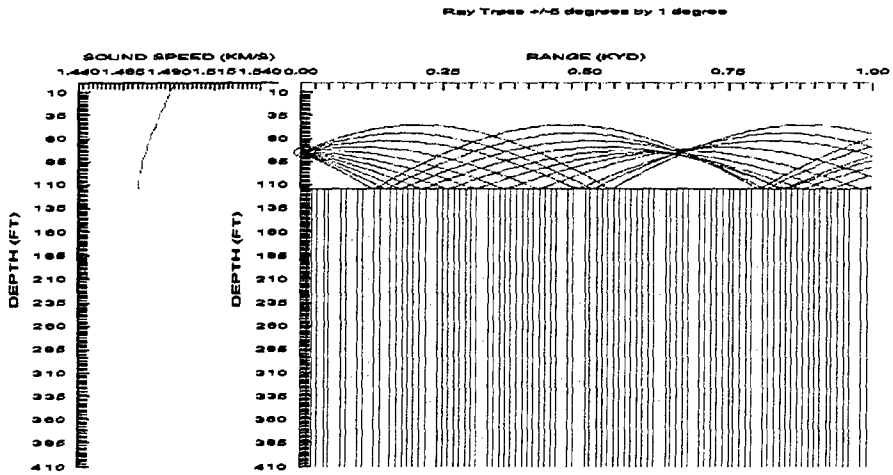

a. Maximum Detection Range (DR) for a Bottom Target Depth = 35 yd, ΔDR = 655 yd

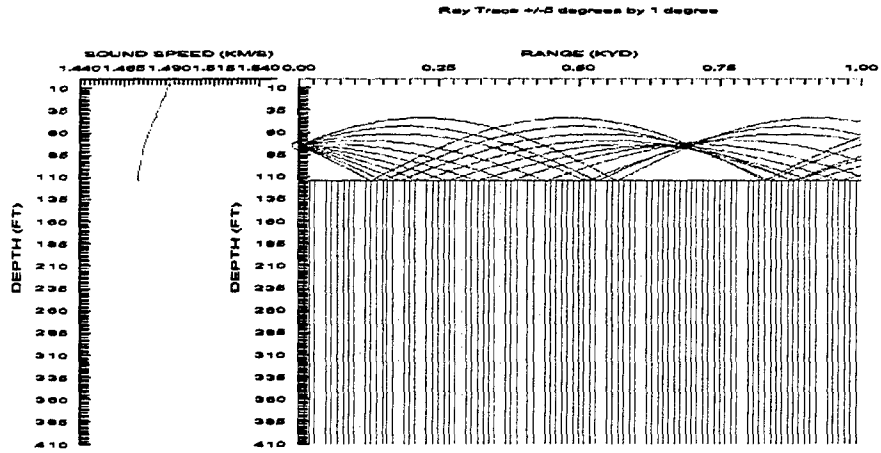

b. Maximum Detection Range (DR) for a Bottom Target Depth = 35 yd, ΔDR = 655 yd

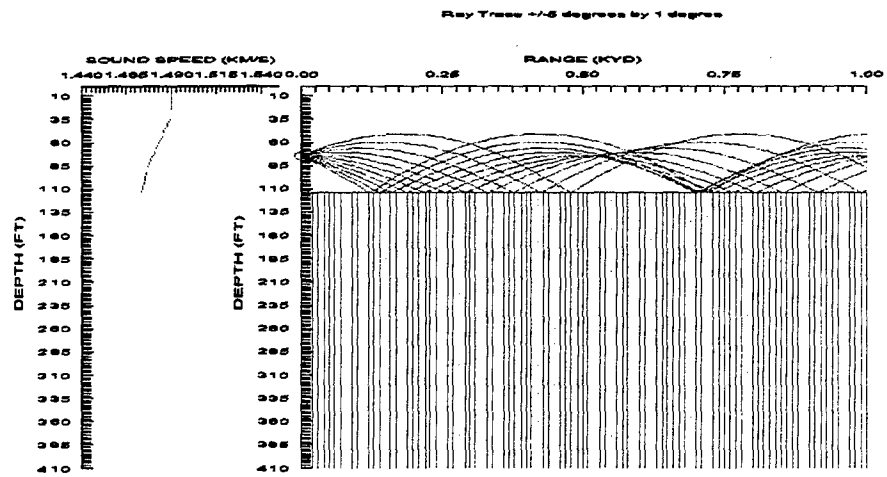

c. Maximum Detection Range (DR) for a Bottom Target Depth = 690 yd

Gravel Bottom/ August/ 38.9 N 122.2 E/ Source Depth = 50 ft/ a. MODAS 1999, b. MOODS

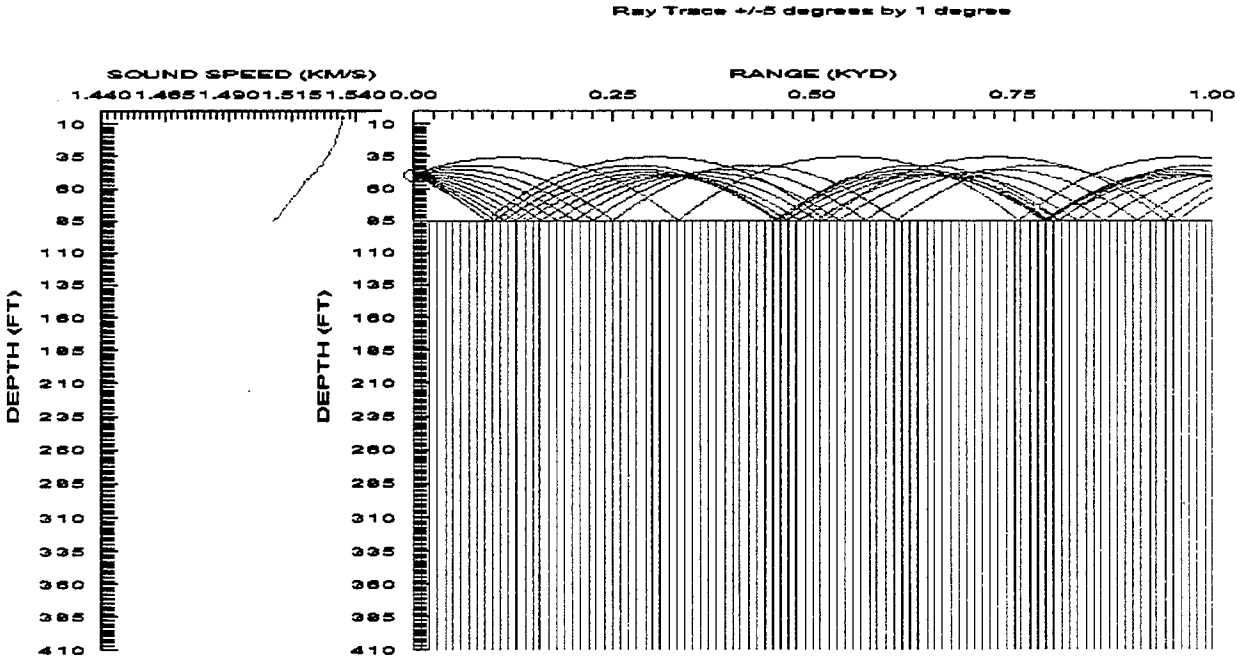

a. **Maximum Detection Range (DR) for a Bottom Target Depth = 445 yd, ΔDR = 425 yd**

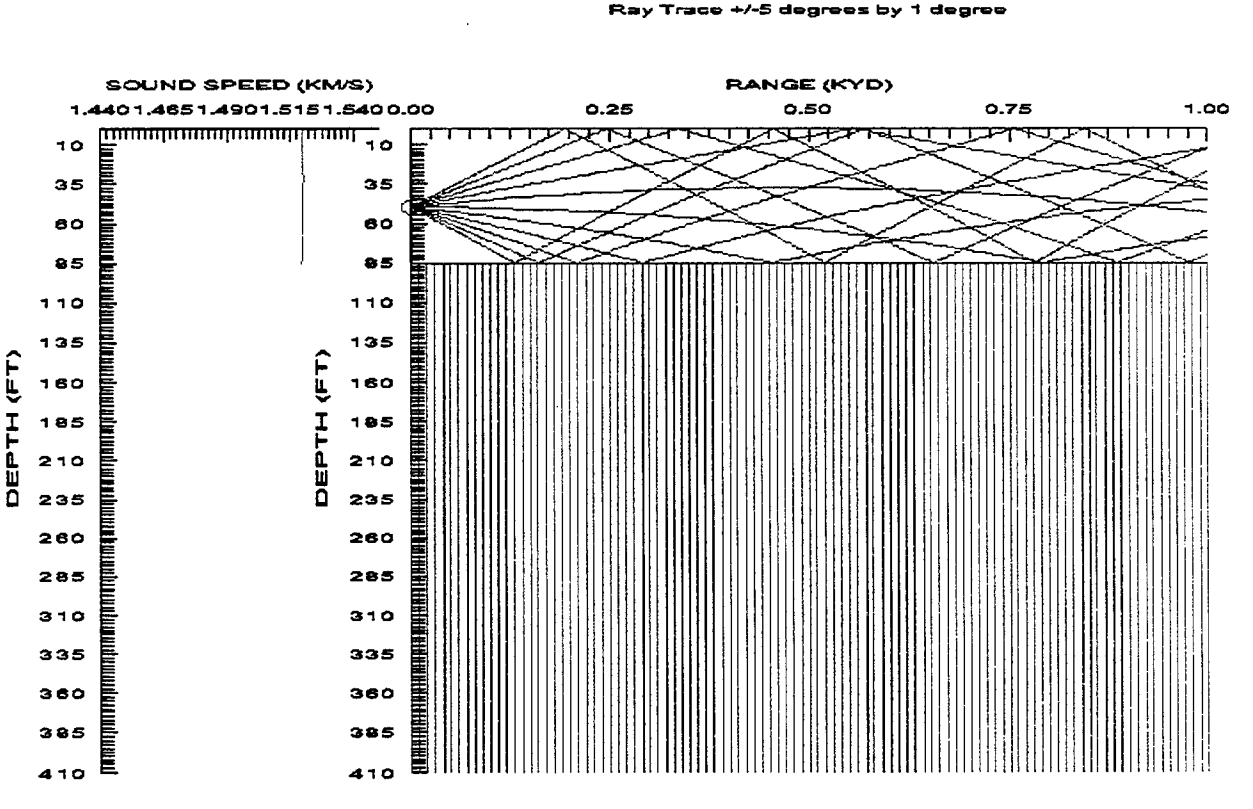

b. **Maximum Detection Range (DR) for a Bottom Target Depth = 20 yd**

Gravel Bottom/ November/ 38.4 N 122.1 E/ Source Depth = 125 ft/ a. MODAS 1999, b. MODAS 2000, c. MOODS

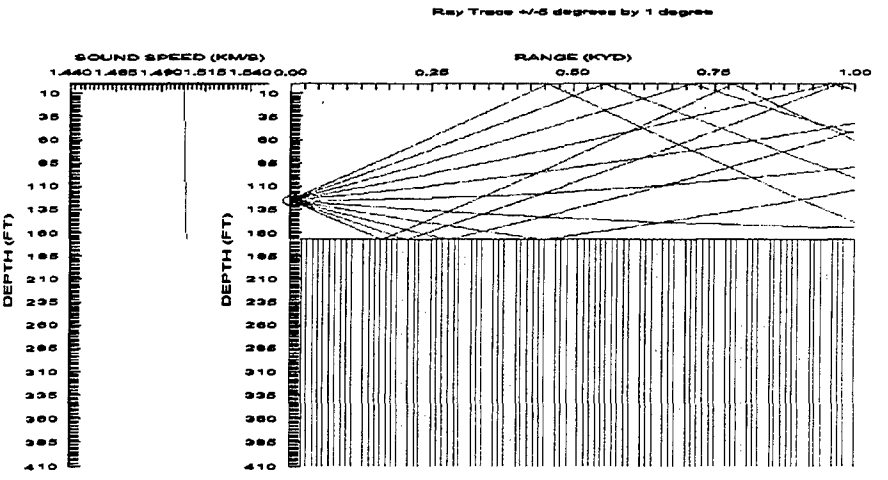

a. Maximum Detection Range (DR) for a Bottom Target Depth = 245 yd, ΔDR = 220 yd

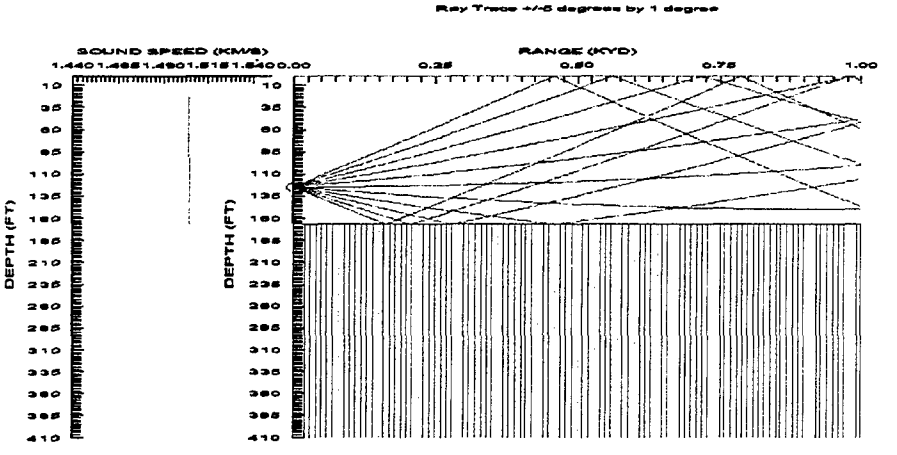

b. Maximum Detection Range (DR) for a Bottom Target Depth = 250 yd, ΔDR = 225 yd

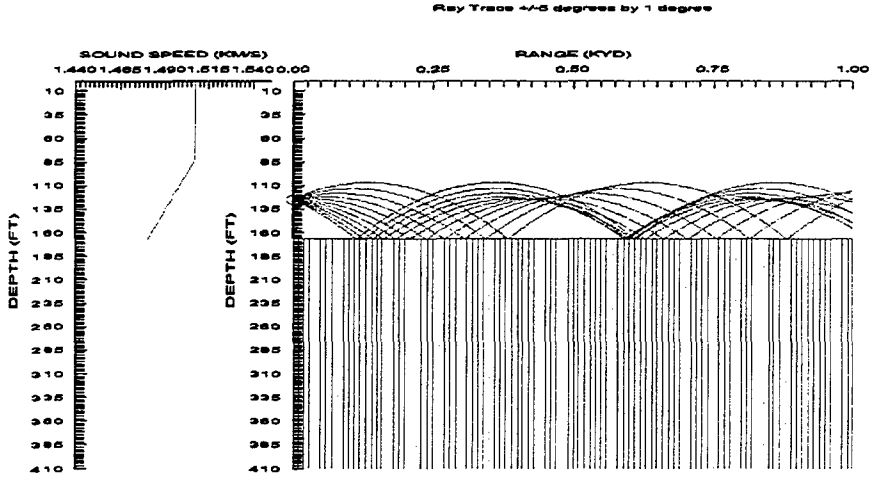

c. Maximum Detection Range (DR) for a Bottom Target Depth = 25 yd

Rock Bottom/ May/ 37.5 N 123.0 E/ Source Depth = 125 ft/ a. MODAS 1999, b. MODAS 2000, c. MOODS

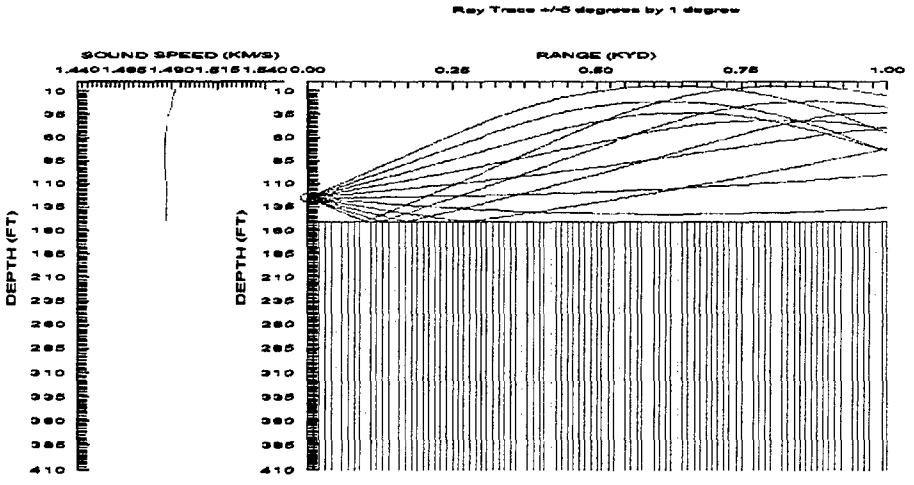

a. Maximum Detection Range (DR) for a Bottom Target Depth = 215 yd, ΔDR = 190 yd

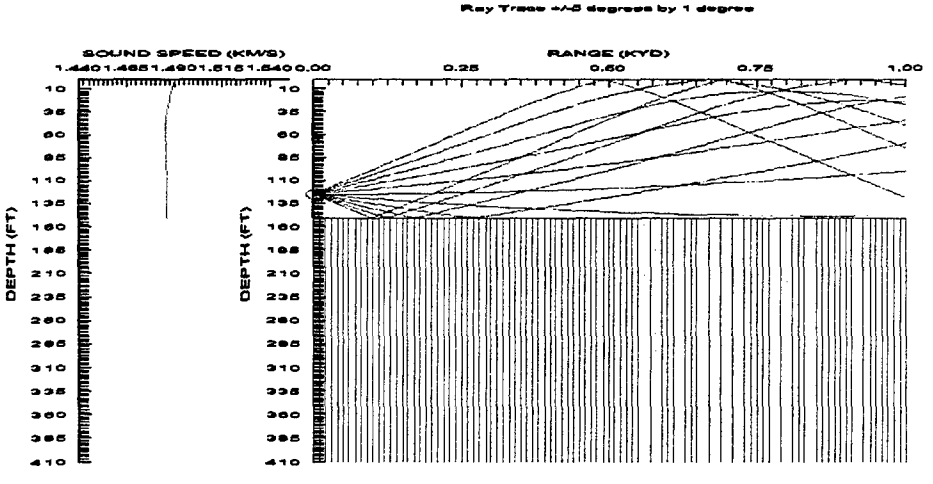

b. Maximum Detection Range (DR) for a Bottom Target Depth = 210 yd, ΔDR = 185 yd

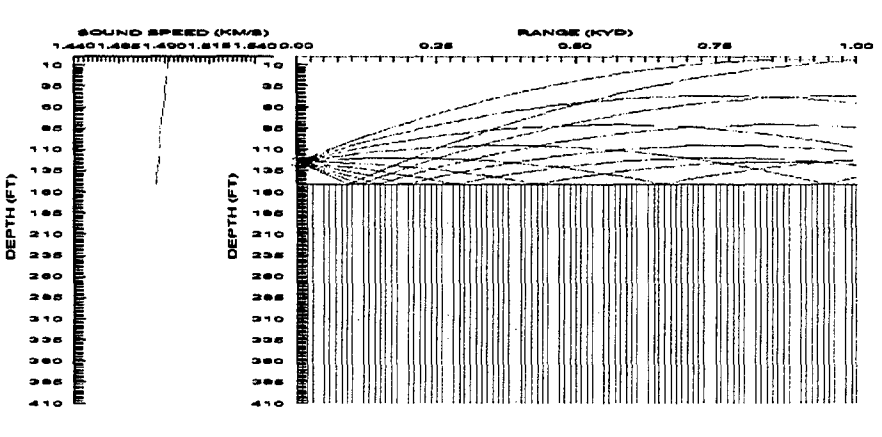

c. Maximum Detection Range (DR) for a Bottom Target Depth = 25 yd

Rock Bottom/ November/ 37.5 N 123.4 E/ Source Depth = 125 ft/ a. MODAS 1999, b. MODAS 2000, c. MOODS

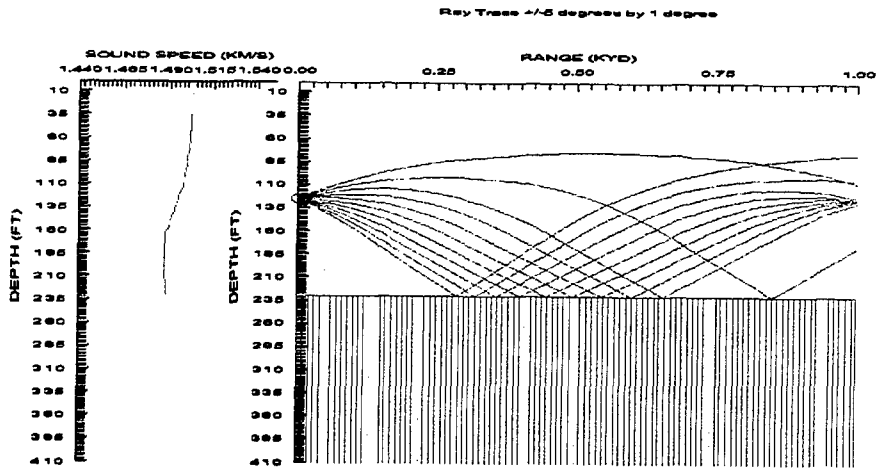

a. **Maximum Detection Range (DR) for a Bottom Target Depth = 40 yd, ΔDR > 960 yd**

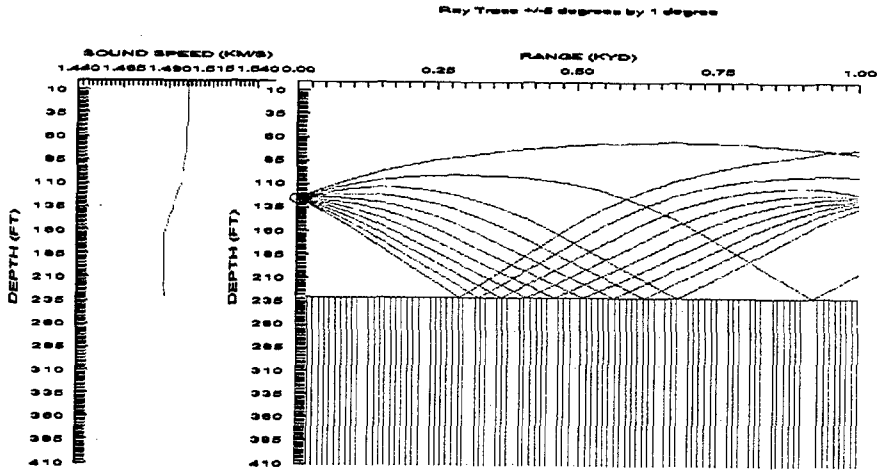

b. **Maximum Detection Range (DR) for a Bottom Target Depth = 40 yd, ΔDR > 960 yd**

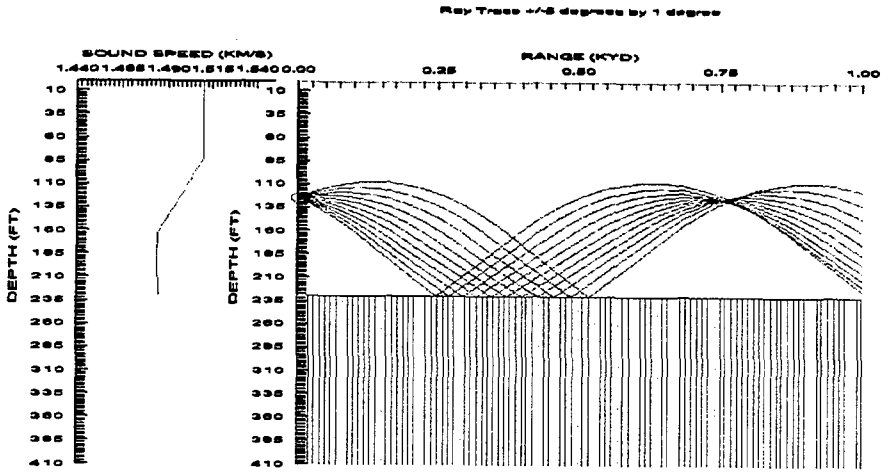

c. **Maximum Detection Range (DR) for a Bottom Target Depth > 1000 yd**

THIS PAGE INTENTIONALLY LEFT BLANK

APPENDIX B. MODAS AND GDEM RAY TRACES

Mud Bottom/ February/ 35.0 N 123.5 E/ Source Depth = 25 ft/ a. MODAS 1999, b. MODAS 2000, c. GDEM

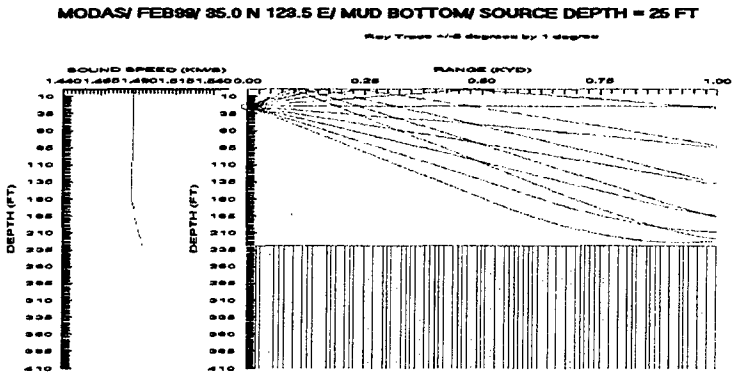

a. **Maximum Detection Range (DR) for a 26 ft. Target Depth >1000 yd ΔDR >755 yd**

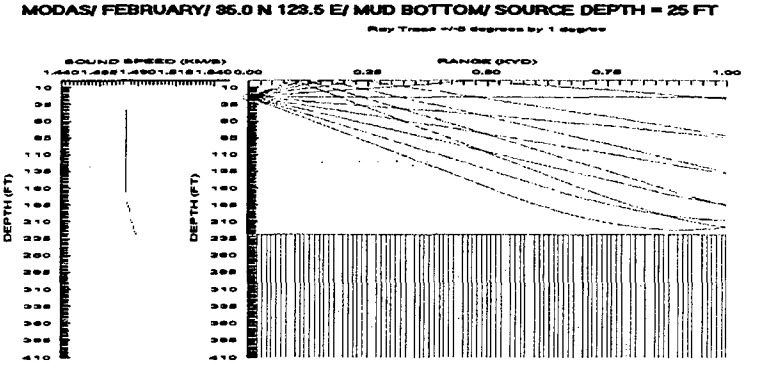

b. **Maximum Detection Range for a 26 ft. Target Depth > 1000 yd ΔDR >755 yd**

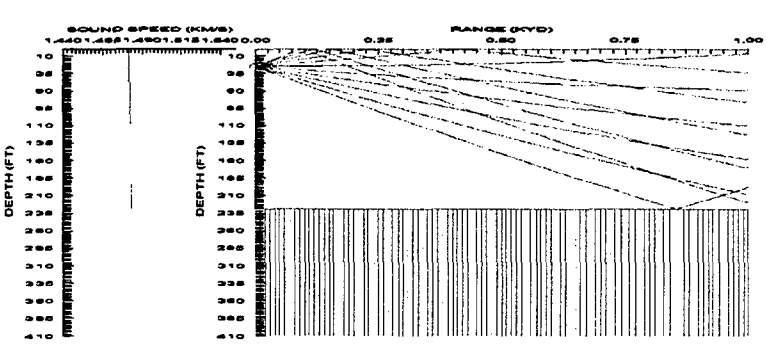

c. **Maximum Detection Range for a 26 ft. Target Depth = 245 yd**

Mud Bottom/ May/ 35.0 N 123.0 E/ Source Depth = 25 ft/ a. MODAS 1999, b. MODAS 2000, c. GDEM

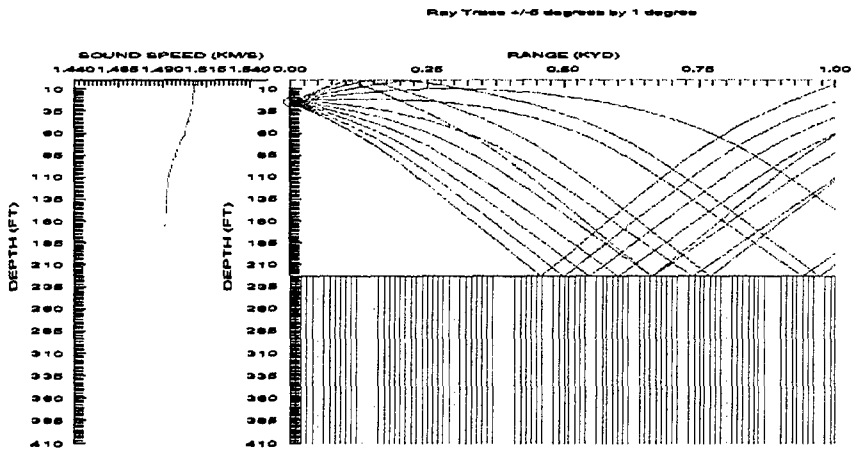

a. **Maximum Detection Range (DR) for a 26 ft. Target Depth = 205 yd ΔDR >795 yd**

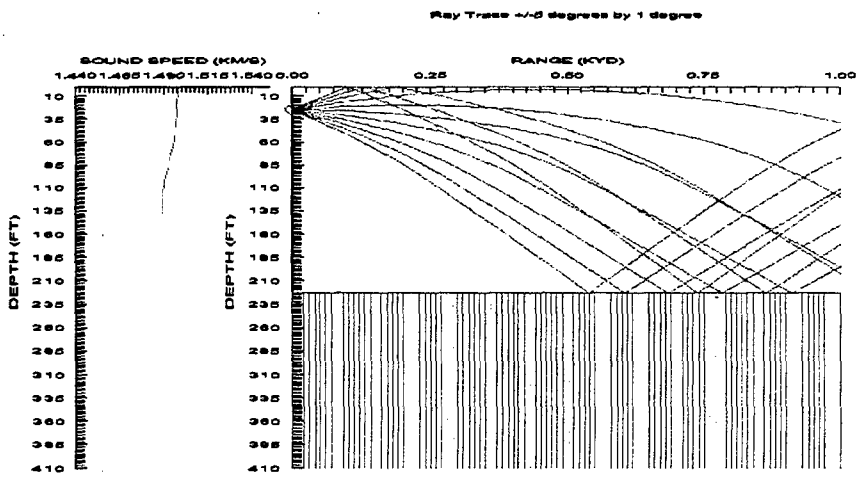

b. **Maximum Detection Range (DR) for a 26 ft. Target Depth = 220 yd, ΔDR >780 yd**

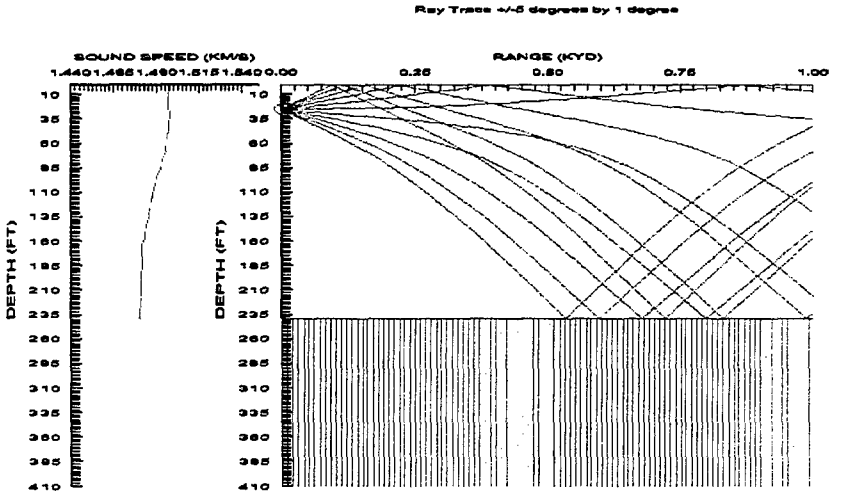

c. **Maximum Detection Range (DR) for a 26 ft. Target Depth >1000 yd**

Mud Bottom/ August/ 35.9 N 124.4 E/ Source Depth = 25 ft/ a. MODAS 1999, b. MODAS 2000, c. GDEM

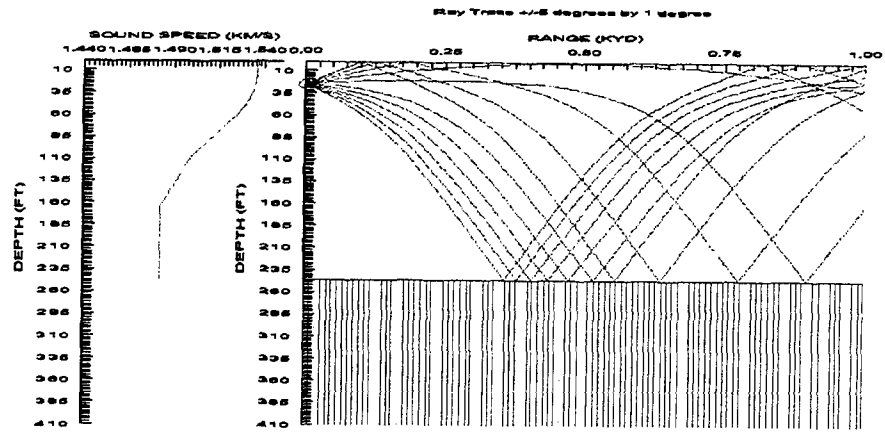

a. **Maximum Detection Range (DR) for a 26 ft. Target Depth = 765 yd, ΔDR = 545 yd**

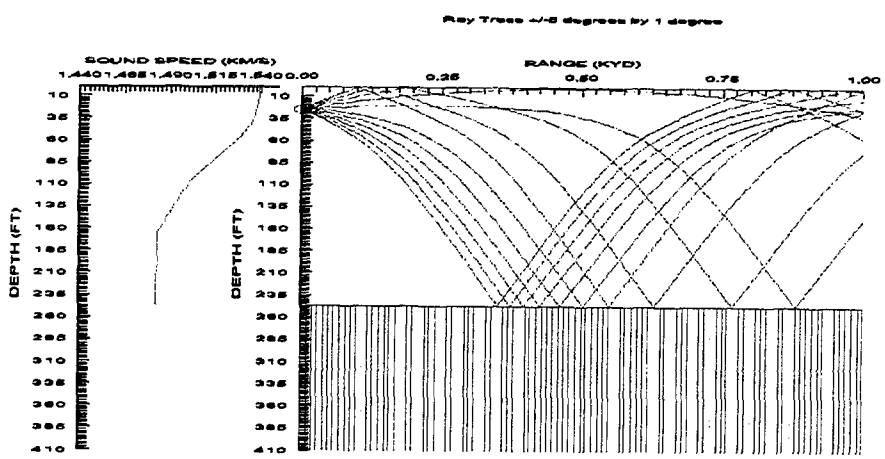

b. **Maximum Detection Range (DR) for a 26 ft. Target Depth = 755 yd, ΔDR = 535 yd**

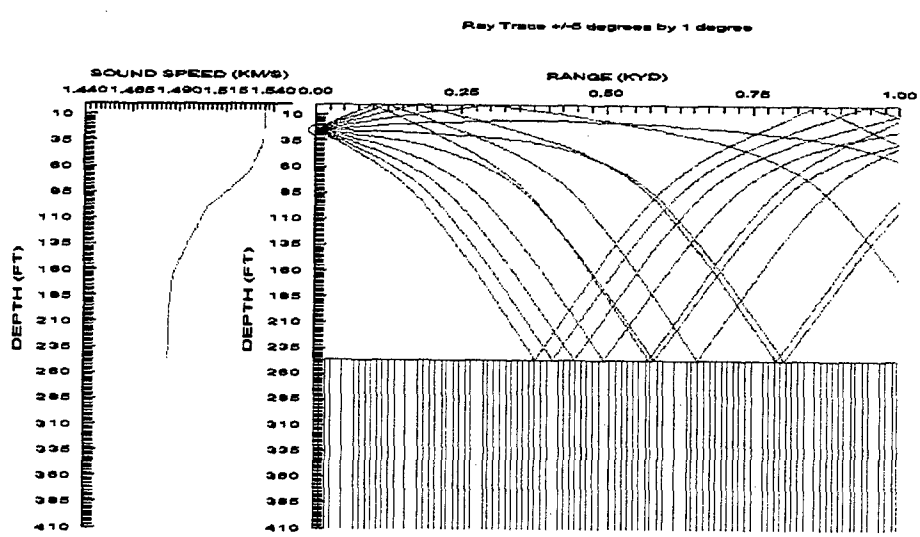

c. **Maximum Detection Range (DR) for a 26 ft. Target Depth = 220 yd**

Mud Bottom/ November/ 36.5 N 123.0 E/ Source Depth = 25 ft/ a. MODAS 1999, b. MODAS 2000, c. GDEM

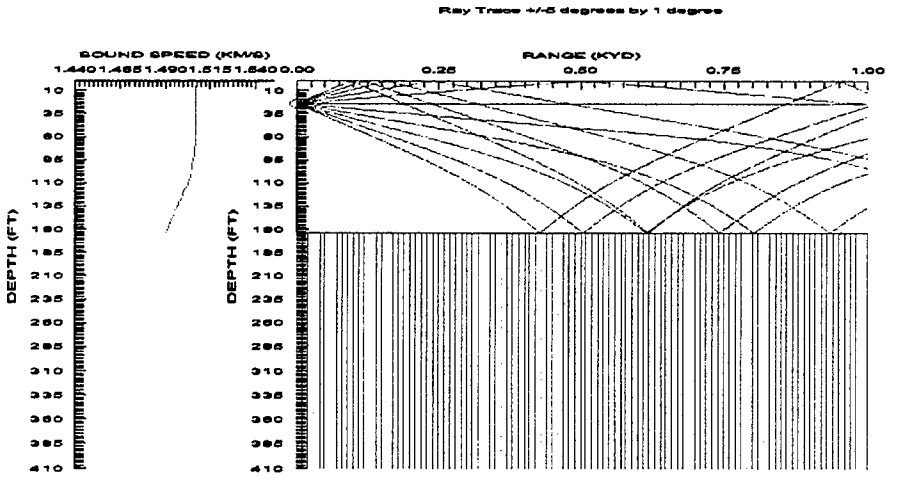

a. Maximum Detection Range (DR) for a 26 ft. Target Depth = 160 yd, ΔDR >840 yd

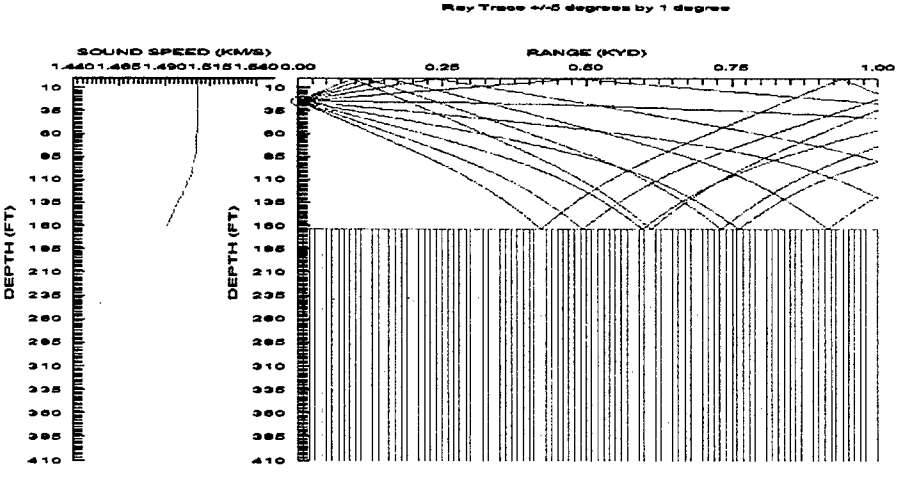

b. Maximum Detection Range (DR) for a 26 ft. Target Depth = 160 yd, ΔDR >840 yd

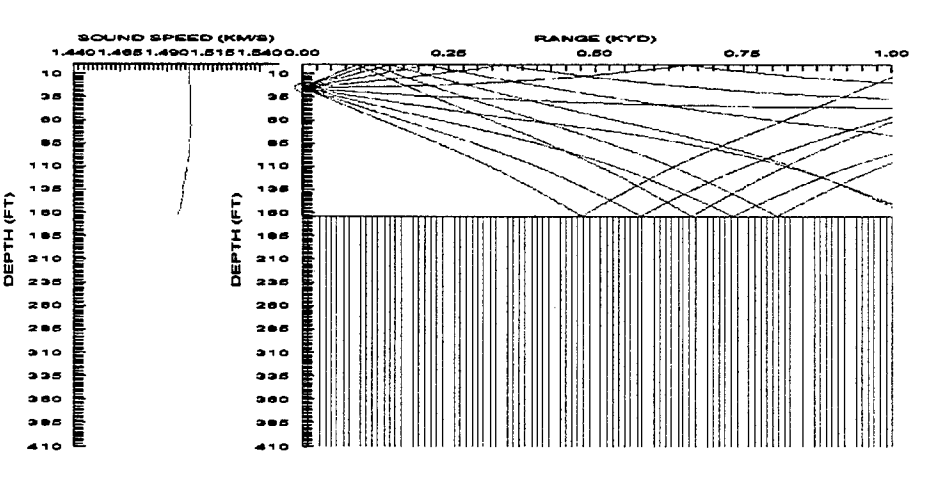

c. Maximum Detection Range (DR) for a 26 ft. Target Depth > 1000 yd

Sand Bottom/ May/ 35.9 N 125.2 E/ Source Depth = 25 ft/ a. MODAS 1999, b. MODAS 2000, c. GDEM

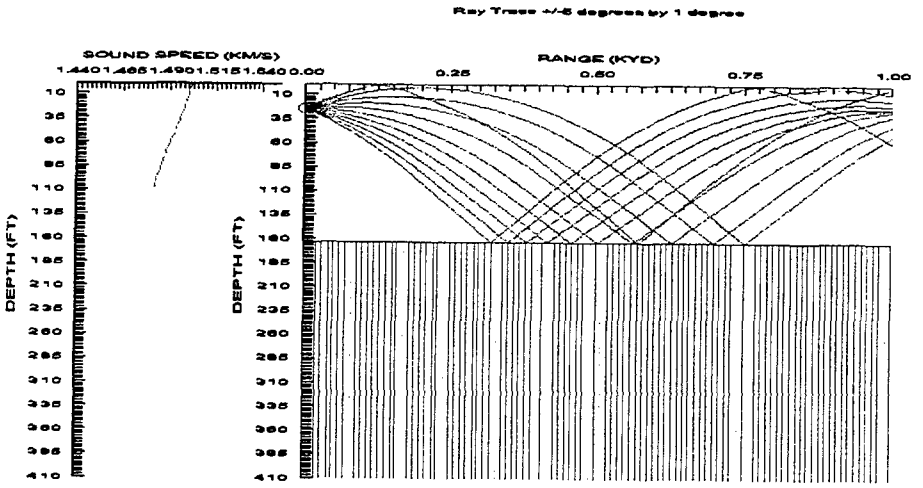

a. Maximum Detection Range (DR) for a 26 ft. Target Depth > 1000 yd, ΔDR >860 yd

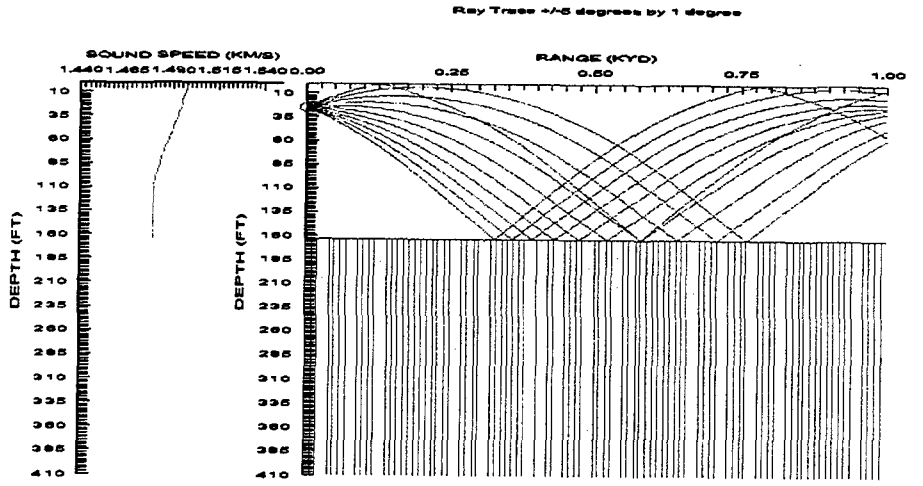

b. Maximum Detection Range (DR) for a 26 ft. Target Depth > 1000 yd, ΔDR >860 yd

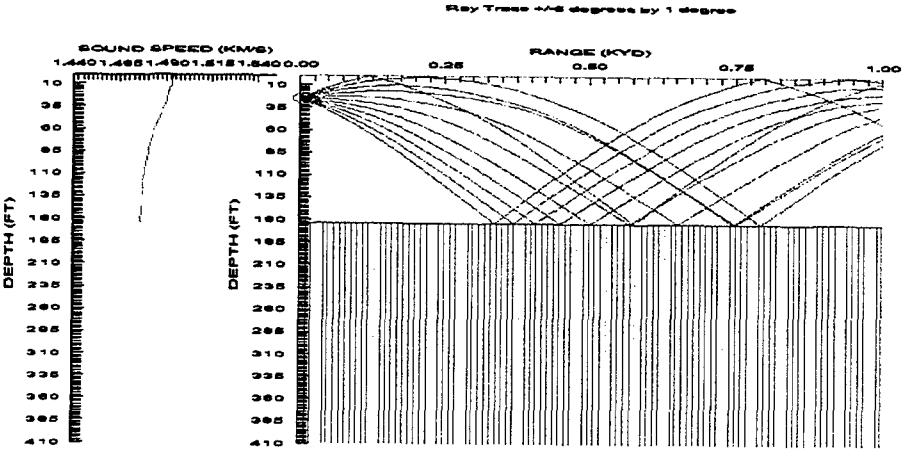

c. Maximum Detection Range (DR) for a 26 ft. Target Depth = 140 yd

Sand Bottom/ August/ 35.9 N 124.8 E/ Source Depth = 25 ft/ a. MODAS 1999, b. MODAS 2000, c. GDEM

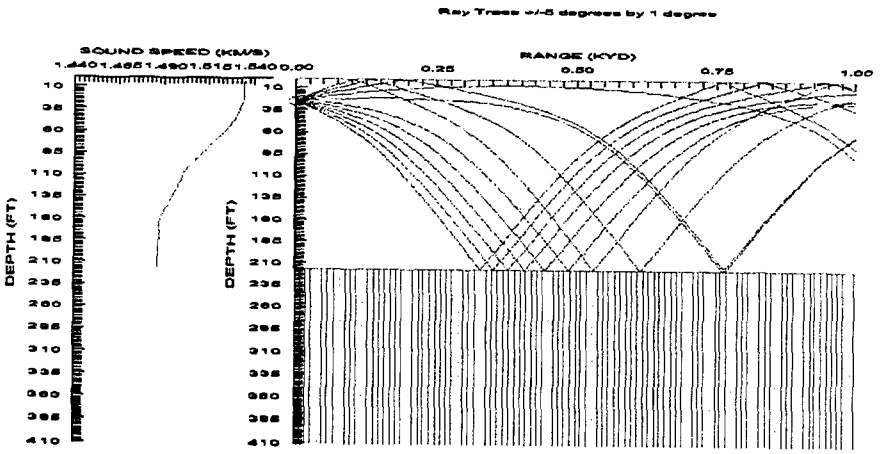

a. **Maximum Detection Range (DR) for a 26 ft. Target Depth > 1000 yd, ΔDR > 390 yd**

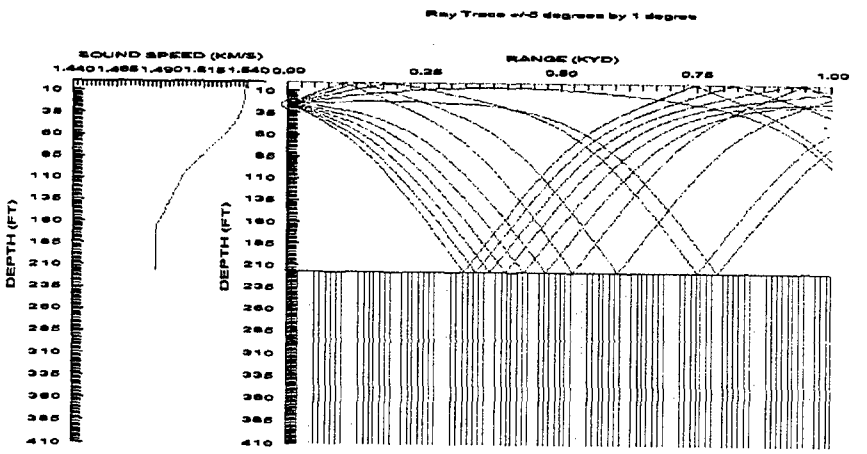

b. **Maximum Detection Range (DR) for a 26 ft. Target Depth = 995 yd, ΔDR = 385 yd**

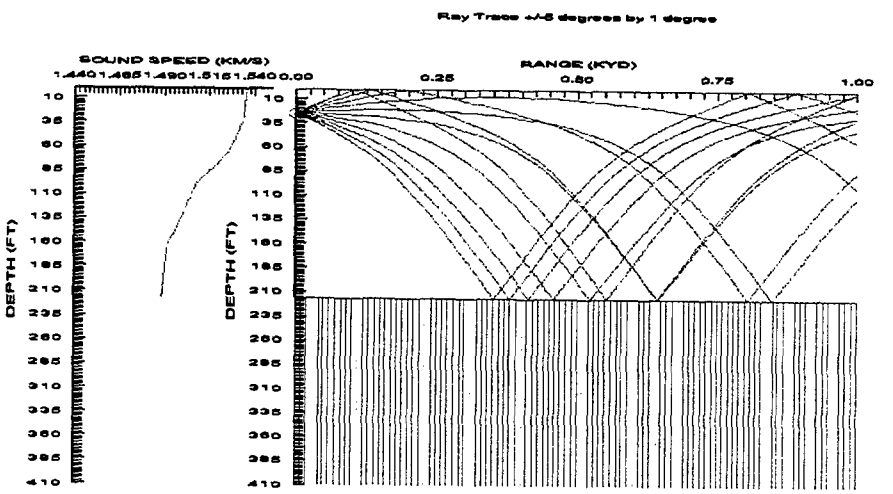

c. **Maximum Detection Range (DR) for a 26 ft. Target Depth = 610 yd**

Mud Bottom/ February/ 35.0 N 123.5 E/ Source Depth = 25 ft/ a. MODAS 1999, b. MODAS 2000, c. GDEM

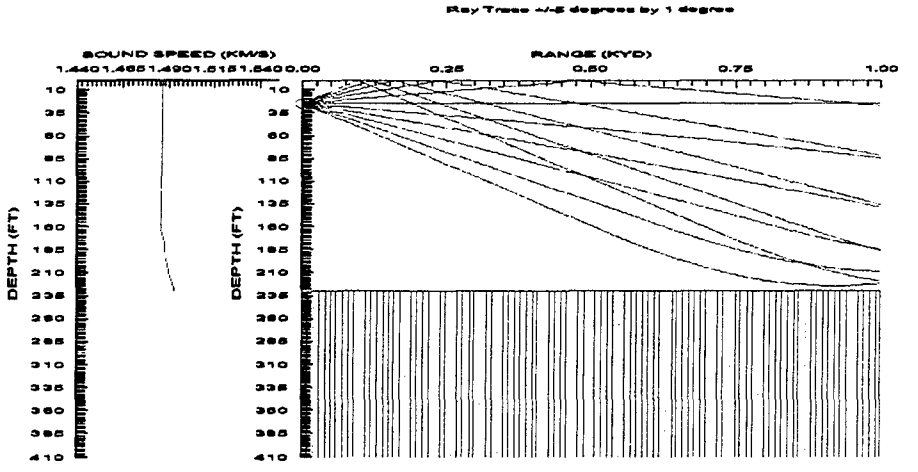

a. **Maximum Detection Range (DR) for a Bottom Target > 1000 yd, ΔDR > 900 yd**

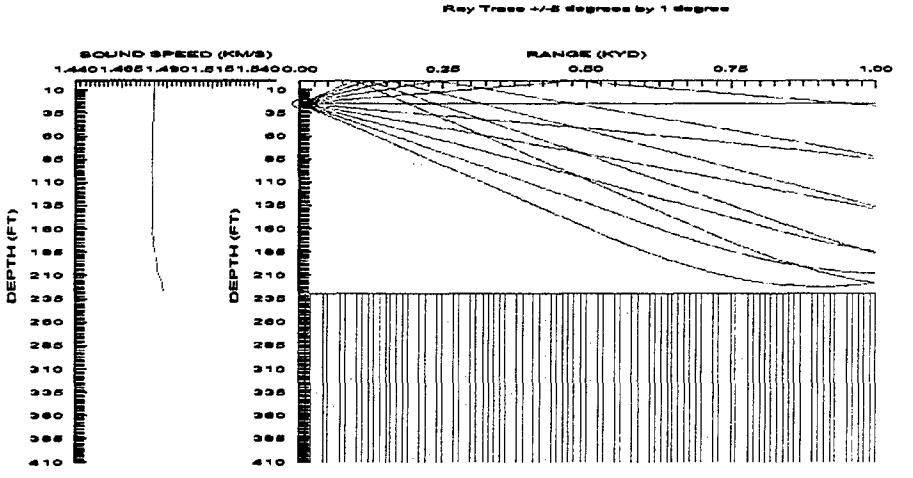

b. **Maximum Detection Range (DR) for a Bottom Target = 990 yd, ΔDR = 100 yd**

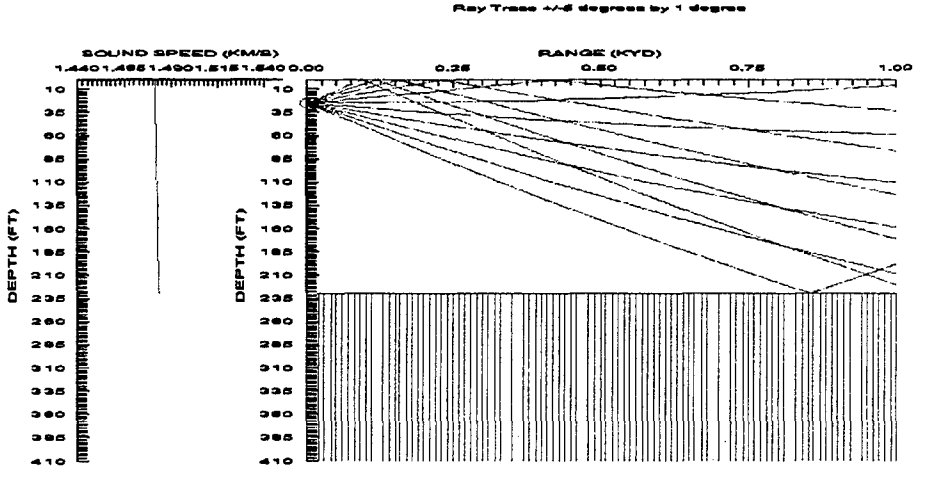

c. **Maximum Detection Range (DR) for a Bottom Target = 100 yd**

Mud Bottom/ May/ 36.3 N 125.0 E/ Source Depth = 25 ft/ a. MODAS 1999, b. MODAS 2000, c. GDEM

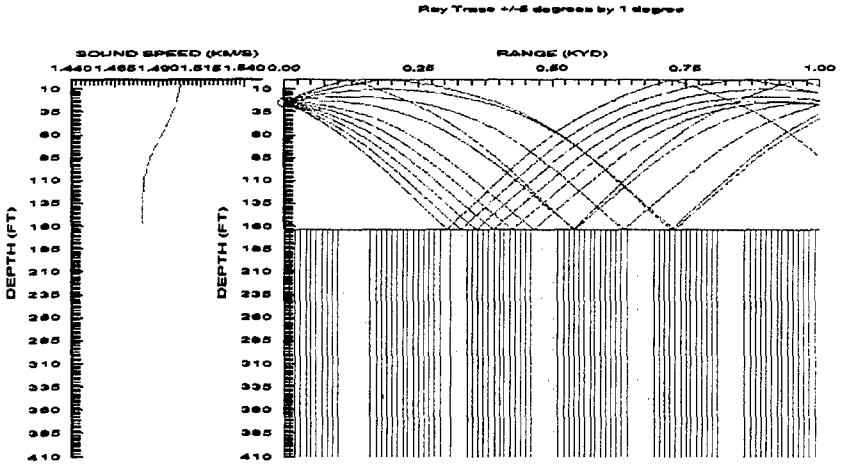

a. **Maximum Detection Range (DR) for a Bottom Target Depth = 0 yd, ΔDR = 655 yd**

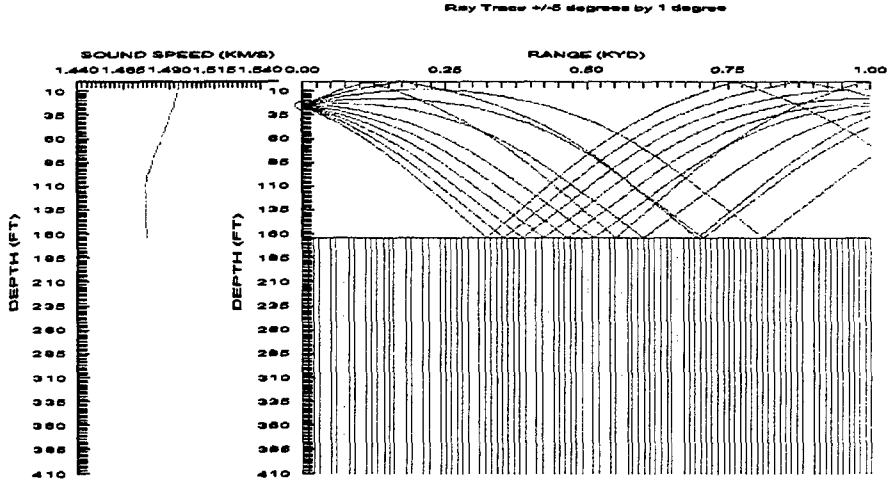

b. **Maximum Detection Range (DR) for a Bottom Target Depth = 0 yd, ΔDR = 655 yd**

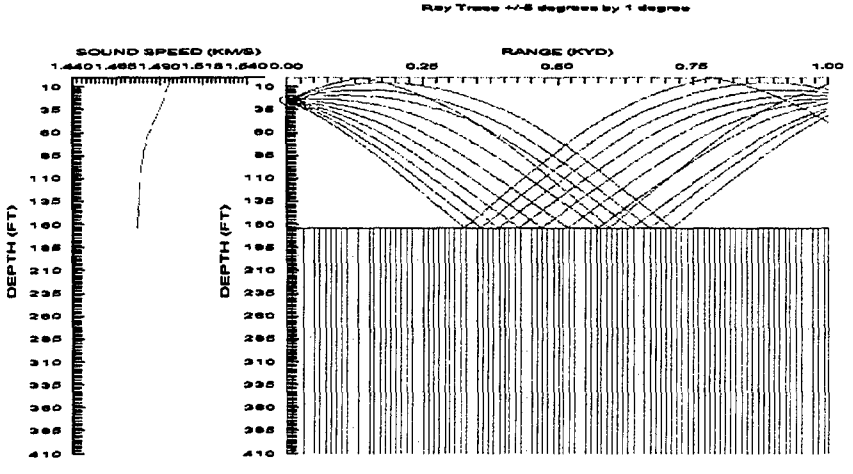

c. **Maximum Detection Range (DR) for a Bottom Target Depth = 655 yd**

Mud Bottom/ February/ 35.0 N 123.5 E/ Source Depth = 125 ft/ a. MODAS 1999, b. MODAS 2000, c. GDEM

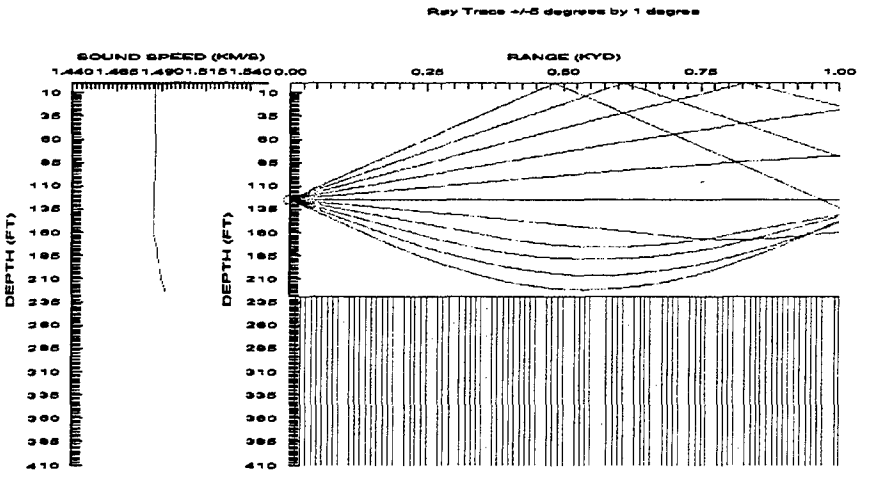

a. Maximum Detection Range (DR) for a 26 ft. Target Depth = 595 yd, ΔDR = 495 yd

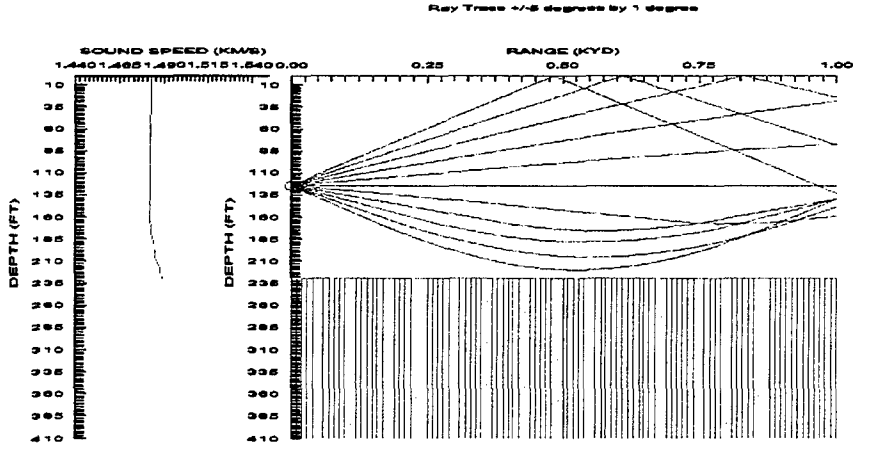

b. Maximum Detection Range (DR) for a 26 ft. Target Depth = 610 yd, ΔDR = 510 yd

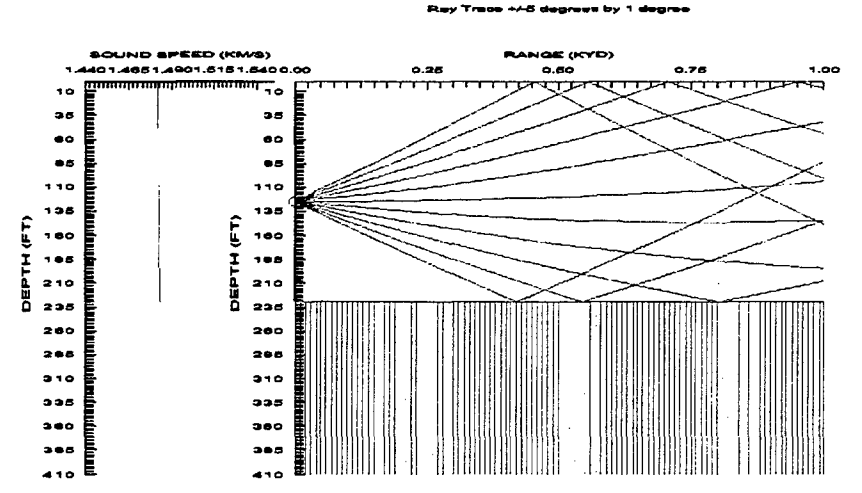

c. Maximum Detection Range (DR) for a 26 ft. Target Depth = 100 yd

Mud Bottom/ November/ 36.5 N 123.0 E/ Source Depth = 125 ft/ a. MODAS 1999, b. MODAS 2000, c. GDEM

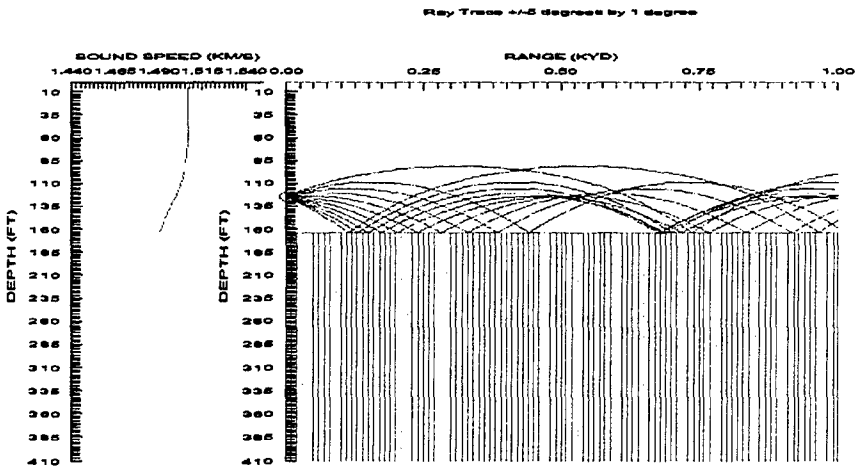

a. **Maximum Detection Range (DR) for a 26 ft. Target Depth = 495 yd, ΔDR = 495 yd**

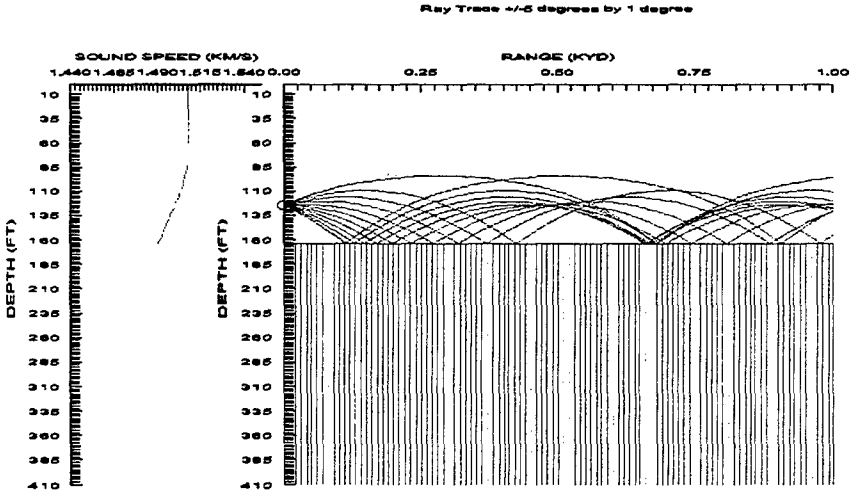

b. **Maximum Detection Range (DR) for a 26 ft. Target Depth = 510 yd, ΔDR = 510 yd**

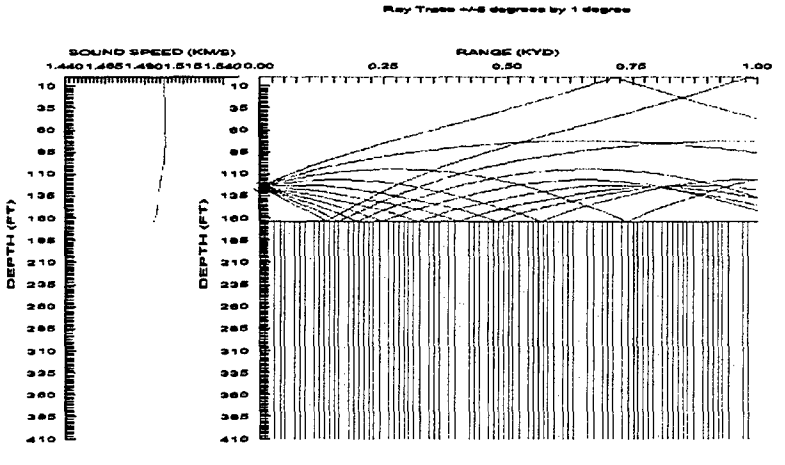

c. **Maximum Detection Range (DR) for a 26 ft. Target Depth = 0 yd**

Sand Bottom/ August/ 35.9 N 124.6 E/ Source Depth = 125 ft/ a. MODAS 1999, b. MODAS 2000, c. GDEM

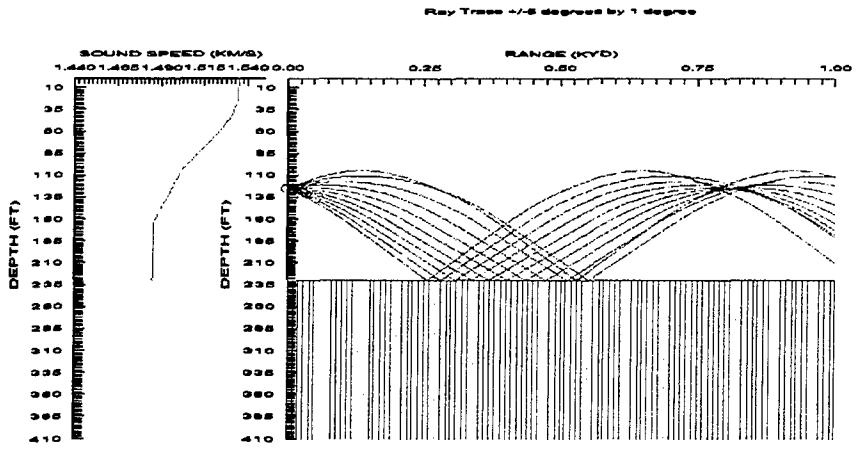

a. **Maximum Detection Range (DR) for a 26 ft. Target Depth = 90 yd, ΔDR = 525 yd**

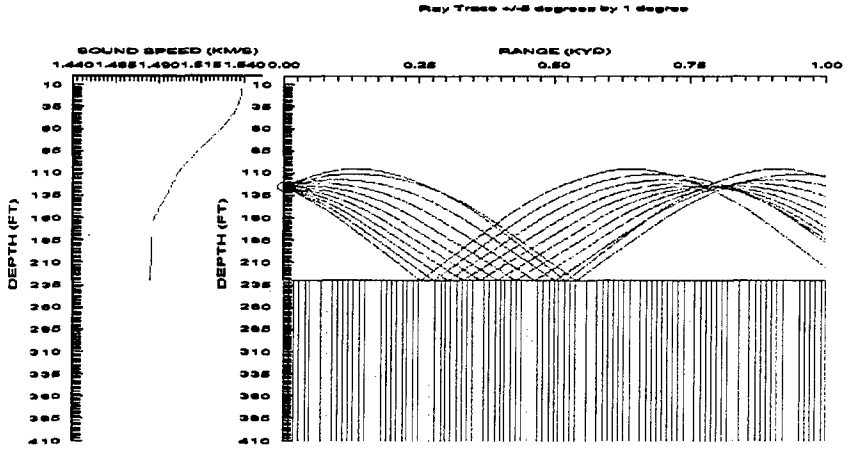

b. **Maximum Detection Range (DR) for a 26 ft. Target Depth = 90 yd, ΔDR = 525 yd**

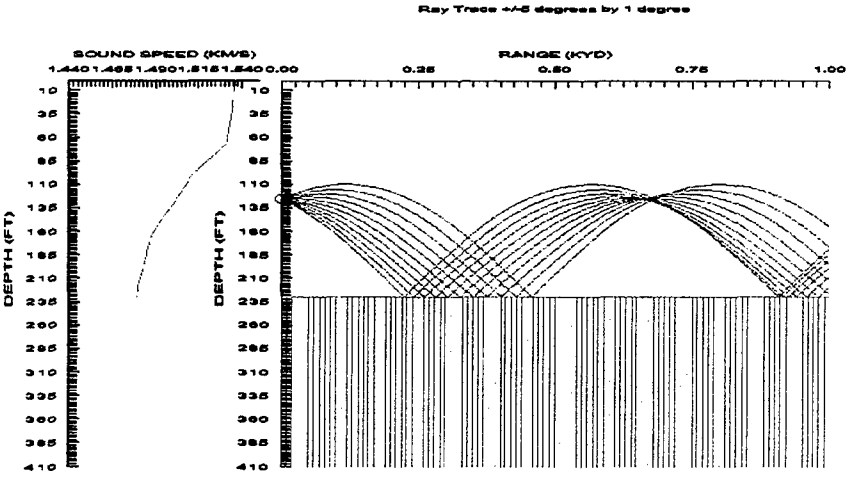

c. **Maximum Detection Range (DR) for a 26 ft. Target Depth = 615 yd**

Sand Bottom/ November/ 35.9 N 124.6 E/ Source Depth = 125 ft/ a. MODAS 2000, b. GDEM

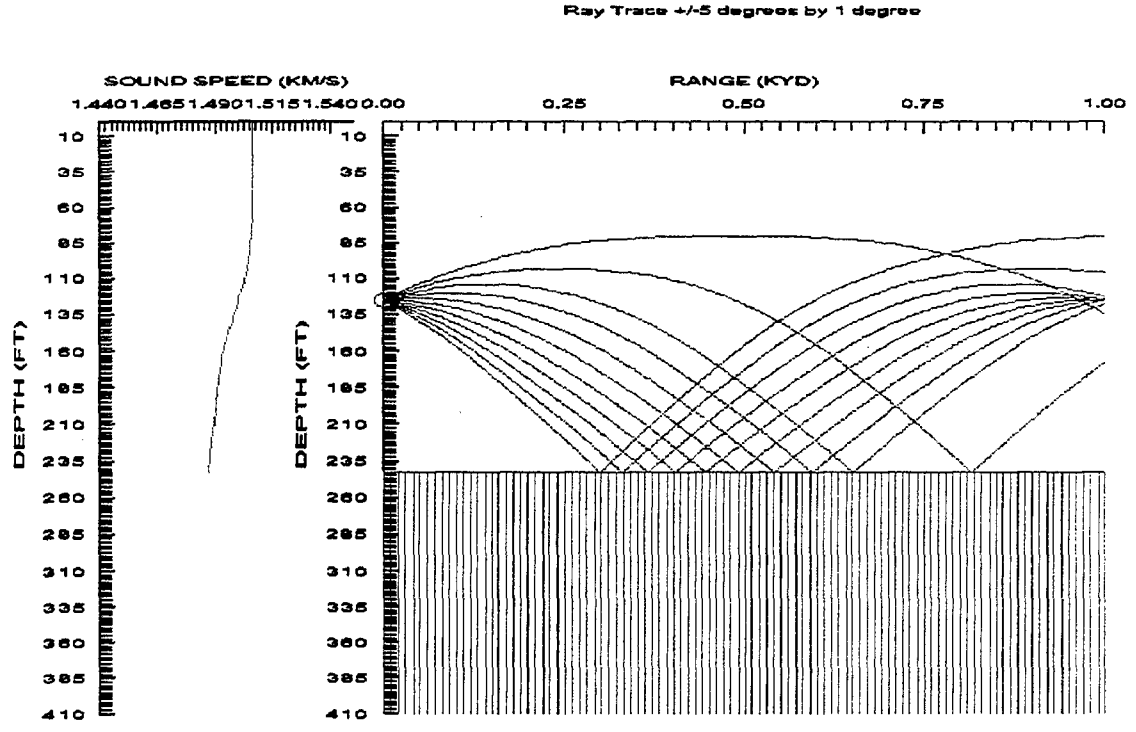

a. **Maximum Detection Range (DR) for a 26 ft. Target Depth = 110 yd, ΔDR = 535 yd**

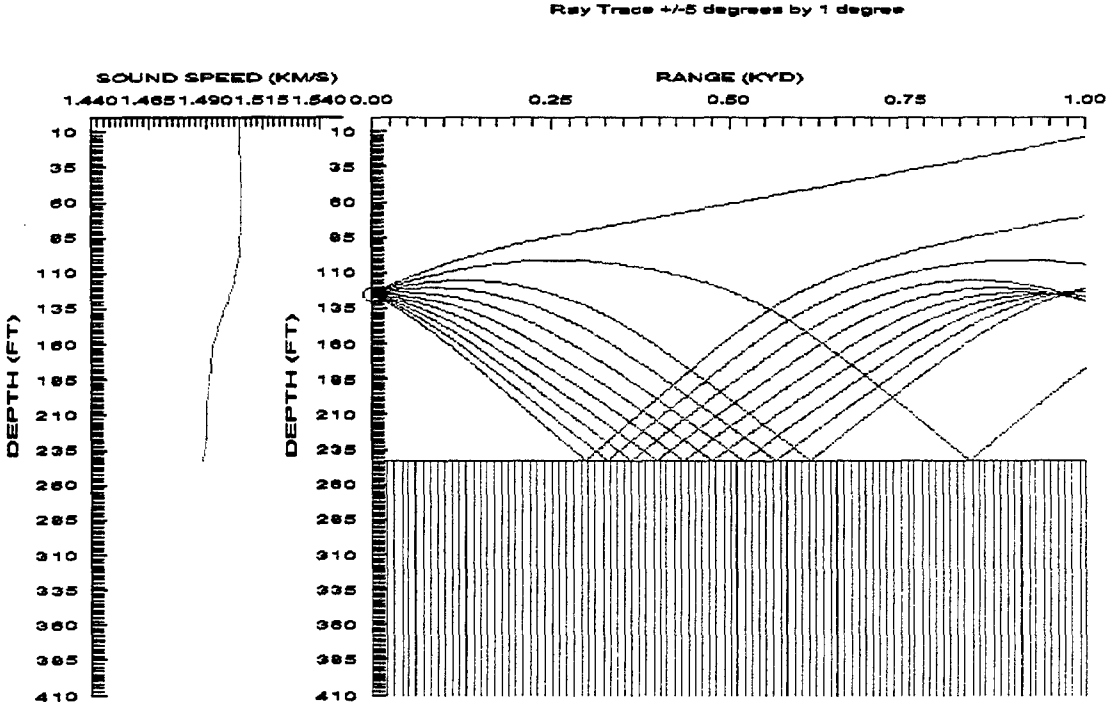

b. **Maximum Detection Range (DR) for a 26 ft. Target Depth = 645 yd**

Mud Bottom/ February/ 35.0 N 123.5 E/ Source Depth = 125 ft/ a. MODAS 1999, b. MODAS 2000, c. GDEM

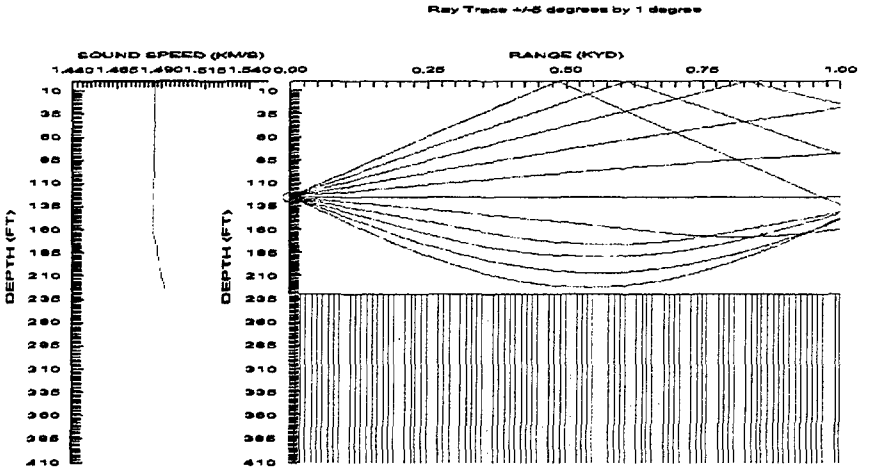

a. Maximum Detection Range (DR) for a Bottom Target = 660 yd, ΔDR = 340 yd

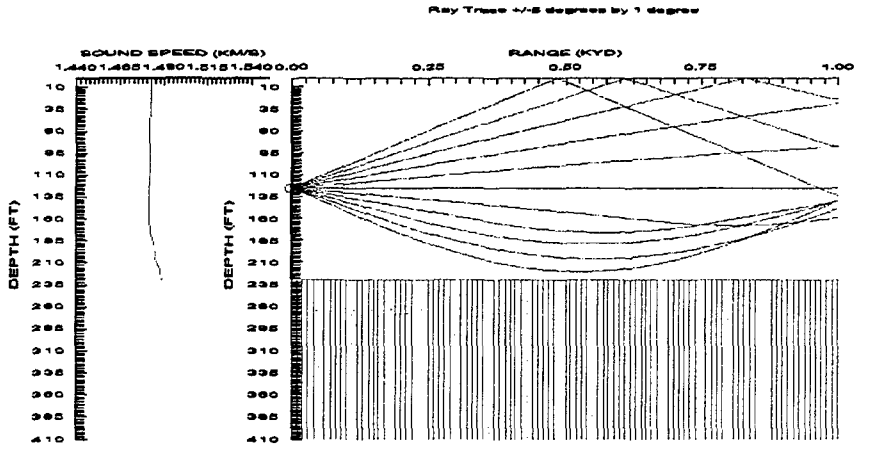

b. Maximum Detection Range (DR) for a Bottom Target = 645 yd, ΔDR > 355 yd

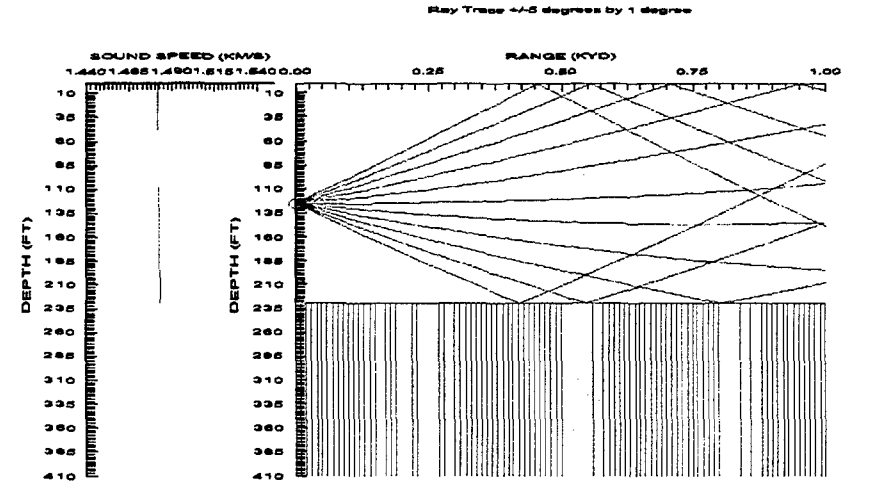

c. Maximum Detection Range (DR) for a Bottom Target > 1000 yd

Mud Bottom/ May/ 35.0 N 123.5 E/ Source Depth = 125 ft/ a. MODAS 1999, b. MODAS 2000, c. GDEM

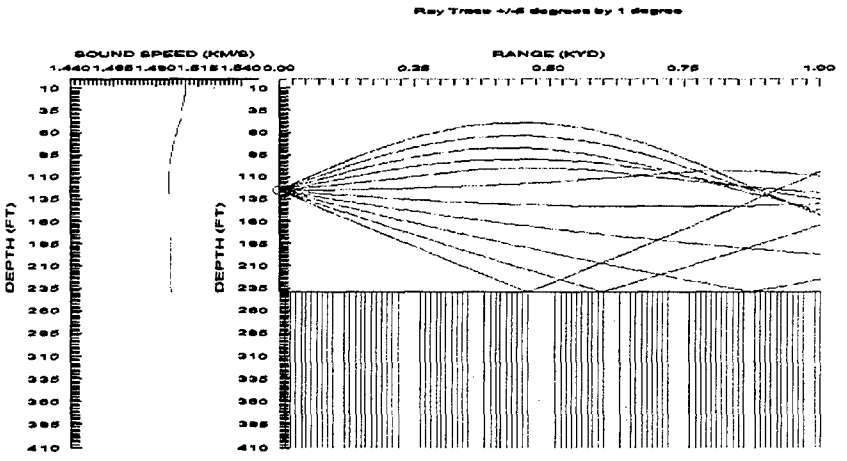

a. **Maximum Detection Range (DR) for a Bottom Target > 1000 yd, ΔDR > 895 yd**

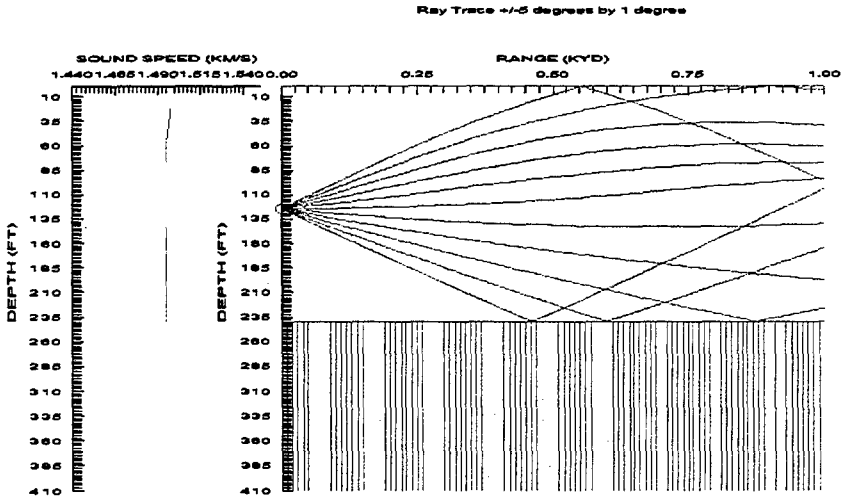

b. **Maximum Detection Range (DR) for a Bottom Target > 1000 yd, ΔDR > 895 yd**

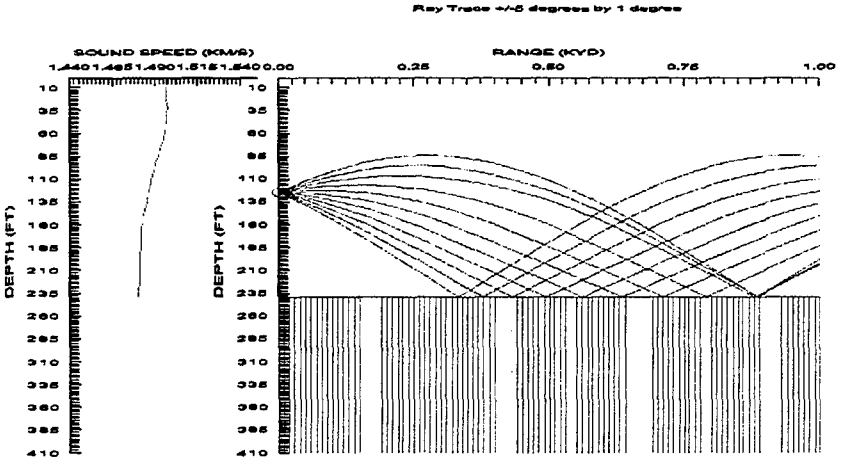

c. **Maximum Detection Range (DR) for a Bottom Target = 105 yd**

Mud Bottom/ November/ 36.5 N 123.0 E/ Source Depth = 125 ft/ a. MODAS 1999, b. MODAS 2000, c. GDEM

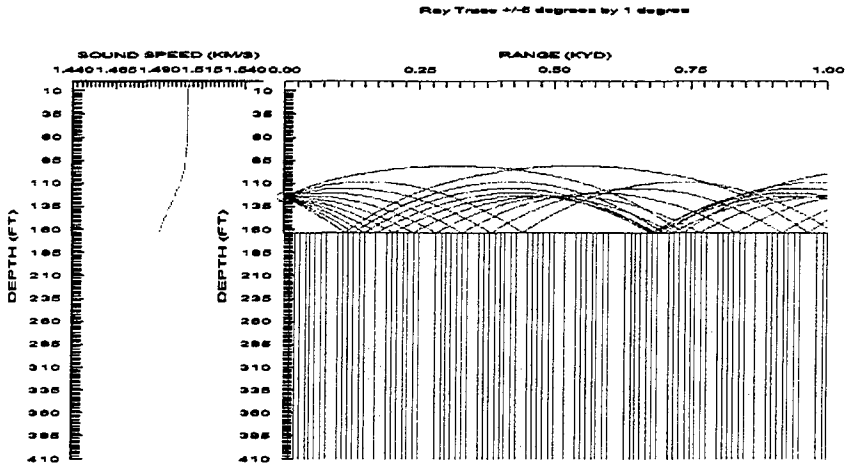

a. **Maximum Detection Range (DR) for a Bottom Target = 670 yd, ΔDR = 250 yd**

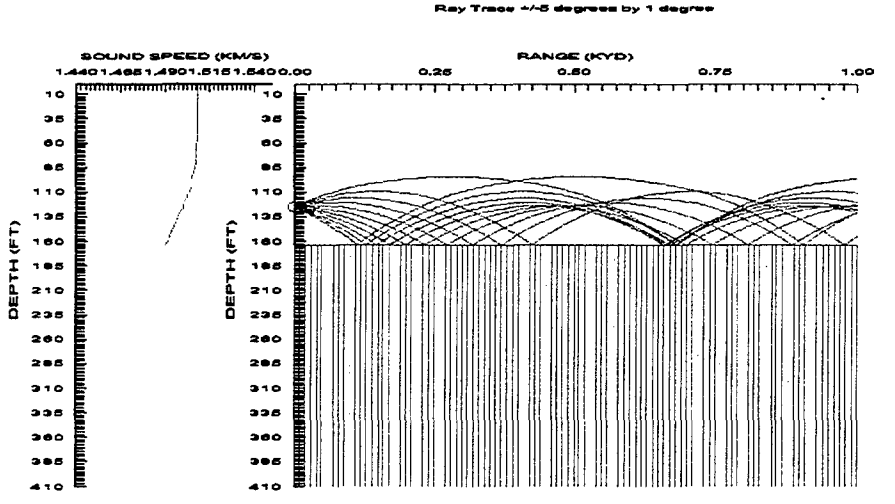

b. **Maximum Detection Range (DR) for a Bottom Target = 655 yd, ΔDR = 235 yd**

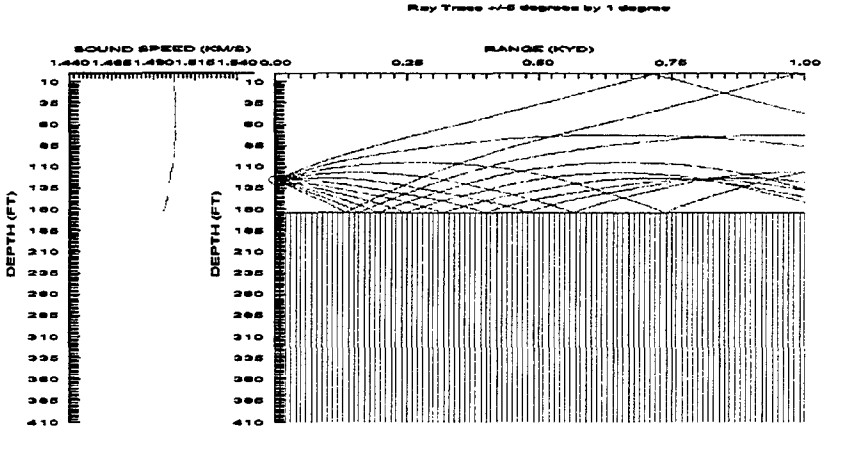

c. **Maximum Detection Range (DR) for a Bottom Target = 420 yd**

Sand Bottom/ August/ 35.9 N 124.6 E/ Source Depth = 125 ft/ a. MODAS 1999, b. MODAS 2000, c. GDEM

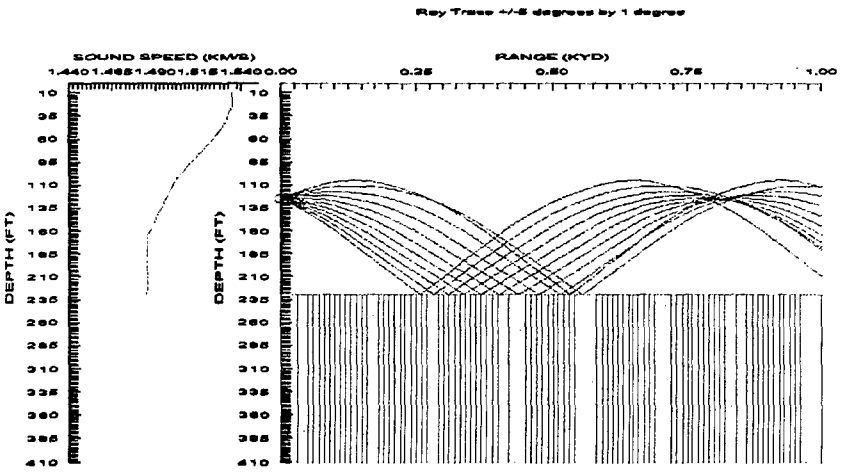

a. **Maximum Detection Range (DR) for a Bottom Target = 885 yd, ΔDR = 385 yd**

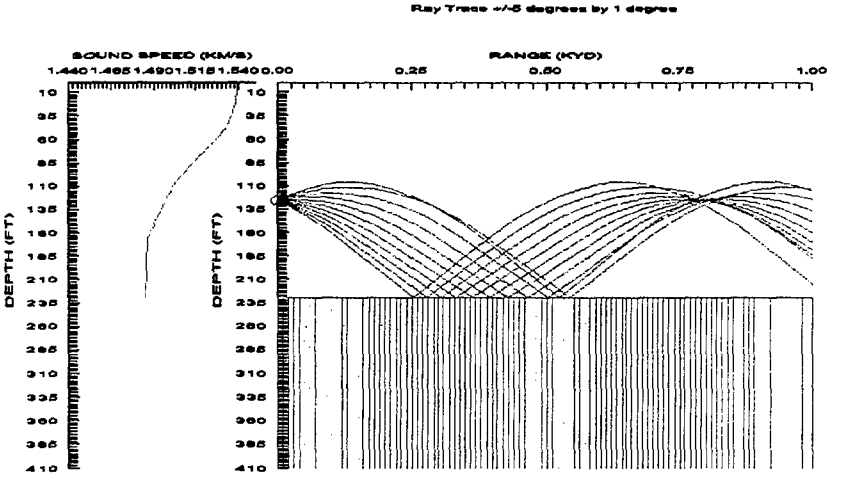

b. **Maximum Detection Range (DR) for a Bottom Target = 860 yd, ΔDR = 360 yd**

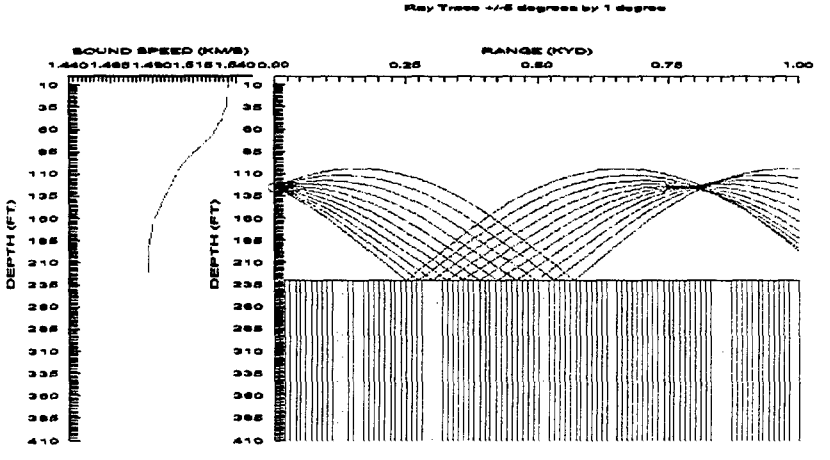

c. **Maximum Detection Range (DR) for a Bottom Target = 500 yd**

Gravel Bottom/ May/ 39.0 N 122.8 E/ Source Depth = 25 ft/ a. MODAS 2000, b. GDEM

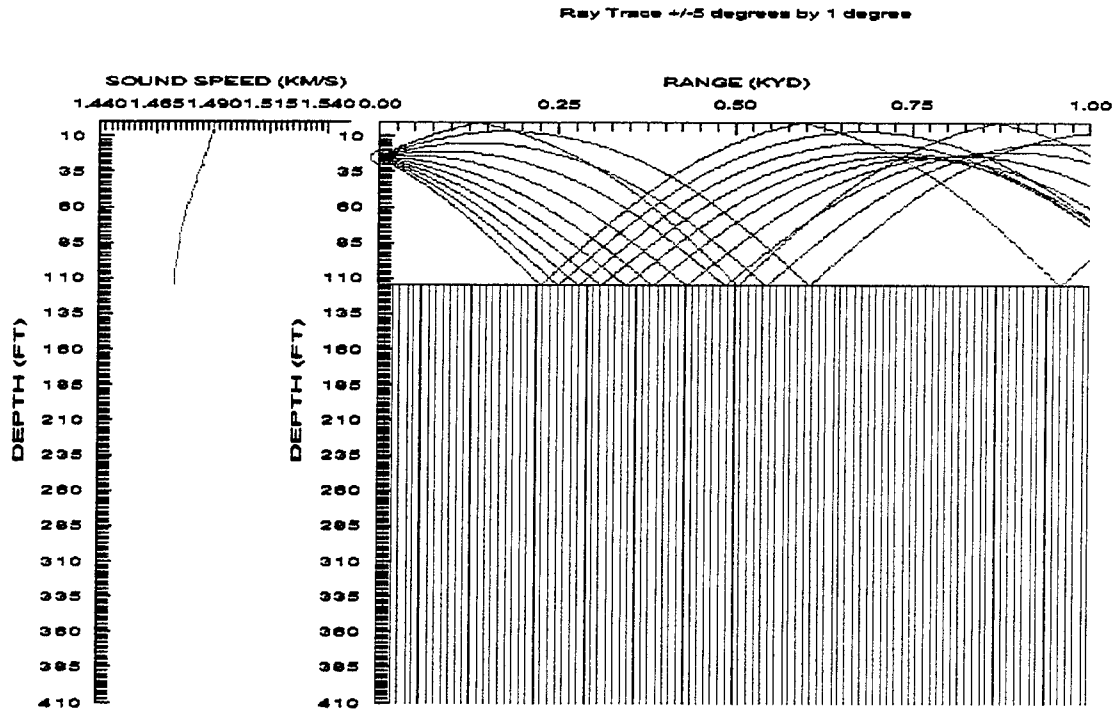

a. **Maximum Detection Range (DR) for a 26 ft. Target Depth = 80 yd, ΔDR = 775 yd**

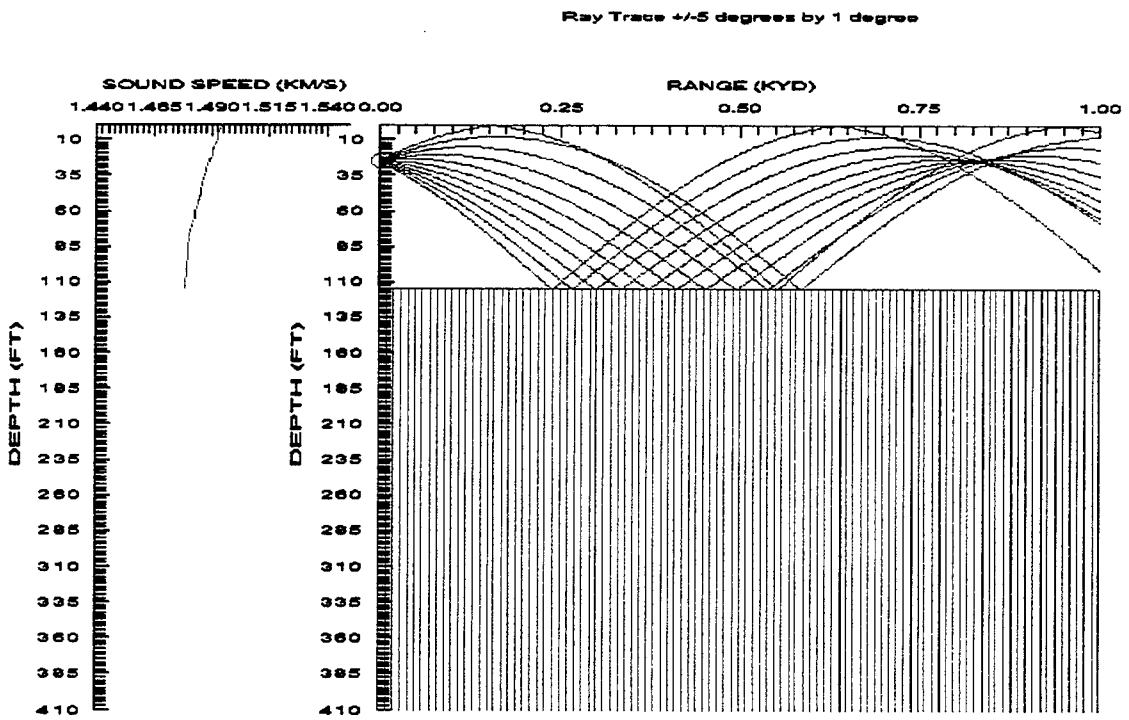

b. **Maximum Detection Range (DR) for a 26 ft. Target Depth = 855 yd**

Gravel Bottom/ August/ 38.6 N 122.0 E/ Source Depth = 25 ft/ a. MODAS 1999, b. MODAS 2000, c. GDEM

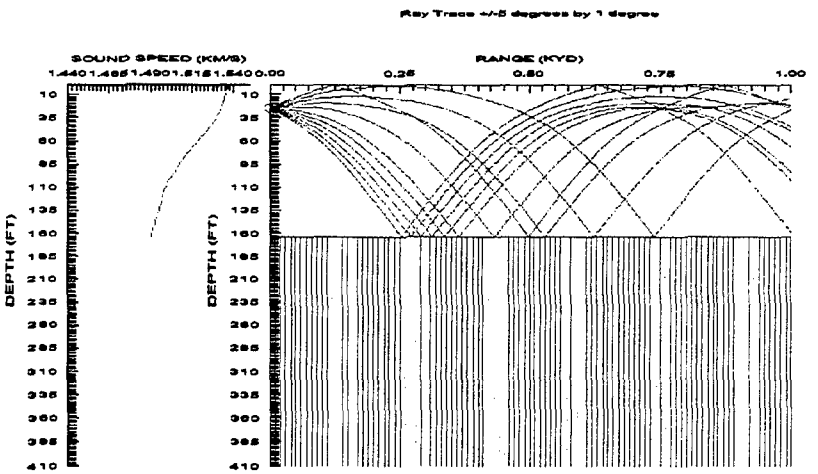

a. Maximum Detection Range (DR) for a 26 ft. Target Depth = 100 yd, ΔDR = 850 yd

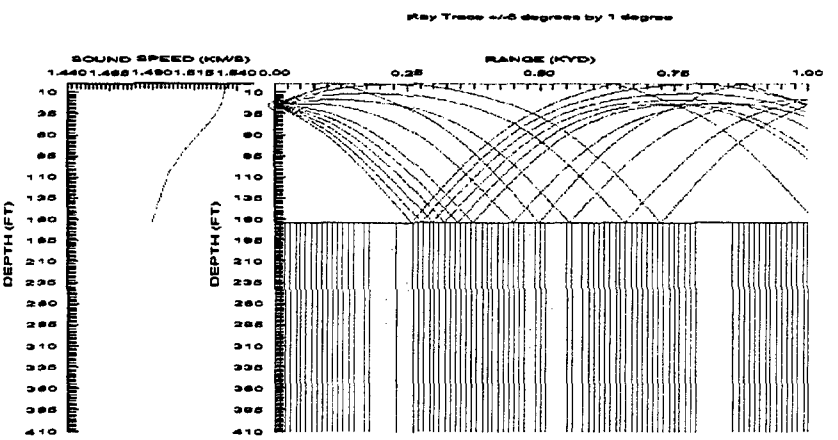

b. Maximum Detection Range (DR) for a 26 ft. Target Depth = 100 yd, ΔDR = 850 yd

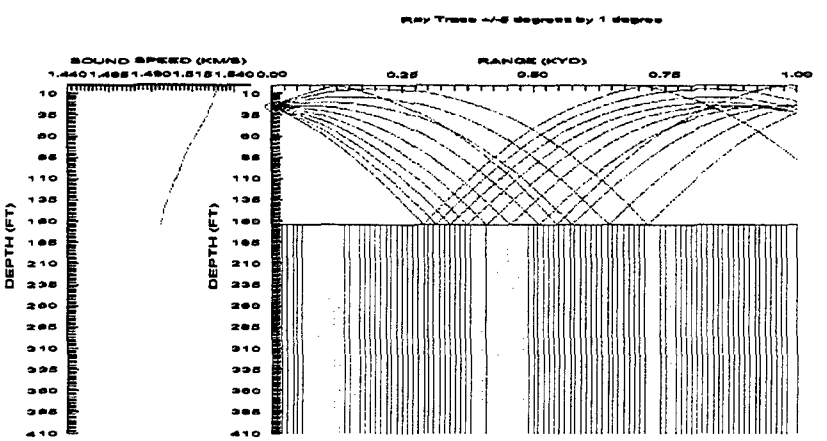

c. Maximum Detection Range (DR) for a 26 ft. Target Depth = 950 yd

Gravel Bottom/ August/ 38.6 N 122.0 E/ Source Depth = 75 ft/ a. MODAS 1999, b. MODAS 2000, c. GDEM

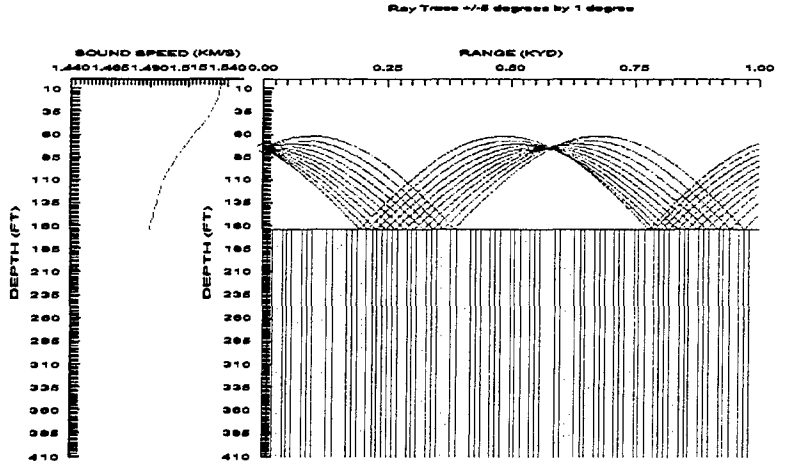

a. **Maximum Detection Range (DR) for a Bottom Target = 0 yd, ΔDR = 955 yd**

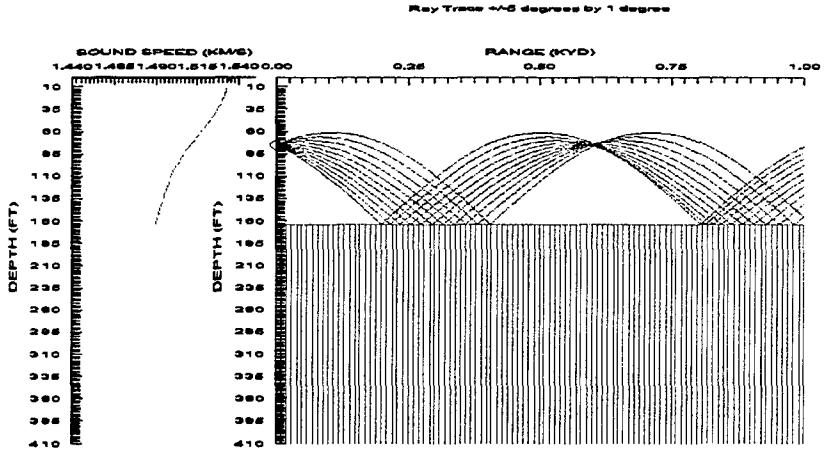

b. **Maximum Detection Range (DR) for a Bottom Target = 0 yd, ΔDR = 955 yd**

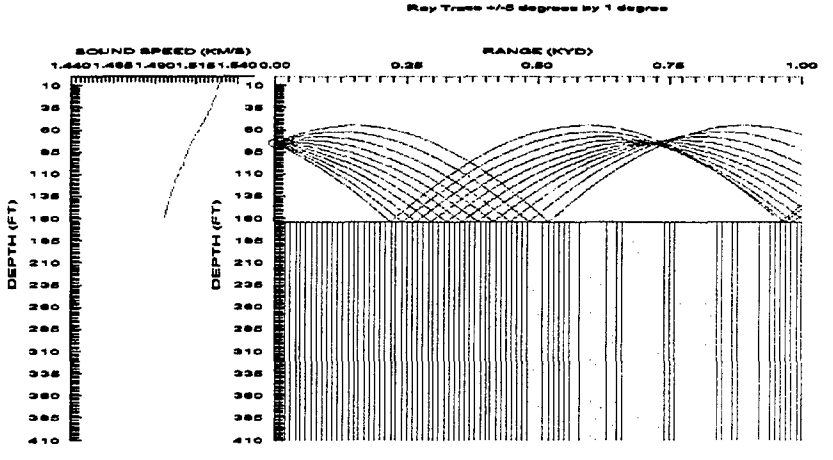

c. **Maximum Detection Range (DR) for a Bottom Target = 955 yd**

Gravel Bottom/ November/ 38.4 N 122.1 E/ Source Depth = 125 ft/ a. MODAS 1999, b. MODAS 2000, c. GDEM

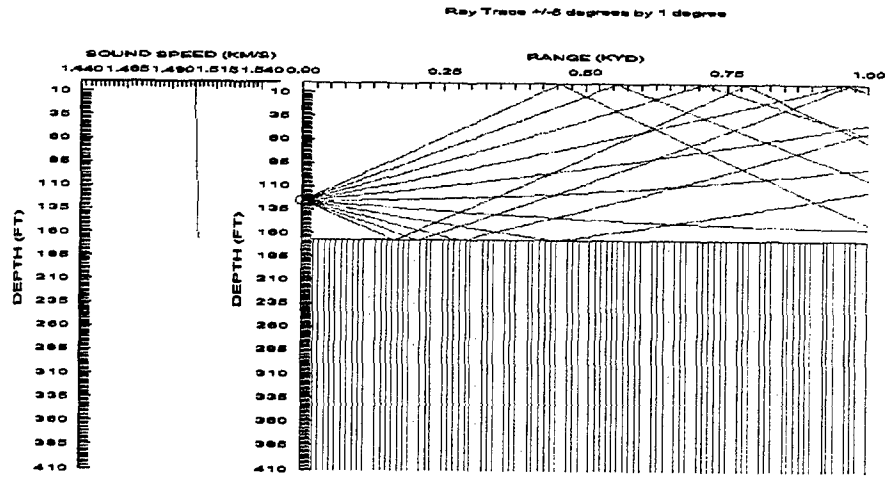

a. **Maximum Detection Range (DR) for a Bottom Target Depth = 245 yd, ΔDR = 220 yd**

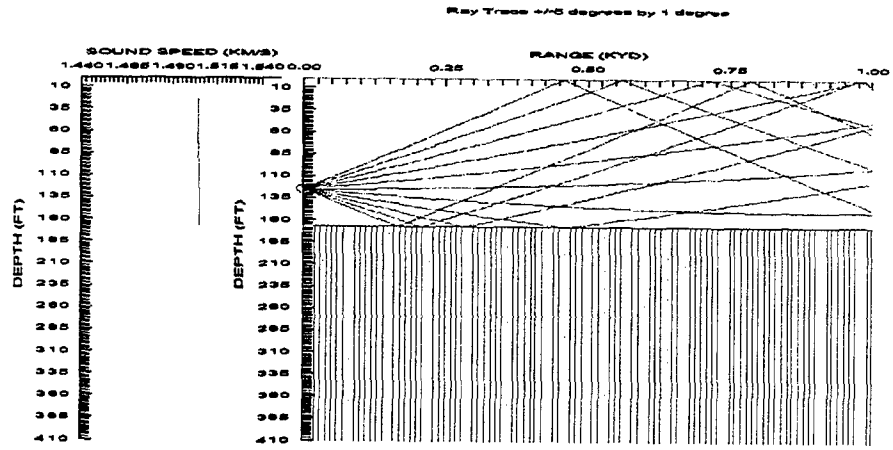

b. **Maximum Detection Range (DR) for a Bottom Target Depth = 250 yd, ΔDR = 225 yd**

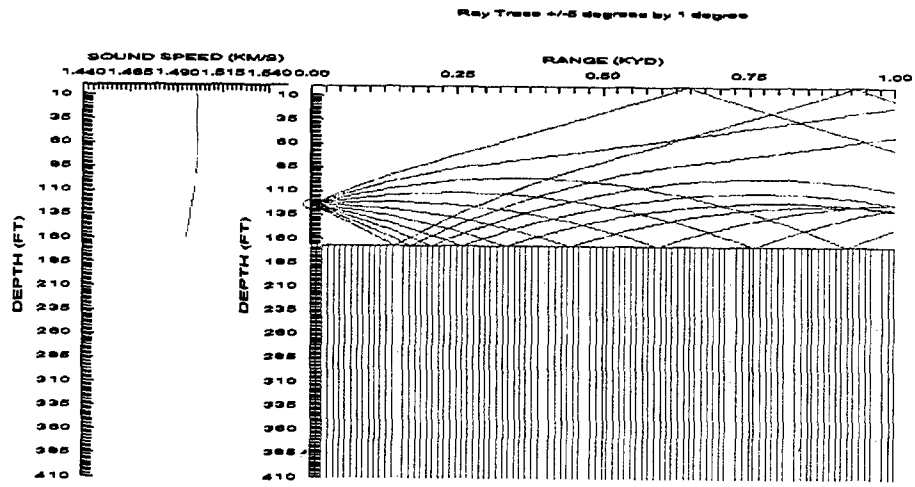

c. **Maximum Detection Range (DR) for a Bottom Target Depth = 25 yd**

Rock Bottom/ May/ 37.5 N 123.0 E/ Source Depth = 125 ft/ a. MODAS 1999, b. MODAS 2000, c. GDEM

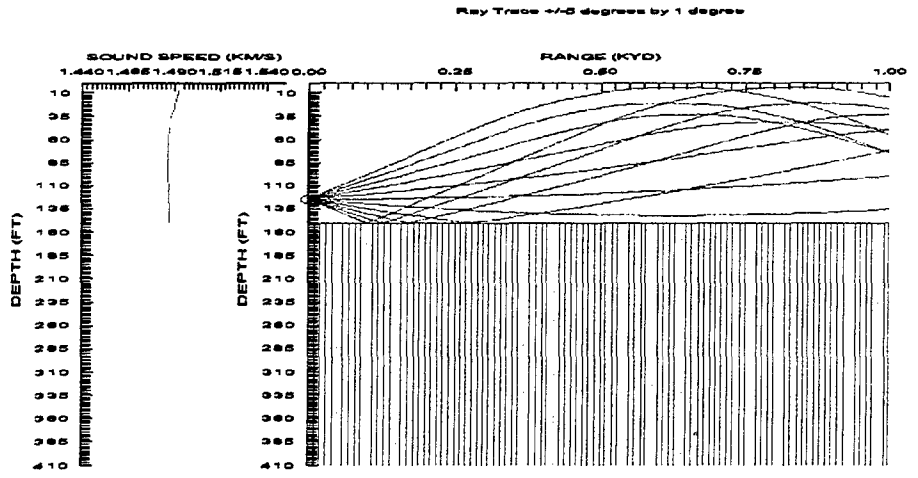

a. **Maximum Detection Range (DR) for a Bottom Target Depth = 215 yd, ΔDR = 190 yd**

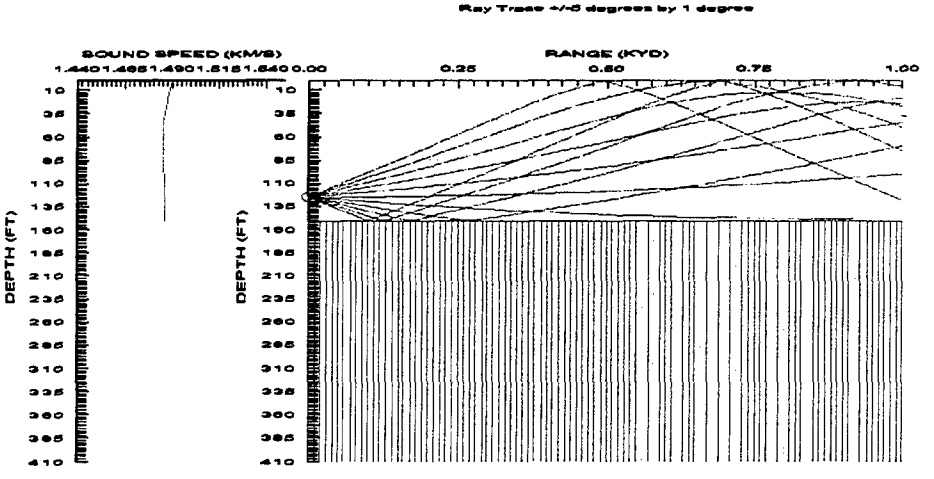

b. **Maximum Detection Range (DR) for a Bottom Target Depth = 210 yd, ΔDR = 185 yd**

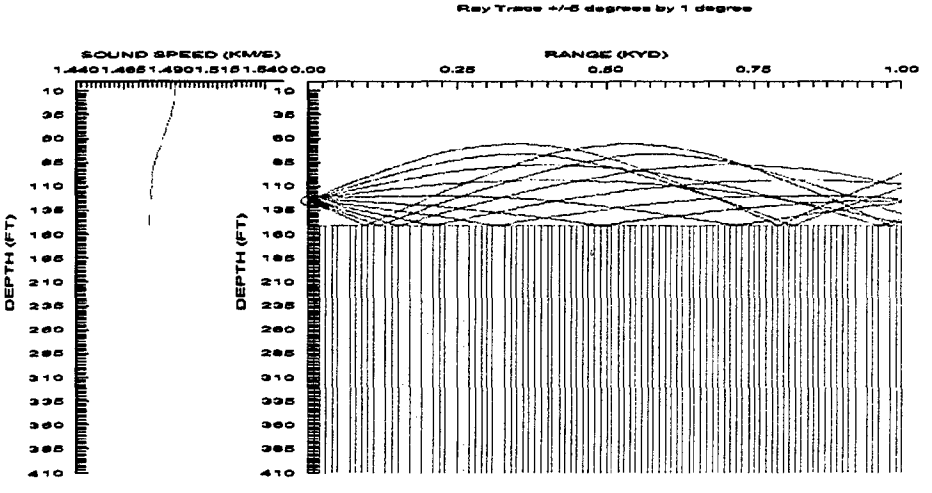

c. **Maximum Detection Range (DR) for a Bottom Target Depth = 25 yd**

THIS PAGE INTENTIONALLY LEFT BLANK

APPENDIX C. HISTOGRAMS FOR HYDROGRAPHIC DATA COMPARISONS

HISTOGRAMS FOR DIFFERENCES IN MAXIMUM DETECTION RANGES FOR ALL TARGET DEPTHS/ FEBRUARY 2000/ MUD BOTTOM/ SOURCE DEPTH = 125 FT.

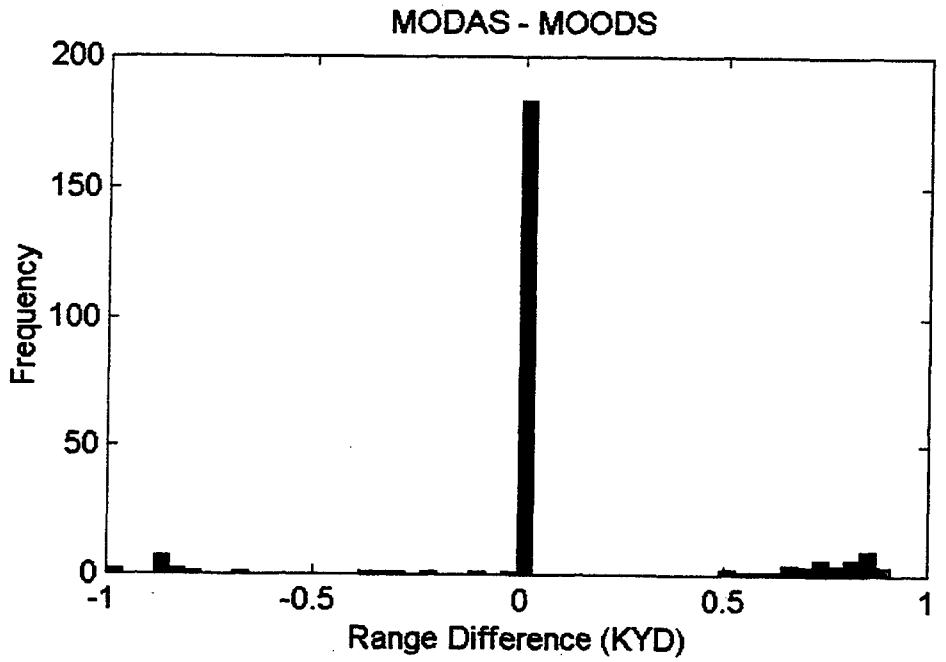

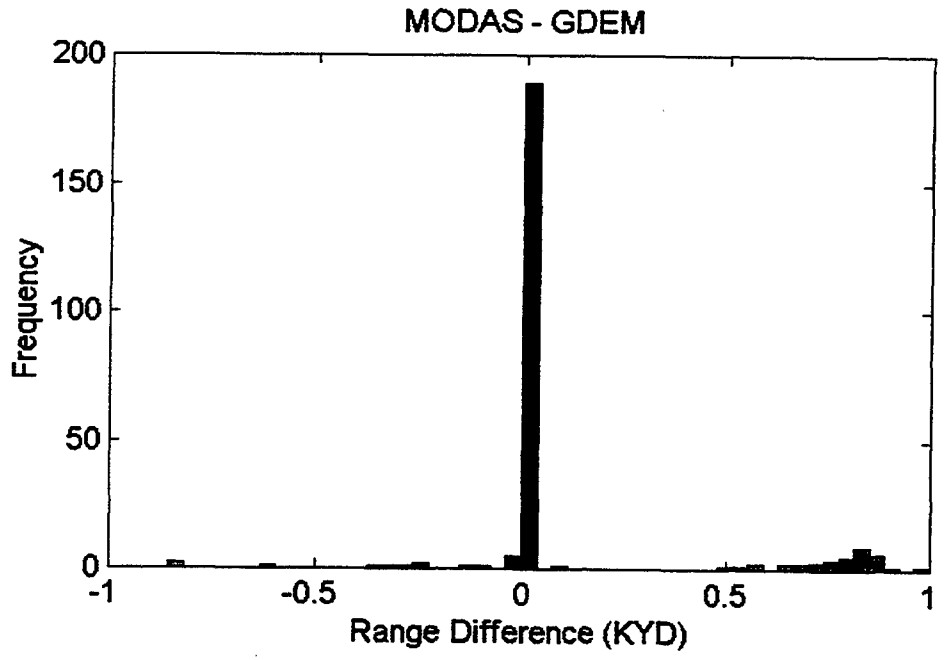

HISTOGRAMS FOR DIFFERENCES IN MAXIMUM DETECTION RANGES FOR ALL TARGET DEPTHS/ FEBRUARY 1999/ MUD BOTTOM/ SOURCE DEPTH = 25 FT.

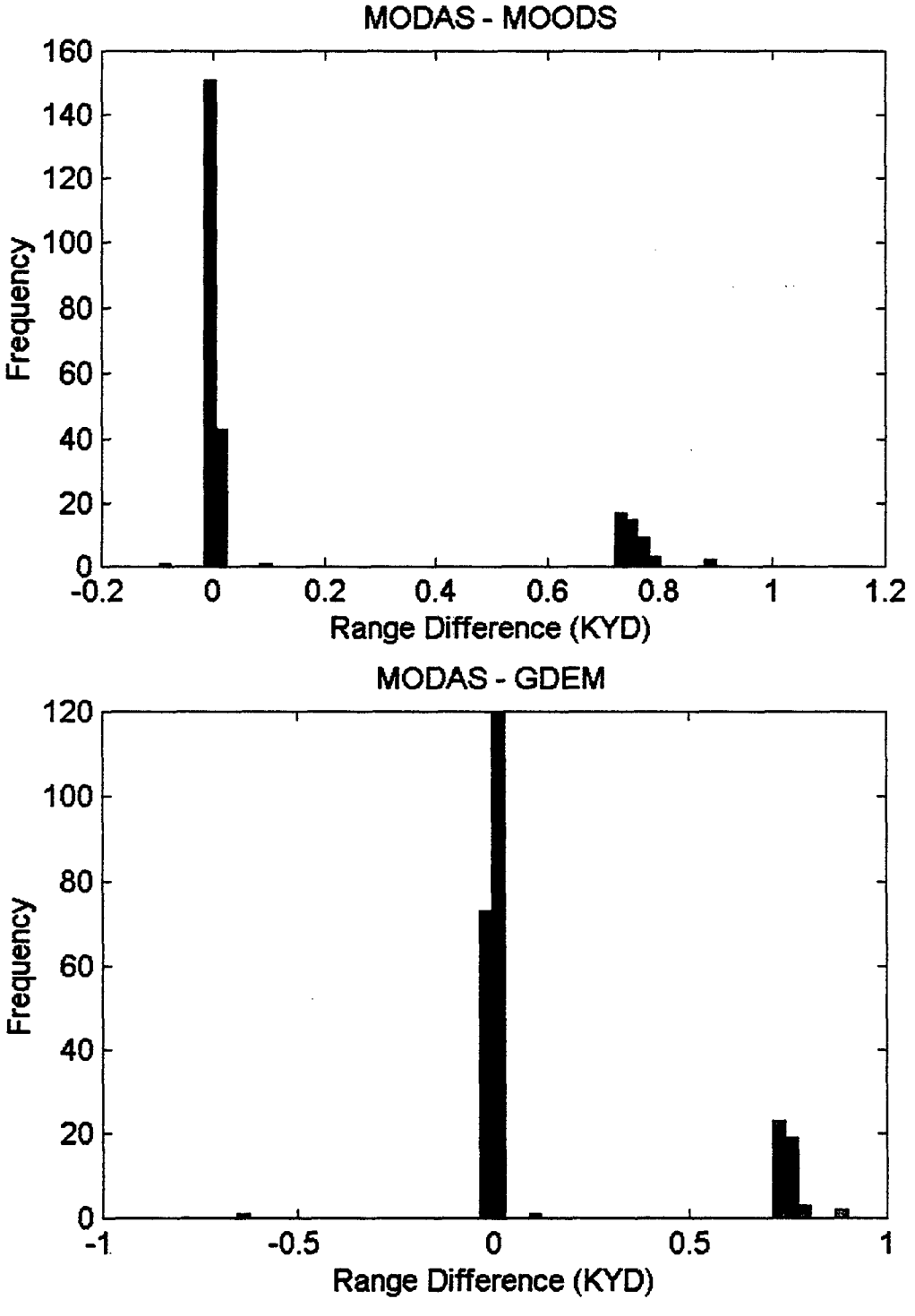

HISTOGRAMS FOR DIFFERENCES IN MAXIMUM DETECTION RANGES FOR ALL TARGET DEPTHS/ FEBRUARY 1999/ MUD BOTTOM/ SOURCE DEPTH = 125 FT.

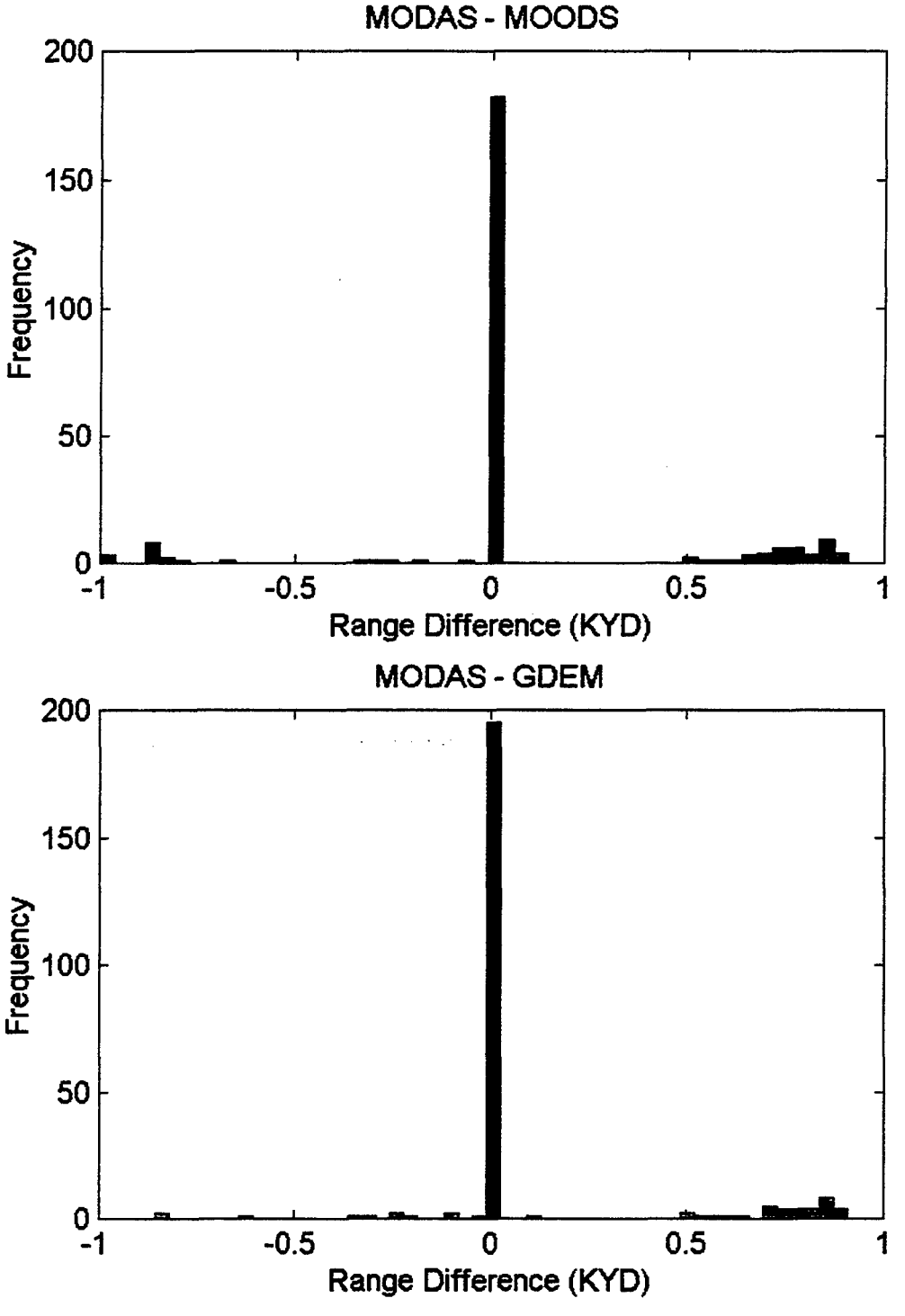

HISTOGRAMS FOR DIFFERENCES IN MAXIMUM DETECTION RANGES FOR ALL TARGET DEPTHS/ MAY 2000/ MUD BOTTOM/ SOURCE DEPTH = 25 FT.

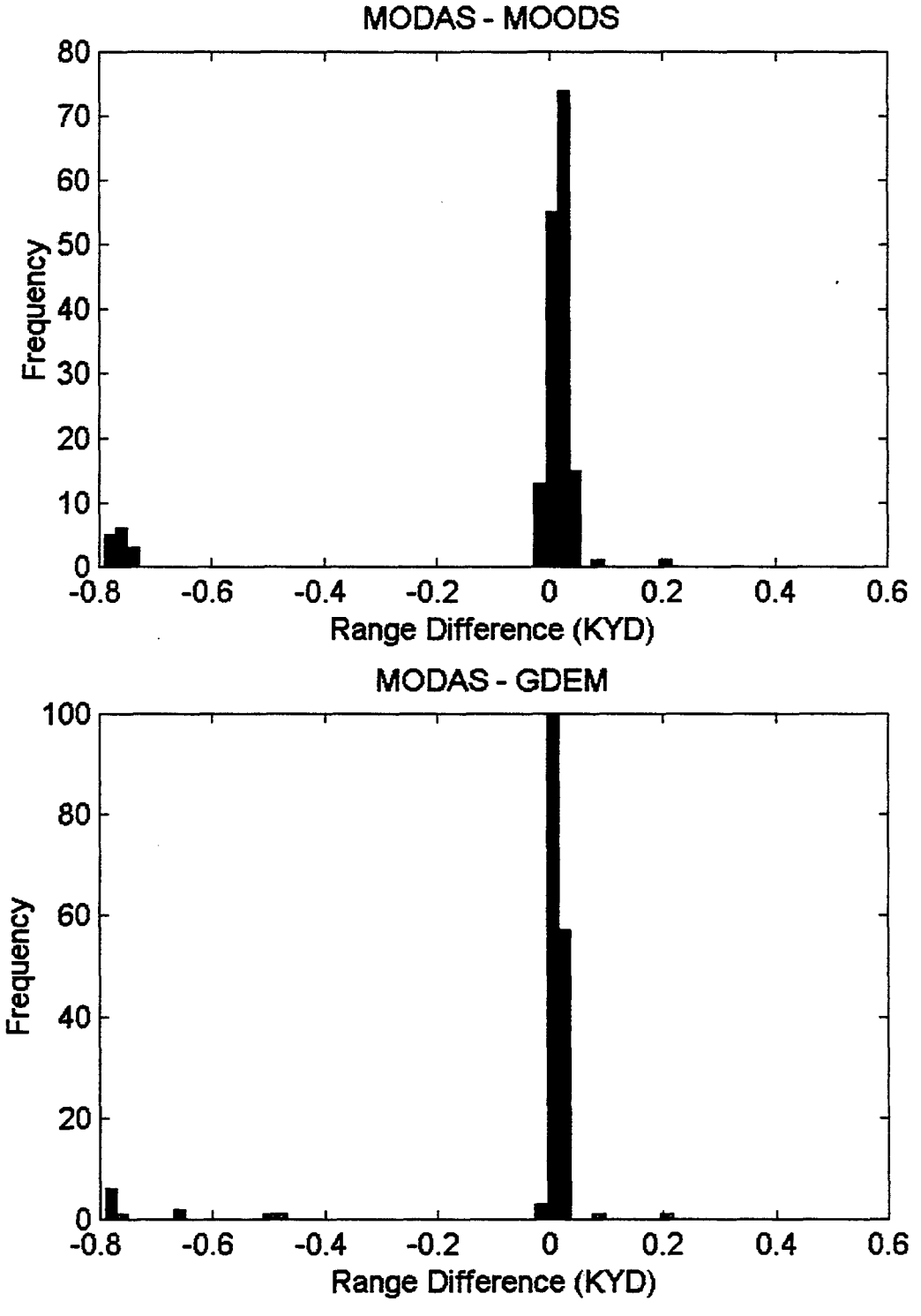

HISTOGRAMS FOR DIFFERENCES IN MAXIMUM DETECTION RANGES FOR ALL TARGET DEPTHS/ MAY 2000/ MUD BOTTOM/ SOURCE DEPTH = 125 FT.

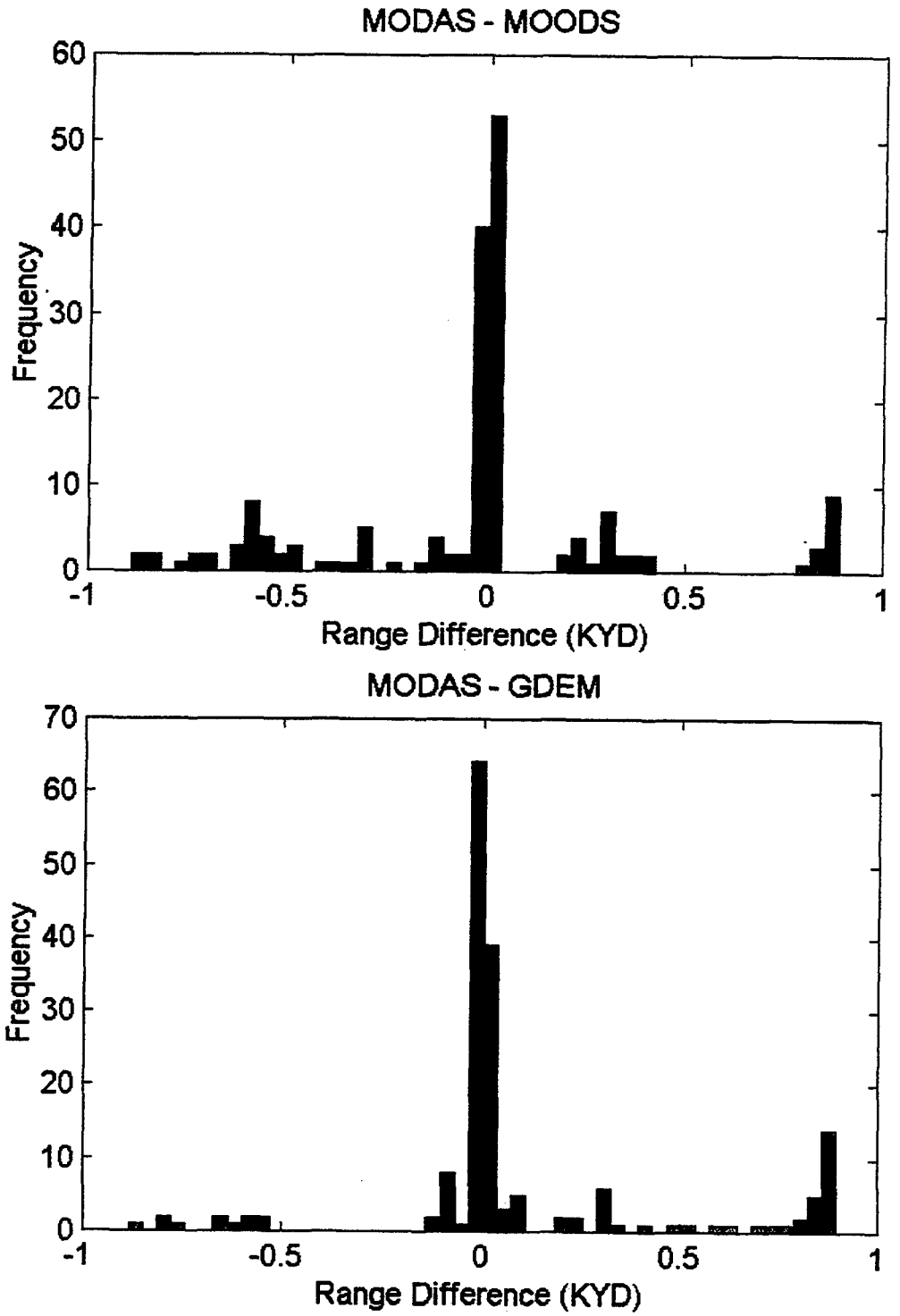

HISTOGRAMS FOR DIFFERENCES IN MAXIMUM DETECTION RANGES FOR ALL TARGET DEPTHS/ MAY 1999/ MUD BOTTOM/ SOURCE DEPTH = 25 FT.

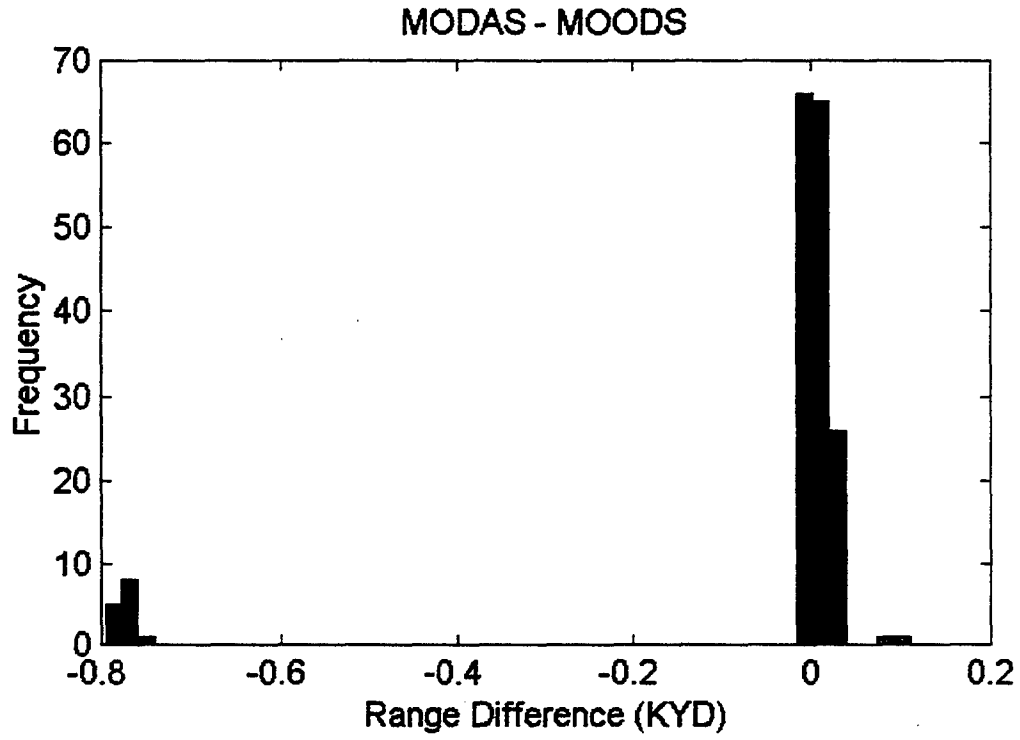

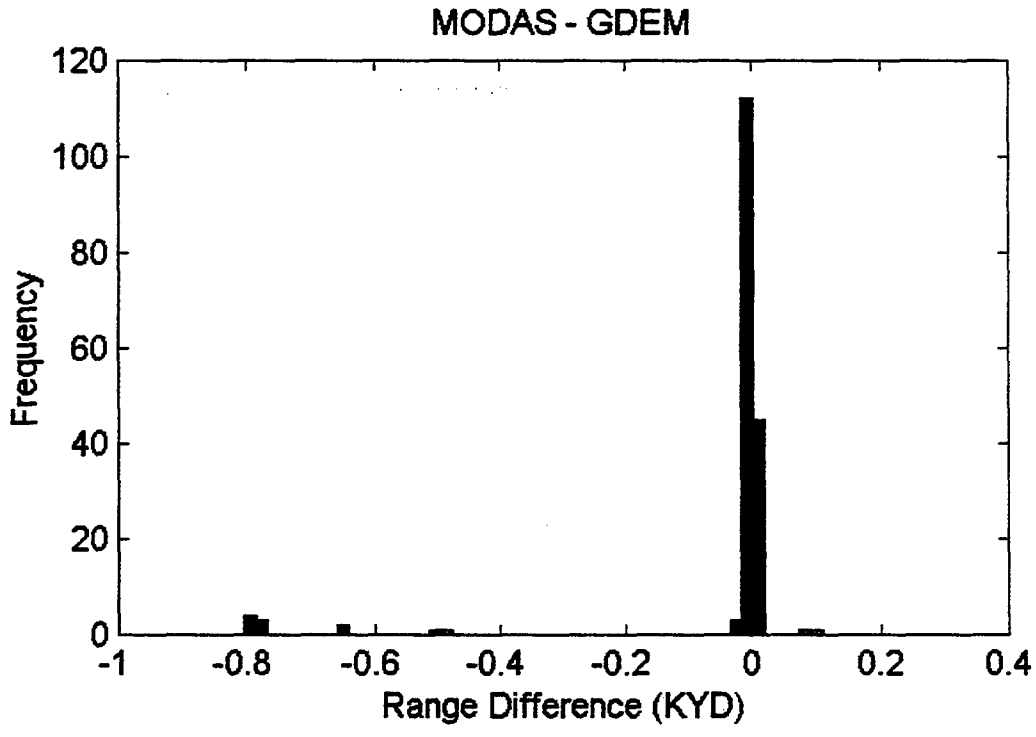

HISTOGRAMS FOR DIFFERENCES IN MAXIMUM DETECTION RANGES FOR ALL TARGET DEPTHS/ MAY 1999/ MUD BOTTOM/ SOURCE DEPTH = 125 FT.

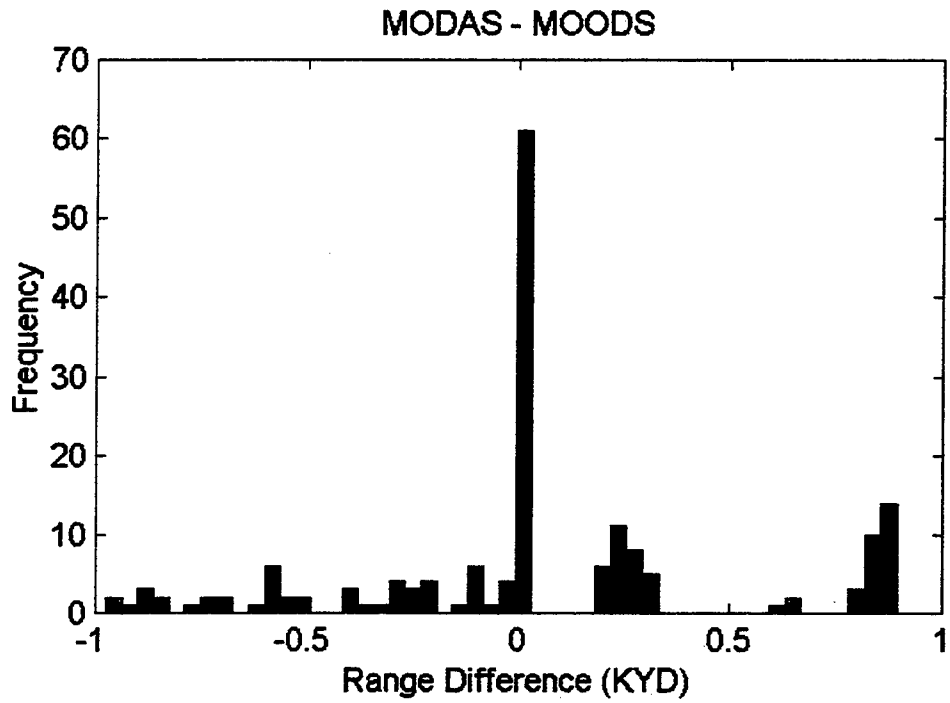

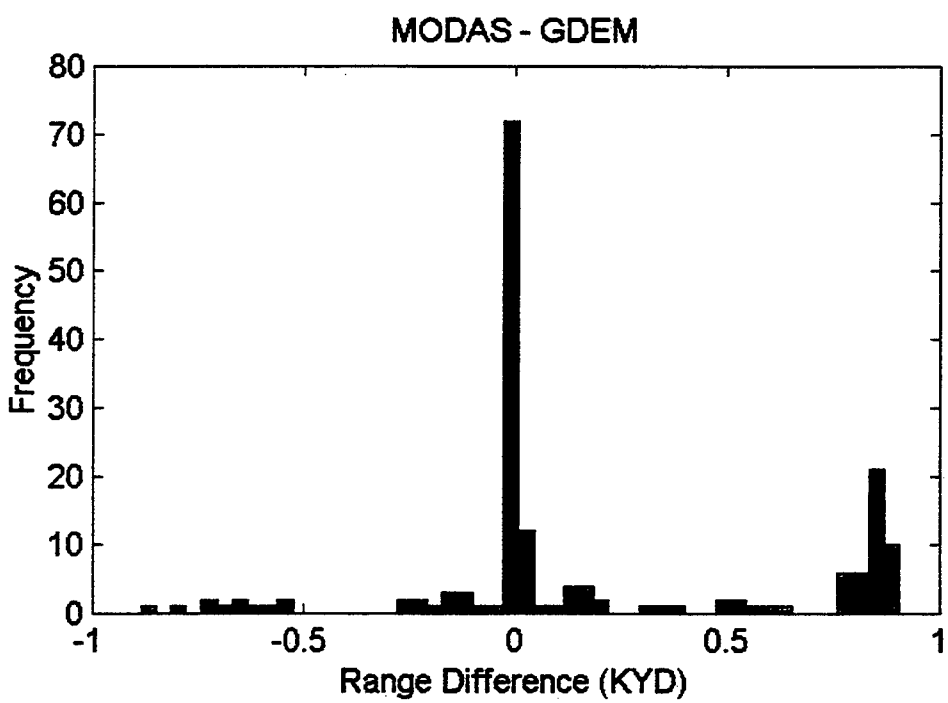

HISTOGRAMS FOR DIFFERENCES IN MAXIMUM DETECTION RANGES FOR ALL TARGET DEPTHS/ AUGUST 2000/ MUD BOTTOM/ SOURCE DEPTH = 25 FT.

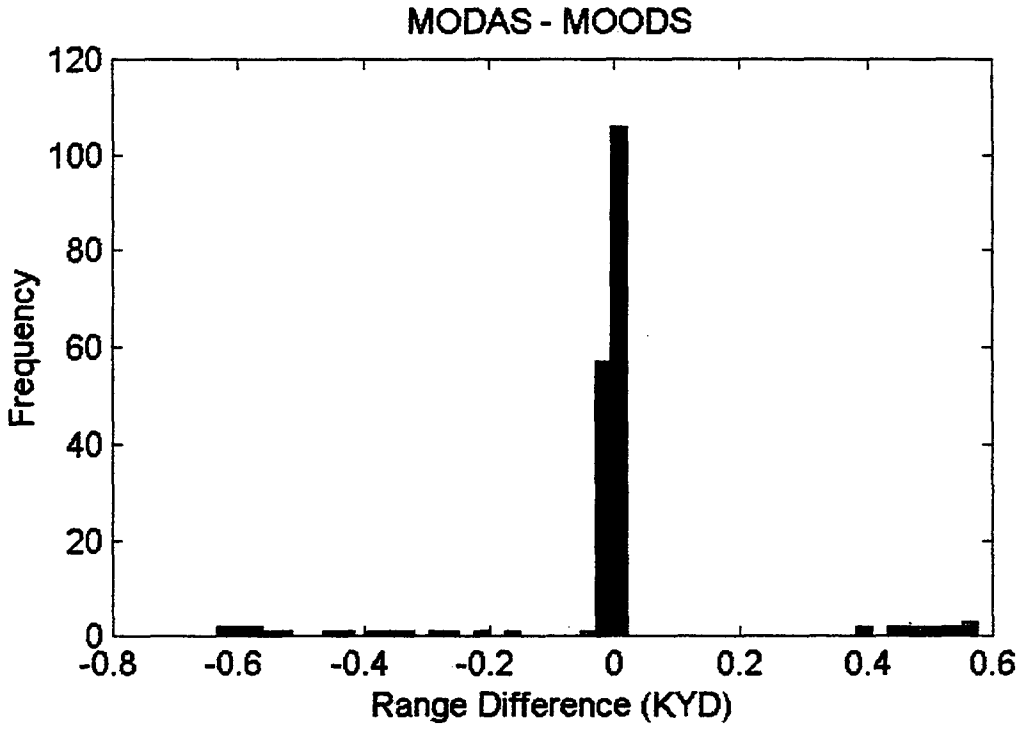

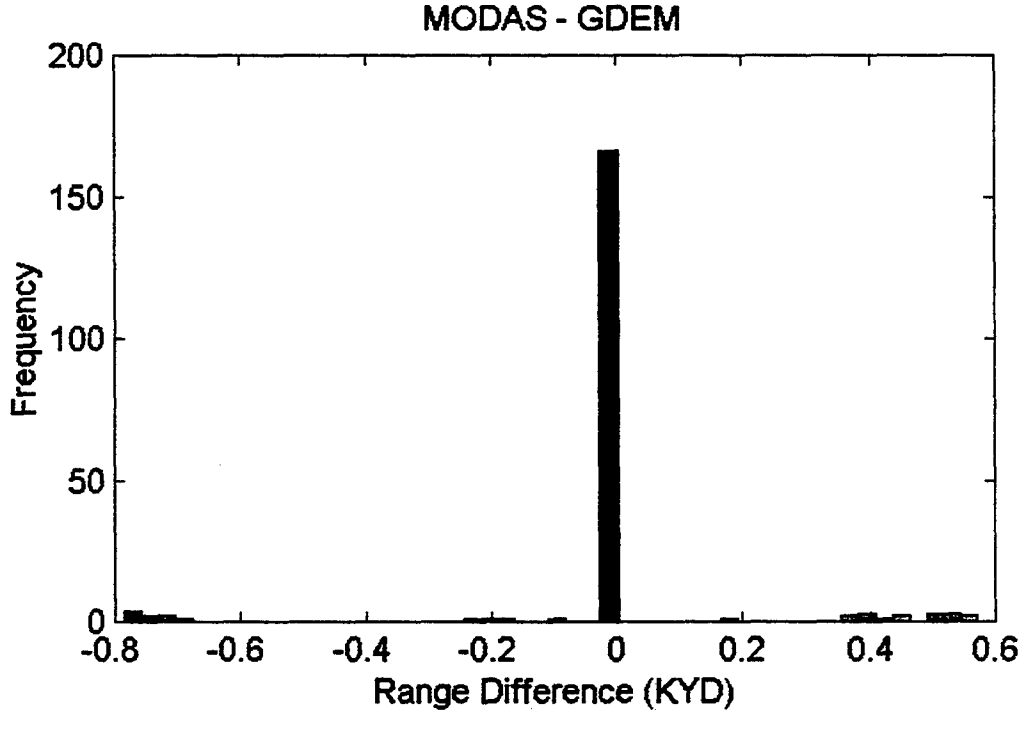

HISTOGRAMS FOR DIFFERENCES IN MAXIMUM DETECTION RANGES FOR ALL TARGET DEPTHS/ AUGUST 2000/ MUD BOTTOM/ SOURCE DEPTH = 125 FT.

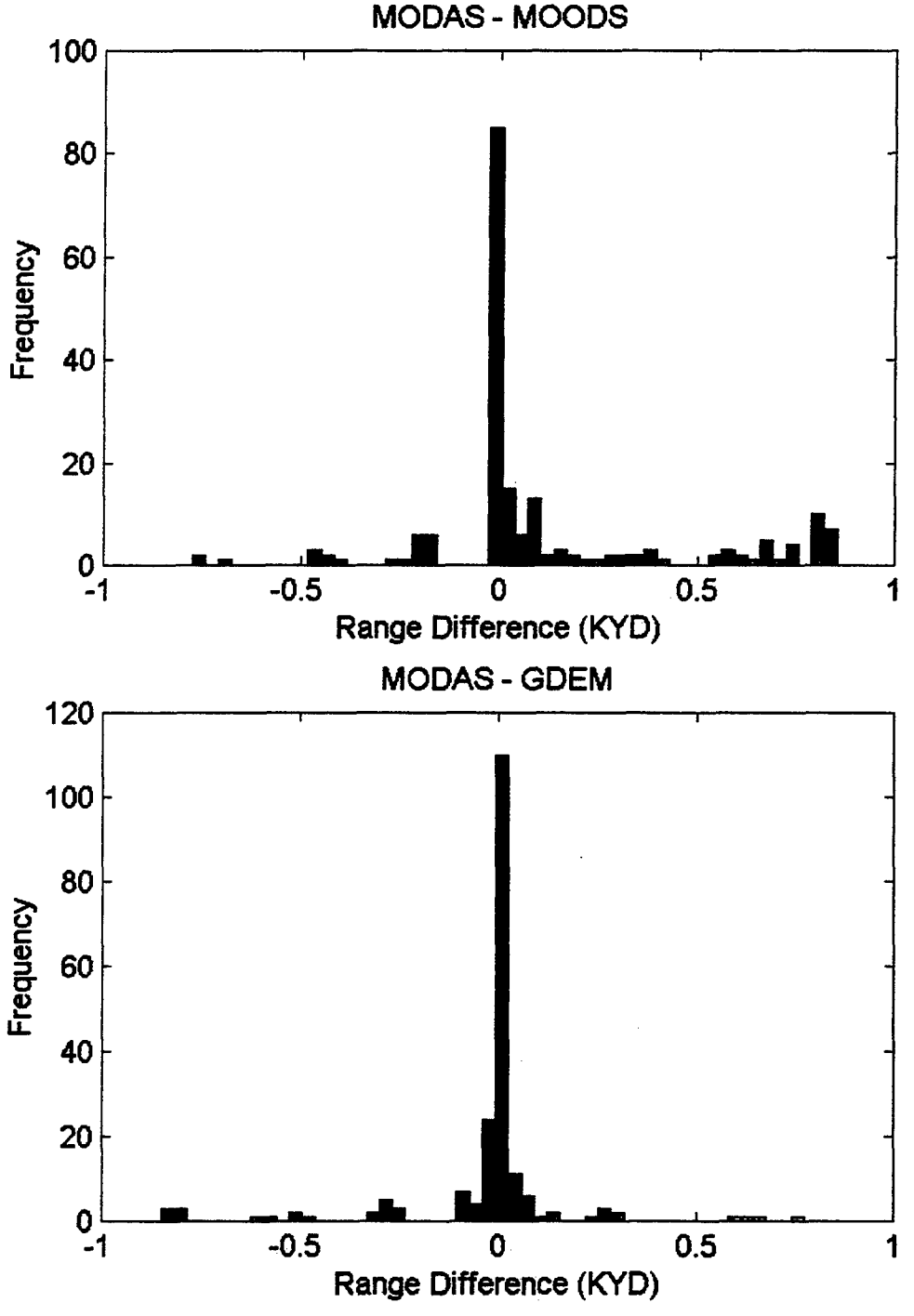

HISTOGRAMS FOR DIFFERENCES IN MAXIMUM DETECTION RANGES FOR ALL TARGET DEPTHS/ AUGUST 1999/ MUD BOTTOM/ SOURCE DEPTH = 25 FT.

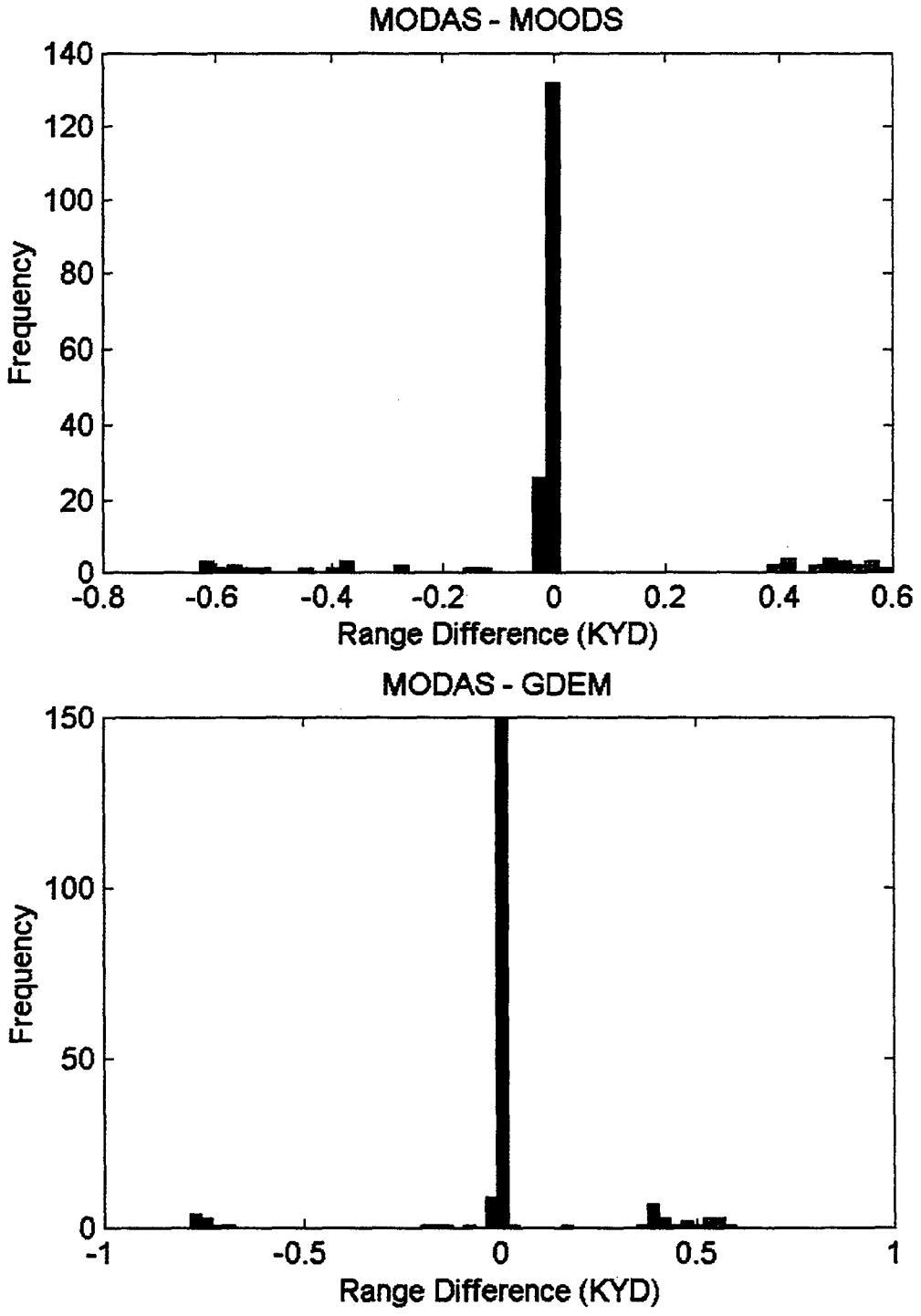

HISTOGRAMS FOR DIFFERENCES IN MAXIMUM DETECTION RANGES FOR ALL TARGET DEPTHS/ AUGUST 1999/ MUD BOTTOM/ SOURCE DEPTH = 125 FT.

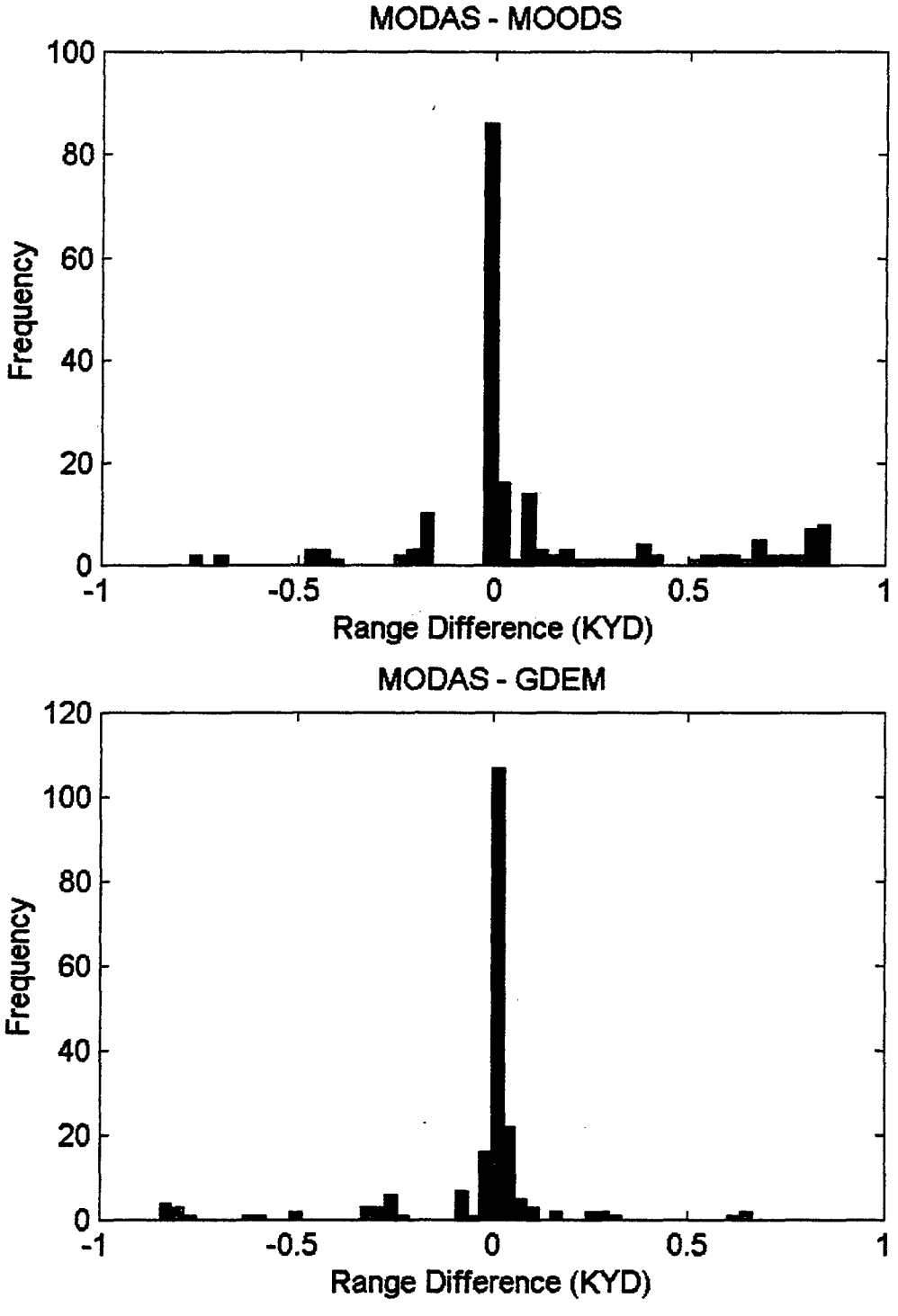

HISTOGRAMS FOR DIFFERENCES IN MAXIMUM DETECTION RANGES FOR ALL TARGET DEPTHS/ NOVEMBER 2000/ MUD BOTTOM/ SOURCE DEPTH = 25 FT.

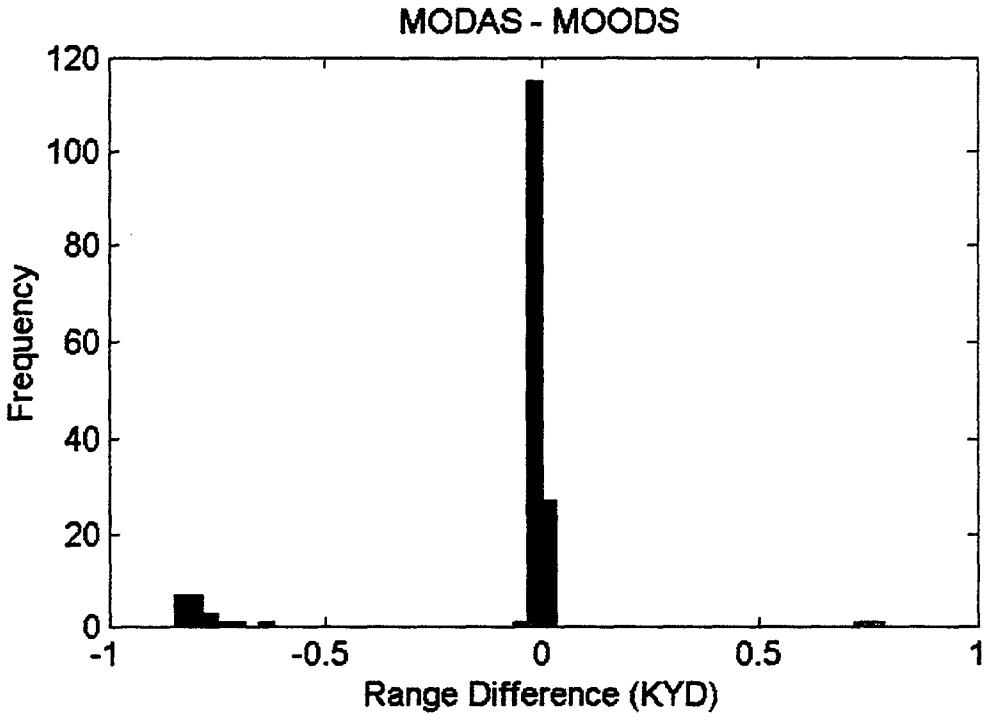

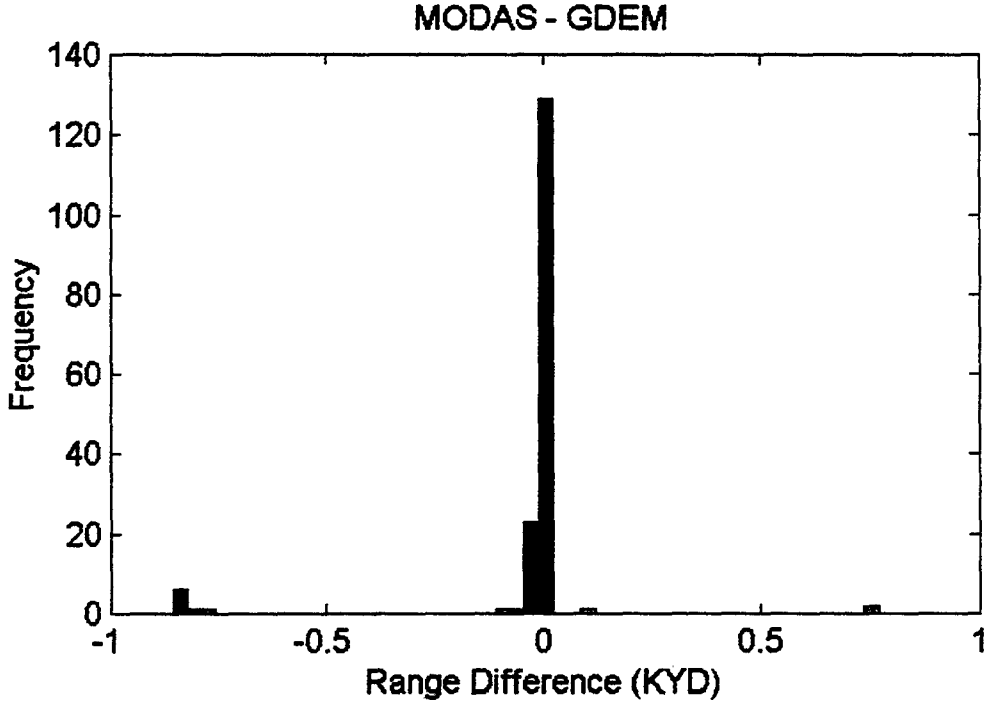

HISTOGRAMS FOR DIFFERENCES IN MAXIMUM DETECTION RANGES FOR ALL TARGET DEPTHS/ NOVEMBER 2000/ MUD BOTTOM/ SOURCE DEPTH = 125 FT.

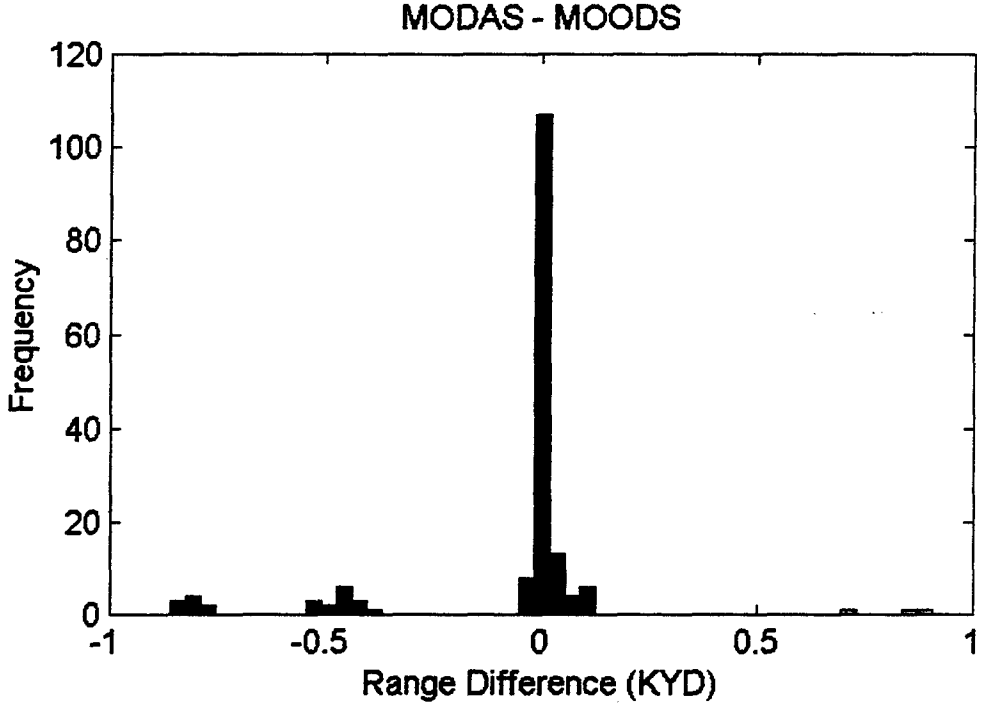

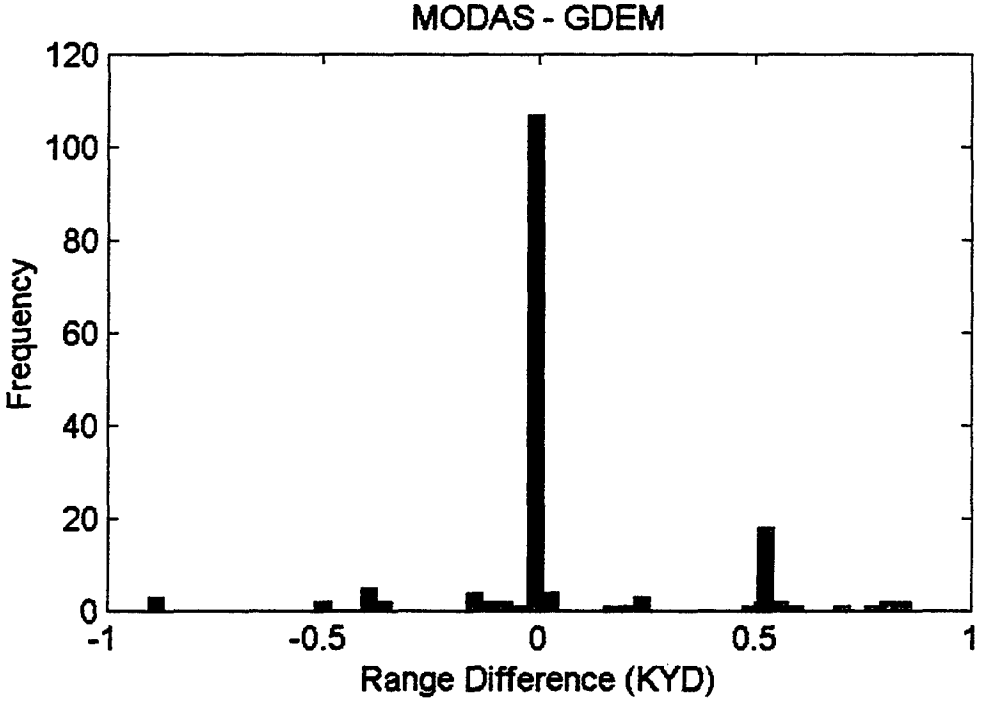

HISTOGRAMS FOR DIFFERENCES IN MAXIMUM DETECTION RANGES FOR ALL TARGET DEPTHS/ NOVEMBER 1999/ MUD BOTTOM/ SOURCE DEPTH = 25 FT.

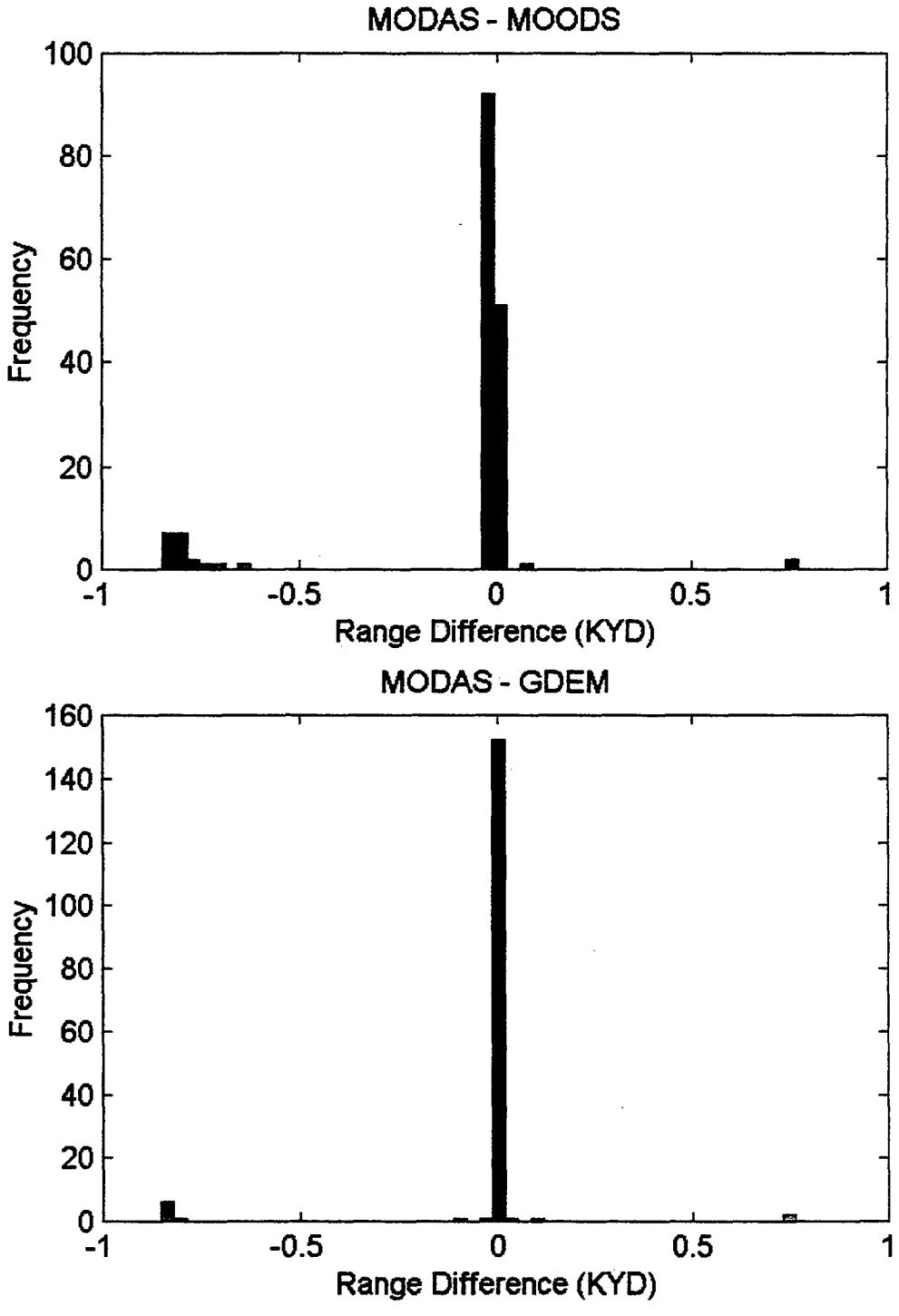

HISTOGRAMS FOR DIFFERENCES IN MAXIMUM DETECTION RANGES FOR ALL TARGET DEPTHS/ NOVEMBER 1999/ MUD BOTTOM/ SOURCE DEPTH = 125 FT.

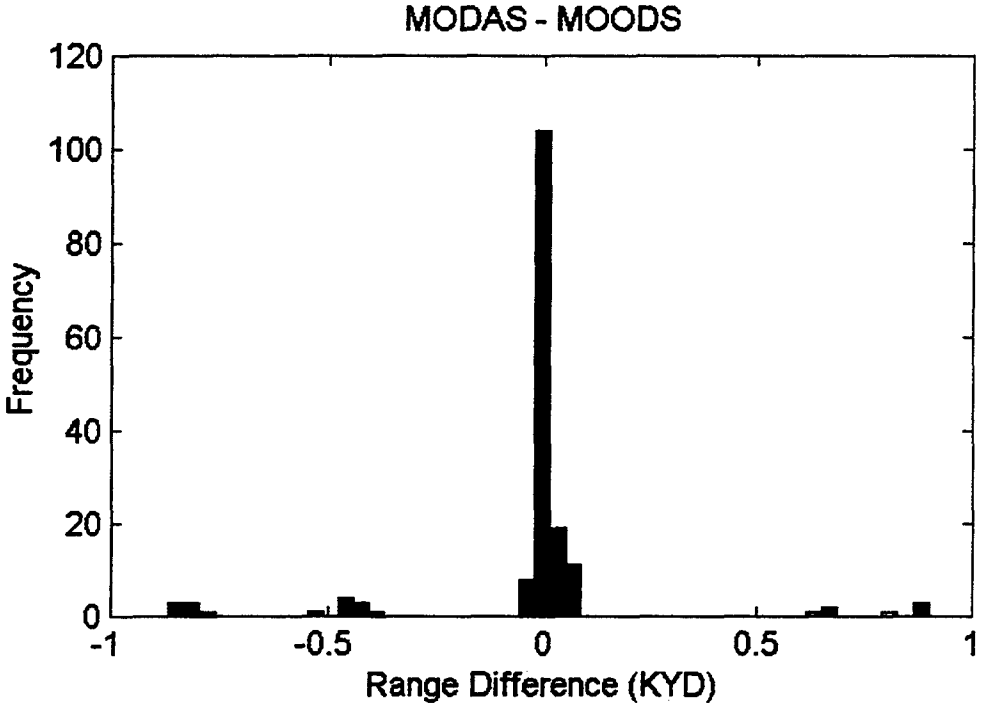

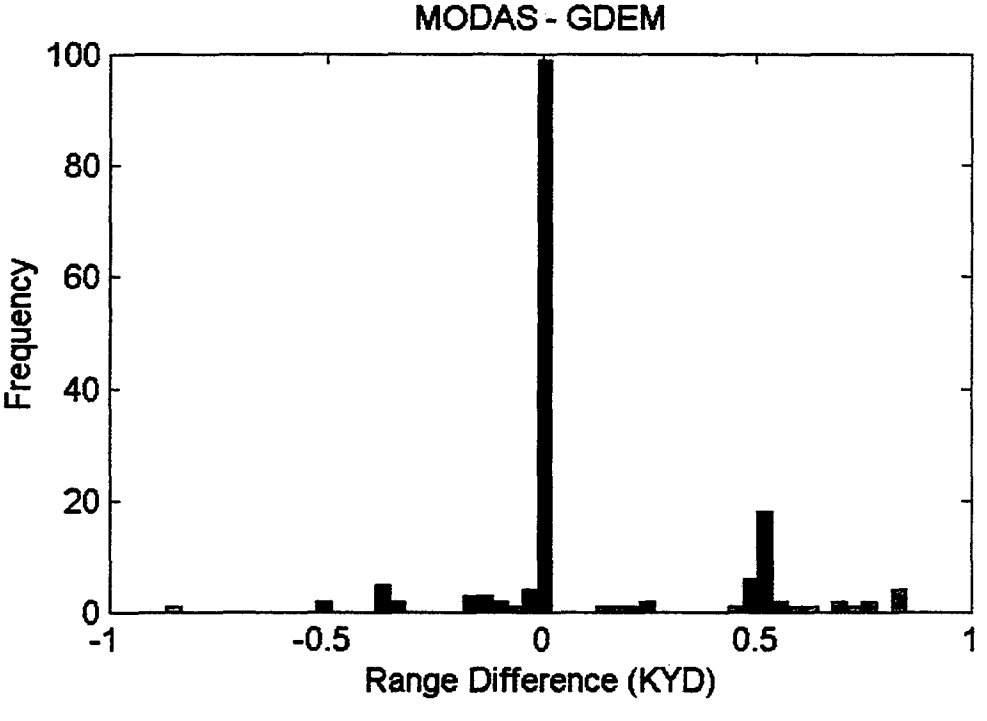

HISTOGRAMS FOR DIFFERENCES IN MAXIMUM DETECTION RANGES FOR ALL TARGET DEPTHS/ FEBRUARY 2000/ SAND BOTTOM/ SOURCE DEPTH = 25 FT.

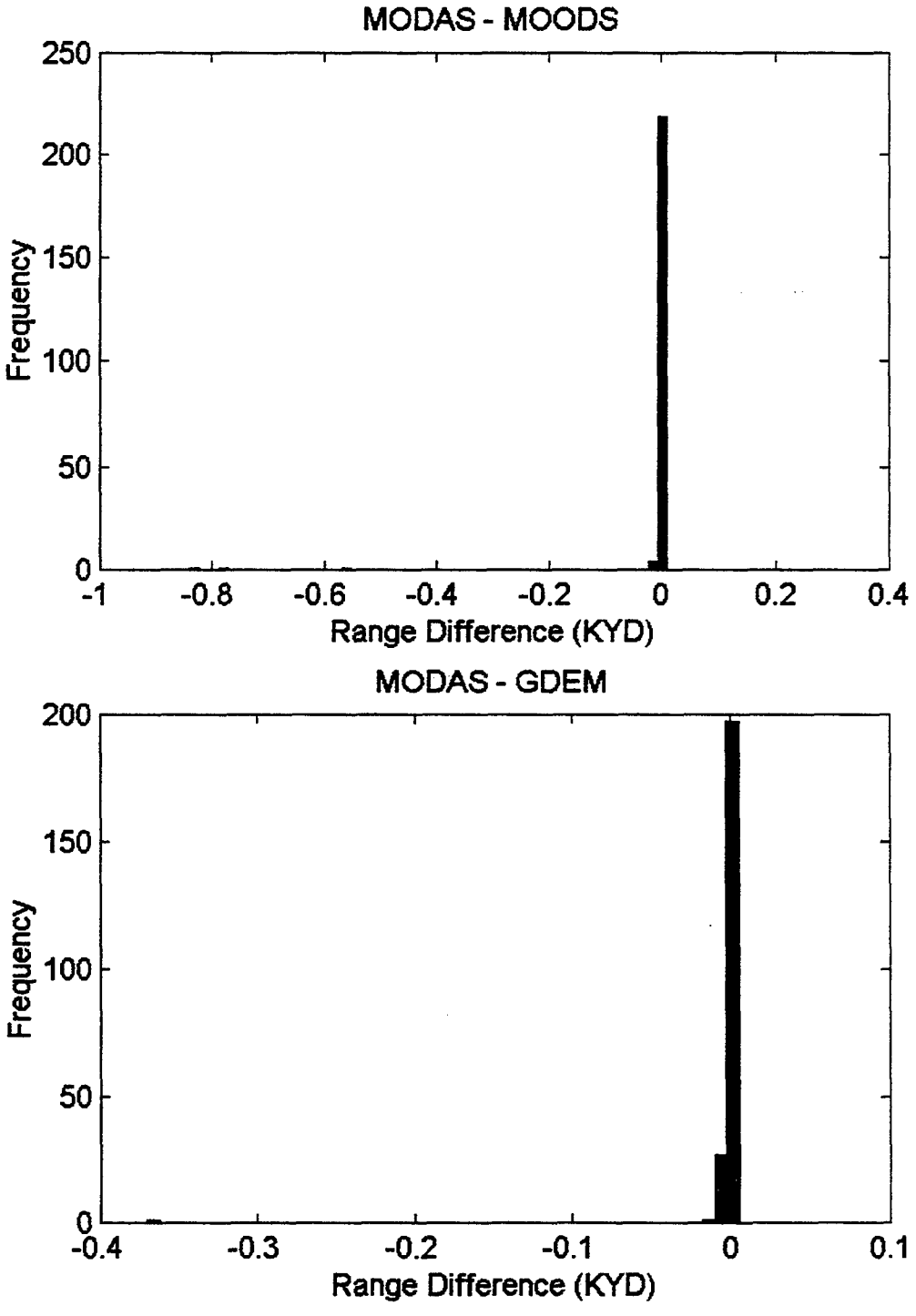

HISTOGRAMS FOR DIFFERENCES IN MAXIMUM DETECTION RANGES FOR ALL TARGET DEPTHS/ FEBRUARY 2000/ SAND BOTTOM/ SOURCE DEPTH = 125 FT.

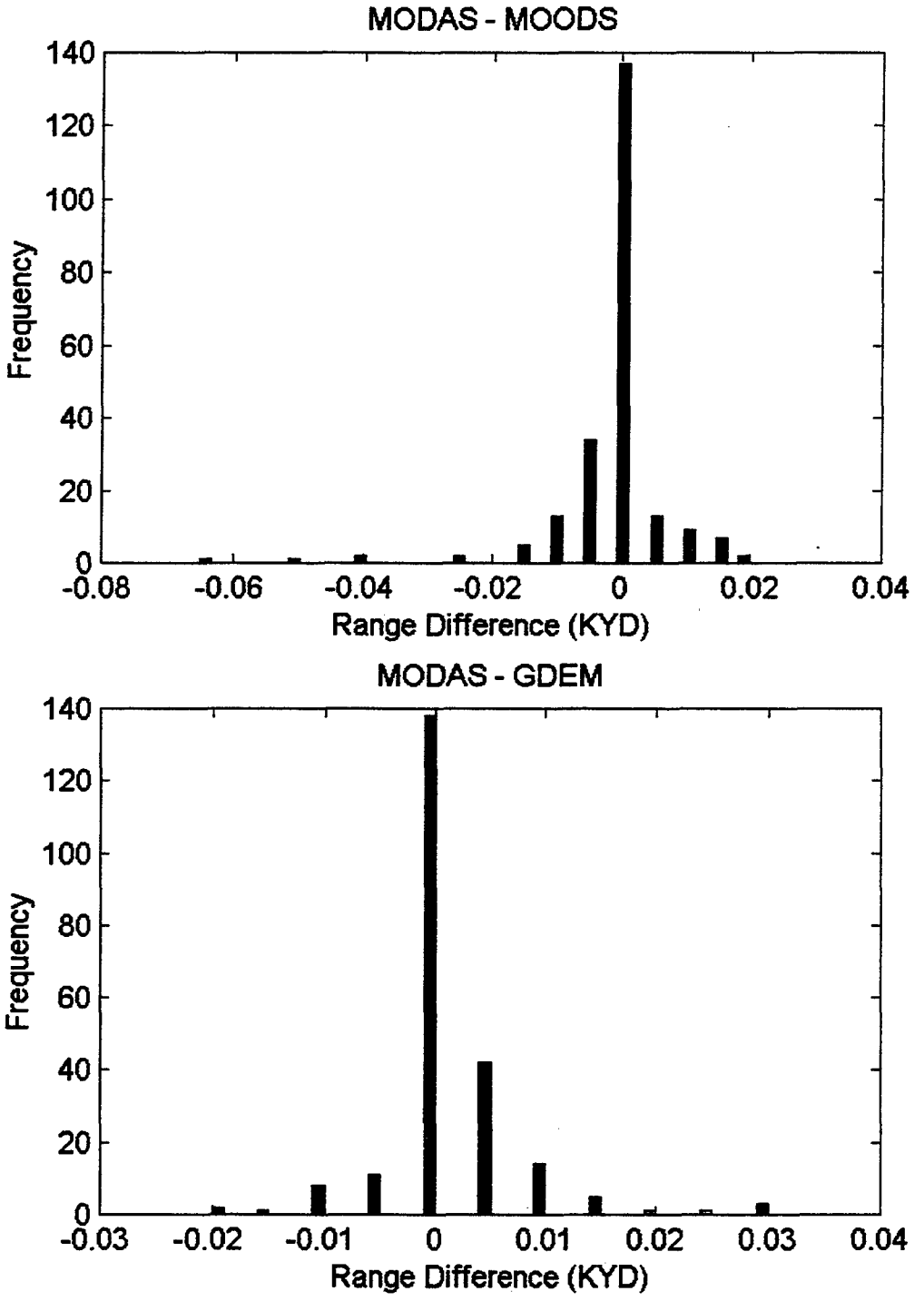

HISTOGRAMS FOR DIFFERENCES IN MAXIMUM DETECTION RANGES FOR ALL TARGET DEPTHS/ FEBRUARY 1999/ SAND BOTTOM/ SOURCE DEPTH = 25 FT.

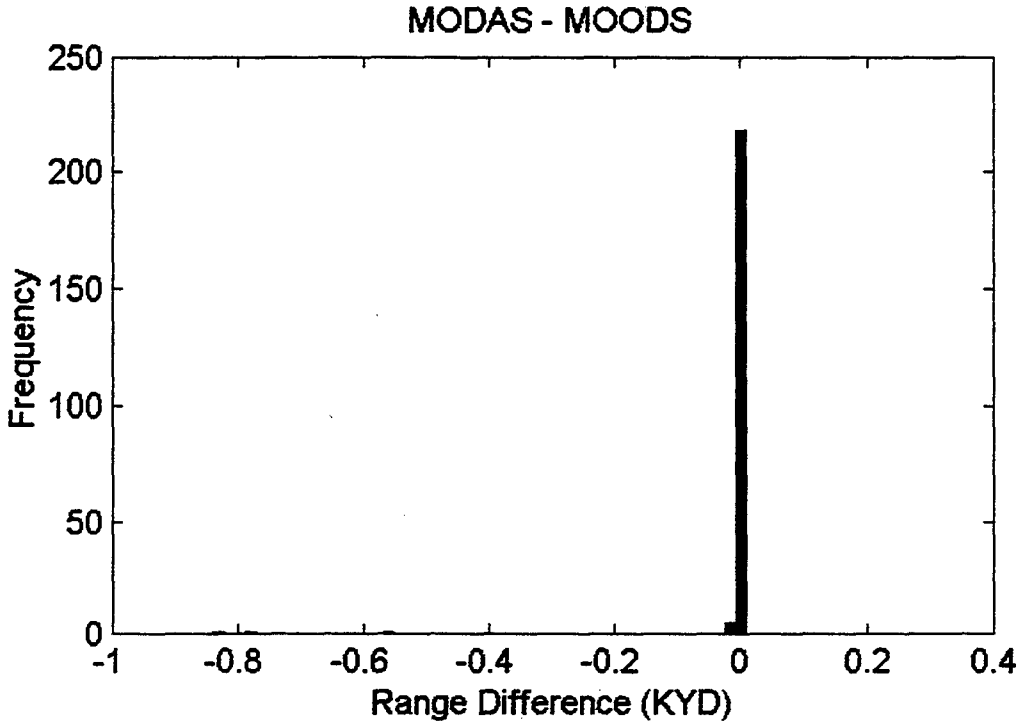

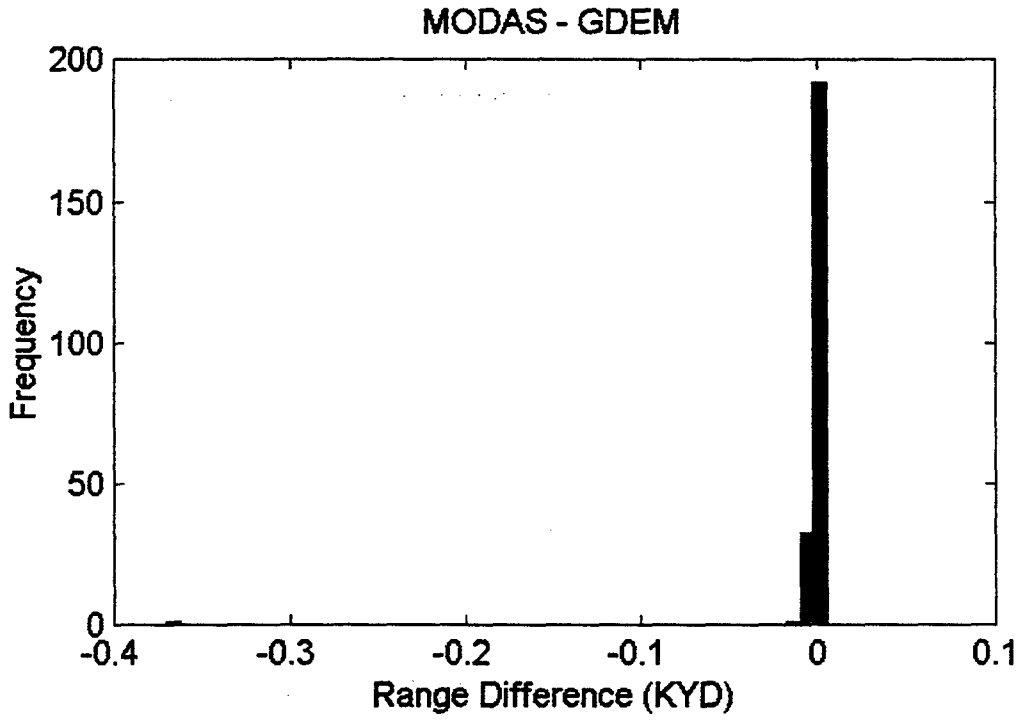

HISTOGRAMS FOR DIFFERENCES IN MAXIMUM DETECTION RANGES FOR ALL TARGET DEPTHS/ FEBRUARY 1999/ SAND BOTTOM/ SOURCE DEPTH = 125 FT.

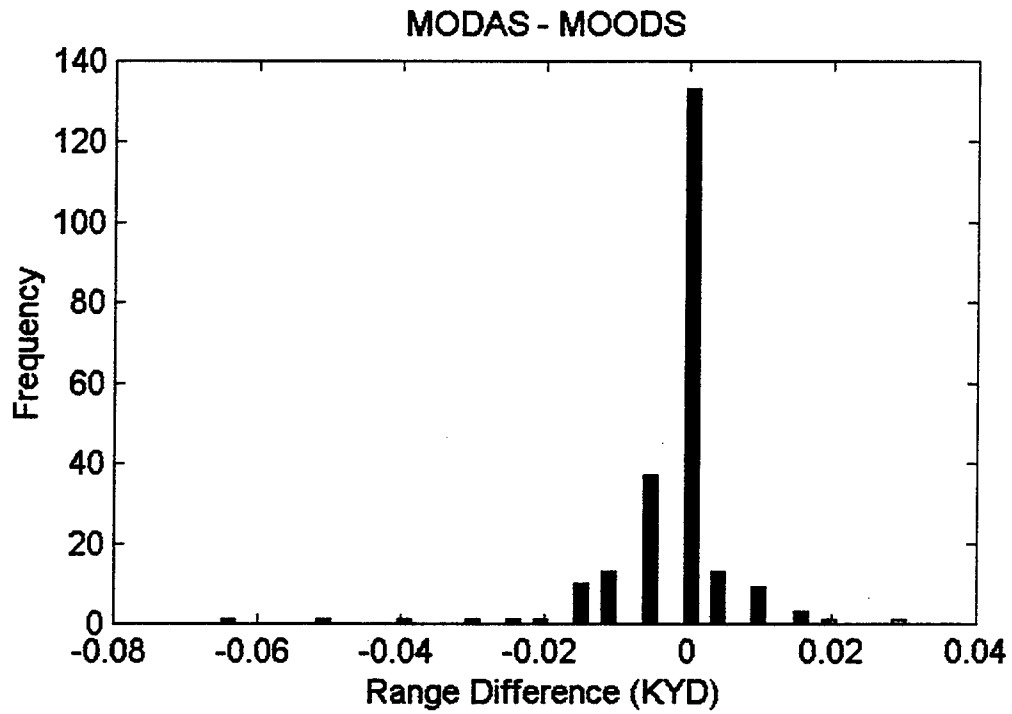

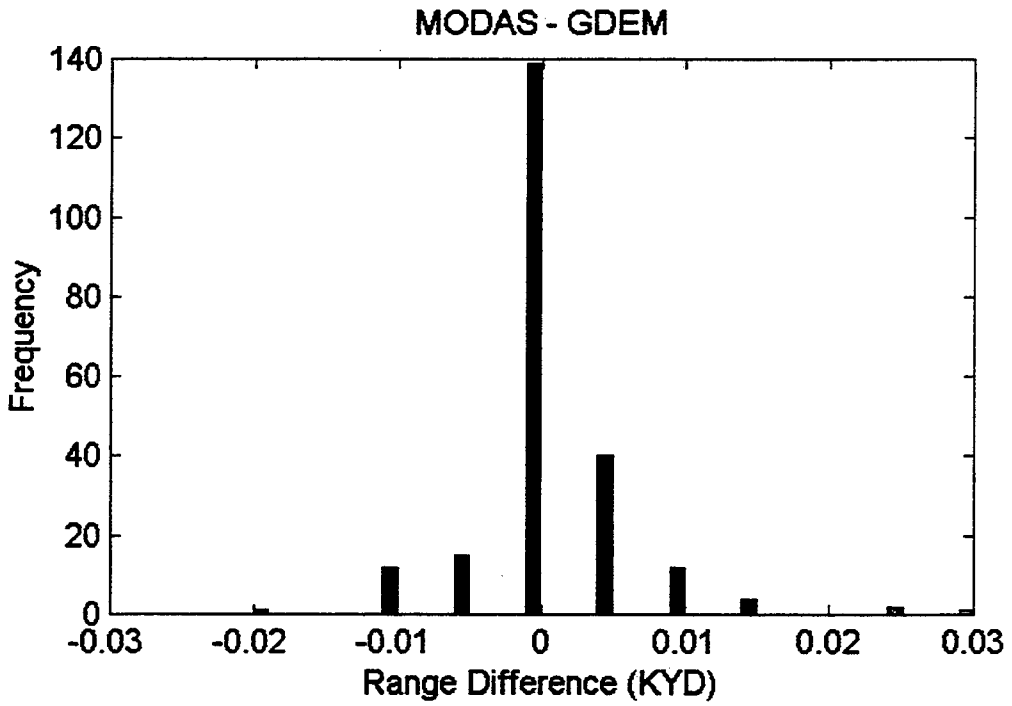

HISTOGRAMS FOR DIFFERENCES IN MAXIMUM DETECTION RANGES FOR ALL TARGET DEPTHS/ MAY 2000/ SAND BOTTOM/ SOURCE DEPTH = 25 FT.

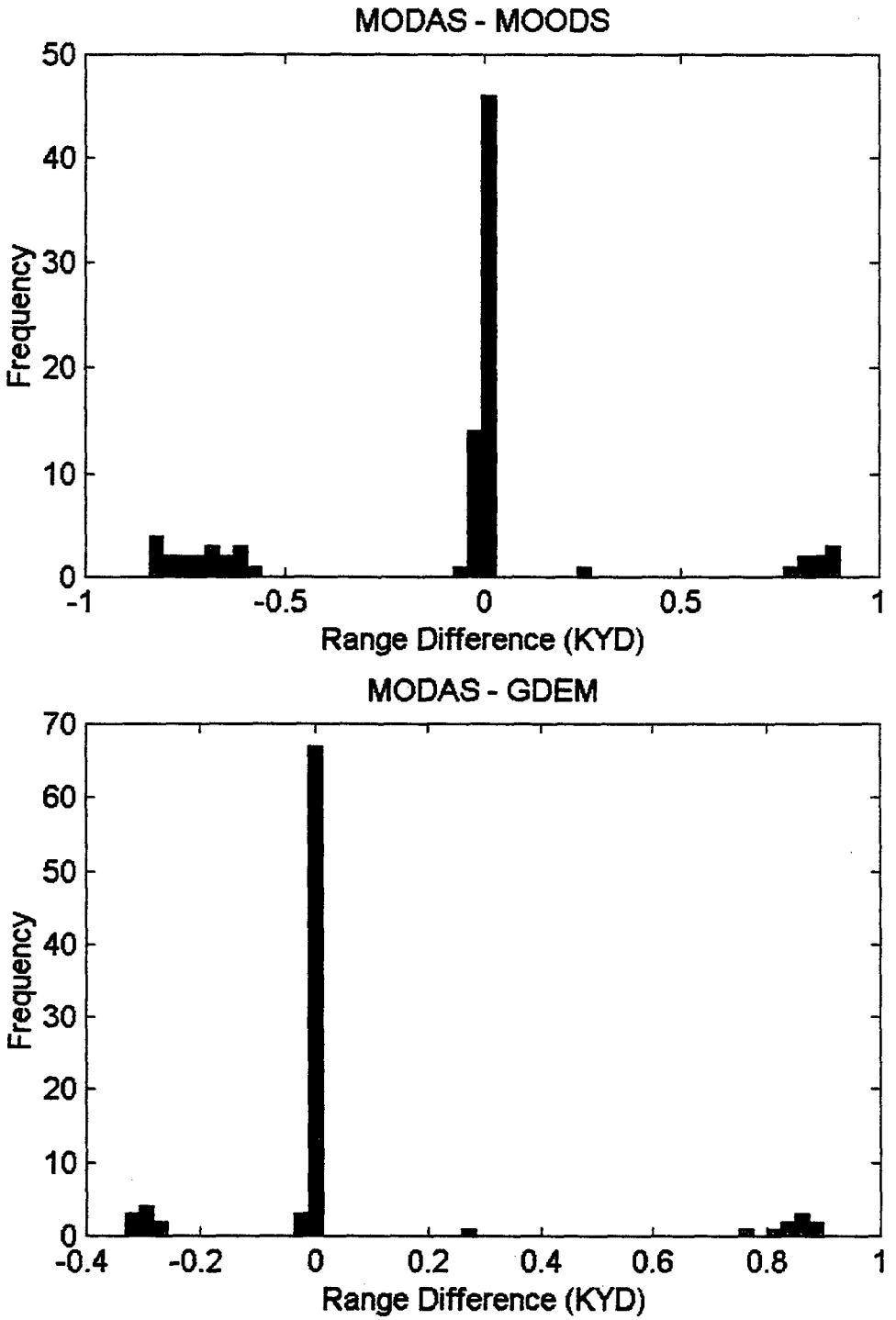

HISTOGRAMS FOR DIFFERENCES IN MAXIMUM DETECTION RANGES FOR ALL TARGET DEPTHS/ MAY 1999/ SAND BOTTOM/ SOURCE DEPTH = 25 FT.

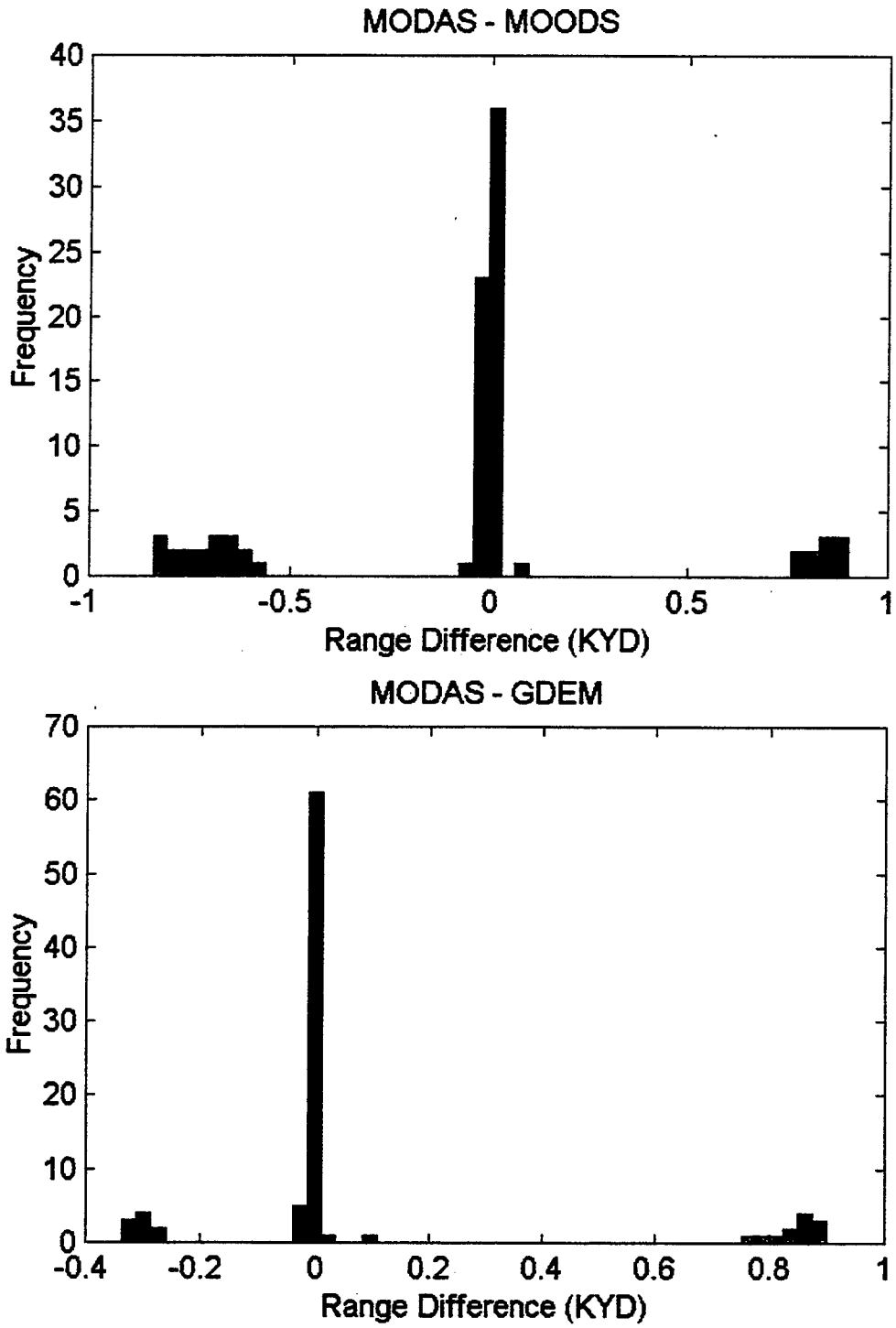

HISTOGRAMS FOR DIFFERENCES IN MAXIMUM DETECTION RANGES FOR ALL TARGET DEPTHS/ AUGUST 2000/ SAND BOTTOM/ SOURCE DEPTH = 25 FT.

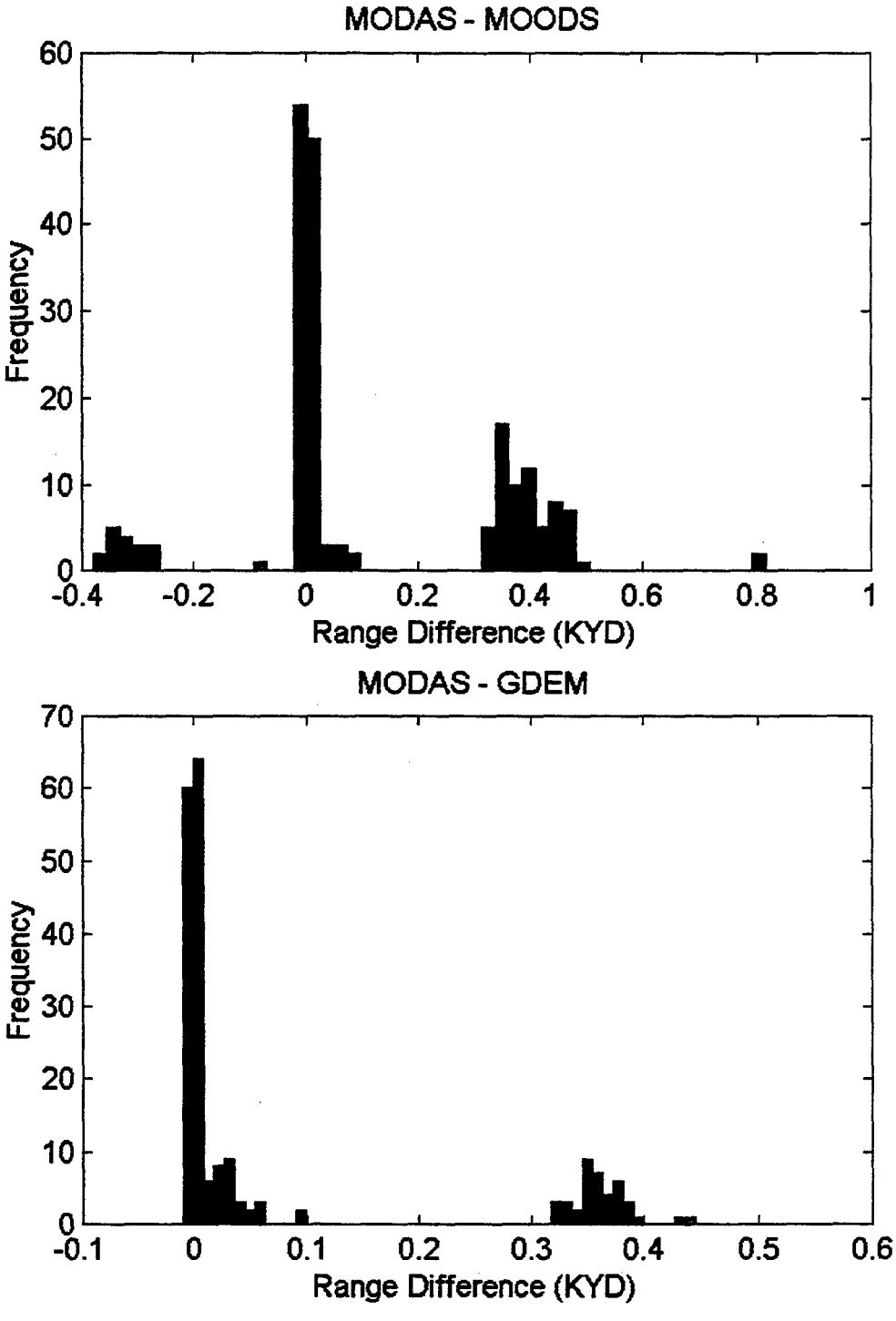

HISTOGRAMS FOR DIFFERENCES IN MAXIMUM DETECTION RANGES FOR ALL TARGET DEPTHS/ AUGUST 2000/ SAND BOTTOM/ SOURCE DEPTH = 125 FT.

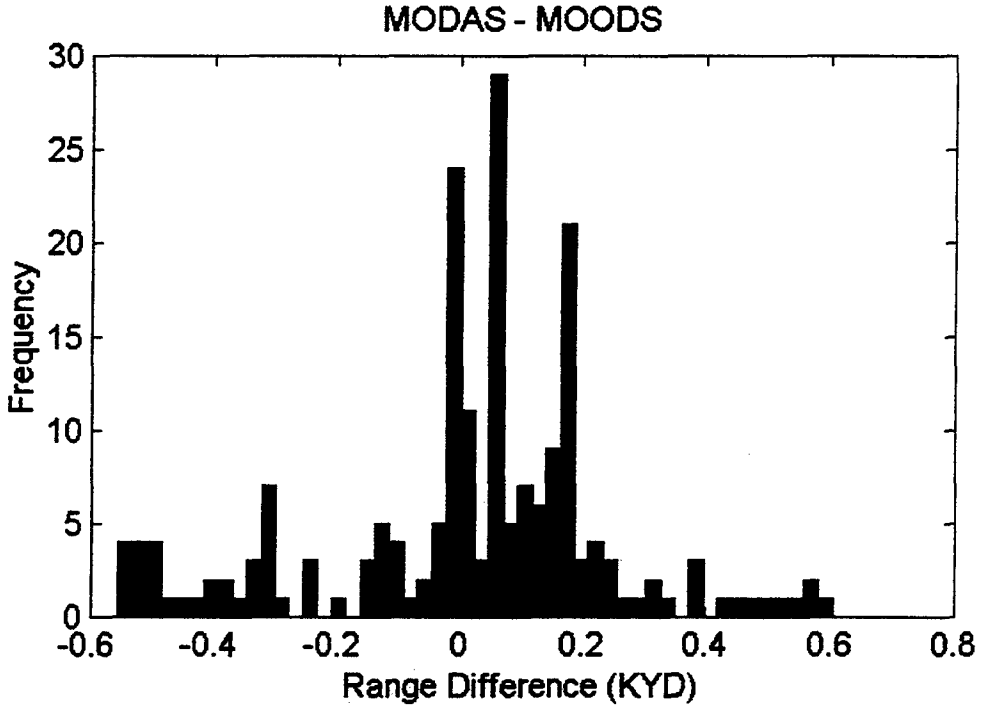

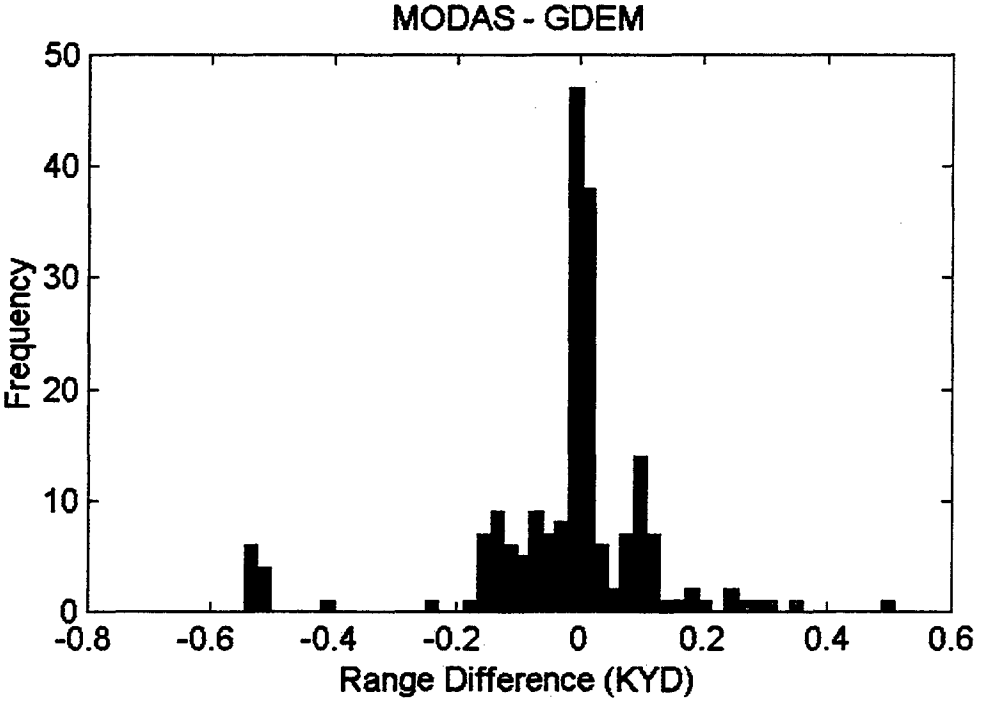

HISTOGRAMS FOR DIFFERENCES IN MAXIMUM DETECTION RANGES FOR ALL TARGET DEPTHS/ AUGUST 1999/ SAND BOTTOM/ SOURCE DEPTH = 25 FT.

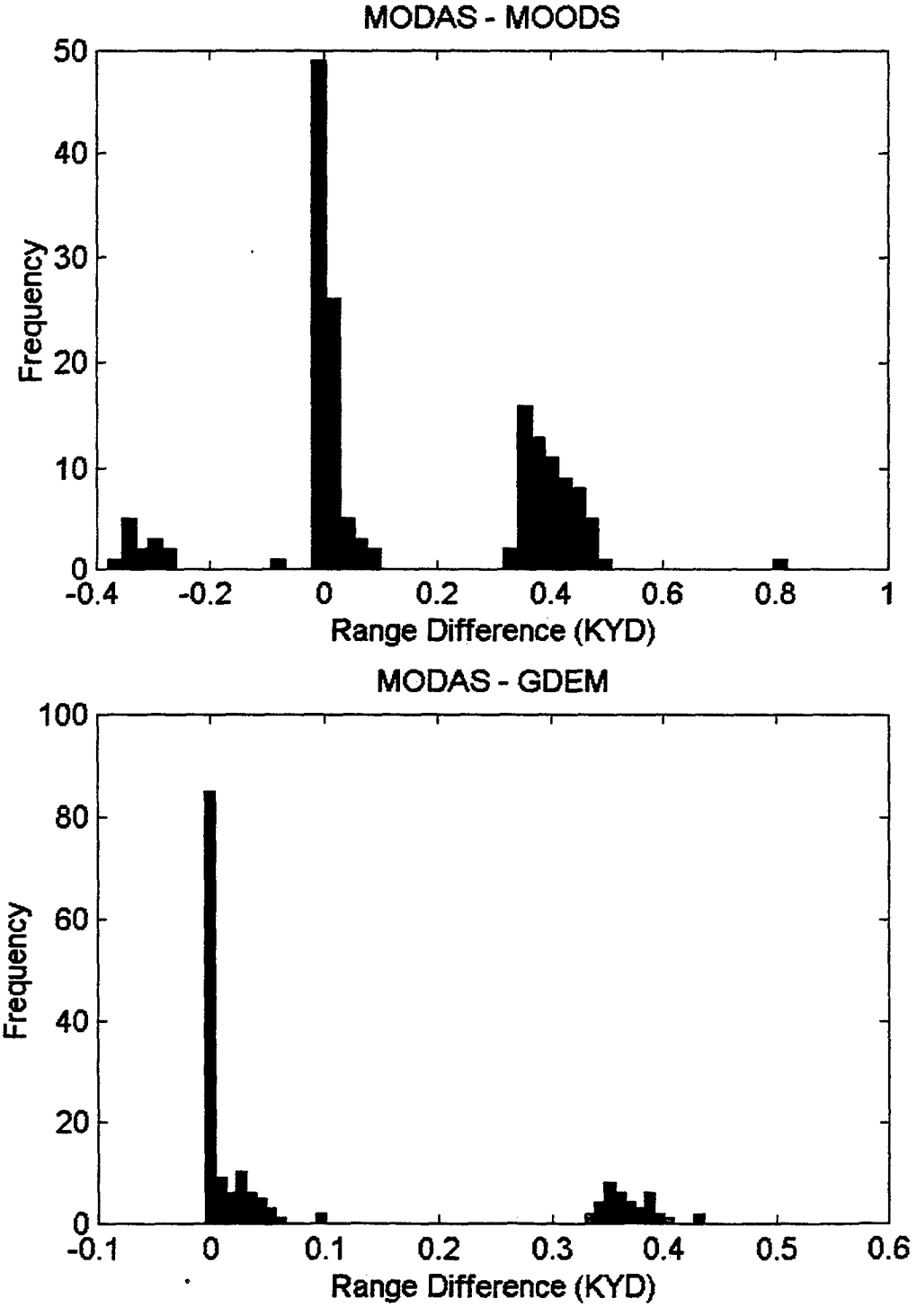

HISTOGRAMS FOR DIFFERENCES IN MAXIMUM DETECTION RANGES FOR ALL TARGET DEPTHS/ AUGUST 1999/ SAND BOTTOM/ SOURCE DEPTH = 125 FT.

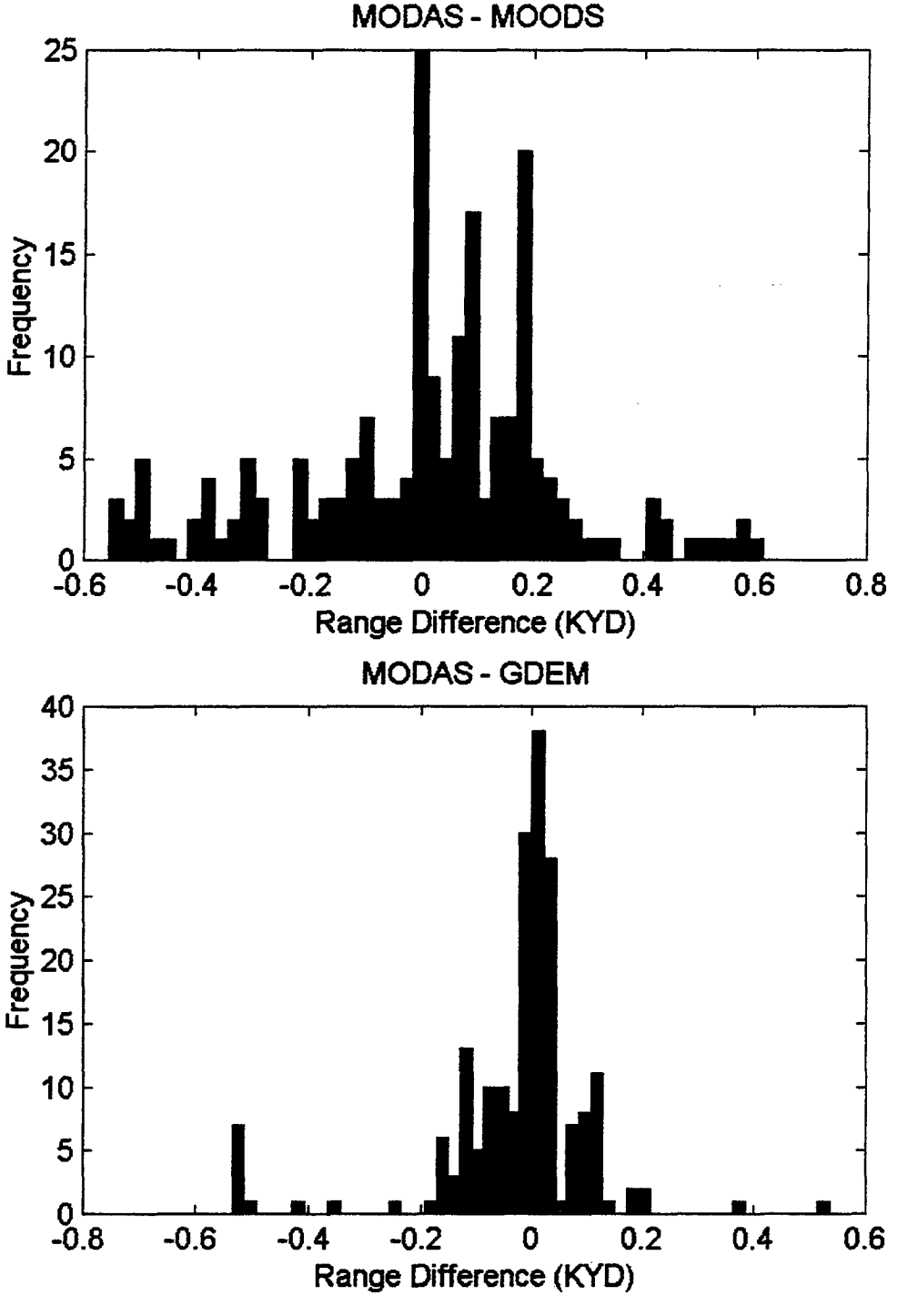

HISTOGRAMS FOR DIFFERENCES IN MAXIMUM DETECTION RANGES FOR ALL TARGET DEPTHS/ NOVEMBER 2000/ SAND BOTTOM/ SOURCE DEPTH = 25 FT.

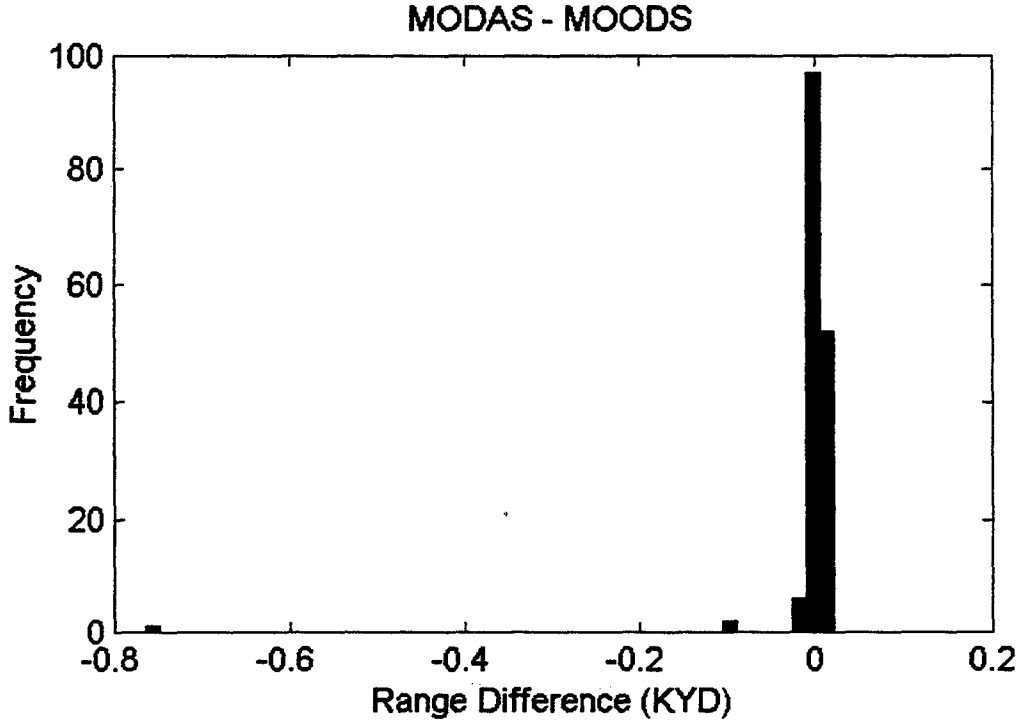

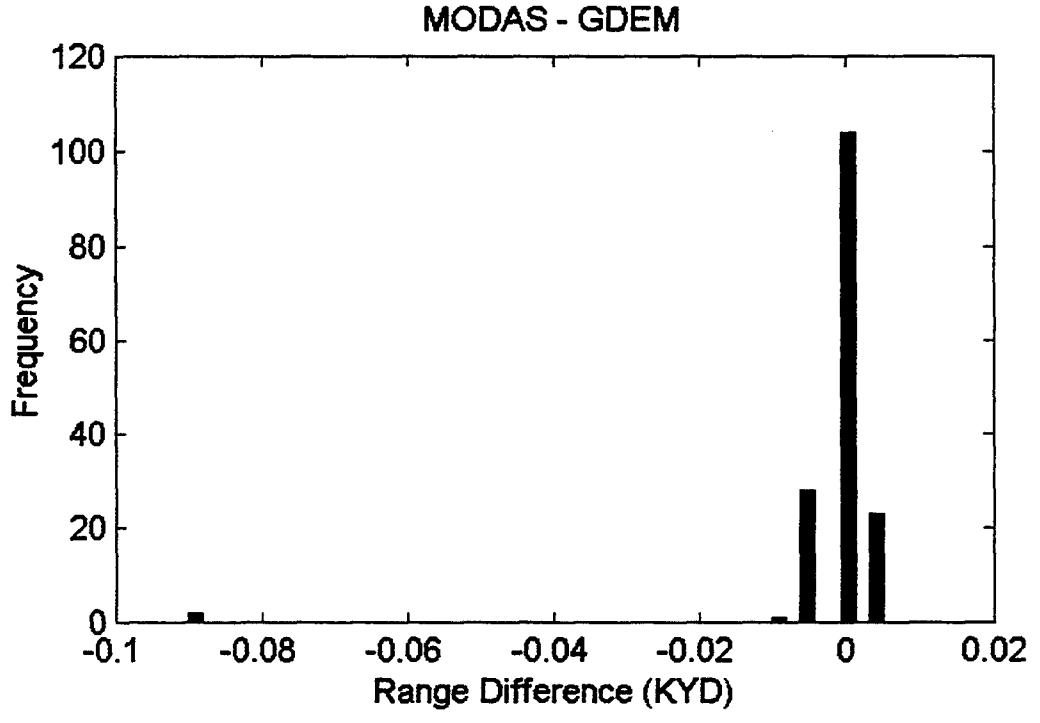

HISTOGRAMS FOR DIFFERENCES IN MAXIMUM DETECTION RANGES FOR ALL TARGET DEPTHS/ NOVEMBER 2000/ SAND BOTTOM/ SOURCE DEPTH = 125 FT.

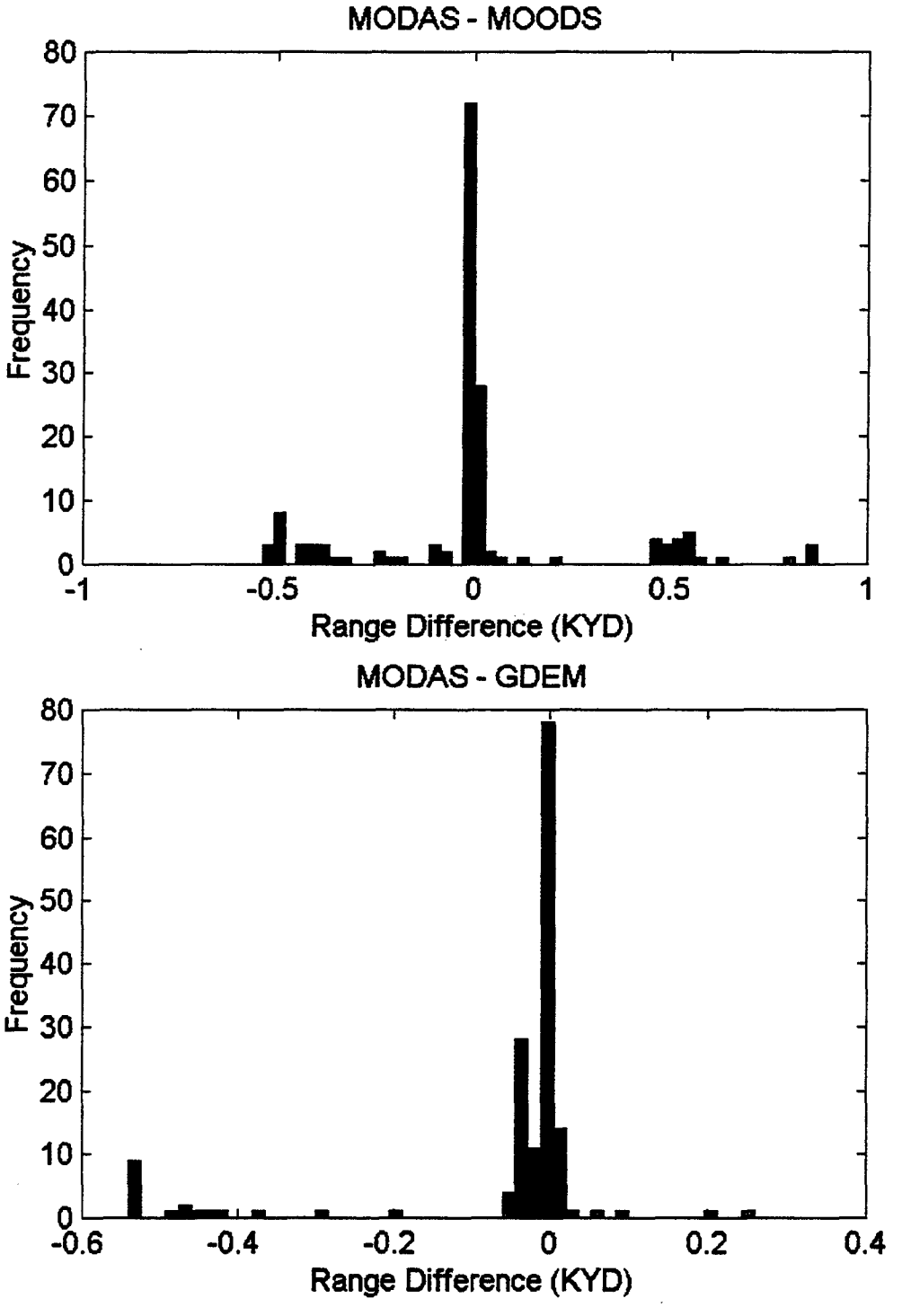

HISTOGRAMS FOR DIFFERENCES IN MAXIMUM DETECTION RANGES FOR ALL TARGET DEPTHS/ NOVEMBER 1999/ SAND BOTTOM/ SOURCE DEPTH = 25 FT.

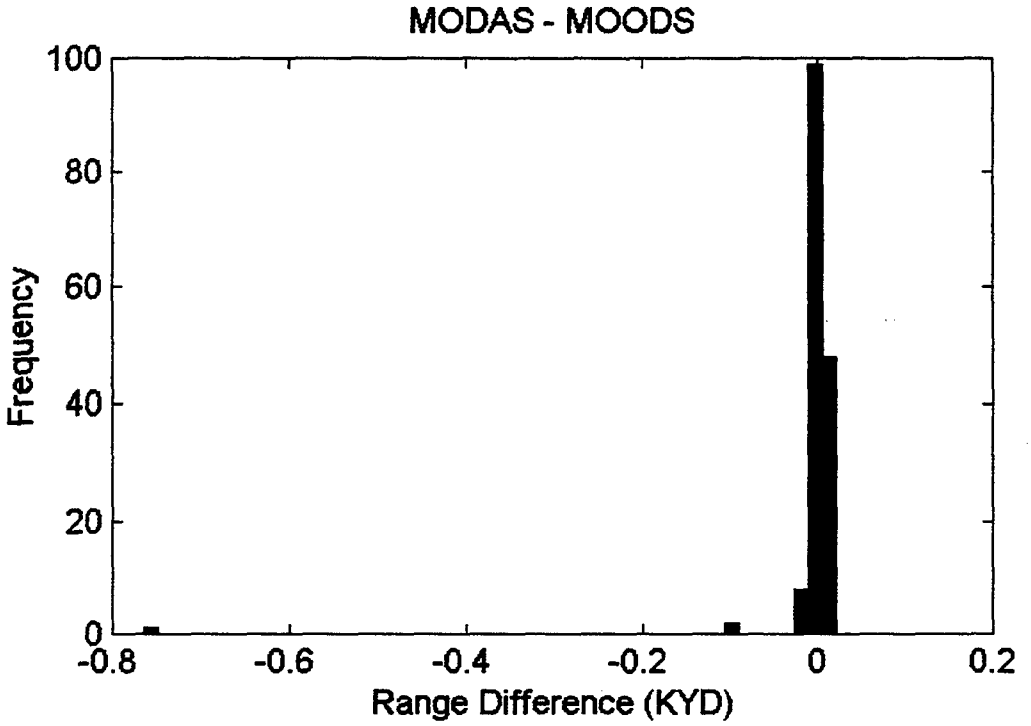

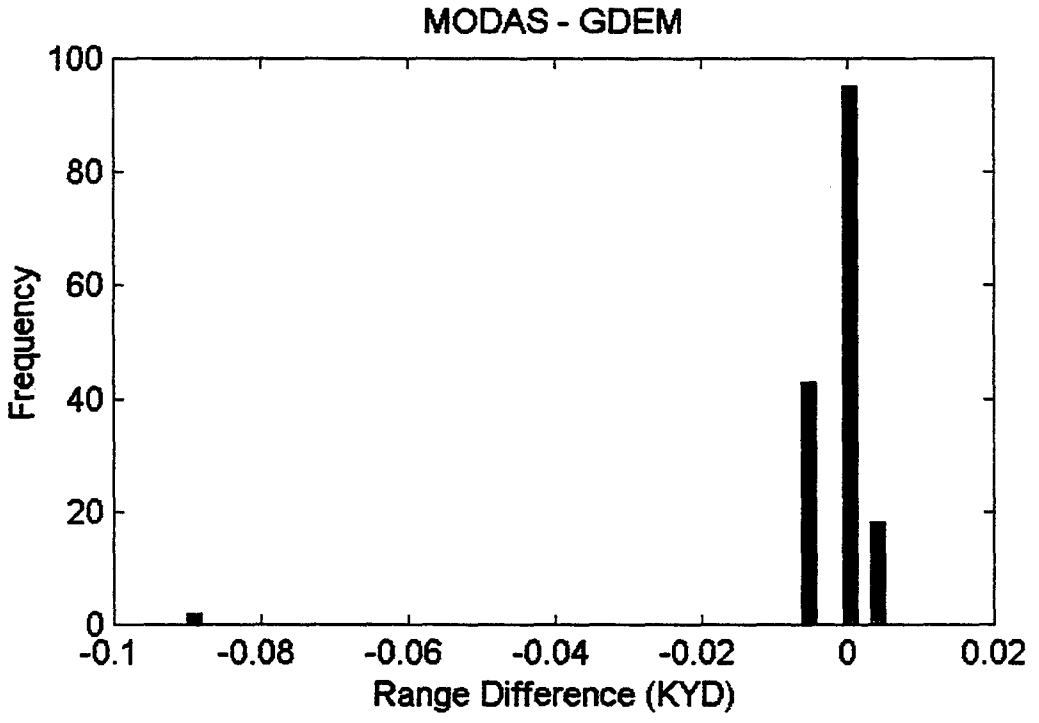

HISTOGRAMS FOR DIFFERENCES IN MAXIMUM DETECTION RANGES FOR ALL TARGET DEPTHS/ NOVEMBER 1999/ SAND BOTTOM/ SOURCE DEPTH = 125 FT.

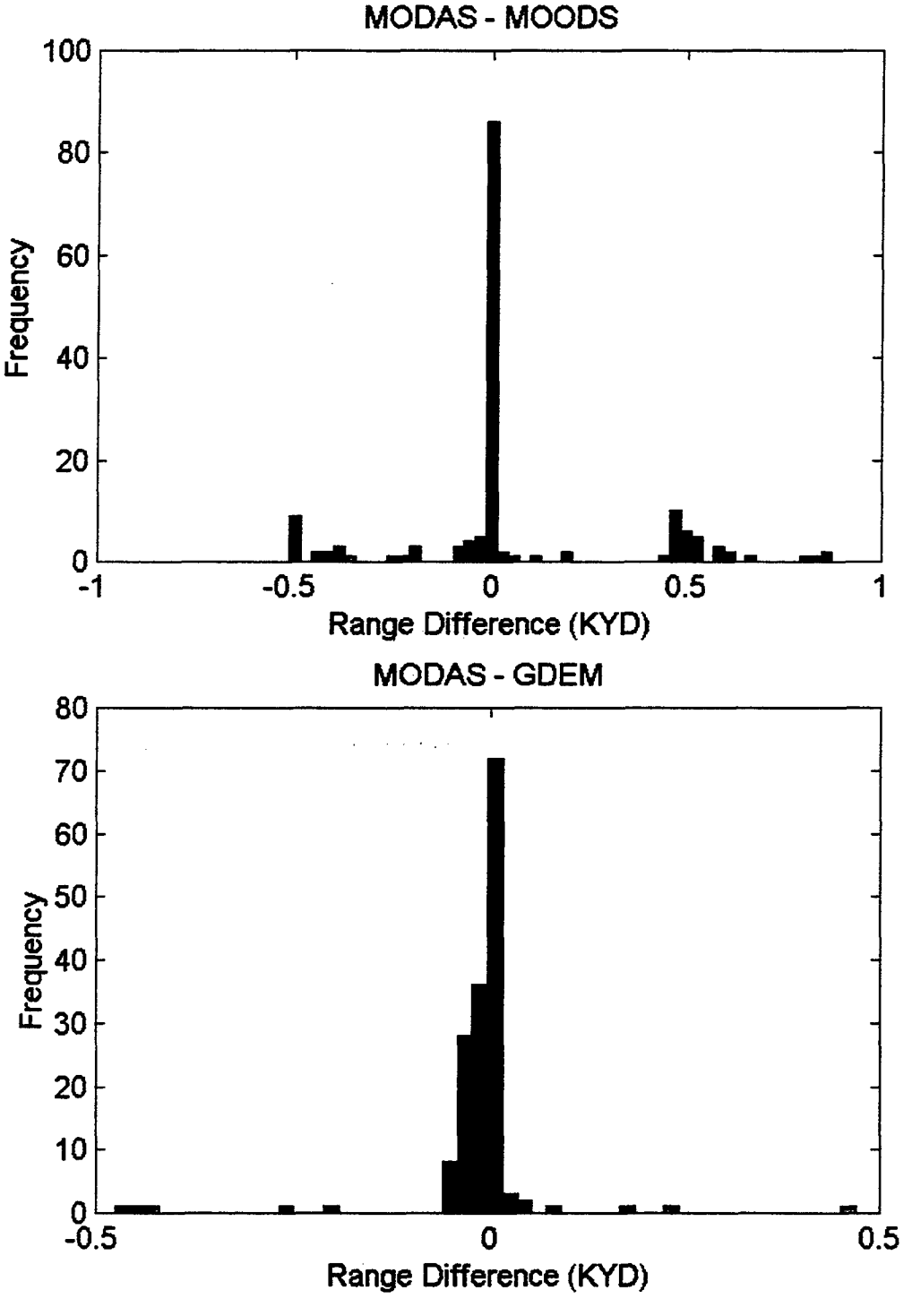

HISTOGRAMS FOR DIFFERENCES IN MAXIMUM DETECTION RANGES FOR ALL TARGET DEPTHS/ FEBRUARY 2000/ MUD BOTTOM/ SOURCE DEPTH = 25 FT.

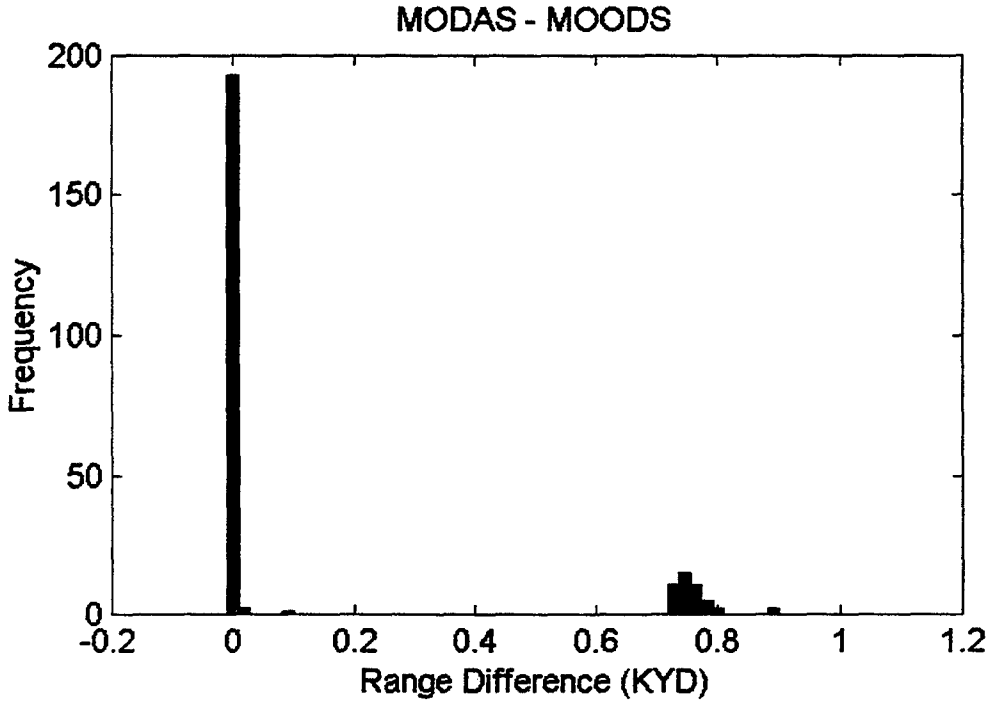

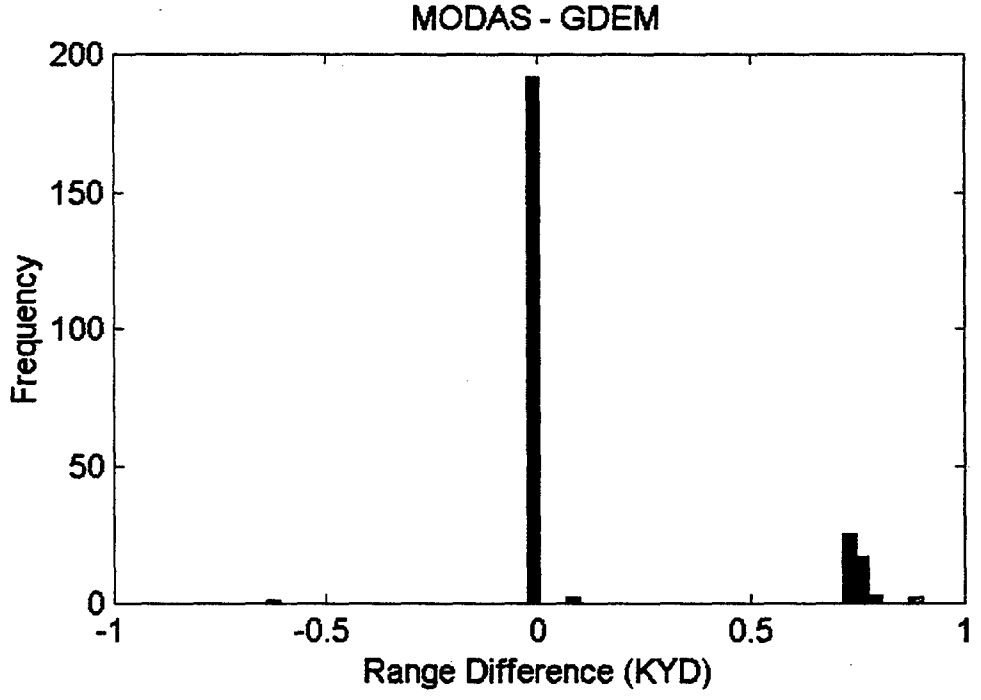

HISTOGRAMS FOR DIFFERENCES IN MAXIMUM DETECTION RANGES FOR ALL TARGET DEPTHS/ FEBRUARY 2000/ GRAVEL BOTTOM/ SOURCE DEPTH = 25 FT.

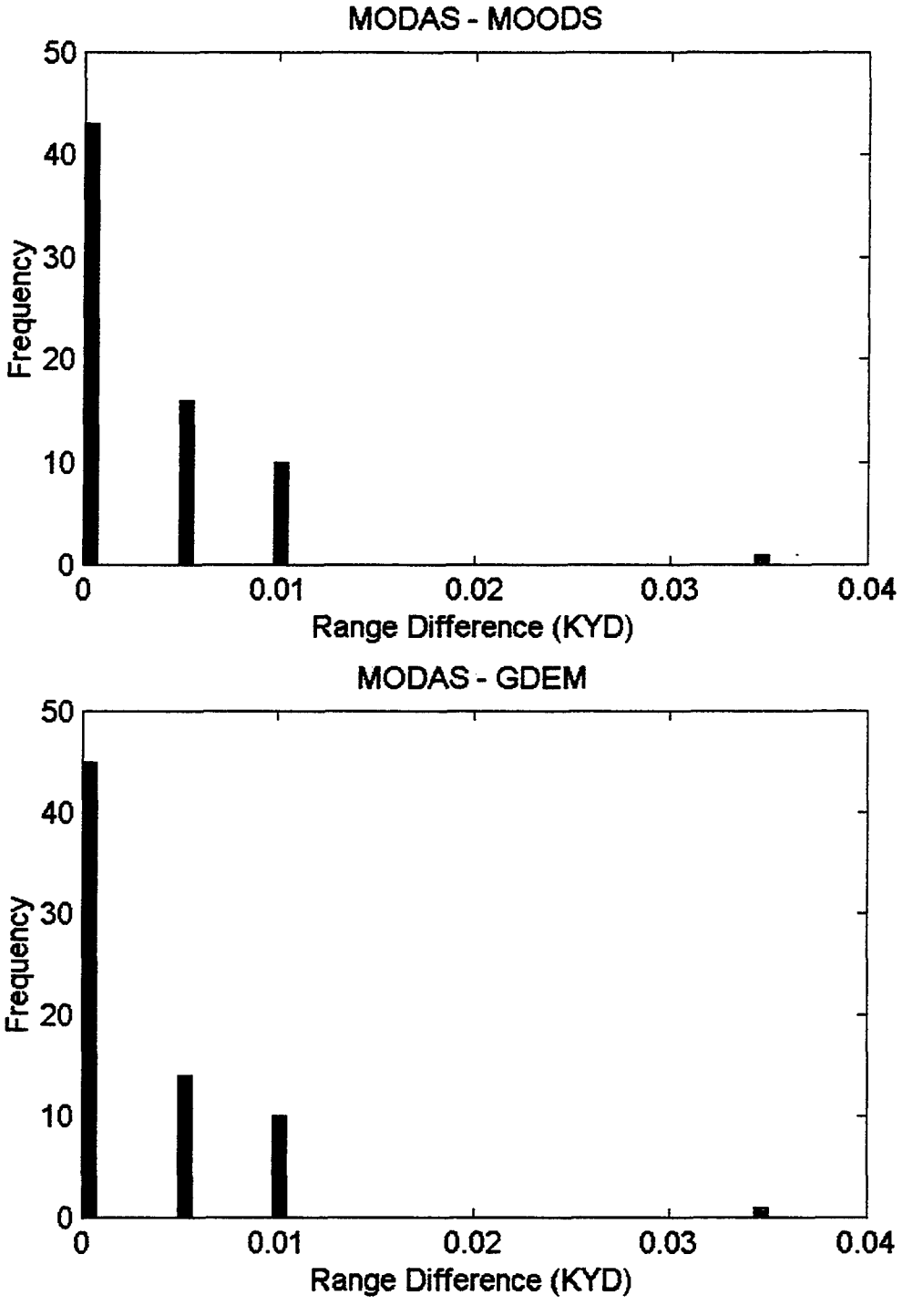

HISTOGRAMS FOR DIFFERENCES IN MAXIMUM DETECTION RANGES FOR ALL TARGET DEPTHS/ FEBRUARY 2000/ GRAVEL BOTTOM/ SOURCE DEPTH = 125 FT.

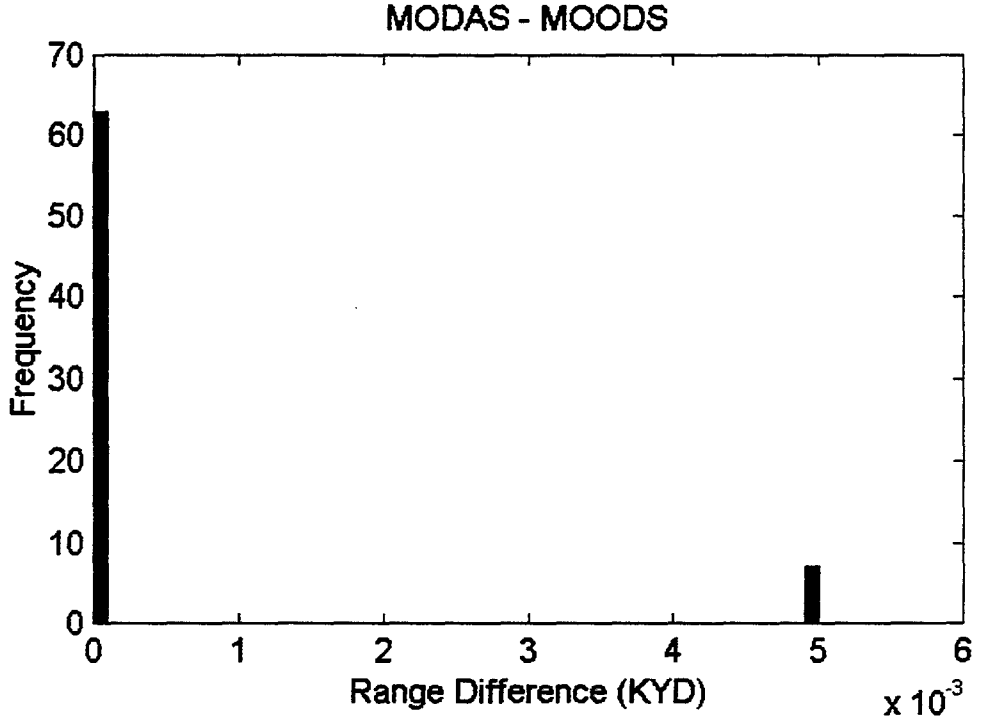

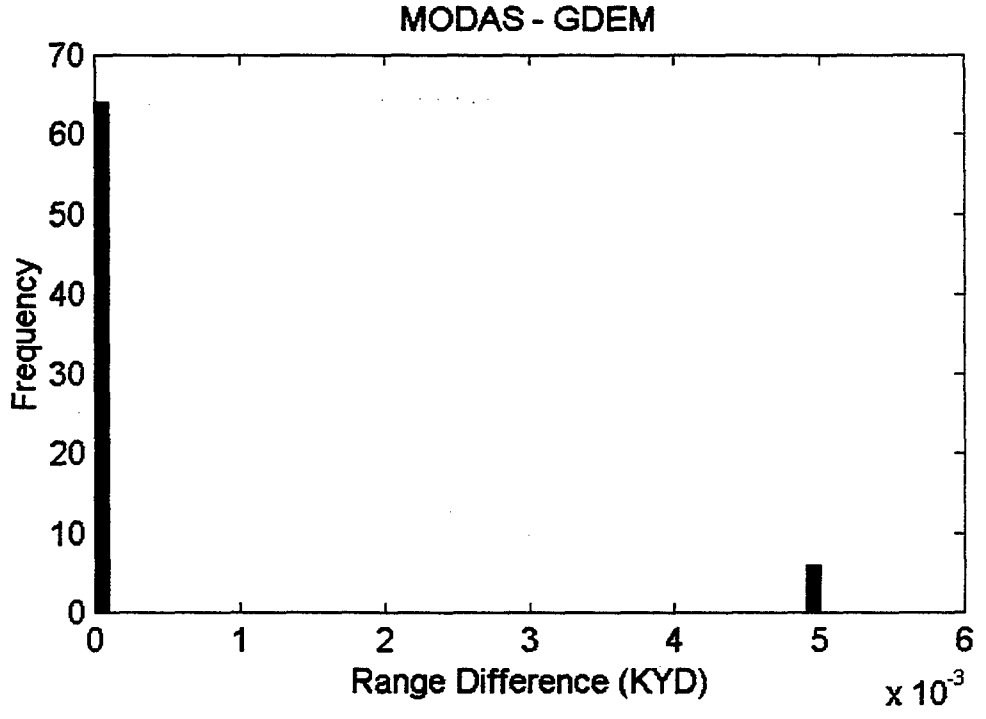

HISTOGRAMS FOR DIFFERENCES IN MAXIMUM DETECTION RANGES FOR ALL TARGET DEPTHS/ FEBRUARY 1999/ GRAVEL BOTTOM/ SOURCE DEPTH = 25 FT.

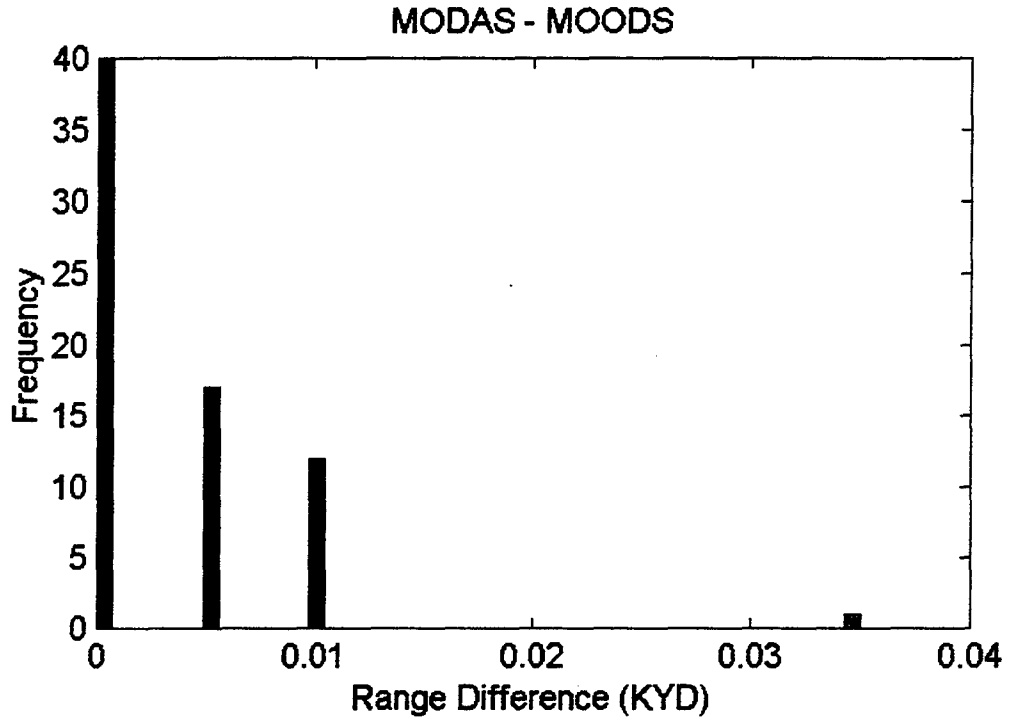

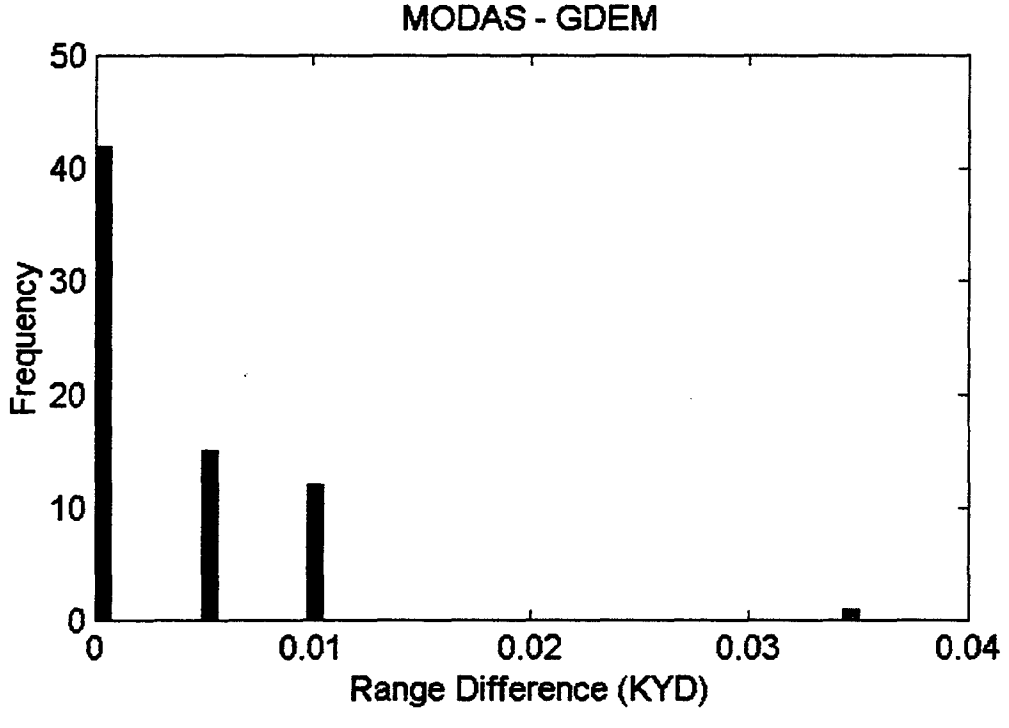

HISTOGRAMS FOR DIFFERENCES IN MAXIMUM DETECTION RANGES FOR ALL TARGET DEPTHS/ FEBRUARY 1999/ GRAVEL BOTTOM/ SOURCE DEPTH = 125 FT.

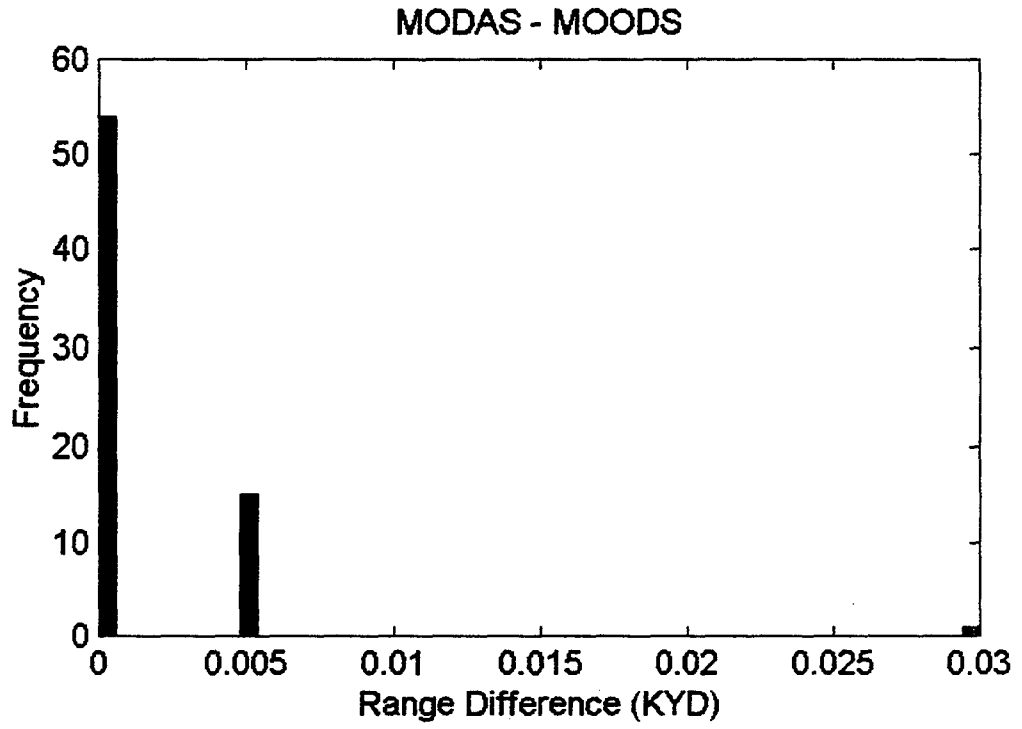

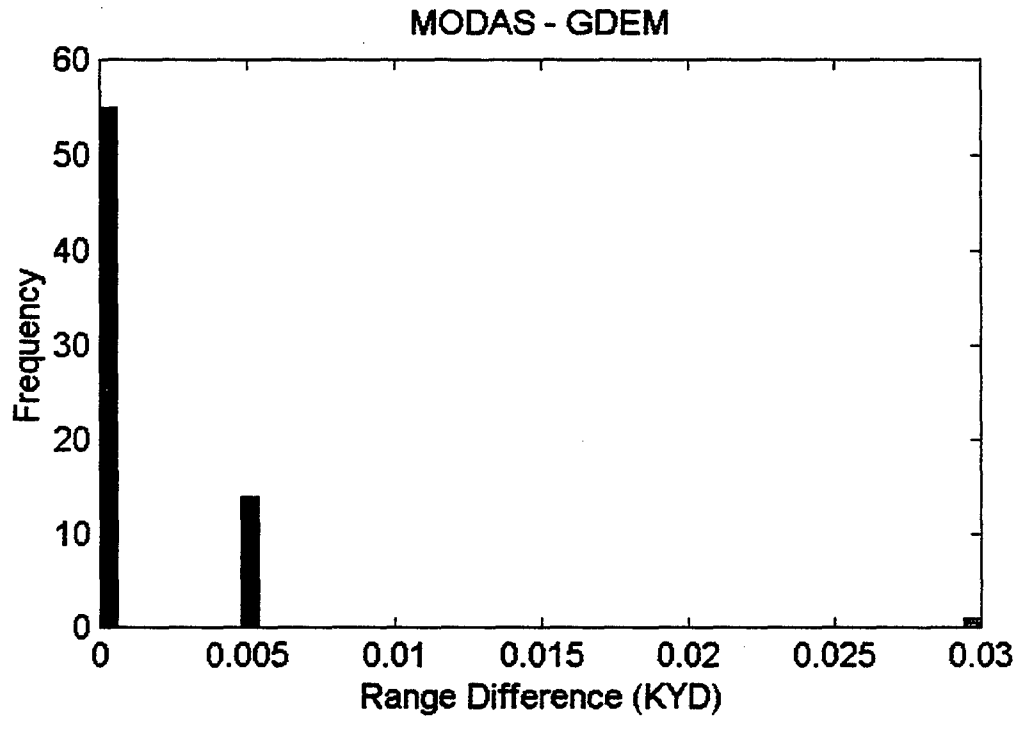

HISTOGRAMS FOR DIFFERENCES IN MAXIMUM DETECTION RANGES FOR ALL TARGET DEPTHS/ MAY 2000/ GRAVEL BOTTOM/ SOURCE DEPTH = 25 FT.

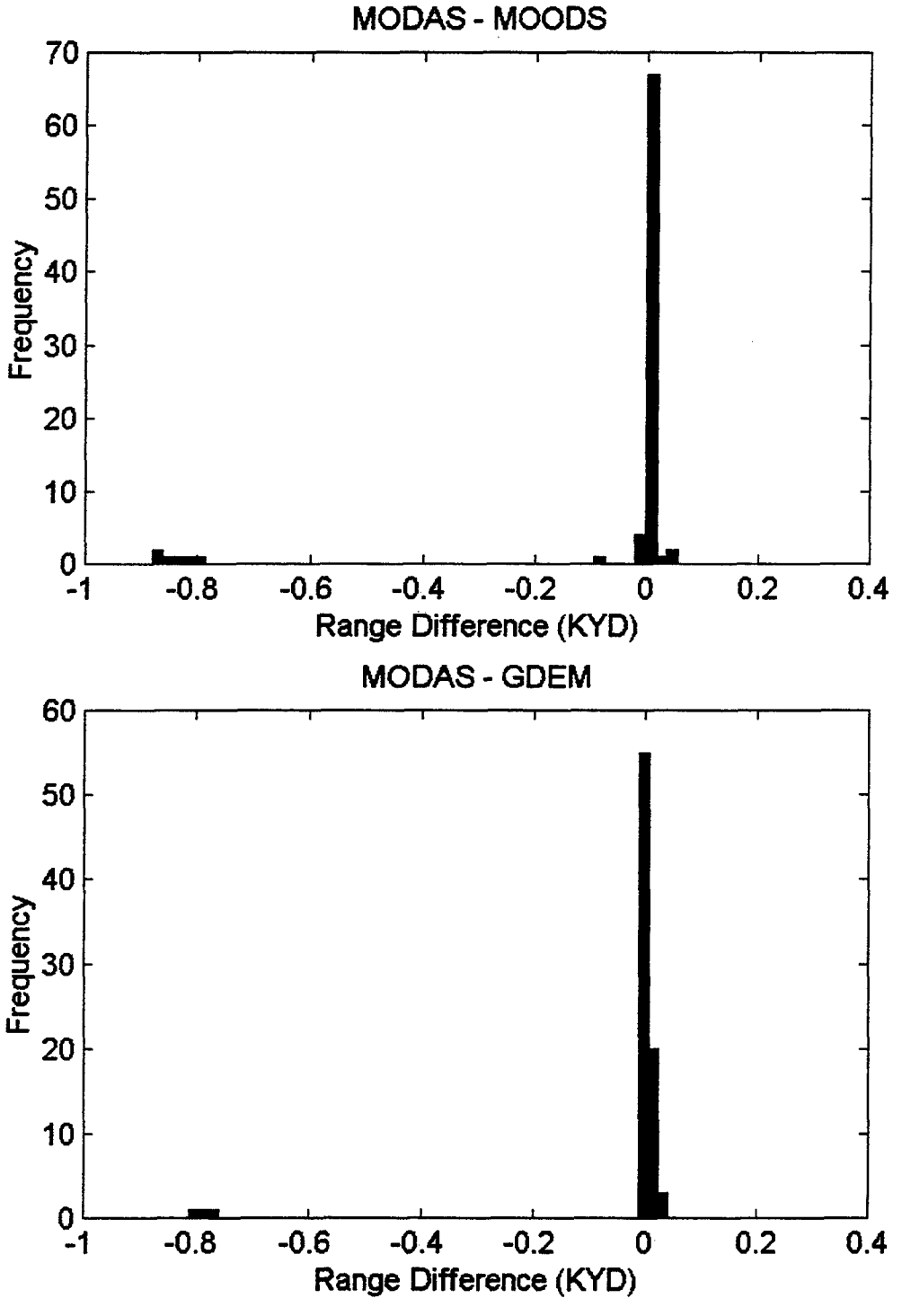

HISTOGRAMS FOR DIFFERENCES IN MAXIMUM DETECTION RANGES FOR ALL TARGET DEPTHS/ MAY 2000/ GRAVEL BOTTOM/ SOURCE DEPTH = 125 FT.

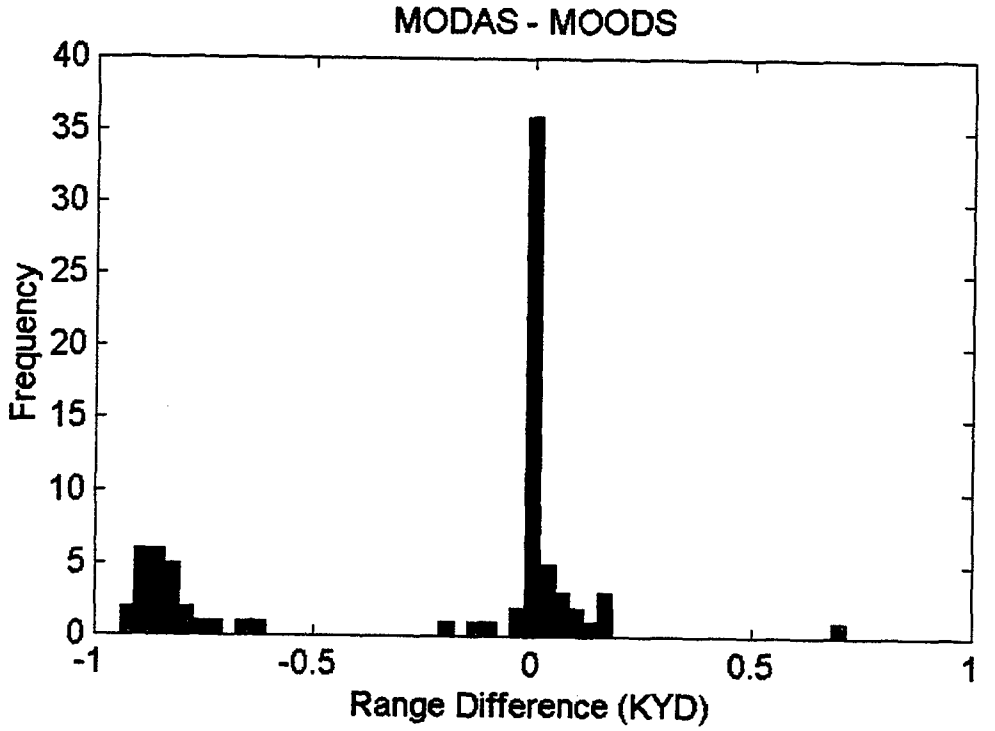

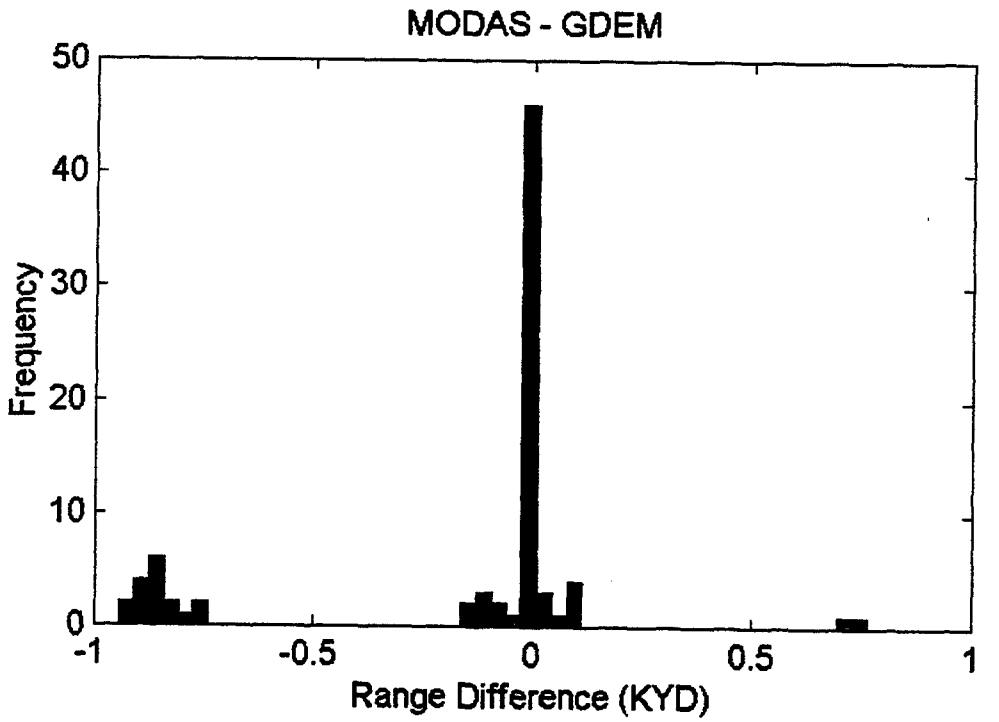

HISTOGRAMS FOR DIFFERENCES IN MAXIMUM DETECTION RANGES FOR ALL TARGET DEPTHS/ MAY 1999/ GRAVEL BOTTOM/ SOURCE DEPTH = 25 FT.

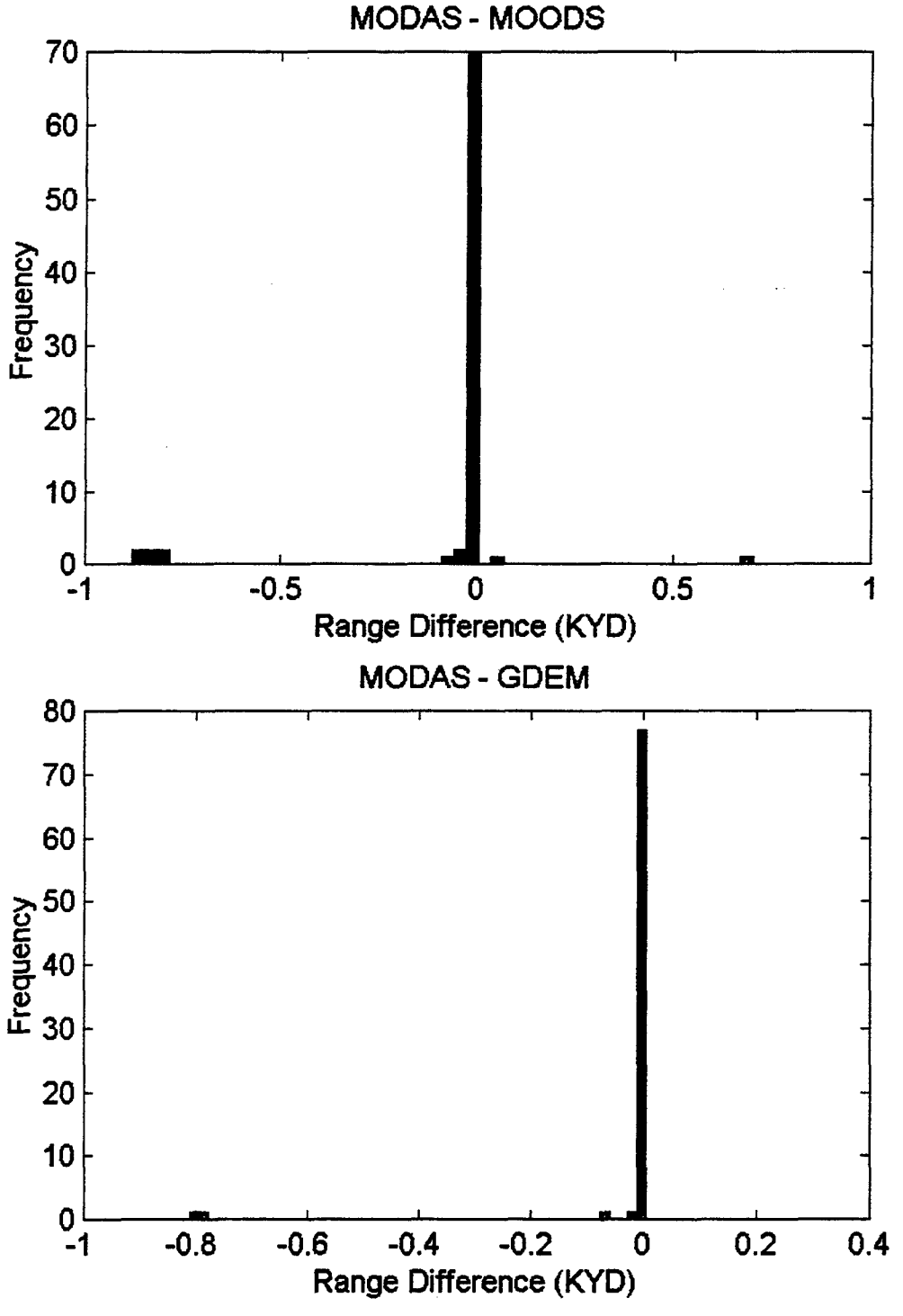

HISTOGRAMS FOR DIFFERENCES IN MAXIMUM DETECTION RANGES FOR ALL TARGET DEPTHS/ MAY 1999/ GRAVEL BOTTOM/ SOURCE DEPTH = 125 FT.

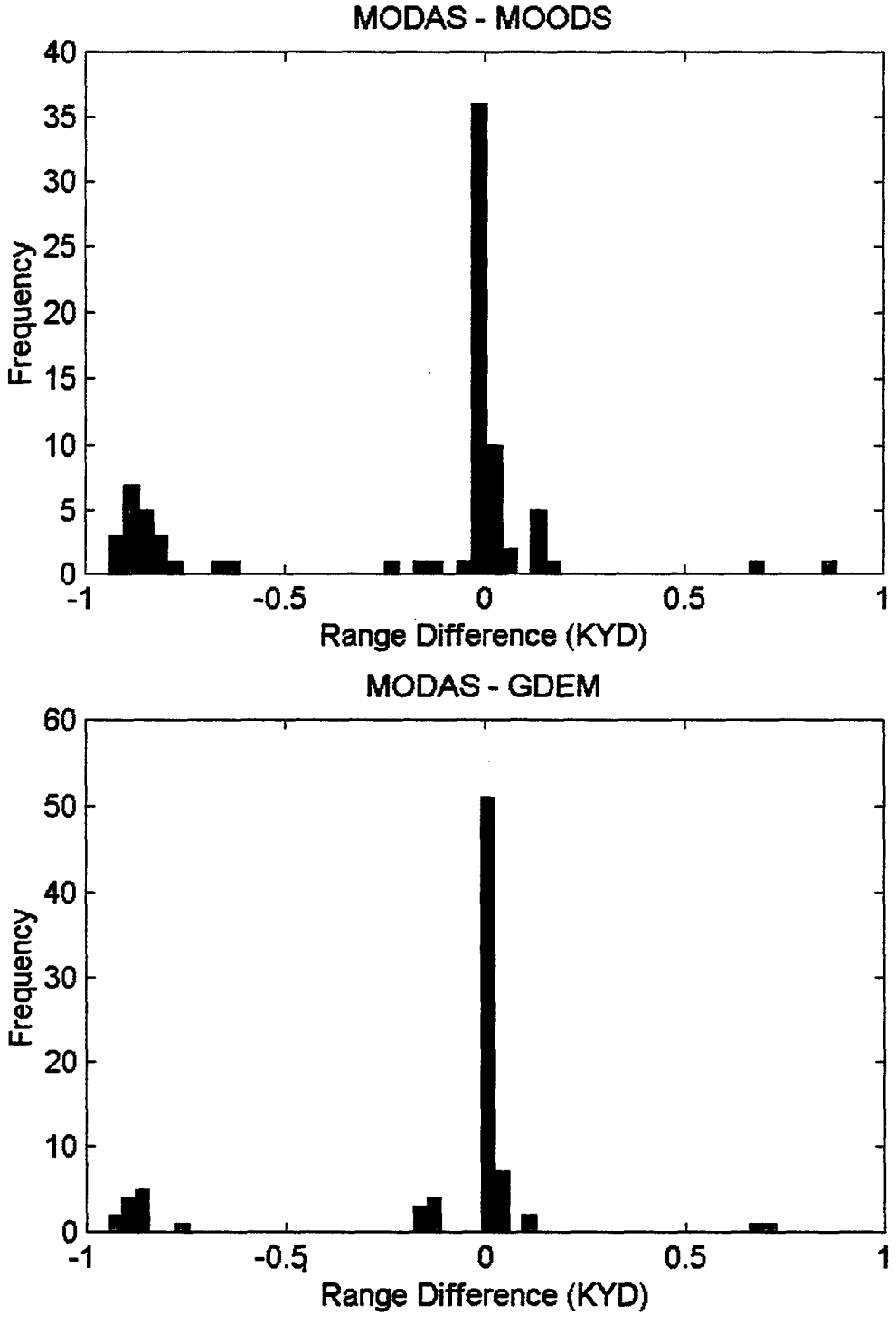

HISTOGRAMS FOR DIFFERENCES IN MAXIMUM DETECTION RANGES FOR ALL TARGET DEPTHS/ AUGUST 2000/ GRAVEL BOTTOM/ SOURCE DEPTH = 25 FT.

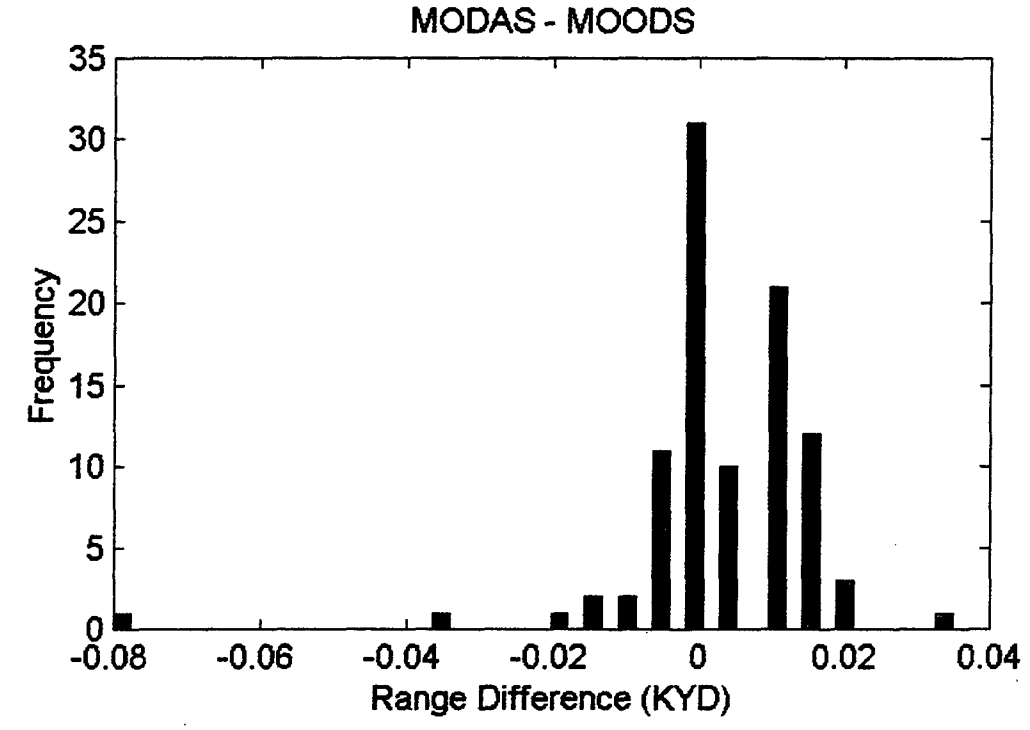

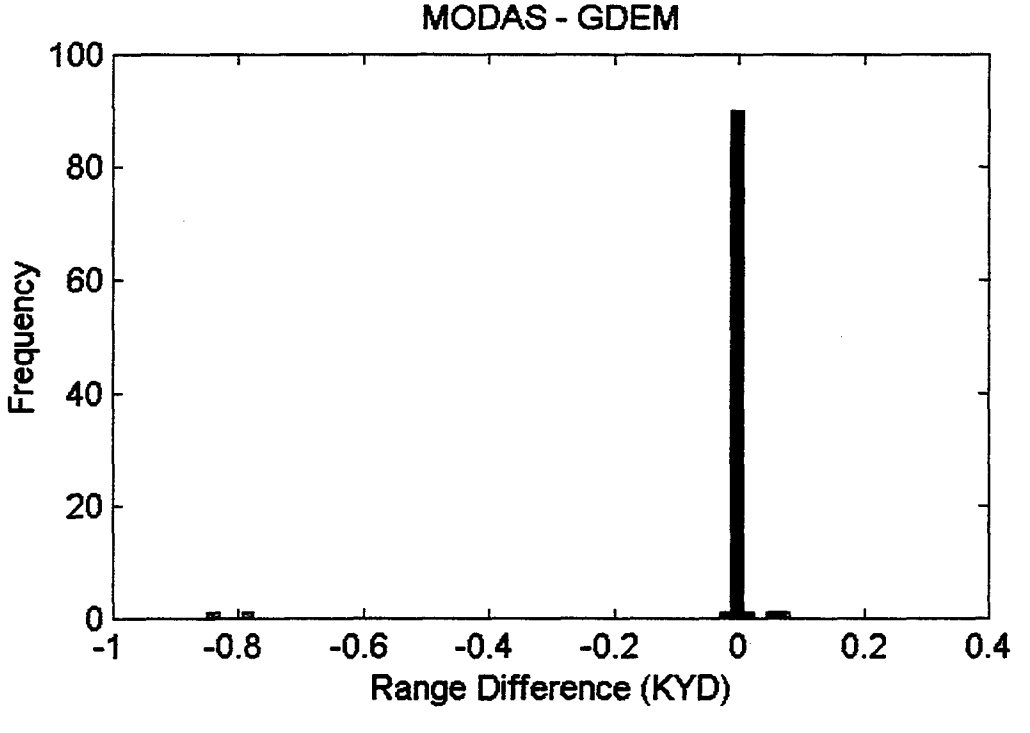

HISTOGRAMS FOR DIFFERENCES IN MAXIMUM DETECTION RANGES FOR ALL TARGET DEPTHS/ AUGUST 2000/ GRAVEL BOTTOM/ SOURCE DEPTH = 125 FT.

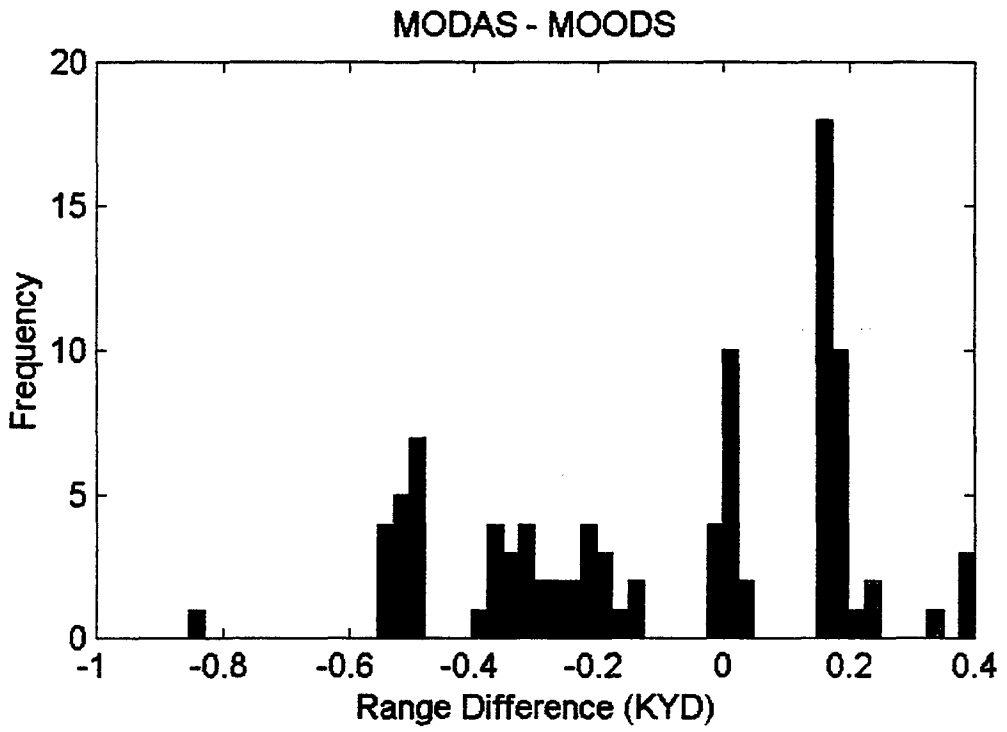

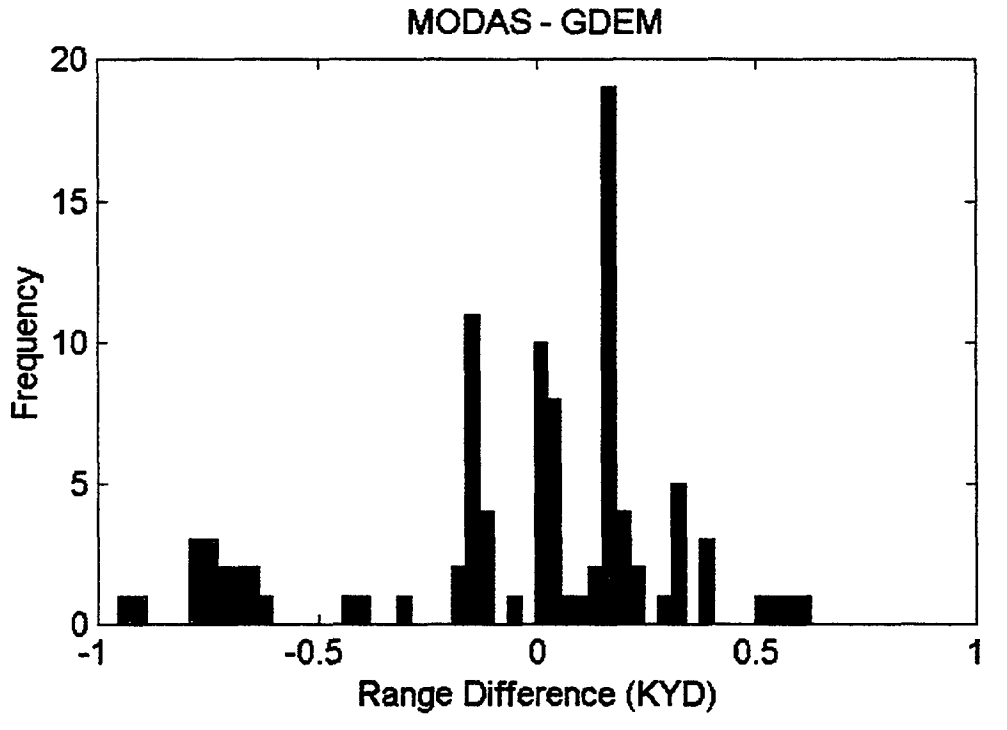

HISTOGRAMS FOR DIFFERENCES IN MAXIMUM DETECTION RANGES FOR ALL TARGET DEPTHS/ AUGUST 1999/ GRAVEL BOTTOM/ SOURCE DEPTH = 25 FT.

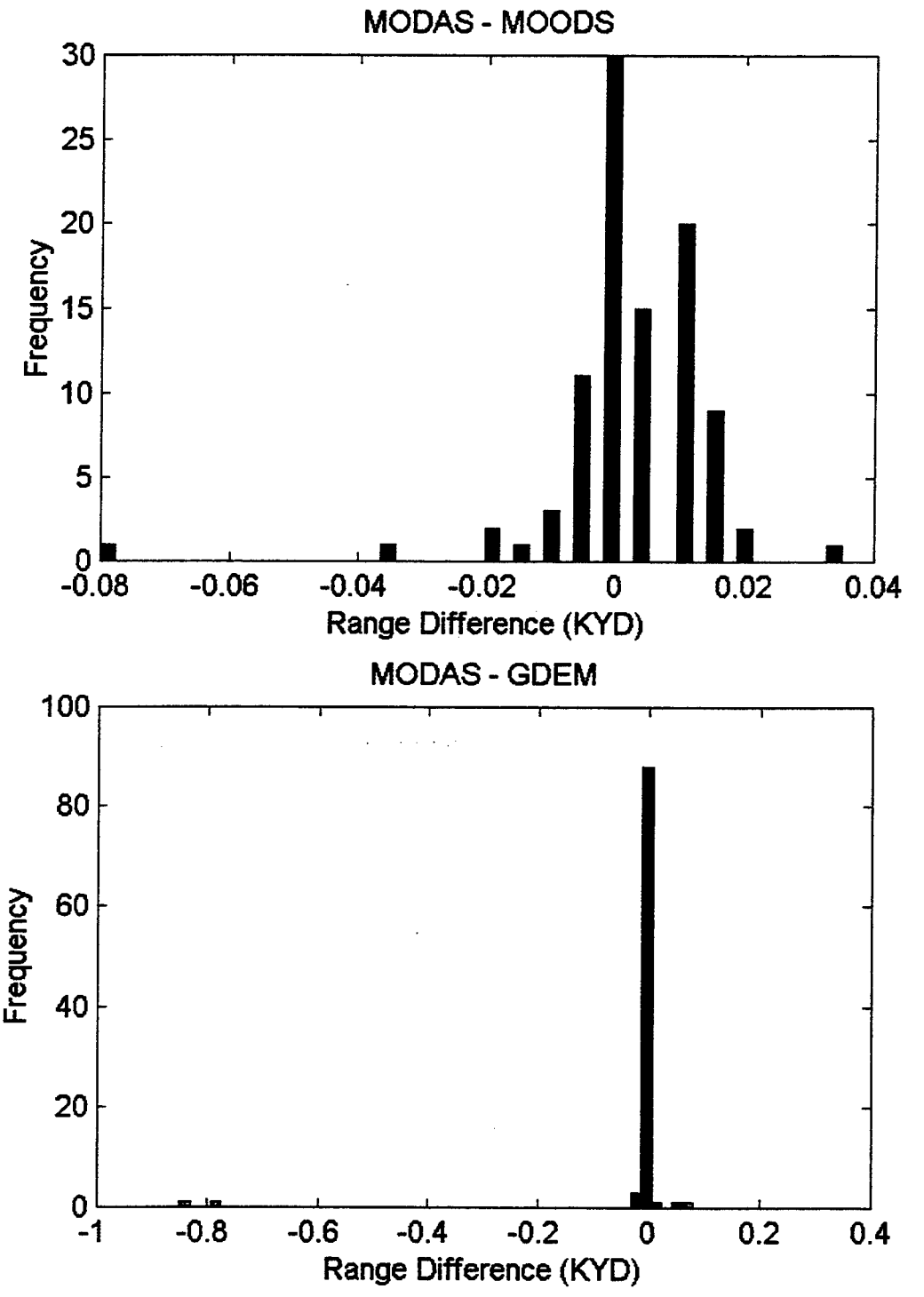

HISTOGRAMS FOR DIFFERENCES IN MAXIMUM DETECTION RANGES FOR ALL TARGET DEPTHS/ AUGUST 1999/ GRAVEL BOTTOM/ SOURCE DEPTH = 125 FT.

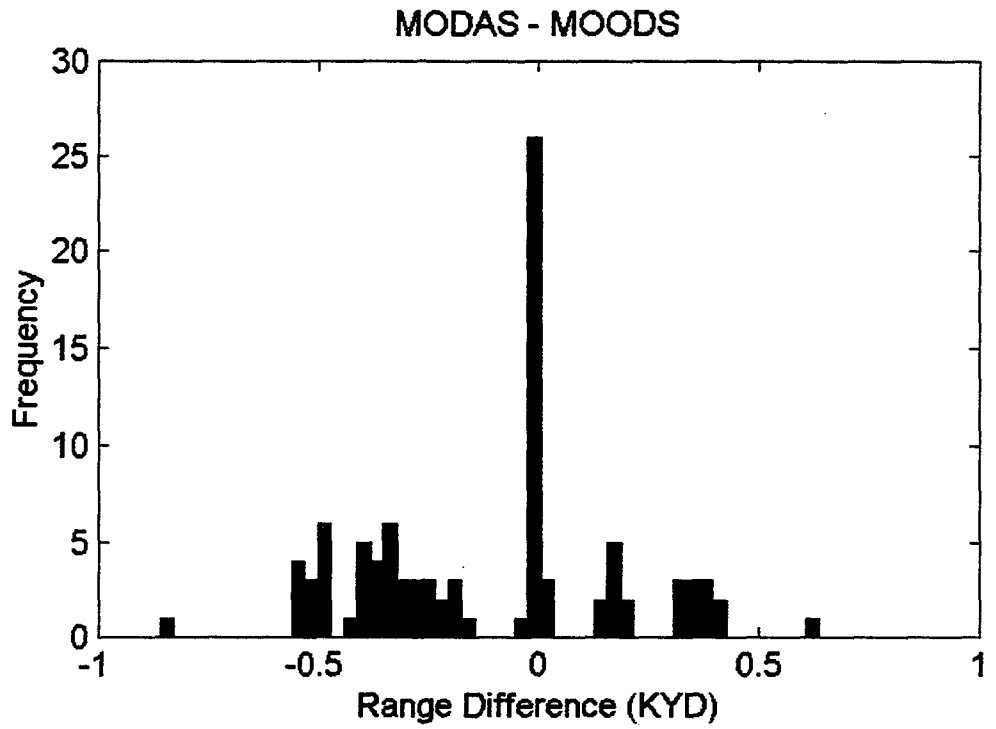

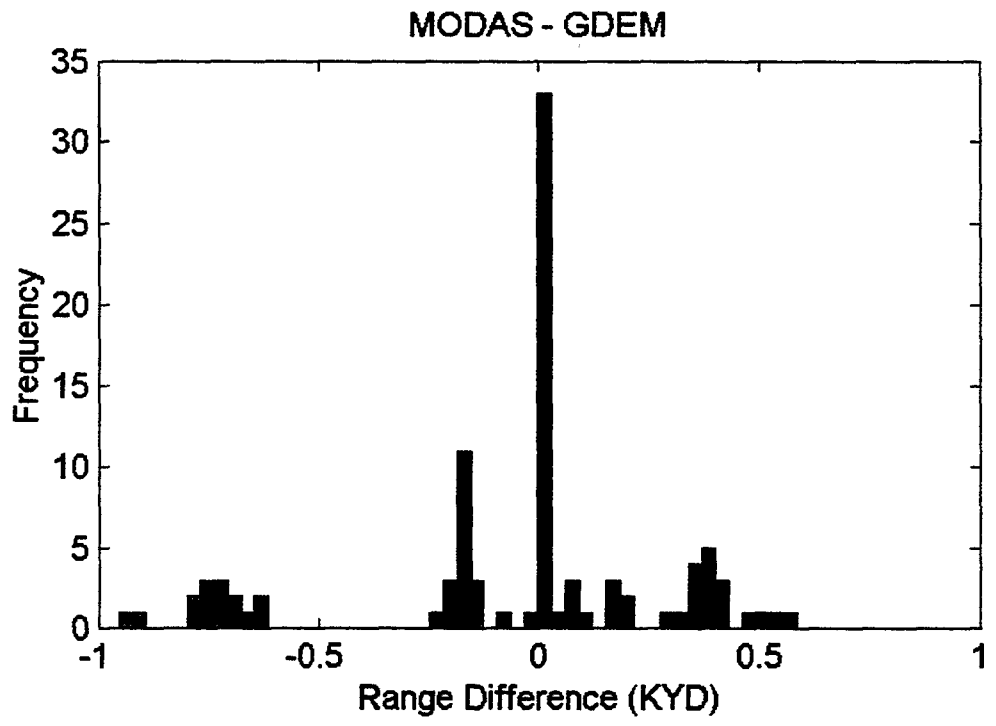

HISTOGRAMS FOR DIFFERENCES IN MAXIMUM DETECTION RANGES FOR ALL TARGET DEPTHS/ NOVEMBER 2000/ GRAVEL BOTTOM/ SOURCE DEPTH = 25 FT.

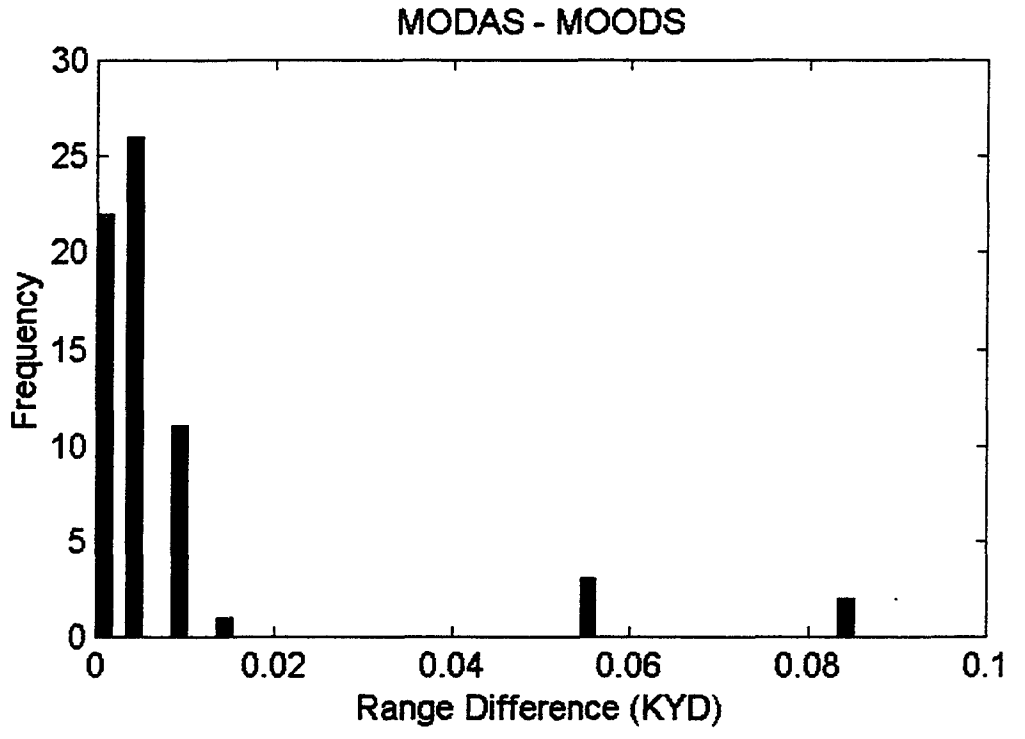

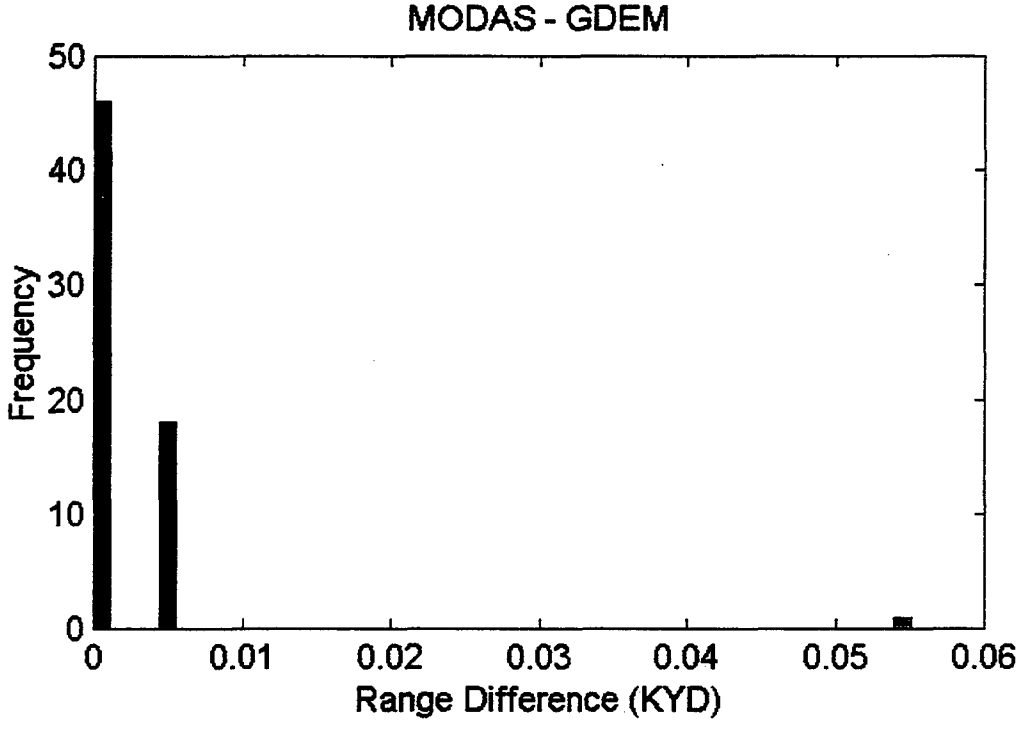

HISTOGRAMS FOR DIFFERENCES IN MAXIMUM DETECTION RANGES FOR ALL TARGET DEPTHS/ NOVEMBER 2000/ GRAVEL BOTTOM/ SOURCE DEPTH=125 FT.

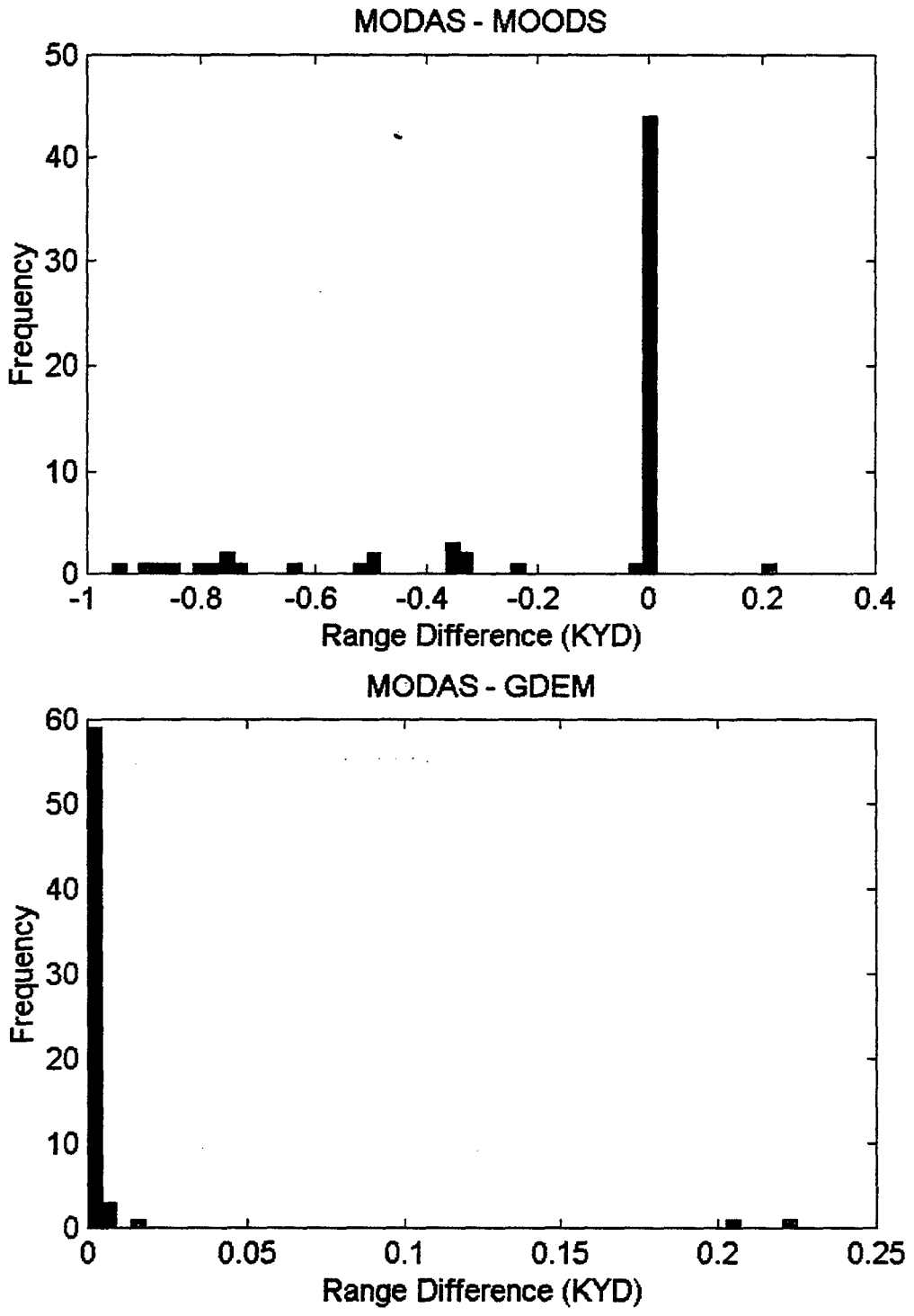

HISTOGRAMS FOR DIFFERENCES IN MAXIMUM DETECTION RANGES FOR ALL TARGET DEPTHS/ NOVEMBER 1999/ GRAVEL BOTTOM/ SOURCE DEPTH = 25 FT.

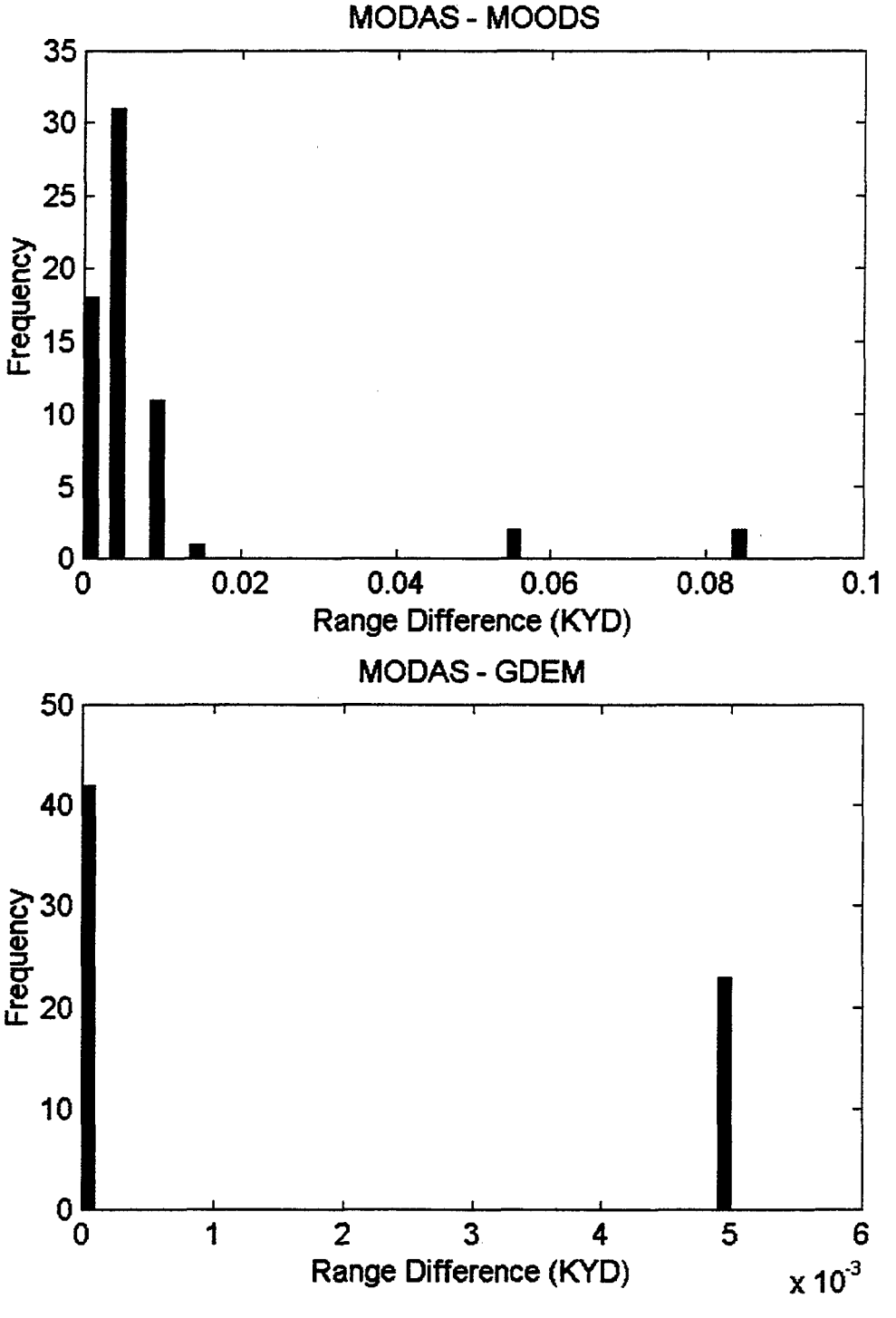

HISTOGRAMS FOR DIFFERENCES IN MAXIMUM DETECTION RANGES FOR ALL TARGET DEPTHS/ NOVEMBER 1999/ GRAVEL BOTTOM/ SOURCE DEPTH=125 FT.

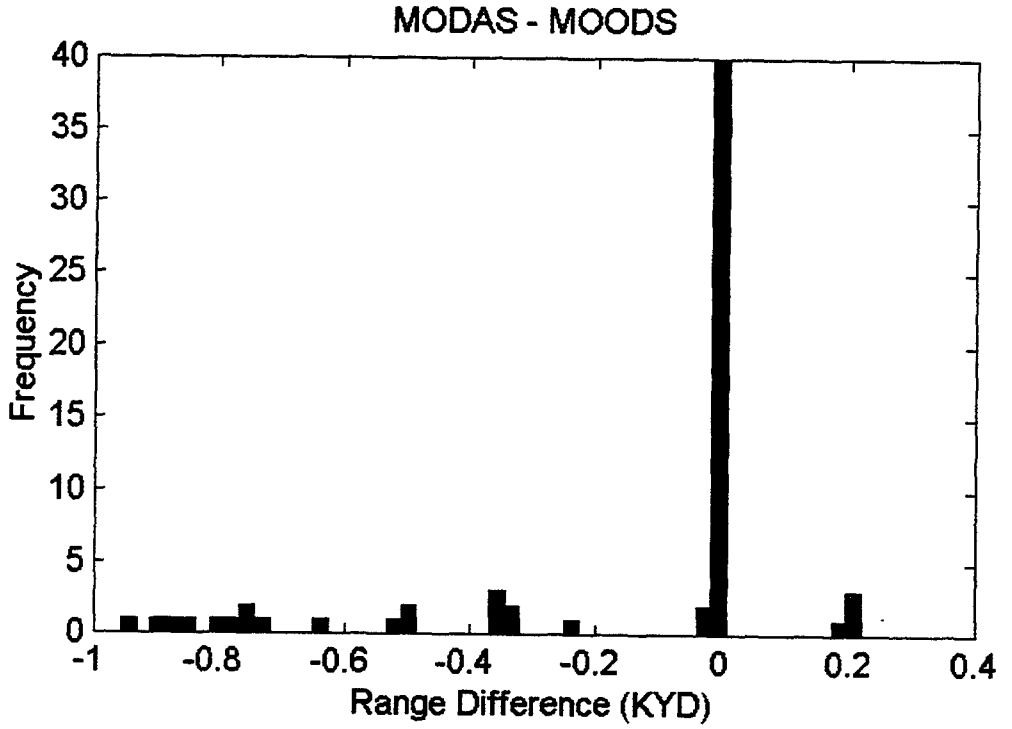

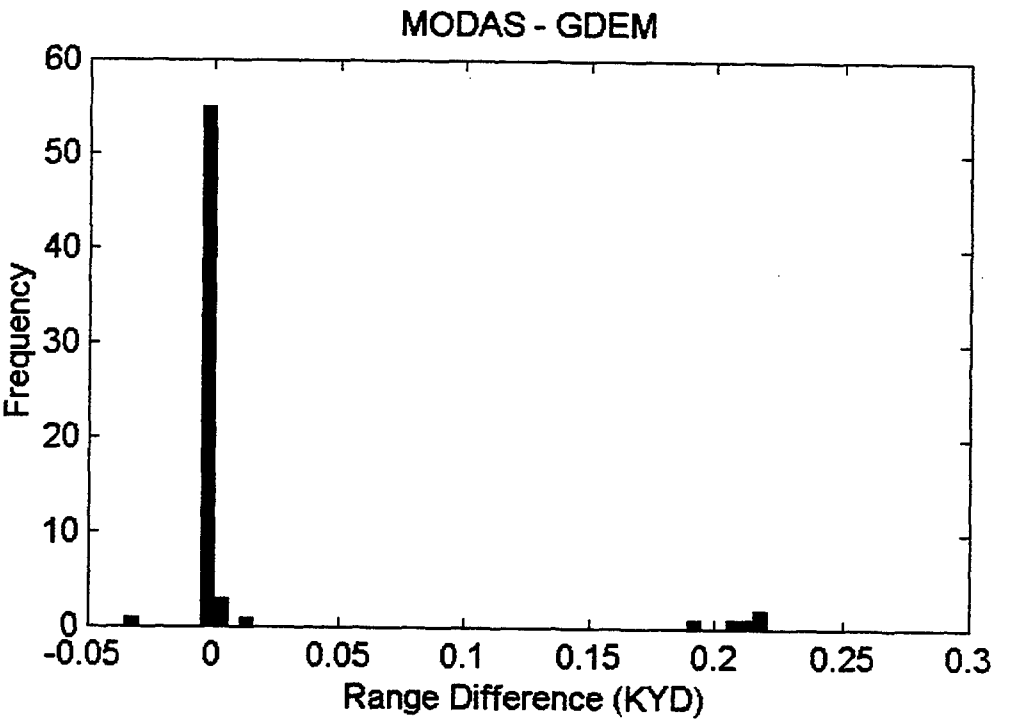

HISTOGRAMS FOR DIFFERENCES IN MAXIMUM DETECTION RANGES FOR ALL TARGET DEPTHS/ FEBRUARY 2000/ ROCK BOTTOM/ SOURCE DEPTH = 25 FT.

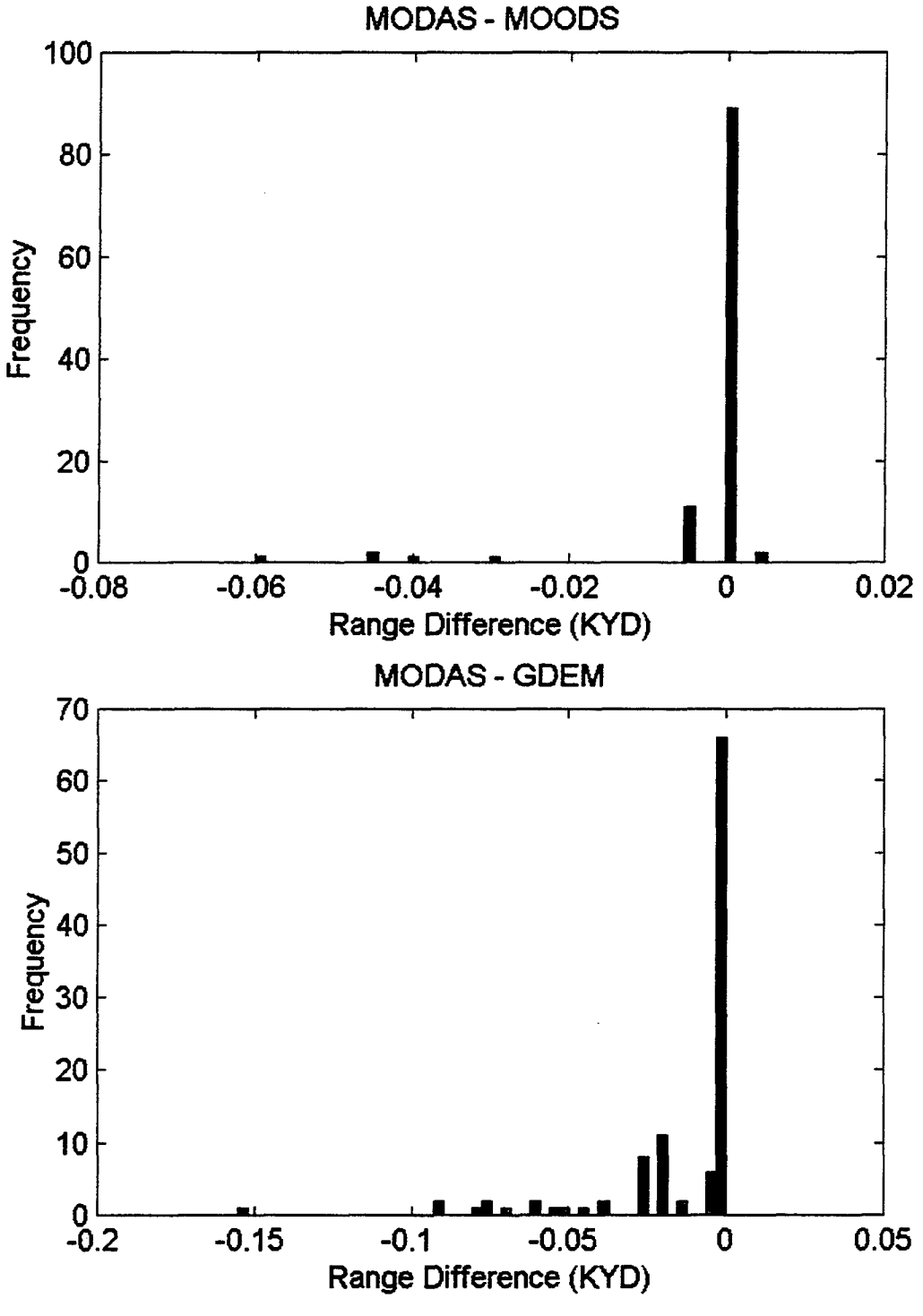

HISTOGRAMS FOR DIFFERENCES IN MAXIMUM DETECTION RANGES FOR ALL TARGET DEPTHS/ FEBRUARY 2000/ ROCK BOTTOM/ SOURCE DEPTH = 125 FT.

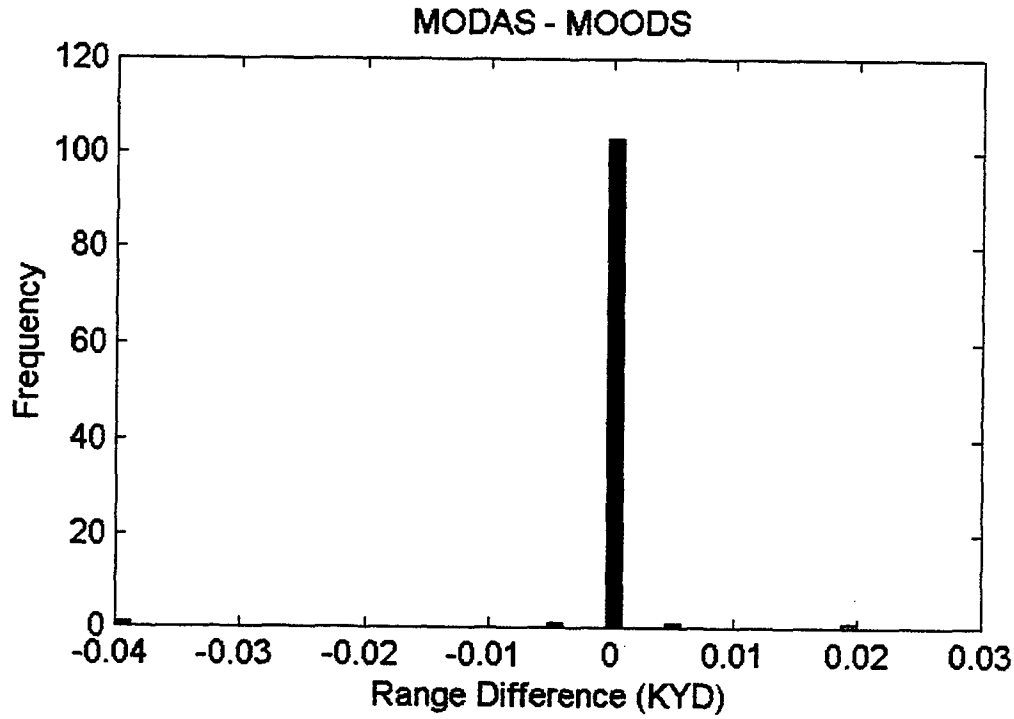

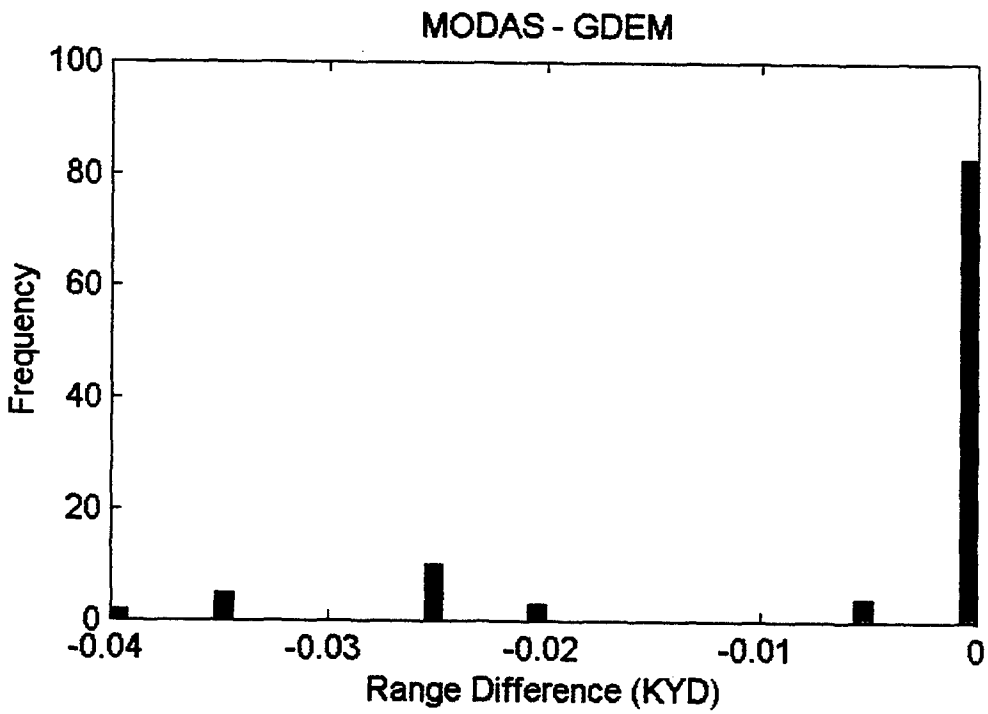

HISTOGRAMS FOR DIFFERENCES IN MAXIMUM DETECTION RANGES FOR ALL TARGET DEPTHS/ FEBRUARY 1999/ ROCK BOTTOM/ SOURCE DEPTH = 25 FT.

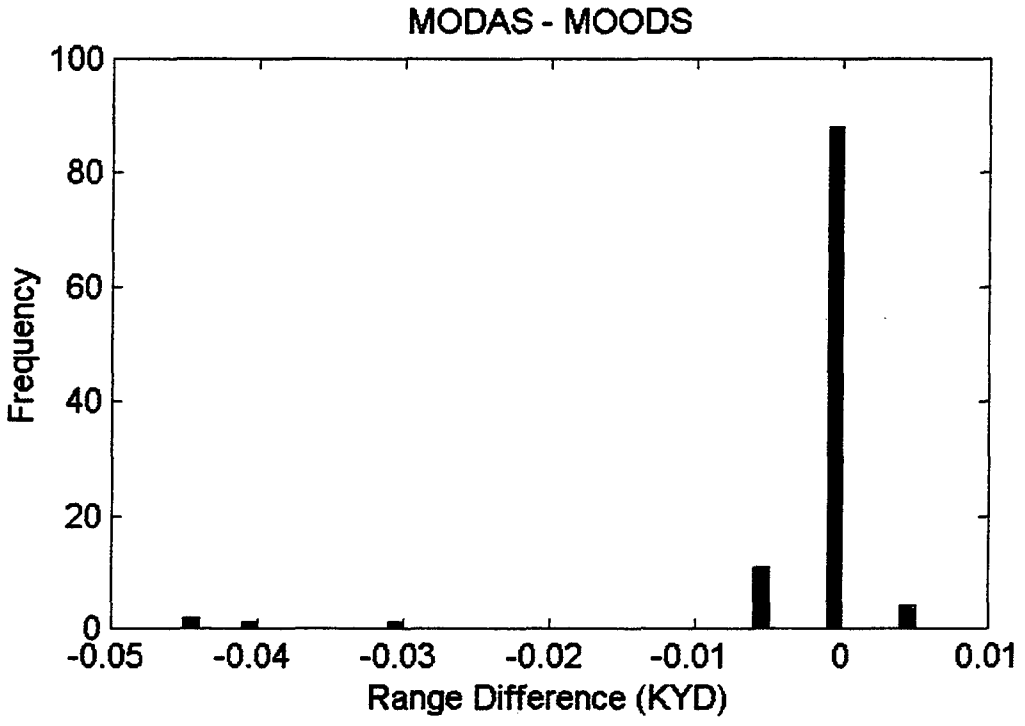

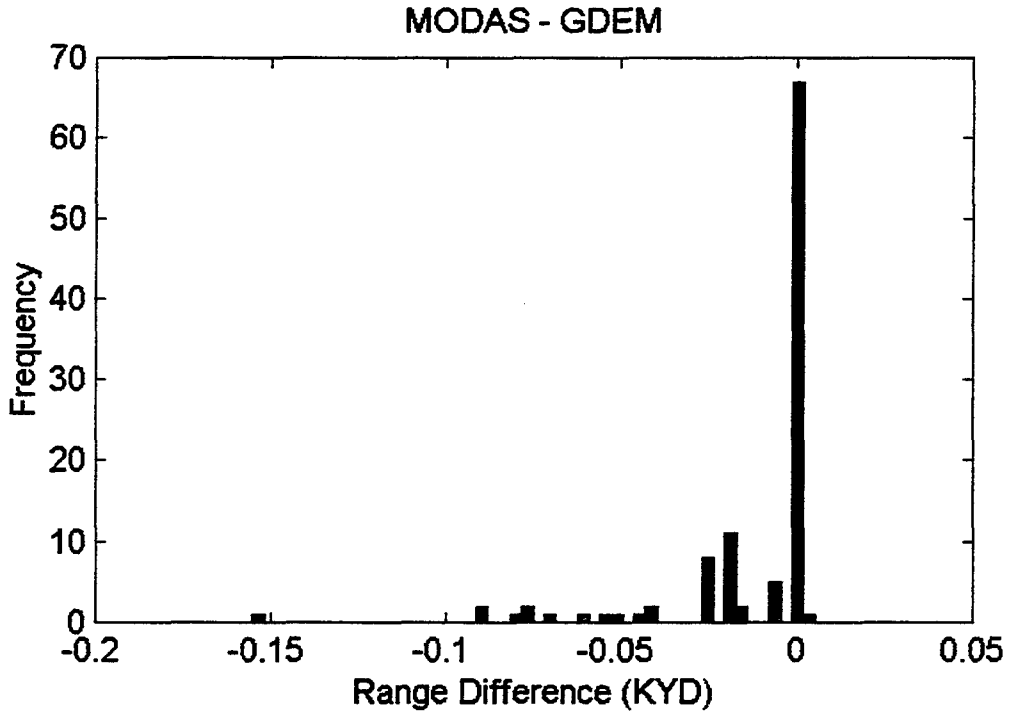

HISTOGRAMS FOR DIFFERENCES IN MAXIMUM DETECTION RANGES FOR ALL TARGET DEPTHS/ FEBRUARY 1999/ ROCK BOTTOM/ SOURCE DEPTH = 125 FT.

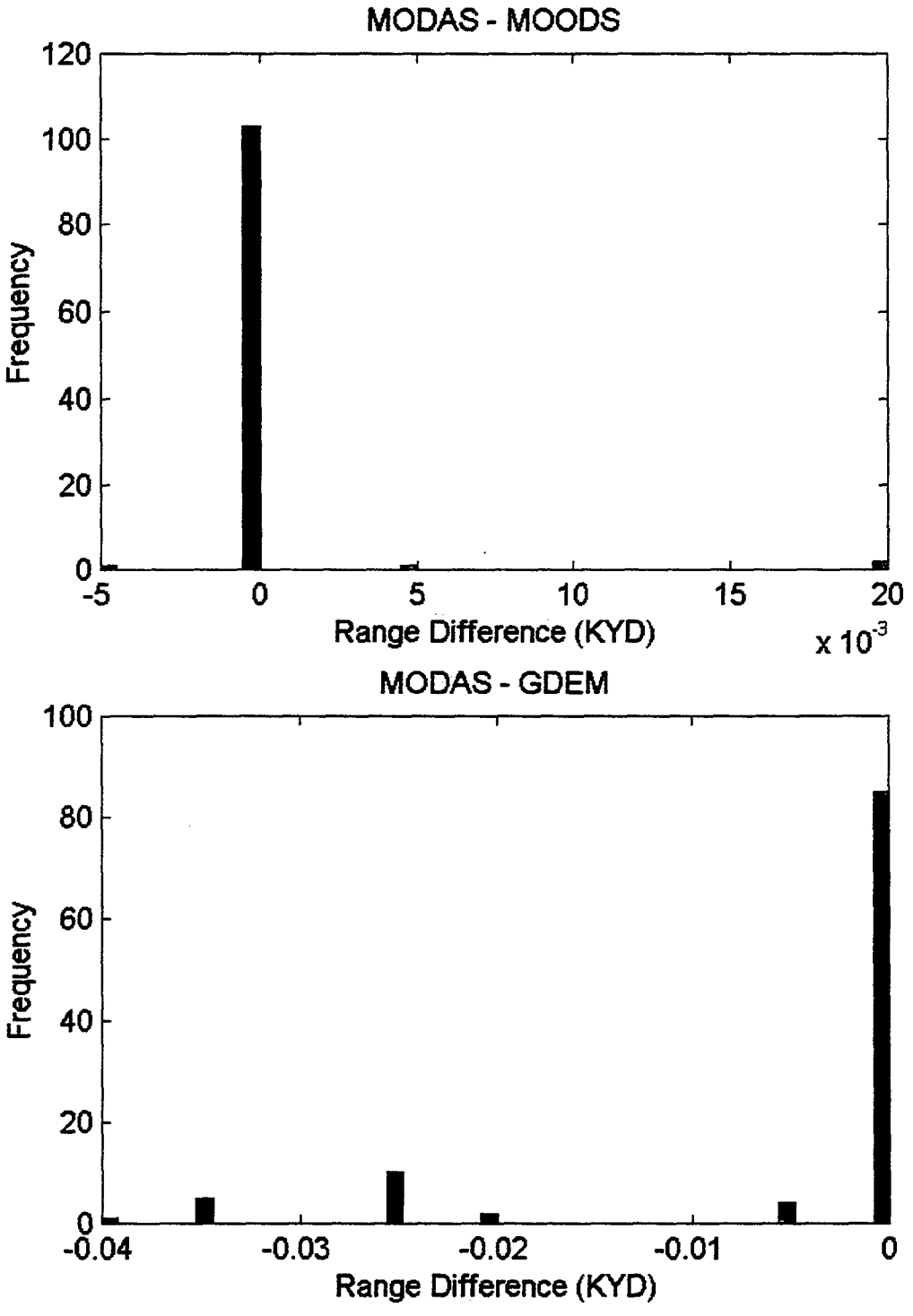

HISTOGRAMS FOR DIFFERENCES IN MAXIMUM DETECTION RANGES FOR ALL TARGET DEPTHS/ MAY 2000/ ROCK BOTTOM/ SOURCE DEPTH = 25 FT.

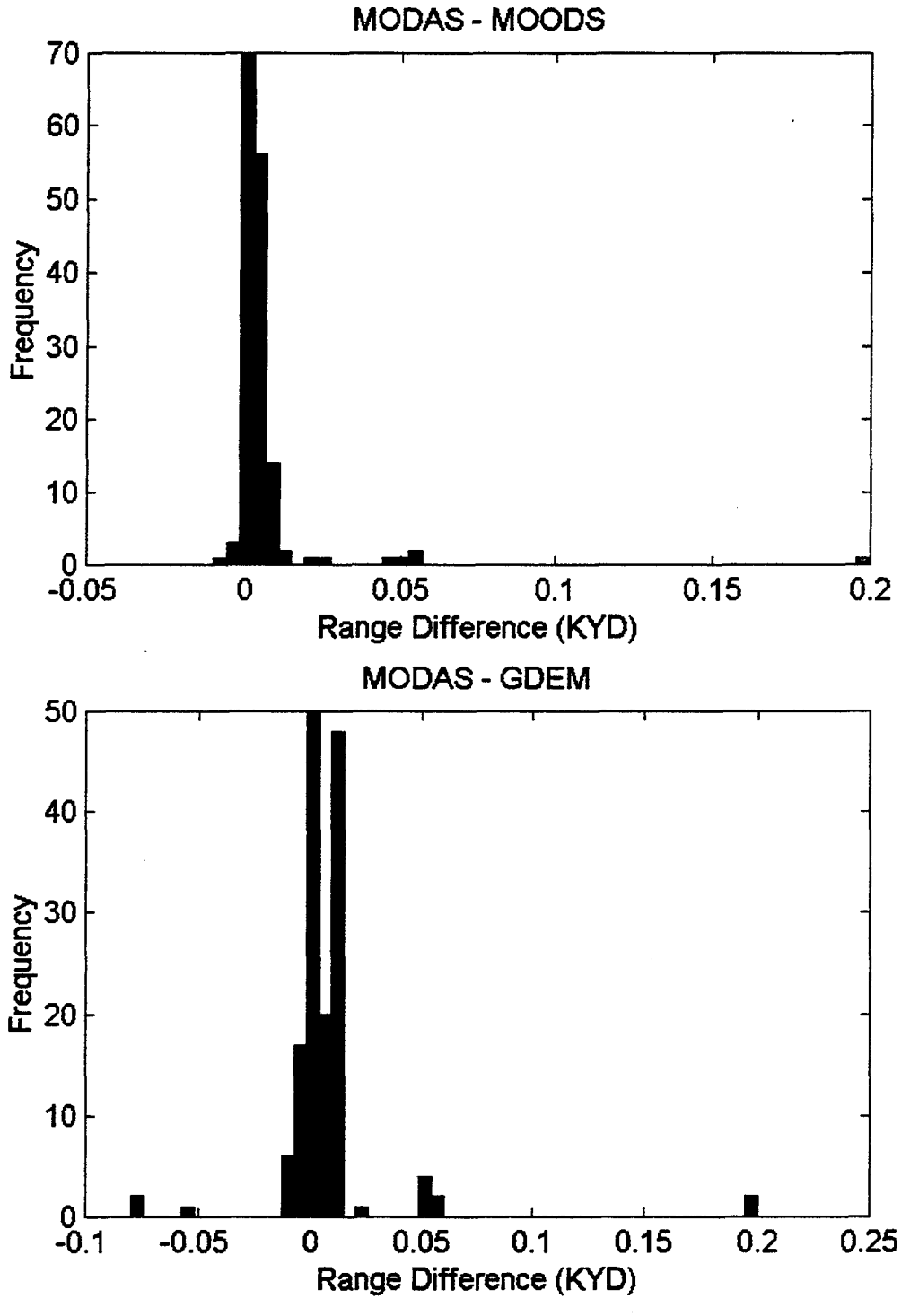

HISTOGRAMS FOR DIFFERENCES IN MAXIMUM DETECTION RANGES FOR ALL TARGET DEPTHS/ MAY 2000/ ROCK BOTTOM/ SOURCE DEPTH = 125 FT.

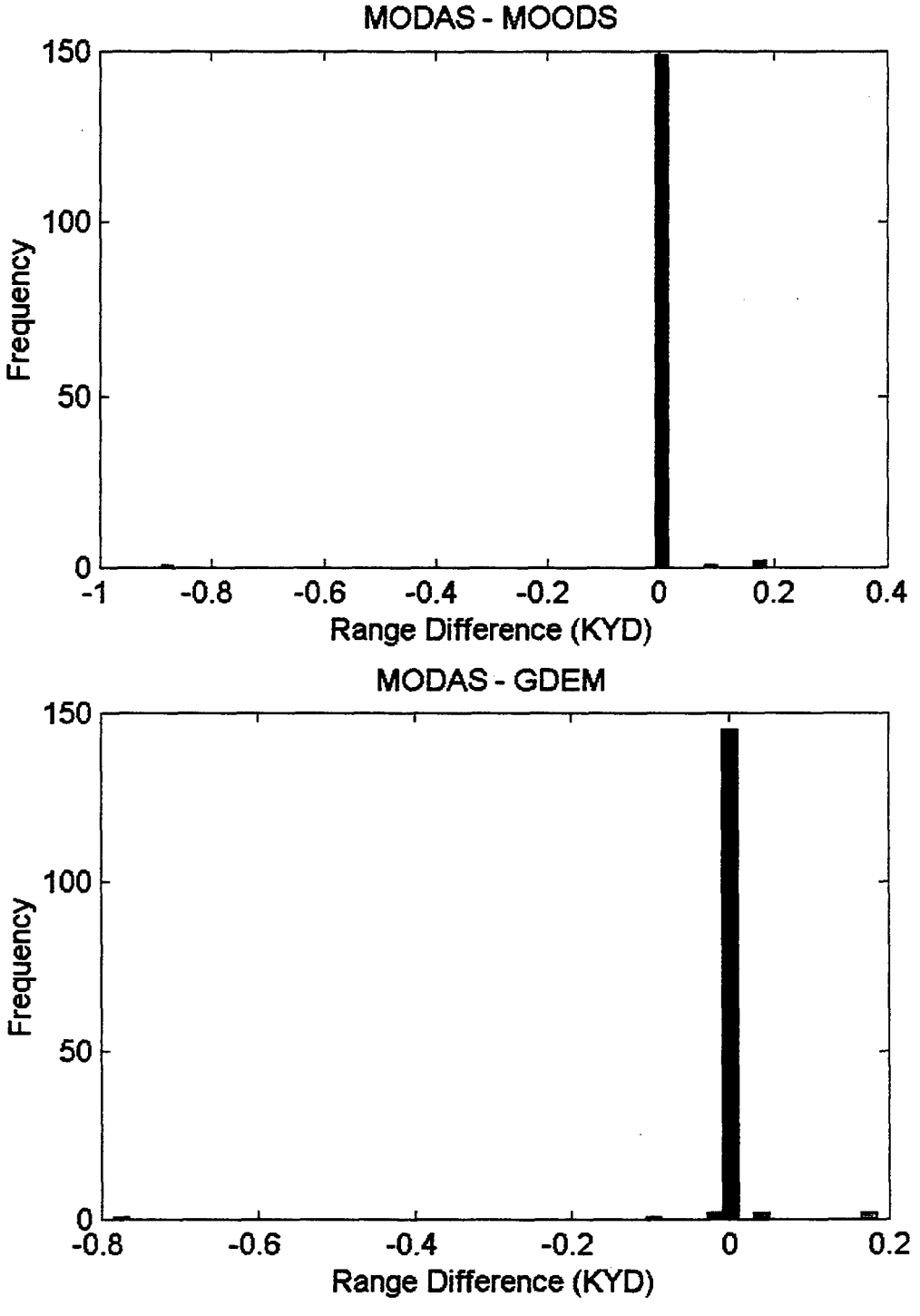

HISTOGRAMS FOR DIFFERENCES IN MAXIMUM DETECTION RANGES FOR ALL TARGET DEPTHS/ MAY 1999/ ROCK BOTTOM/ SOURCE DEPTH = 25 FT.

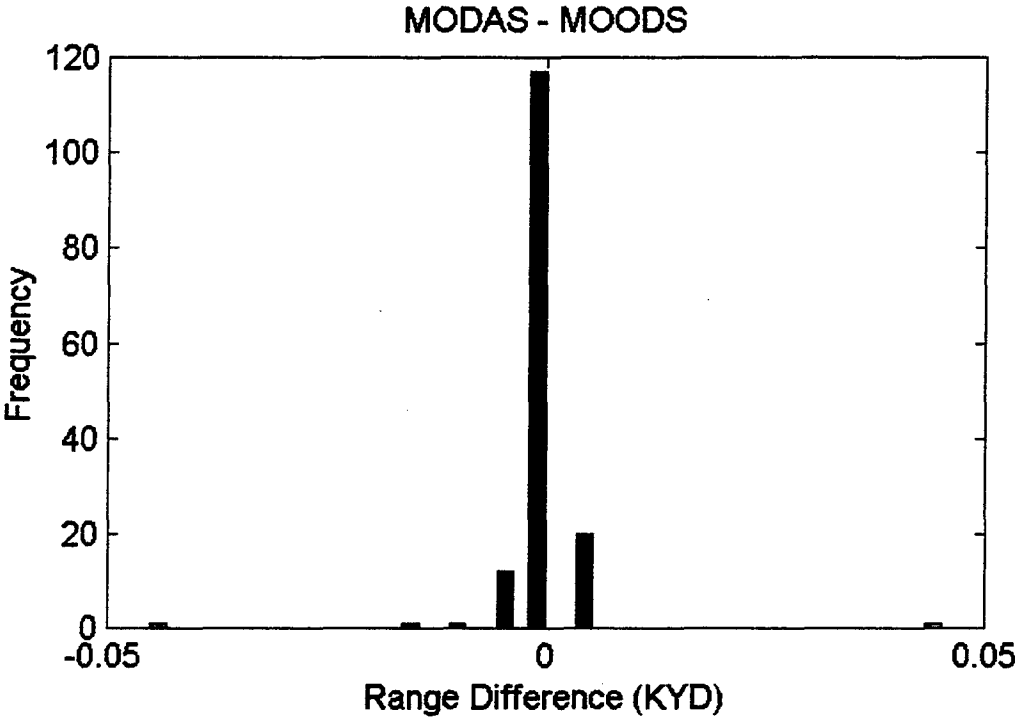

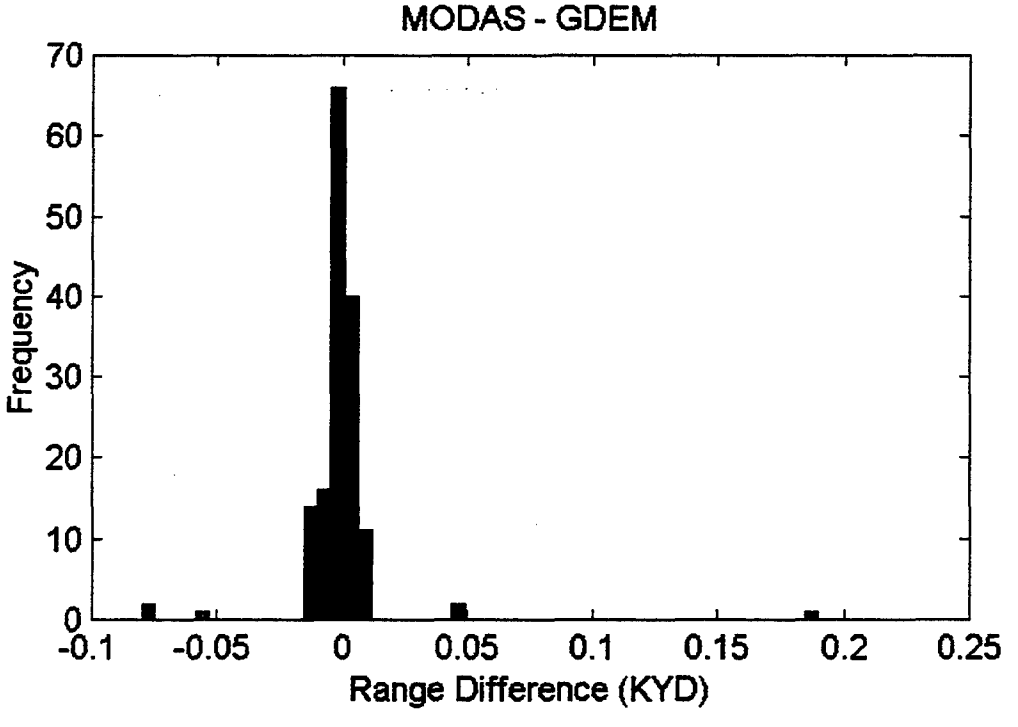

HISTOGRAMS FOR DIFFERENCES IN MAXIMUM DETECTION RANGES FOR ALL TARGET DEPTHS/ MAY 1999/ ROCK BOTTOM/ SOURCE DEPTH = 125 FT.

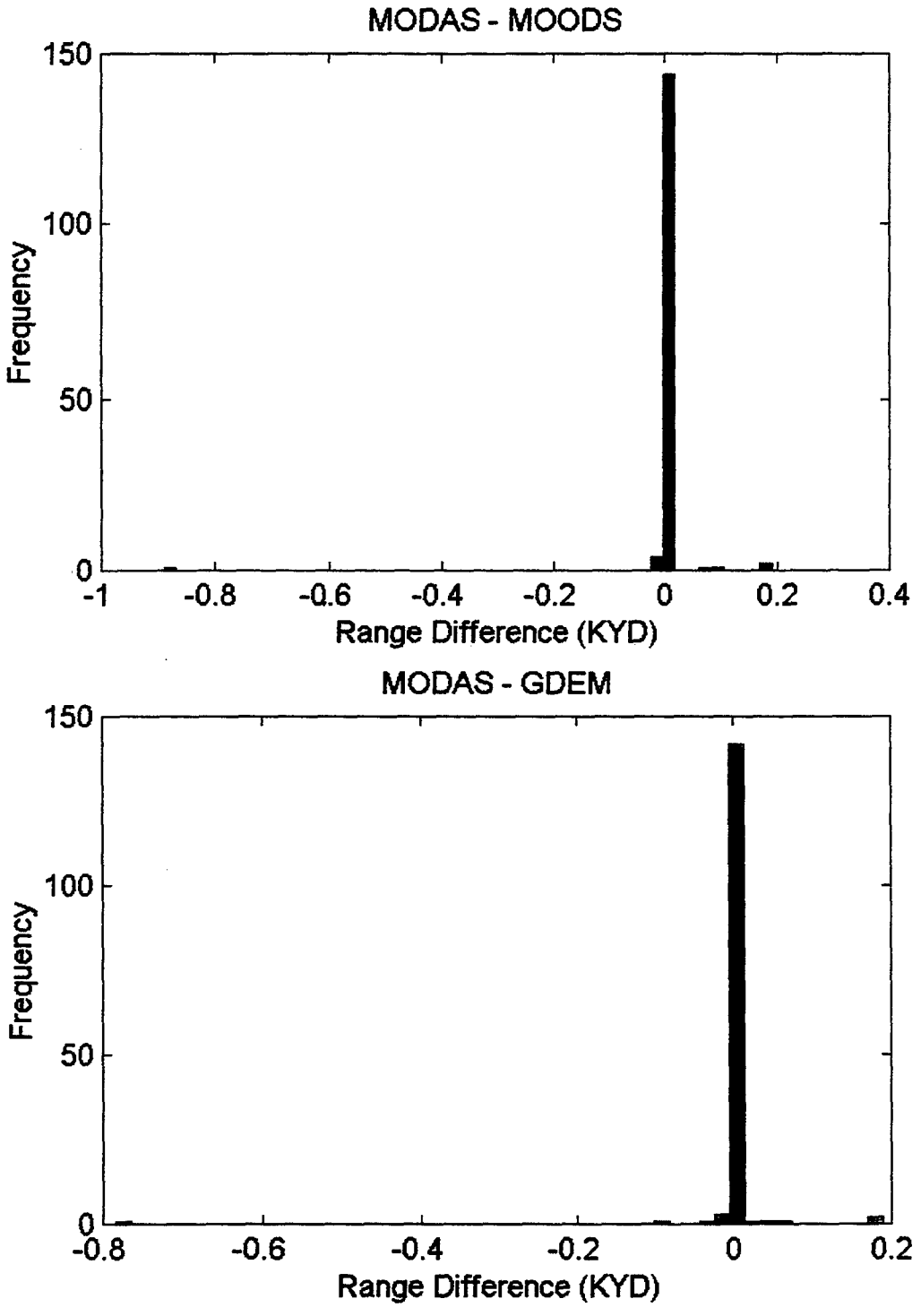

HISTOGRAMS FOR DIFFERENCES IN MAXIMUM DETECTION RANGES FOR ALL TARGET DEPTHS/ AUGUST 2000/ ROCK BOTTOM/ SOURCE DEPTH = 25 FT.

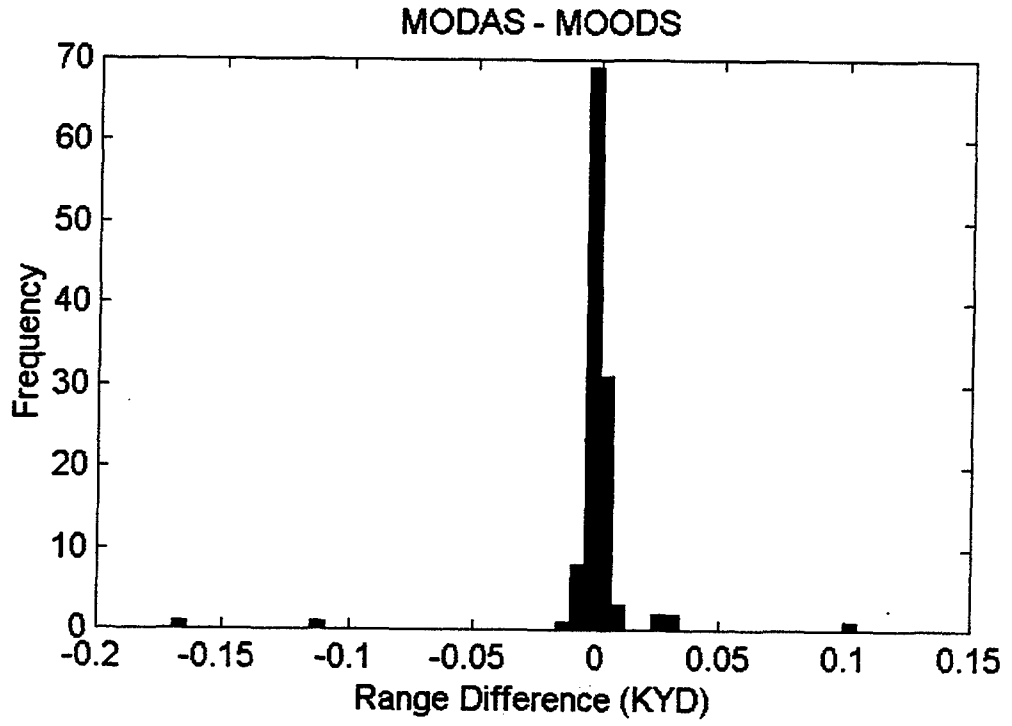

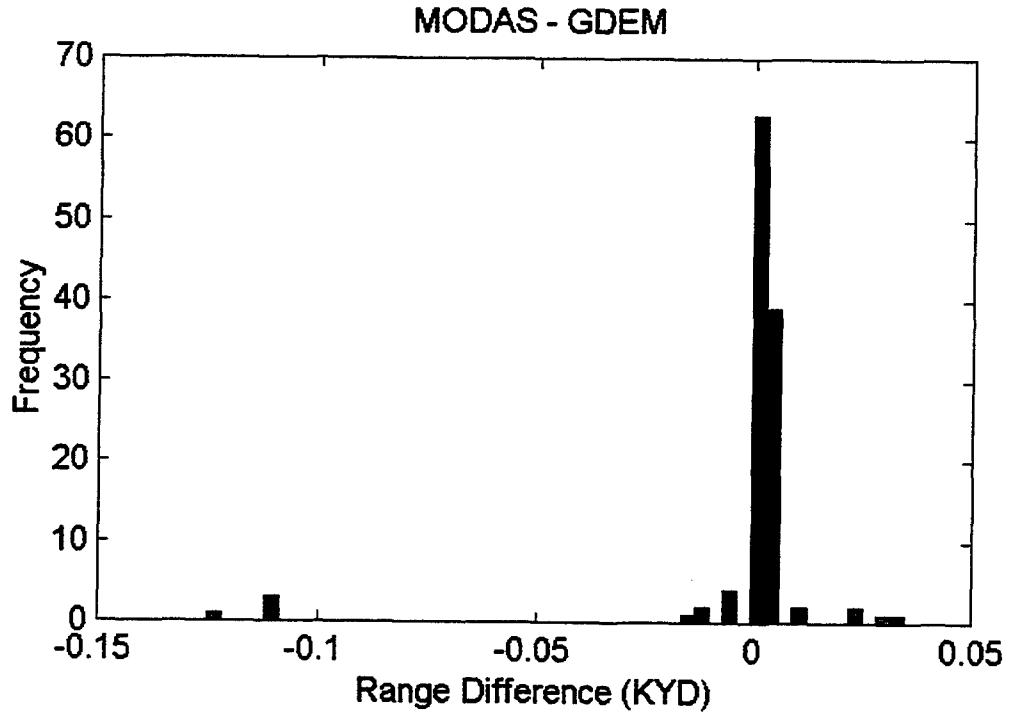

HISTOGRAMS FOR DIFFERENCES IN MAXIMUM DETECTION RANGES FOR ALL TARGET DEPTHS/ AUGUST 2000/ ROCK BOTTOM/ SOURCE DEPTH = 125 FT.

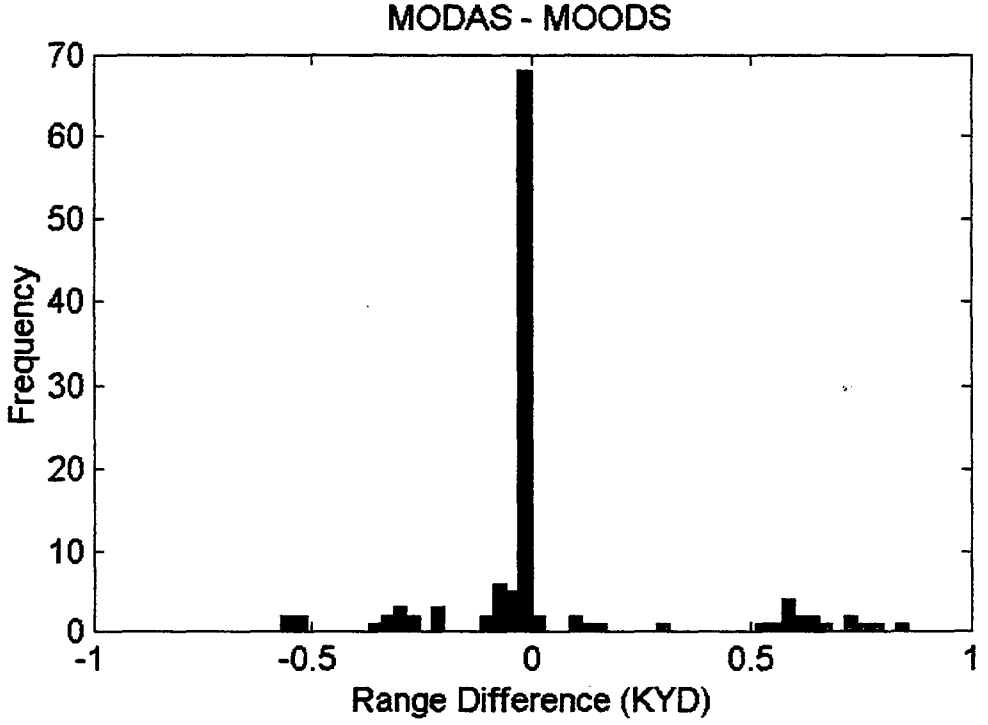

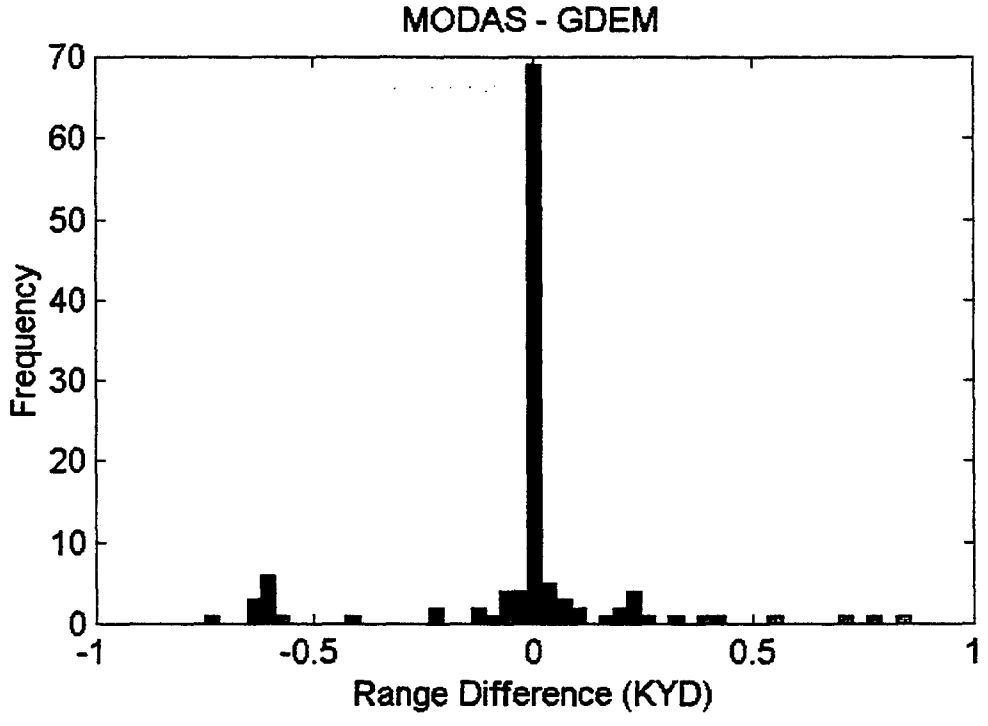

HISTOGRAMS FOR DIFFERENCES IN MAXIMUM DETECTION RANGES FOR ALL TARGET DEPTHS/ AUGUST 1999/ ROCK BOTTOM/ SOURCE DEPTH = 25 FT.

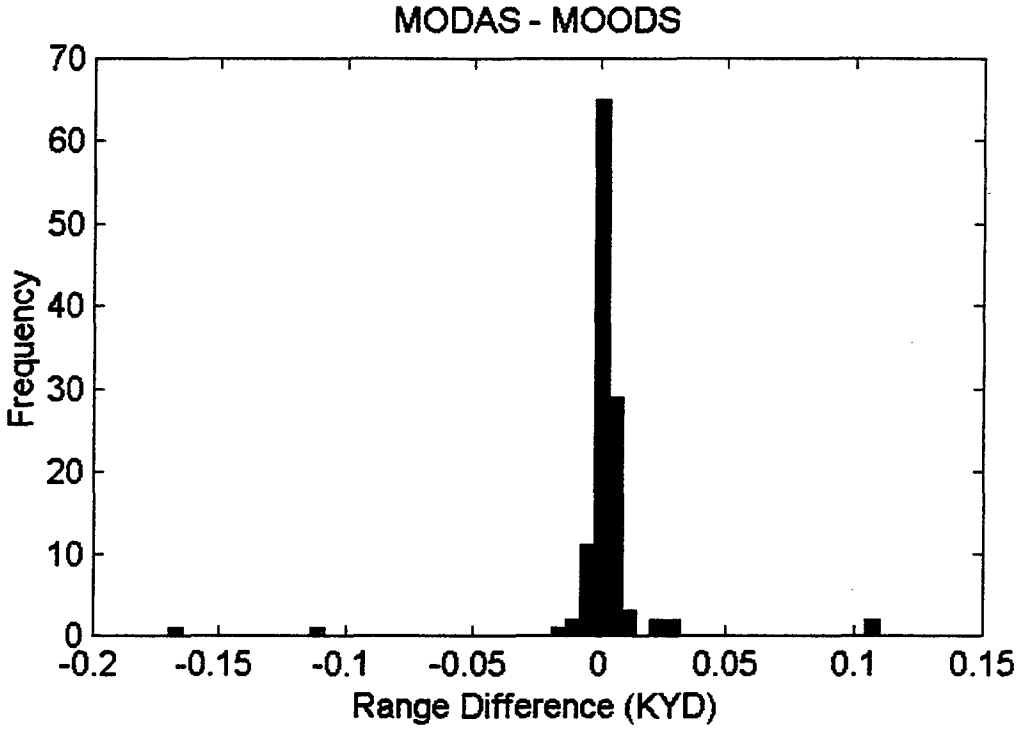

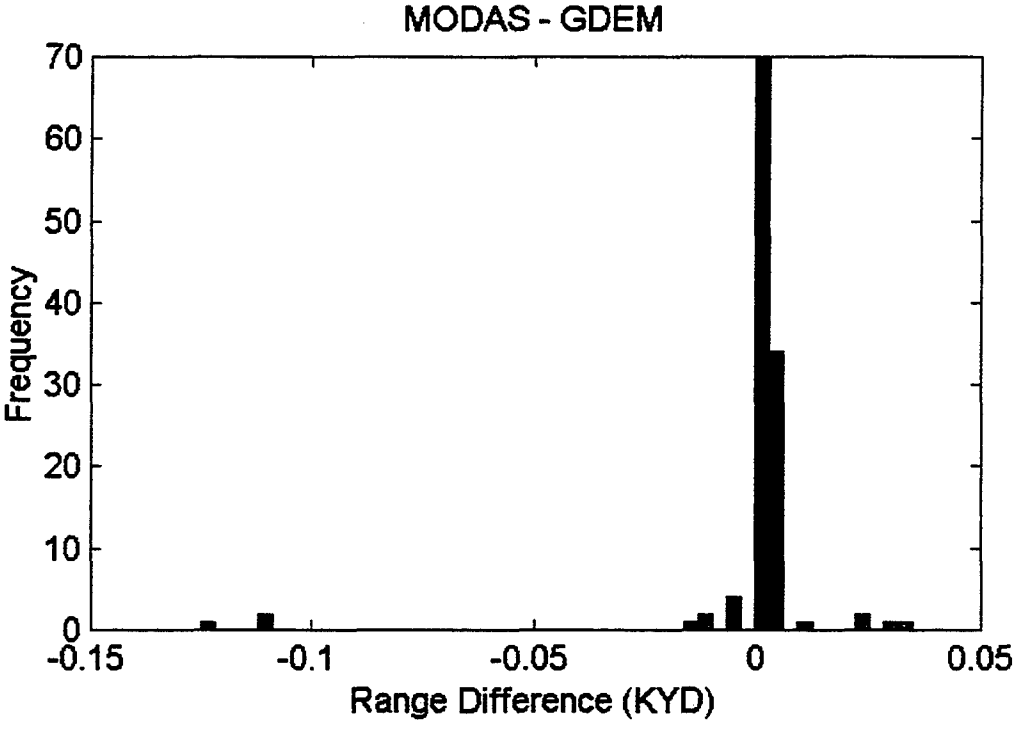

HISTOGRAMS FOR DIFFERENCES IN MAXIMUM DETECTION RANGES FOR ALL TARGET DEPTHS/ AUGUST 1999/ ROCK BOTTOM/ SOURCE DEPTH = 125 FT.

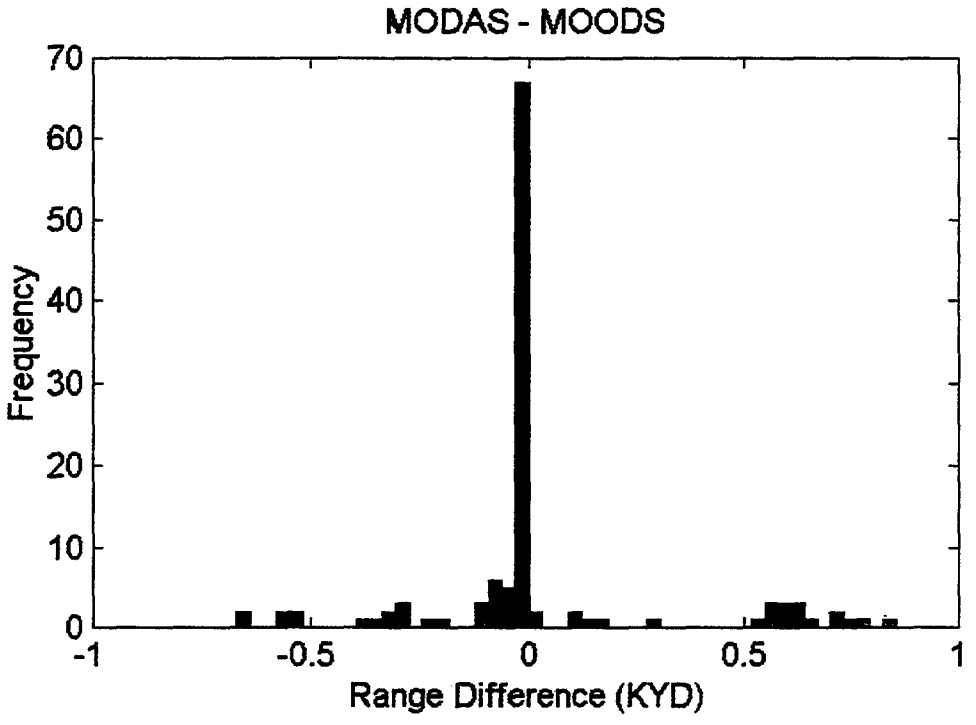

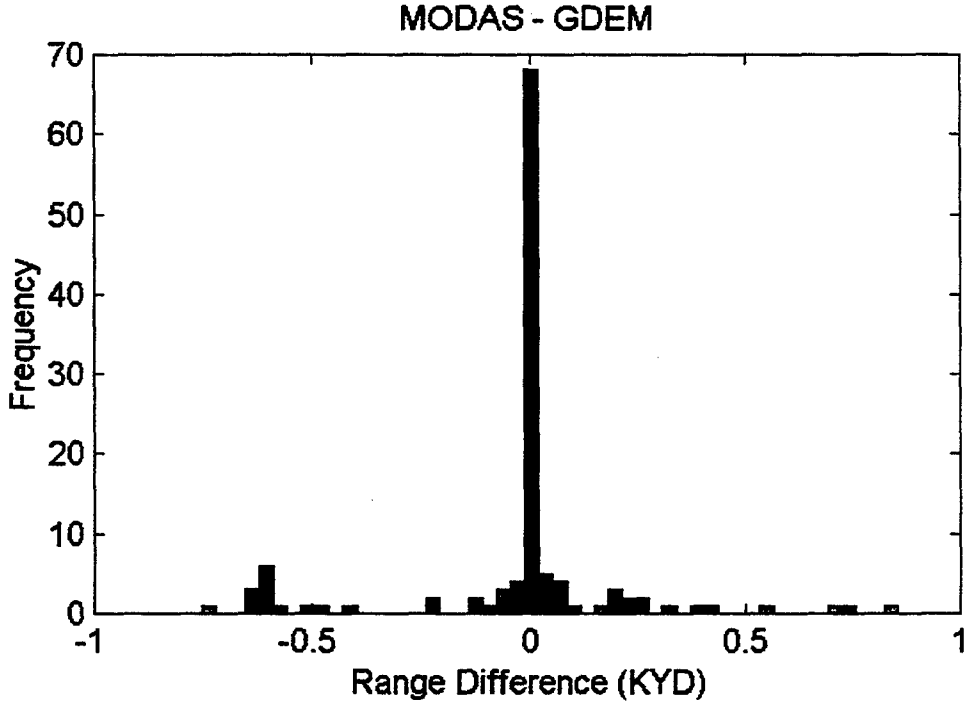

HISTOGRAMS FOR DIFFERENCES IN MAXIMUM DETECTION RANGES FOR ALL TARGET DEPTHS/ NOVEMBER 2000/ ROCK BOTTOM/ SOURCE DEPTH = 25 FT.

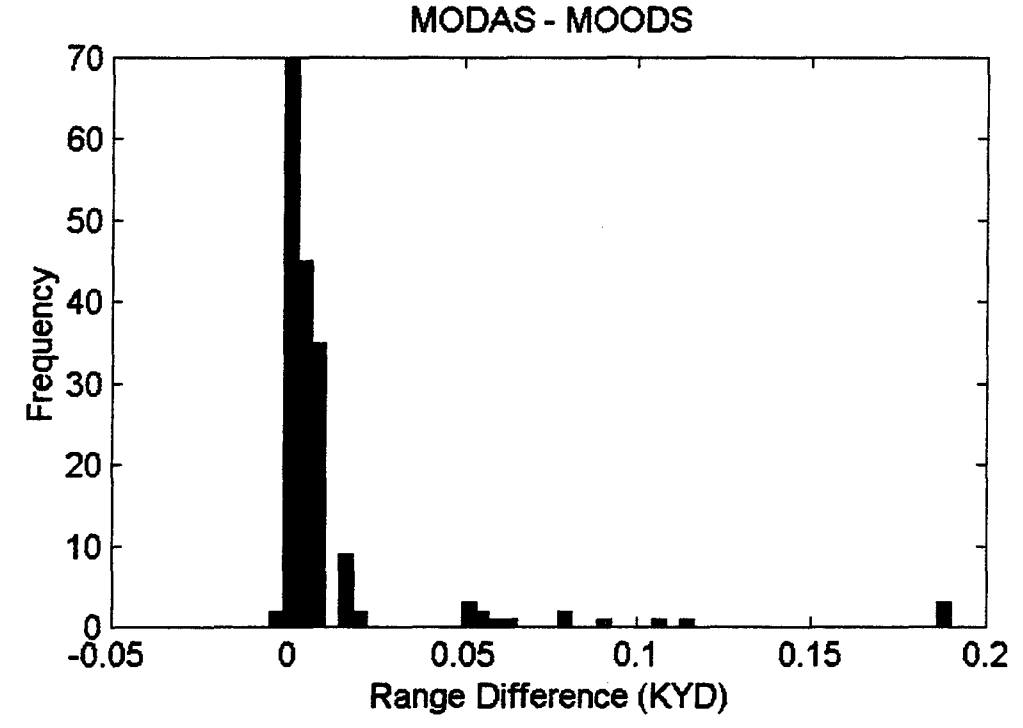

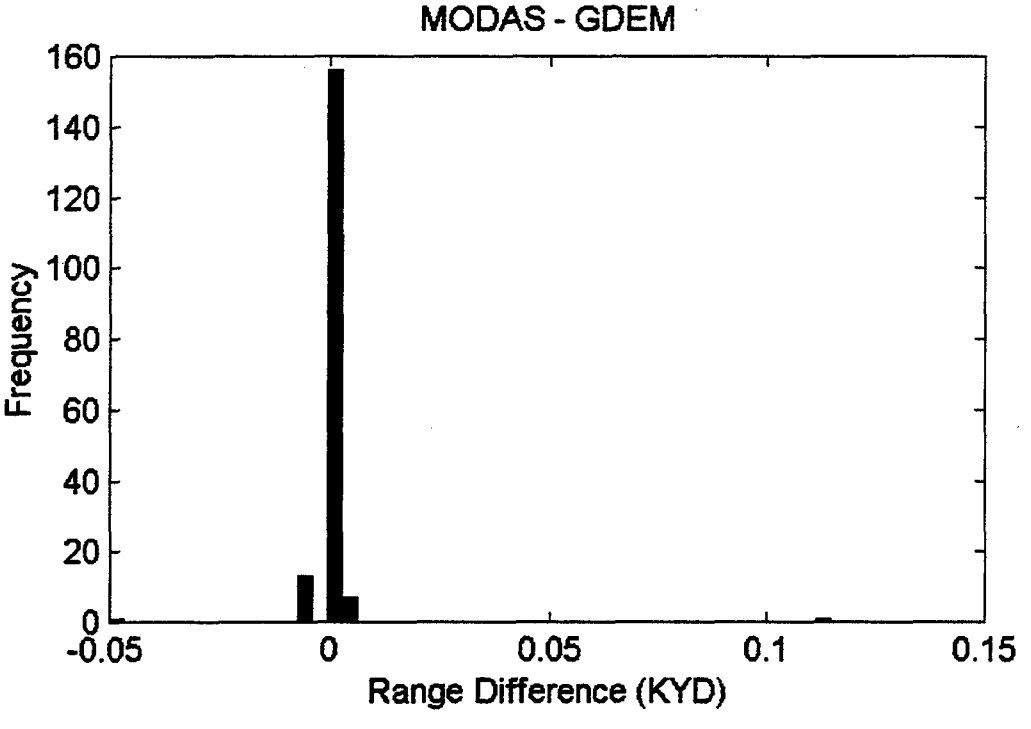

HISTOGRAMS FOR DIFFERENCES IN MAXIMUM DETECTION RANGES FOR ALL TARGET DEPTHS/ NOVEMBER 2000/ ROCK BOTTOM/ SOURCE DEPTH = 125 FT.

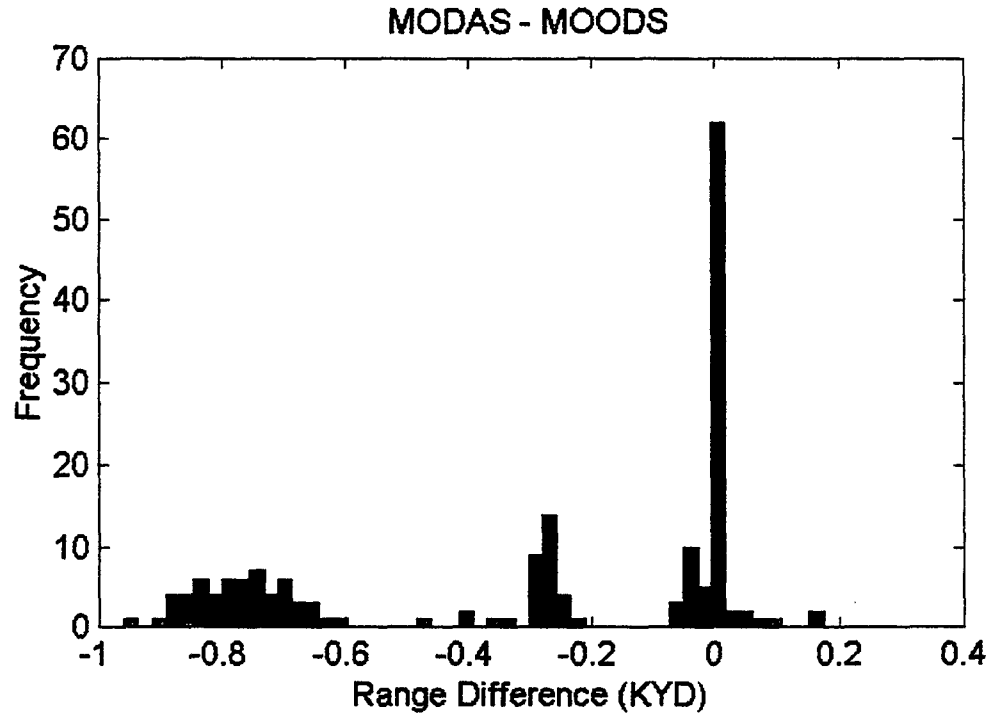

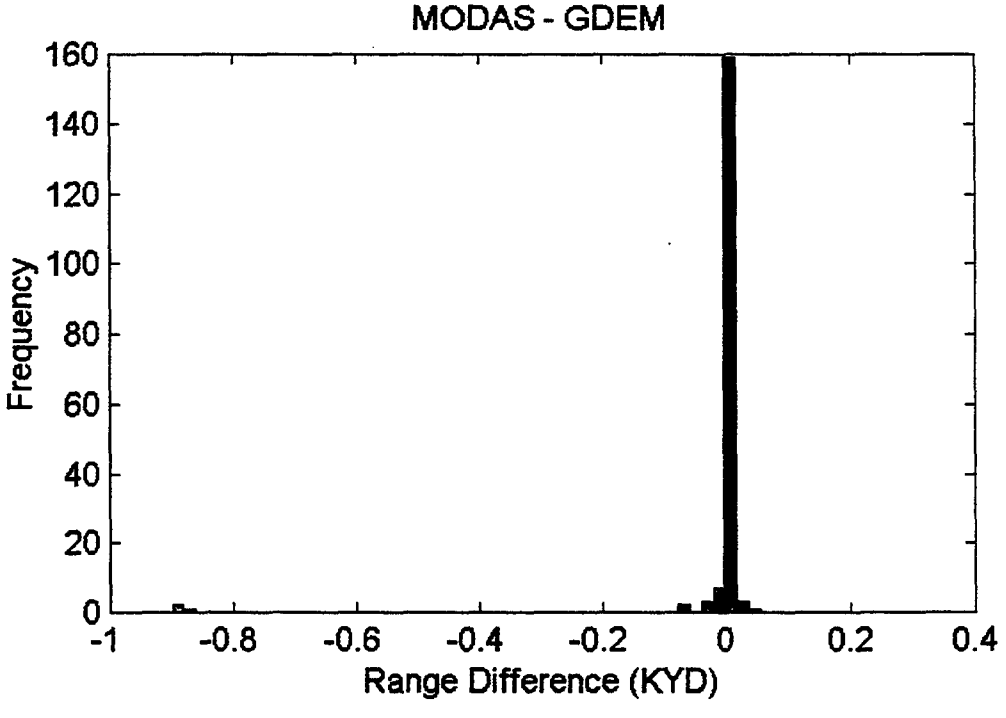

HISTOGRAMS FOR DIFFERENCES IN MAXIMUM DETECTION RANGES FOR ALL TARGET DEPTHS/ NOVEMBER 1999/ ROCK BOTTOM/ SOURCE DEPTH = 25 FT.

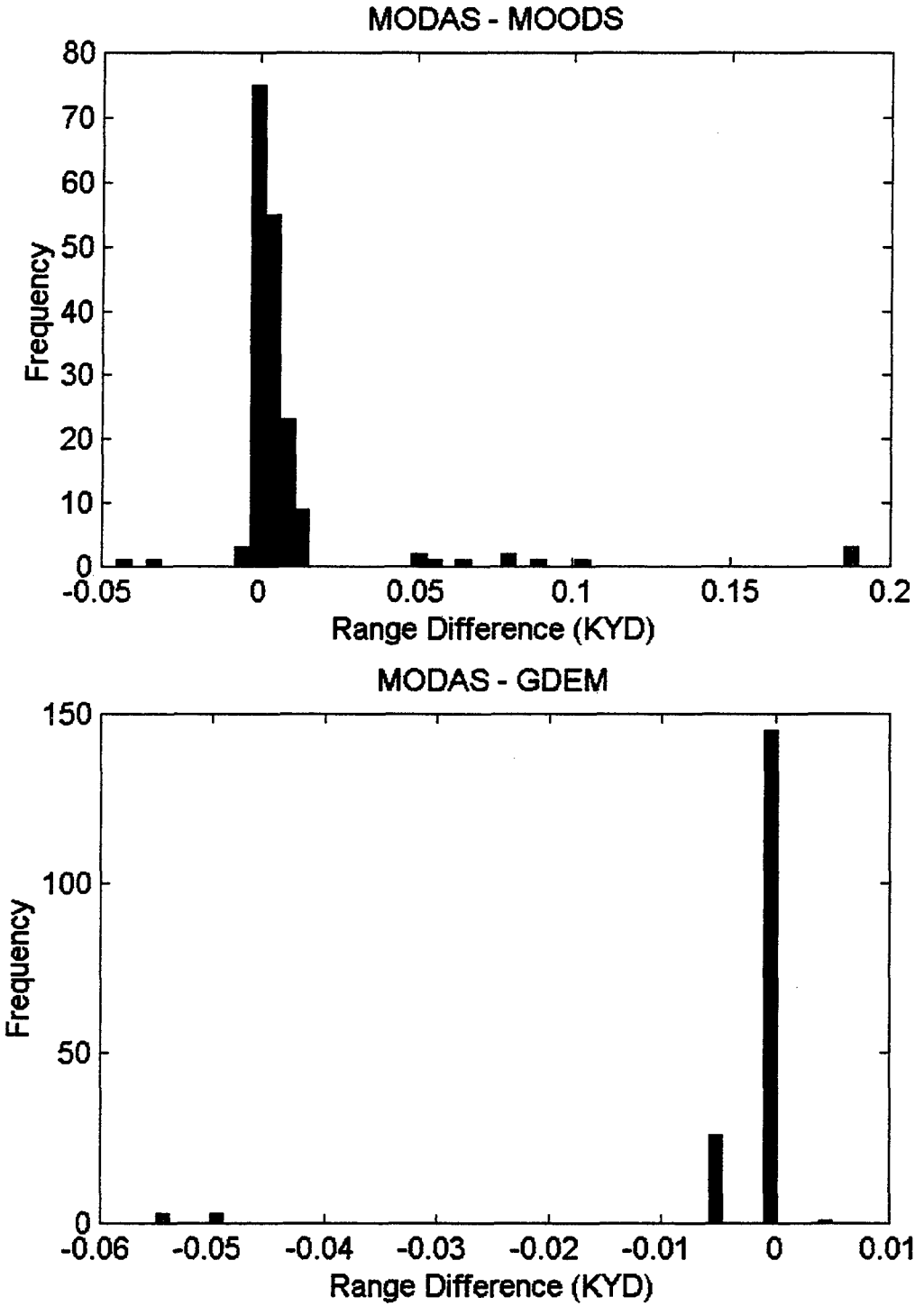

HISTOGRAMS FOR DIFFERENCES IN MAXIMUM DETECTION RANGES FOR ALL TARGET DEPTHS/ NOVEMBER 1999/ ROCK BOTTOM/ SOURCE DEPTH = 125 FT.

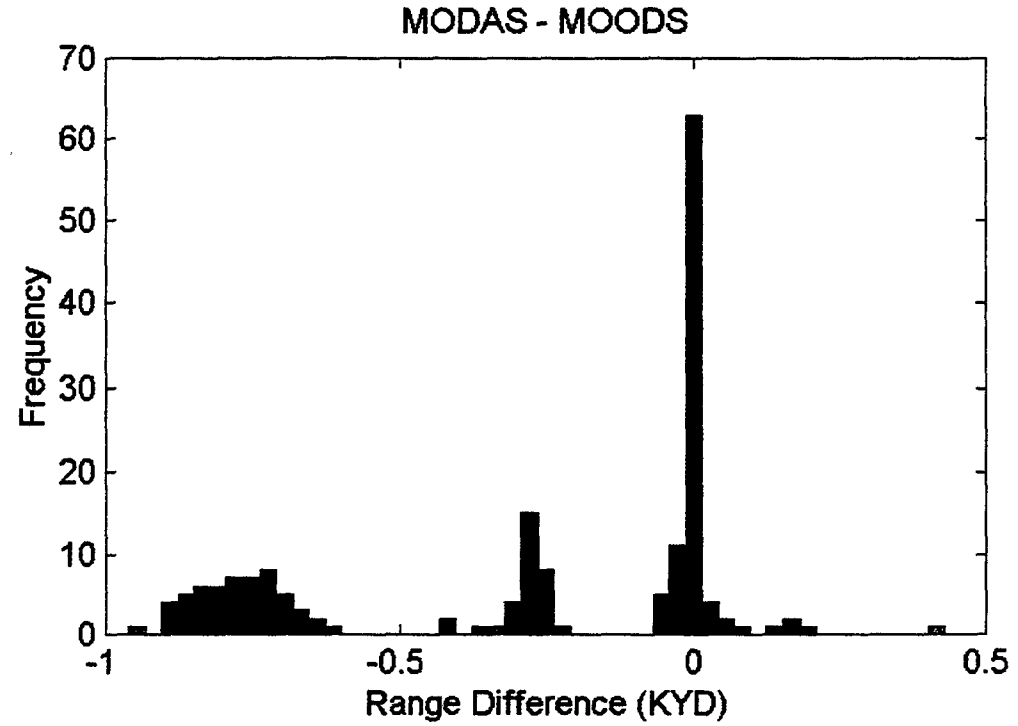

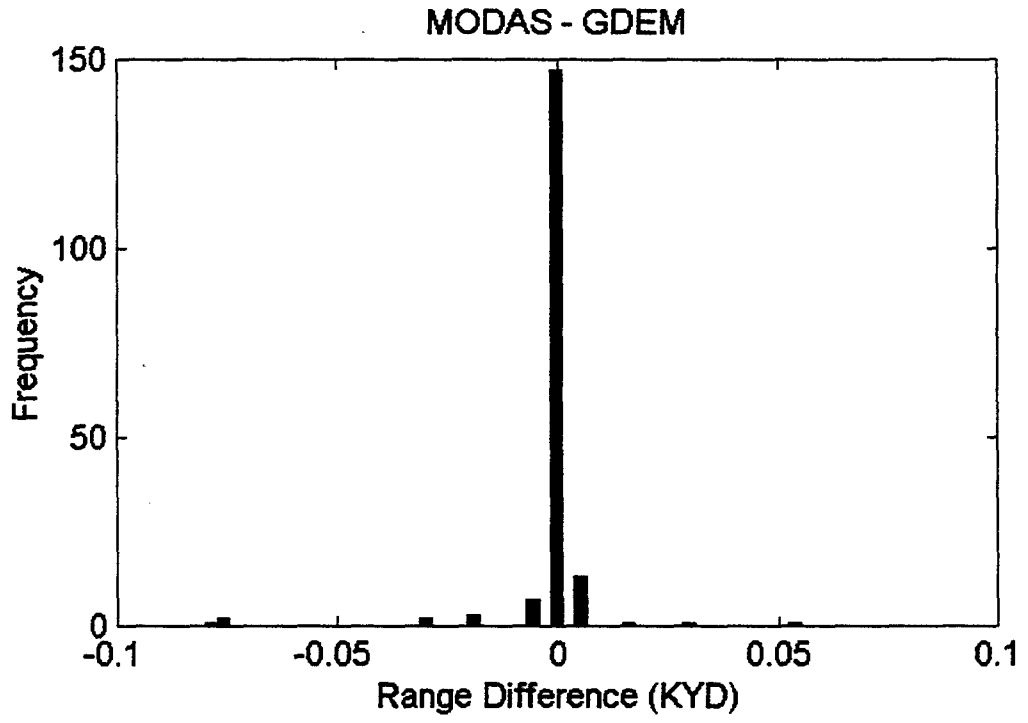

APPENDIX D. HISTOGRAMS FOR ACOUSTIC UNCERTAINTY

HISTOGRAMS FOR DIFFERENCES IN MAXIMUM DETECTION RANGES FOR ALL TARGET DEPTHS/ FEBRUARY 2000/ MUD BOTTOM/ SOURCE DEPTH = 25 FT.

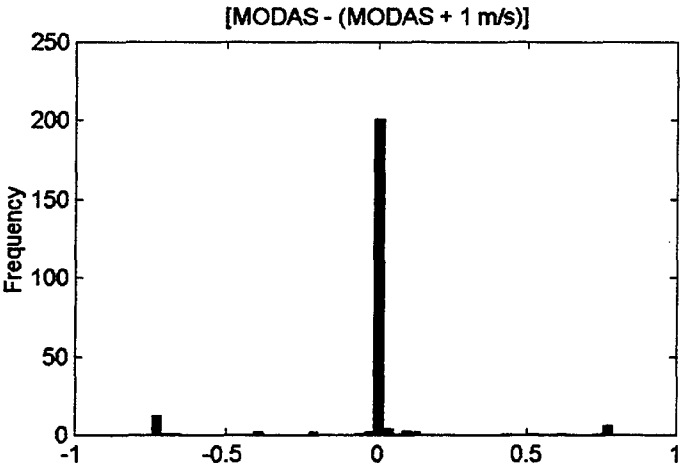

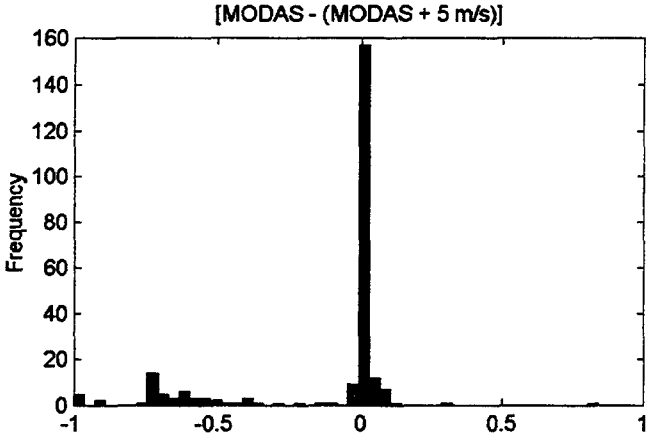

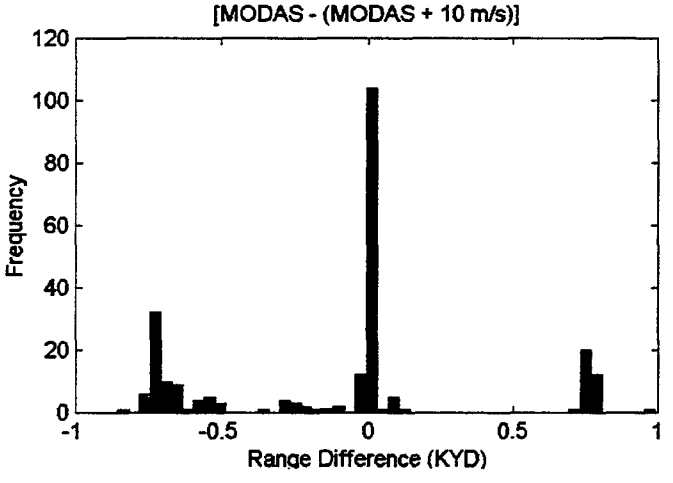

HISTOGRAMS FOR DIFFERENCES IN MAXIMUM DETECTION RANGES FOR ALL TARGET DEPTHS/ FEBRUARY 2000/ MUD BOTTOM/ SOURCE DEPTH = 125 FT.

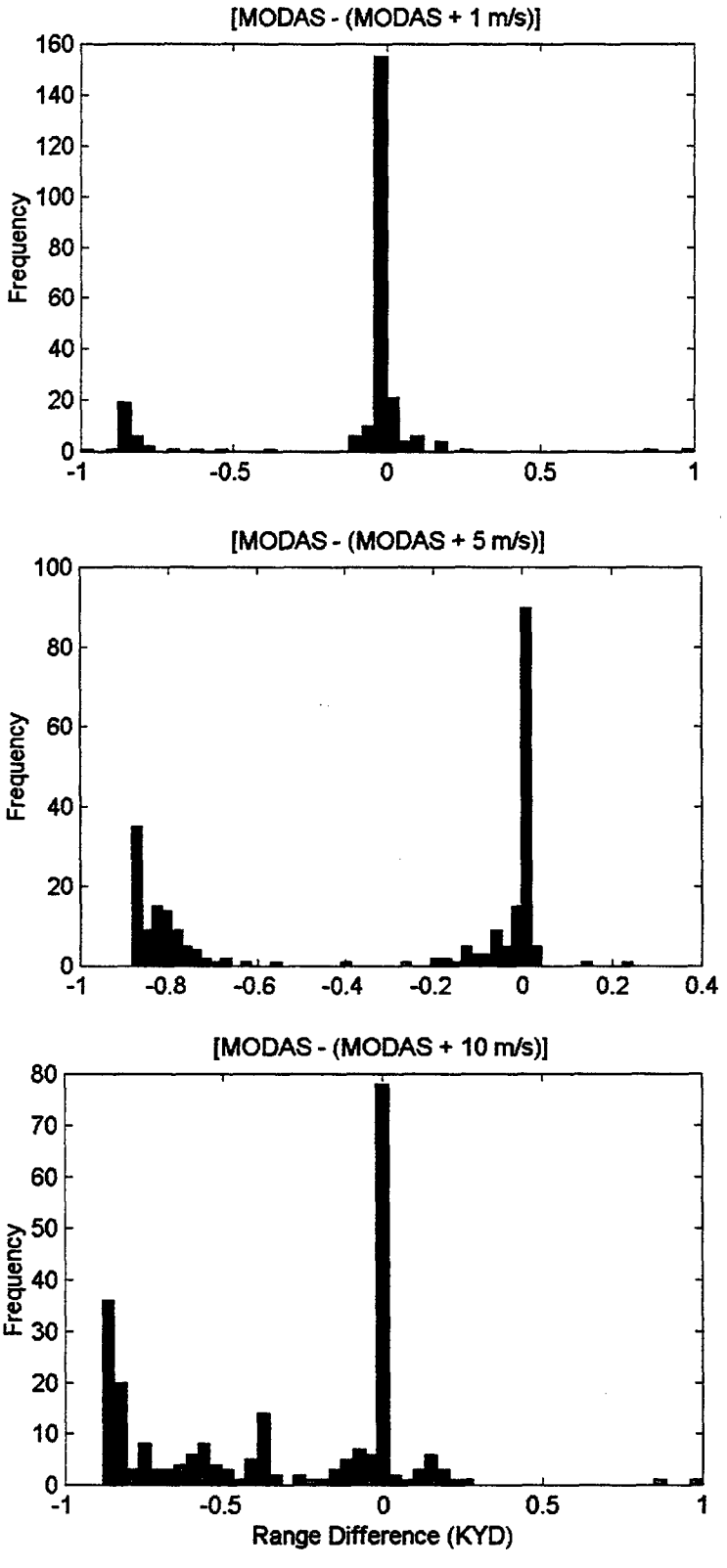

HISTOGRAMS FOR DIFFERENCES IN MAXIMUM DETECTION RANGES FOR ALL TARGET DEPTHS/ AUGUST 2000/ MUD BOTTOM/ SOURCE DEPTH = 25 FT.

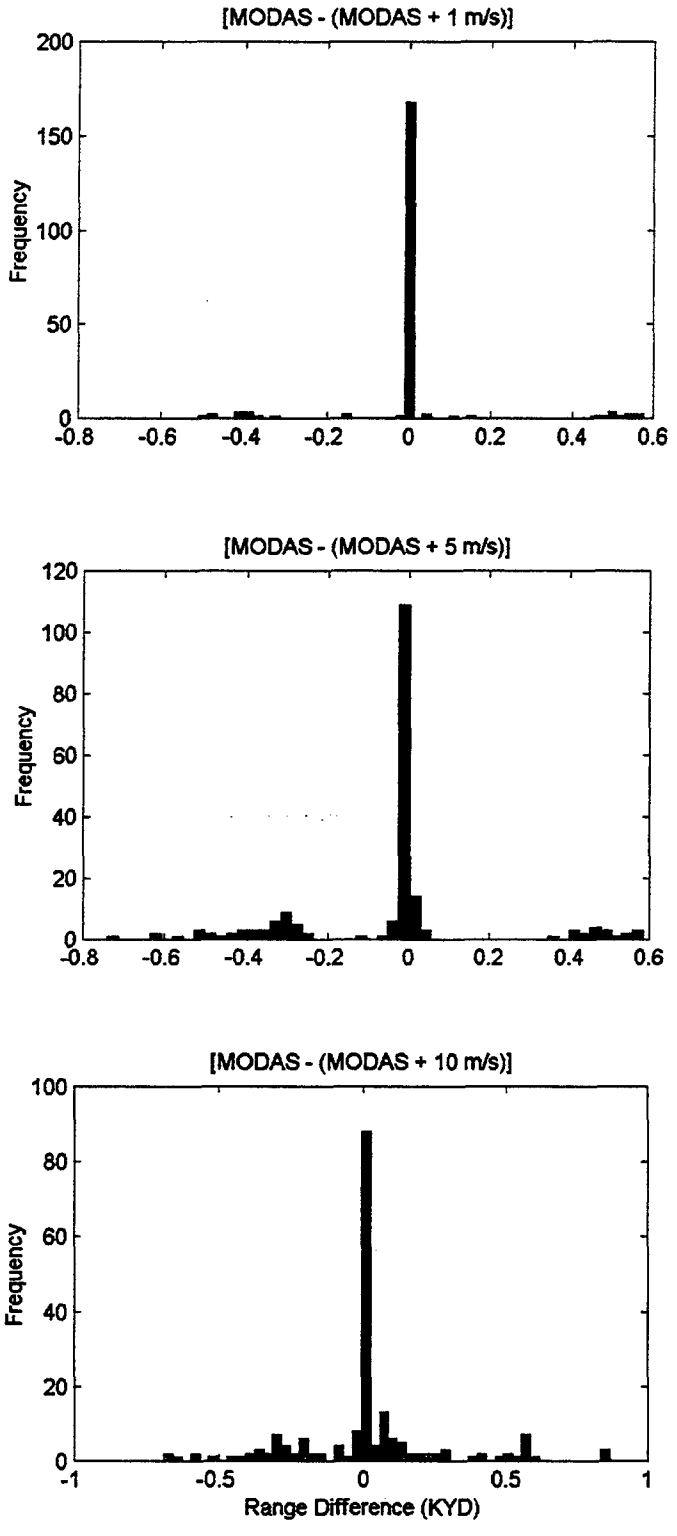

HISTOGRAMS FOR DIFFERENCES IN MAXIMUM DETECTION RANGES FOR ALL TARGET DEPTHS/ AUGUST 2000/ MUD BOTTOM/ SOURCE DEPTH = 125 FT.

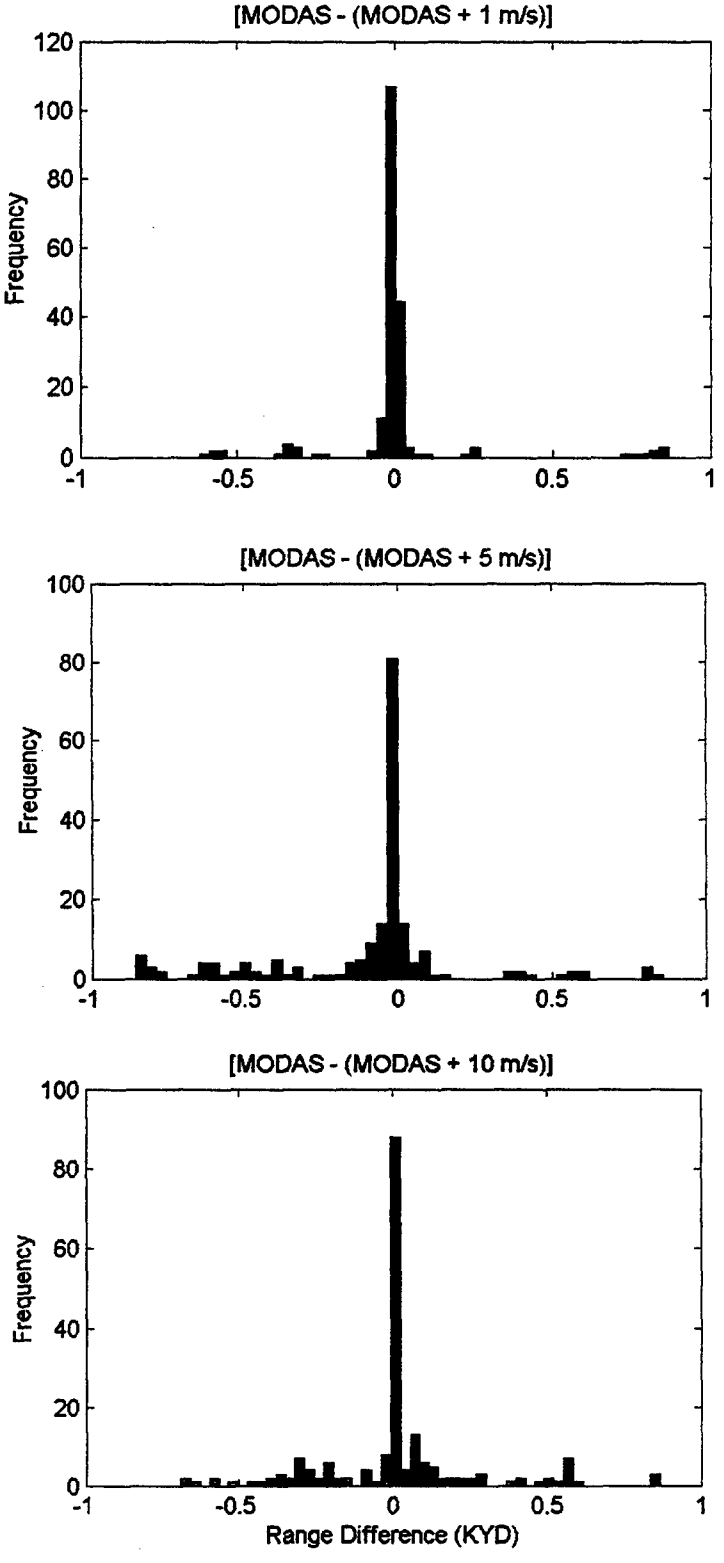

HISTOGRAMS FOR DIFFERENCES IN MAXIMUM DETECTION RANGES FOR ALL TARGET DEPTHS/ FEBRUARY 2000/ SAND BOTTOM/ SOURCE DEPTH = 25 FT.

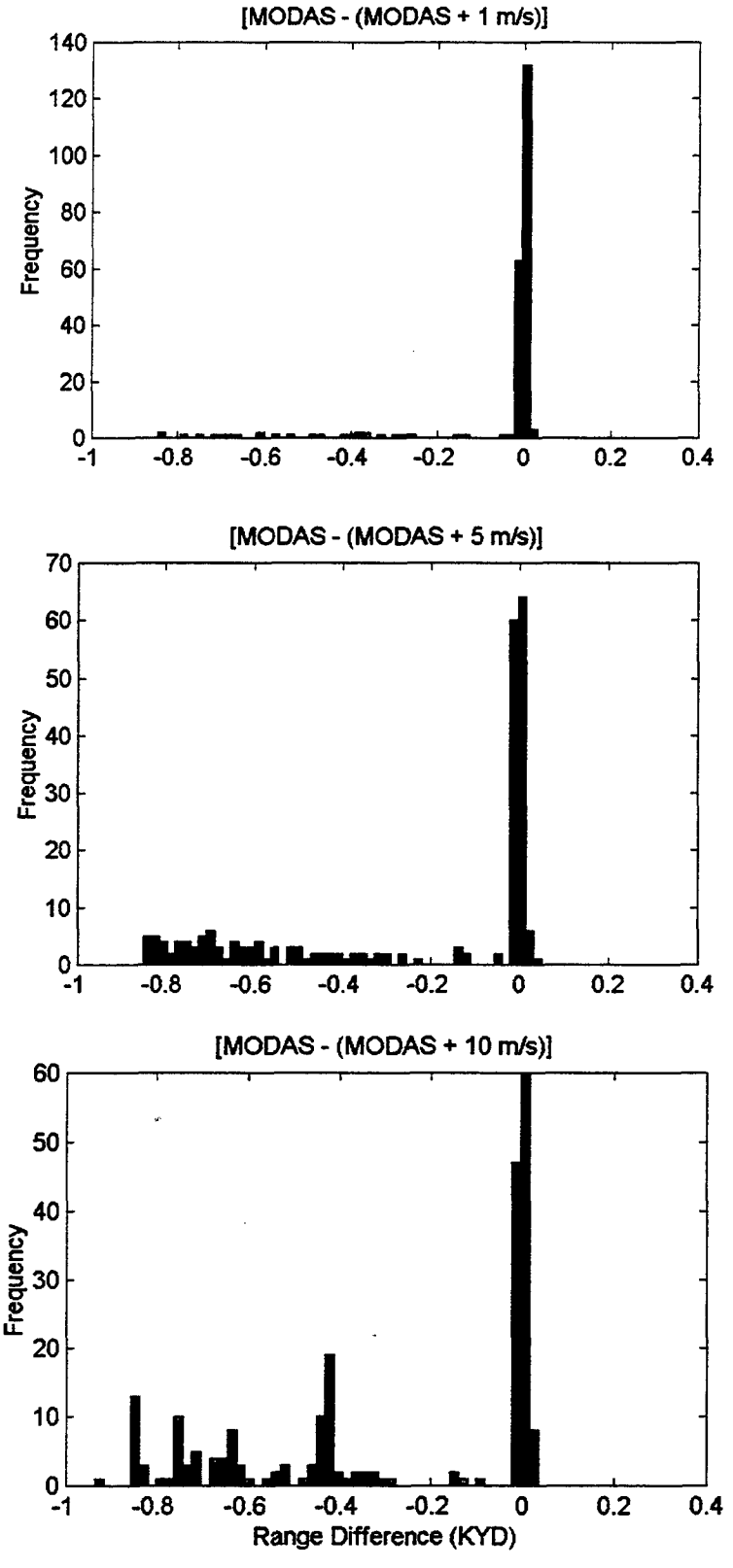

HISTOGRAMS FOR DIFFERENCES IN MAXIMUM DETECTION RANGES FOR ALL TARGET DEPTHS/ FEBRUARY 2000/ SAND BOTTOM/ SOURCE DEPTH = 125 FT.

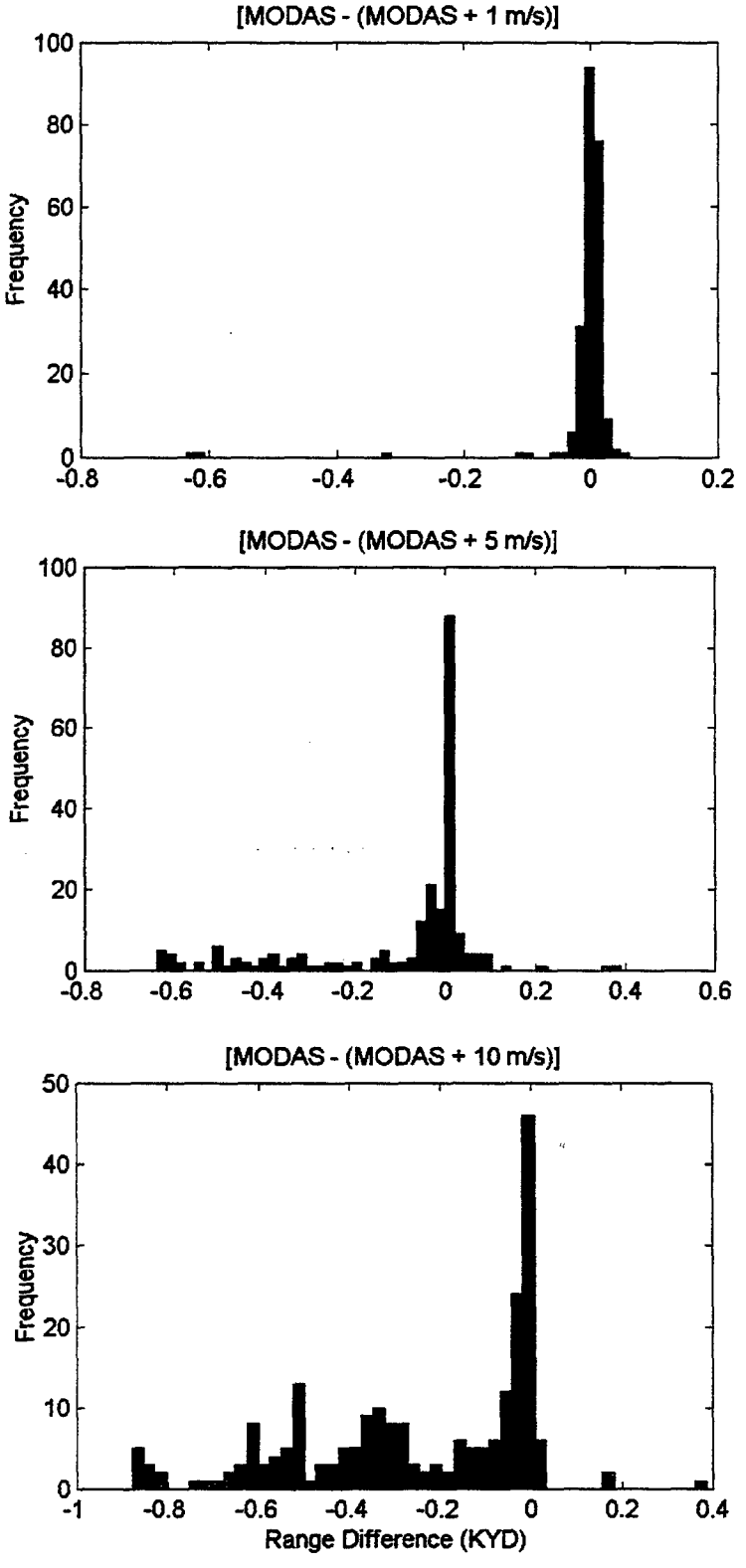

HISTOGRAMS FOR DIFFERENCES IN MAXIMUM DETECTION RANGES FOR ALL TARGET DEPTHS/ AUGUST 2000/ SAND BOTTOM/ SOURCE DEPTH = 25 FT.

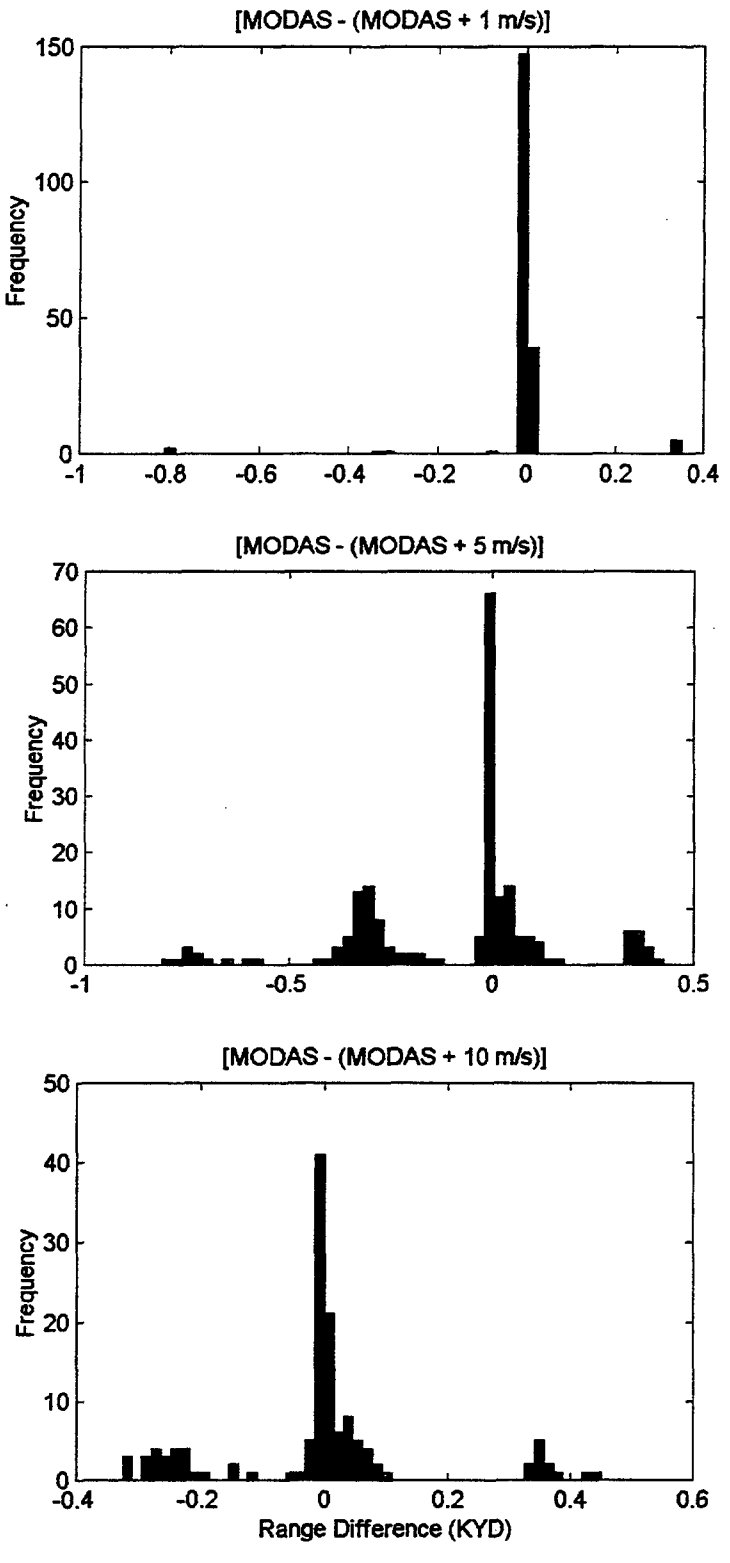

HISTOGRAMS FOR DIFFERENCES IN MAXIMUM DETECTION RANGES FOR ALL TARGET DEPTHS/ AUGUST 2000/ SAND BOTTOM/ SOURCE DEPTH = 125 FT.

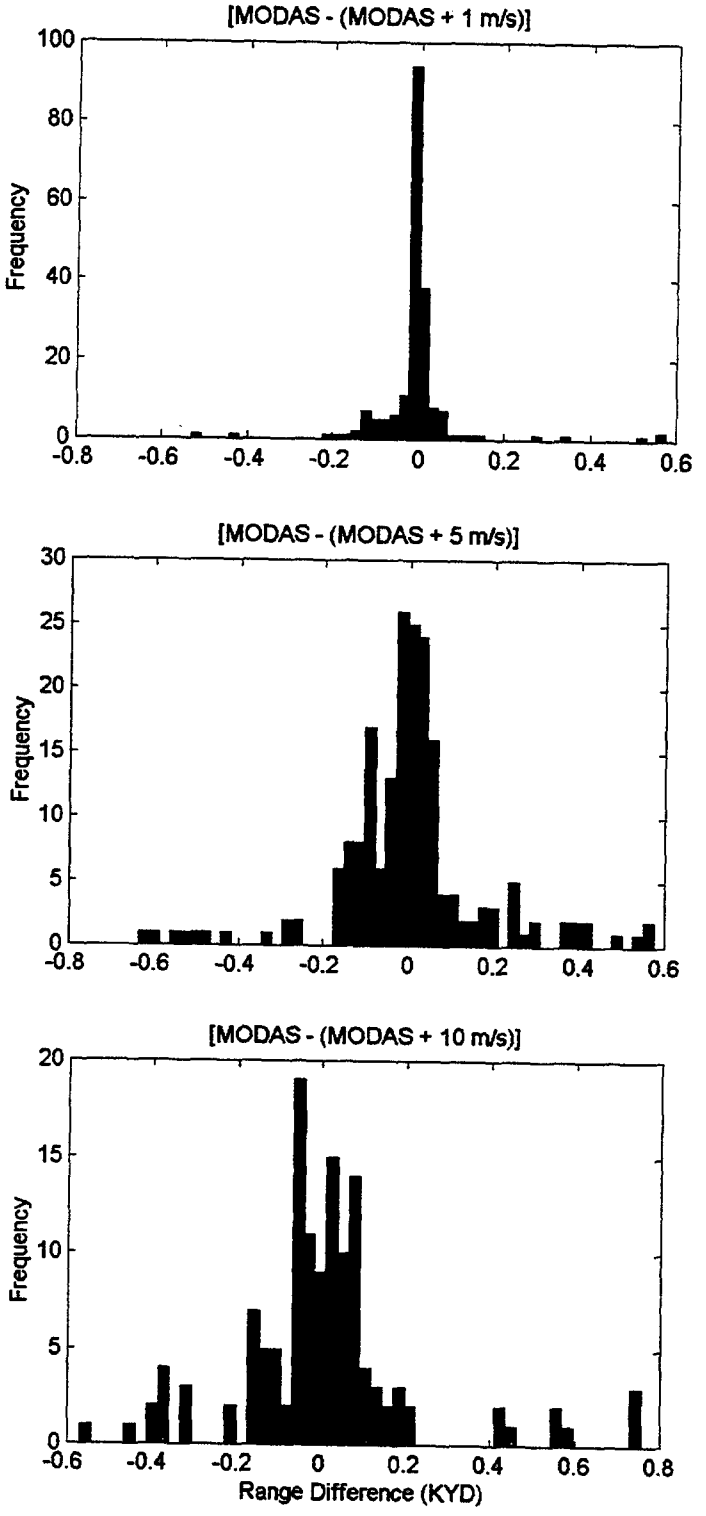

APPENDIX E. CASS/GRAB MODEL INPUT CARD

```
X OFFSET          = 0.05 IN
BACKGROUND COLOR = WHITE
FOREGROUND COLOR = BLUE
PLOT DEVICE       = VISUAL
PLOT LIBRARY      = CASS
ERROR STATUS      = CONTINUE
FOREGROUND COLOR = BLUE
BACKGROUND COLOR = WHITE
EIGENRAY MODEL    = GRAB
OUTPUT FILE       = SAV
RESET OUTPUT DEVICE
RESET PLOT DEVICE
EIGENRAY MODEL       = GRAB
FREQUENCY MINIMUM    = XXXXX  HZ
FREQUENCY MAXIMUM    = XXXXX  HZ
FREQUENCY INCREMENT =     1  HZ
VERTICAL ANGLE UNIT             =    DEG
VERTICAL ANGLE MINIMUM          =  0 DEG
VERTICAL ANGLE MAXIMUM          = 90 DEG
VERTICAL ANGLE INCREMENT        =  1 DEG
VERTICAL ANGLE AXIS LENGTH      =  7 IN
VERTICAL ANGLE AXIS MINIMUM     =  0 DEG
VERTICAL ANGLE AXIS MAXIMUM     = 90 DEG
VERTICAL ANGLE AXIS INCREMENT = 10 DEG
FUNCTION UNIT                   =    DB
FUNCTION AXIS LENGTH            =  5 IN
FUNCTION AXIS MINIMUM           =-20 DB
FUNCTION AXIS MAXIMUM           =  0 DB
FUNCTION AXIS INCREMENT         =  5 DB
DEPTH UNIT                      =  FT
DEPTH AXIS MINIMUM              =  0 FT
DEPTH AXIS MAXIMUM              = 410 FT
DEPTH AXIS INCREMENT            =  25 FT
DEPTH AXIS LENGTH               =   5 IN
LEVEL AXIS MINIMUM              = -50 DB
LEVEL AXIS MAXIMUM              = -20 DB
LEVEL AXIS INCREMENT            =  10 DB
LEVEL AXIS LENGTH               =   5 IN
RANGE UNIT                      =   KYD
RANGE AXIS LENGTH               =   7 IN
RANGE AXIS MINIMUM              =   0 KYD
RANGE AXIS MAXIMUM              =  1.0 KYD
RANGE AXIS INCREMENT            = 0.25 KYD
TIME AXIS LENGTH                =  7 IN
TIME AXIS MINIMUM               =  0 S
TIME AXIS MAXIMUM               =  1.50 S
TIME AXIS INCREMENT             =  0.1 S
SPEED AXIS LENGTH               =  1.75 IN
SPEED AXIS MINIMUM              = 1440.0 M/S
SPEED AXIS MAXIMUM              = 1550.0 M/S
SPEED AXIS INCREMENT            =   25   M/S
BOTTOM REFLECTION COEFFICIENT MODEL   =  RAYLEIGH
```

```
SURFACE REFLECTION COEFFICIENT MODEL  =  APL/UW
BOTTOM SCATTERING STRENGTH MODEL      =  APL/UW
SURFACE SCATTERING STRENGTH MODEL     =  APL/UW
VOLUME SCATTERING STRENGTH MODEL      =  DEPTH TABLE
VOLUME SCATTERING STRENGTH TABLE      =  -80  DB
INPUT FILE                            =  WINSPD
ADD INPUT FILE
INPUT FILE                            =  BTMTYP
ADD INPUT FILE
FUNCTION SYMBOL                 =  BTM_RFL
FUNCTION SYMBOL                 =  BTM_STR
FUNCTION AXIS MINIMUM           =  - 80 DB
FUNCTION SYMBOL                 =  SRF_RFL
FUNCTION AXIS MINIMUM           =  - 10 DB
FUNCTION SYMBOL                 =  SRF_STR
FUNCTION AXIS MINIMUM           =  - 80 DB
INPUT FILE                            =  BTMDP
ADD INPUT FILE
INPUT FILE                            =  svp
ADD INPUT FILE
DEPTH MINIMUM    =  0 M
INPUT FILE                            =  DEPMAX
ADD INPUT FILE
RANGE MINIMUM            =     0  KYD
RANGE MAXIMUM            =  1.00 KYD
RANGE INCREMENT          =     5   YD
INPUT FILE                            =  SUCDP
ADD INPUT FILE
INPUT FILE                            =  TRNSDP
ADD INPUT FILE
VERTICAL ANGLE MINIMUM   = -5 DEG
VERTICAL ANGLE MAXIMUM   =  5 DEG
VERTICAL ANGLE INCREMENT =  1 DEG
PLOT OPTION              = CONTINUE
TITLE TABLE
EOT
PLOT SOUND SPEED
X OFFSET                 = 2.0  IN
RANGE AXIS LENGTH        =   5  IN
PLOT OPTION              =
RAY MODEL                = TWO-DIMENSION
TITLE TABLE
Ray Trace +/-5 degrees by 1 degree
EOT
PLOT OPTION              =
FOREGROUND COLOR         = BLUE
PLOT RAYS
FUNCTION SYMBOL    =  VLM_ATN
FUNCTION UNITS     =      DB/KM
DEPTH MINIMUM      =     0 FT
INPUT FILE                            =  DEPMAX
ADD INPUT FILE
DEPTH INCREMENT    =    25 FT
PRINT FUNCTION VS DEPTH
COMMENT TABLE
the bandwidth only affects the noise level
more bandwidth more noise  =10log(bandwidth)
```

```
EOT
BANDWIDTH TABLE     =    XXXX  HZ
SOURCE LEVEL MODEL =    TABLE
SOURCE LEVEL TABLE =    XXX DB
PULSE LENGTH        =    XXX MS
COMMENT TABLE
the time increment must be < 1/2 pulse length
EOT
TIME MINIMUM              =       0  S
TIME MAXIMUM              =    1.50  S
TIME INCREMENT            =    0.16  MS
RECEIVER HORIZONTAL BEAMWIDTH TABLE  =  XXX DEG
INPUT FILE                           =  BIZONAL
ADD INPUT FILE
TRANSMITTER TILT ANGLE          =  0 DEG
FUNCTION SYMBOL                 = TRN_BMP
TITLE TABLE
TRANSMITTER BEAM PATTERN
EOT
INPUT FILE                           =  RECTA
ADD INPUT FILE
FUNCTION SYMBOL                 = RCV_BMP
TITLE TABLE
RECEIVER BEAM PATTERN
EOT
VERTICAL ANGLE MINIMUM    =  -40.0 DEG
VERTICAL ANGLE MAXIMUM    =   40.0 DEG
VERTICAL ANGLE INCREMENT =    0.1 DEG
AMBIENT NOISE SPECTRUM MODEL = TABLE
AMBIENT NOISE SPECTRUM TABLE
HZ         DB//HZ
XXXXX        XX
EOT
COMMENT TABLE
the bearing is set such that the reverberation
will be calculated using the horizontal beamwidth table
and the single set of eigenrays
the bearing increment command overrides the horizontal beamwidth
and integrates the reverberation over the bearing increments
horizontal beamwidth is used to integrate reverberation
if rcv beamwidth < projector beamwidth then small beamwidth is
applicable
EOT
TRUE TARGET BEARING =    0     DEG
BEARING MINIMUM     =    0     DEG
BEARING MAXIMUM     =    0     DEG
BEARING INCREMENT   =    1.5   DEG
HORIZONTAL BEAMWIDTH TABLE  =  3.8 DEG
REVERBERATION FILE  = REV004
RESET REVERBERATION
TARGET DEPTH        = BOTTOM
EIGENRAY FILE       = BOT004
COMPUTE EIGENRAYS
COMPUTE BOTTOM REVERBERATION
TARGET DEPTH        = SURFACE
EIGENRAY FILE       = SRF004
COMPUTE EIGENRAYS
```

```
COMPUTE SURFACE REVERBERATION
INPUT FILE                              =  MTDP
ADD INPUT FILE
INPUT FILE                              =  SCATDP
ADD INPUT FILE
EIGENRAY FILE                 = VOL004
COMPUTE EIGENRAYS
COMPUTE VOLUME REVERBERATION
X OFFSET                      =    0  IN
RANGE AXIS LENGTH             =    5  IN
LEVEL AXIS MAXIMUM =   200 DB
LEVEL AXIS MINIMUM =     0 DB
PRINT REVERBERATION VS TIME
PLOT OPTION                   =
FOREGROUND COLOR              = BLUE
PLOT REVERBERATION + NOISE VS TIME
DEPTH MINIMUM           =    1 FT
INPUT FILE                              =  DEPMAX
ADD INPUT FILE
DEPTH INCREMENT         =    5 FT
EIGENRAY FILE           =  TRGE004
COMPUTE EIGENRAYS
COMMENT TABLE
the detection threshold is the difference between signal excess
and signal to noise ratio so if we are ambient limited we set
the noise threshold and if we are reverb limited we set the noise
threshold to the same thing
EOT
AMBIENT NOISE THRESHOLD MODEL = TABLE
AMBIENT NOISE THRESHOLD TABLE = XX DB
REVERBERATION THRESHOLD MODEL = TABLE
REVERBERATION THRESHOLD TABLE = XX DB
TARGET STRENGTH MODEL         = FREQUENCY
TARGET STRENGTH TABLE         =  XX DB
SIGNAL EXCESS FILE            = EX004
COMPUTE ACTIVE SIGNAL EXCESS
LEVEL AXIS MAXIMUM =    80 DB
LEVEL AXIS MINIMUM =   -20 DB
PRINT SIGNAL EXCESS VS RANGE
PLOT OPTION                   = CONTINUE
TITLE TABLE
EOT
PLOT OPTION                   =
FOREGROUND COLOR              = BLUE
CONTOUR SIGNAL EXCESS
```

LIST OF REFERENCES

1. Aidala, F. E., Keenan, R. E., and Weinberg, H., Modeling High-Frequency System Performance in Shallow-Water, Range-Dependent Environments with the Comprehensive Acoustic Simulation System (CASS). NUWC Division Newport Technical Digest, 54-61, 1998.

2. Chu, P. C., Wells, S. K., Haeger, S. D., Szczechowski, C., and Carron, M. J., Temporal and Spatial Scales of the Yellow Sea Thermal Variability. Journal of Geophysical Research, 102, C3, 5657-5658, 1997a.

3. Chu, P. C., Fralick, C. R., Haeger, S. D., and Carron, M. J, A Parametric Model for the Yellow Sea Thermal Variability. Journal of Geophysical Research, 102, C5, 10499-10507, 1997b.

4. Chu, P. C., Tseng, H., Chang, C. P., and Chen, J. M., South China Sea Warm Pool Detected in Spring from the Navy's Master Oceanographic Observational Data Set (MOODS). Journal of Geophysical Research, 102, C7, 15761-15762, 1997c.

5. Fox, D. N., Teague, W. J., Barron, C.N., Carnes, M.R., and Lee, C.M., The Modular Ocean Data Assimilation System (MODAS). In preparation for: Journal of Atmospheric Oceanic Technology, pp. 4-11, 2000.

6. Jensen, F. B., Kuperman, W. A., Porter, M. B., and Schmidt, H., Computational Ocean Acoustics, Springer-Verlag, 2000.

7. Keenan, R., Weinberg, H., E., and Aidala, F. E., Software Requirements Specifications for the Gaussian Ray Bundle (GRAB) Eigenray Propagation Model. OAML-SRS-74, Systems Integration Division Stennis Space Center, MS, 1999.

8. Keenan, R. E., An Introduction to GRAB Eigenrays and CASS Reverberation and Signal Excess. Science Applications International Corporation, MA, 2000.

9. Medwin, H., and Clay, C. S., Fundamentals of Acoustical Oceanography, Academic Press, 1998.

10. Mississippi State Center of Air Sea Technology, User's Manual for the Naval Interactive Data Analysis System (NIDAS) Version 3.1. Technical Note 4-97, Stennis Space Center, MS, 1997.

11. Naval Meteorology and Oceanography Command, NAVPACMETOCCEN Yokosuka Japan, "NPMOC Yokosuka Operational Support Web Site."

    [http://207.133.112.37/cgi-bin/show.pl?forecast+westpac+sfcanal+wp00.gif]. February 2001.

12. Naval Oceanographic Office," Yellow Sea Oceanographic Features Analysis-Color Composite Web Site."

    [http://www.navo.navy.mil/LIBRARY/Metoc/Pacific+North+-+West+of+180/Regional+NWPAC/SATANAL/OFA/Color+Composite/index.html]. February 2001.

13. Naval Oceanographic Office Systems Integration Division, Software Design Document for the Gaussian Ray Bundle (GRAB) Eigenray Propagation Model. OAML-SDD-74. Stennis Space Center, MS, 1999.

14. Naval Oceanographic Office Systems Integration Division, Data Base Description for the Generalized Digital Environmental Model (GDEM-V) Version 2.5. OAML-DBD-72C, Stennis Space Center, MS, 2000.

15. Naval Research Laboratory Code 7320, User's Manual for the Modular Ocean Data Assimilation System (MODAS) Version 2.1. PSI Technical Report S-285. Stennis Space Center, MS, 1999.

16. Naval Research Laboratory Code 7323, Confidence Level Assessment of MODAS Appendix 1: Upgraded Altimetry Processing. Stennis Space Center, MS, 2000.

17. Naval Research Laboratory, "NRL Monterey Marine Meteorology Division (Code 7500) Tropical Cyclone Page."

[http://kauai.nrlmry.navy.mil/tcin/tc_home?YEAR=2000&.submit=Submit+Query&.cgifields=YEAR]. August 2000.

18. Ninno, H., and Emery, K. O., Sediments of Shallow Portions of the East China Sea and South China Sea. Geology Society of America BULL., 72, pp. 731-762, 1961.

19. Raytheon Electronic Systems Naval & Maritime Integrated Systems, "AN/SQQ-32 Mine Hunting Sonar System."

[http://www.raytheon.com/systems_integration/brochures/SQQ-32.pdf]. December 2000.

20. Shepard, F. P., Submarine Geology, pp. 246-250, Harper & Row, 1973.

21. Teague, W. J., Carron, M. J., and Hogan, P. J., A Comparison between the Generalized Digital Environmental Model and Levitus Climatologies. Journal of Geophysical Research, 95, C5, 7167-7183, 1990.

DISTRIBUTION LIST

1.	LCDR Jim Berdeguez Chief of Naval Operations 2000 Navy Pentagon N852 Room 5E 613 Washington, D.C. 20350-2000	1
2.	Mr. Landry Bernard Technical Director Naval Oceanographic Office 1002 Balch Blvd Stennis Space Center, MS 39529	1
3.	CDR Jeffrey S. Best Commanding Officer NAVMETOCPRODEVCEN Stennis Space Center, MS 39529	1
4.	Professor Albert Bottoms Mine Warfare Association Naval Postgraduate School Monterey, CA 93943	1
5.	Dr. William Burnett COMMETOCCOM Stennis Space Center, MS 39529	1
6.	Mr. Scott Burleson COMINEWARCOM N00TD/N80 325 5th Street Corpus Christi, TX 78419	1
7.	Mr. Scott Burleson COMINEWARCOM N00TD/N80 325 5th Street Corpus Christi, TX 78419	1
8.	CDR Chris Butler ONR-IFO 223 Old Marylebone Road	1
9.	Dr. Michael Carron N00t Naval Oceanographic Office 1002 Balch Blvd Stennis Space Center, MS 39529	1

10.	Professor Peter C Chu Institute of Joint Warfare Analysis and Department of Oceanography Naval Postgraduate School Monterey, CA 93943	30
11.	Don L. Durham Technical Director COMMETOCCOM Stennis Space Center, MS 39529	1
12.	Herbert Eppert Naval Research Laboratory Superintendent Code 7400, Bldg. 1005 Stennis Space Center, MS 39529	1
13.	Dan Fox Naval Research Laboratory Code 7300 Stennis Space Center, MS 39529-5004	5
14.	Eric Gottshall USS Carl Vinson, CVN 70 FPO, AP 96629-2840	1
15.	Stephane Guyonic DCE/GESMA BP 42 29240 Brest-Naval FRANCE	1
16.	Steven D. Haeger Naval Oceanographic Office 1002 Balch Blvd Stennis Space Center, MS 39529	5
17.	Dr. Jill L. Karsten Office of Naval Research Code 322 GG 800 North Quincy Street Arlington, VA 22217-5660	1
18.	Ruth Keenan Naval Undersea Warfare Center Division Newport 1176 Howell Street Newport, RI 02841-1708	5

19. Larry Kelly — 1
Mine Warfare Association
6436 Randall Dr.
Hughesville, MD 20637

20. Joseph H. Kravitz — 1
Office of Naval Research
Code 322 GG
800 North Quincy Street
Arlington, VA 22217-5660

21. Stephen C. Lingsch — 1
Naval Oceanographic Office
1002 Balch Blvd
Stennis Space Center, MS 39529

22. William C. Lingsch — 1
Naval Oceanographic Office
1002 Balch Blvd
Stennis Space Center, MS 39529

23. Bruce Northridge — 1
COMMETOCCOM
Stennis Space Center, MS 39529

24. Mr. Mark Null — 1
NEPTUNE SCIENCES, INC.
Mine Warfare Environmental Support
325 Fifth Street, SE
Corpus Christi, TX 78419

25. RADM John D. Pearson — 1
MIW Chair
Naval Postgraduate School
Monterey, CA 93943

26. Dr. Michael Richardson — 1
Naval Research Laboratory
Code 7430
Stennis Space Center, MS 39529-5004

27. LCDR Mike Rocheleau — 1
MIW Force Oceanographer
COMINEWARCOM
Attn: N37
325 Fifth Street SE
Corpus Christi, TX 78427

28. Professor Gordon Schacher — 5
Institute of Joint Warfare Analysis and
Department of Physics
Naval Postgraduate School
Monterey, CA 93943

29. Dr. Ruud Schuttenheim — 1
NITG-TNO
Geo-Marine and Coast Dept., P.O. Box 800015
2508 TA Utrecht
NETHERLANDS

30. Dr. Rick Spinrad — 1
Technical Director
CNO-N96
U.S. Naval Observatory
Bldg. 1
3450 Massachusetts Ave., NW
Washington DC 20392

31. CDR Robert Steadley — 1
COMMETOCCOM
Stennis Space Center, MS 39529

32. Dr. Douglas G. Todoroff — 1
Office of Naval Research
Code 322 W
800 North Quincy Street
Arlington, VA 22217-5660

33. Ms. Lisa Tubridy — 1
Coastal System Station
Science Technology, Analysis, and
Special Operation Department, Code R12
6703 West Highway 98
Panama City, FL 32407

34. Dr. Phillip Valent — 1
Naval Research Laboratory
Code 7401, Bldg. 1005
Stennis Space Center, MS 39529

35. Dr. Linwood Vincent — 1
Office of Naval Research
Code 321 CD
800 North Quincy Street
Arlington, VA 22217-5660

36. Dr. Thomas Wever — 1
Federal Armed Forces Underwater Acoustics
And Marine Geophysics Research Institute
FWG-323, Klausdorfer Weg 2-24
24148 Kiel Germany

37. Mr. Cees J. Wiersum — 1
TNO Physics and Electronics Laboratory
Operations Research and Business Management
Or Studies Navy-Mine Warfare
Oude Waalsdorperweg 63
PO Box 96864
2509 JG The Hague
NETHERLANDS

38. Dr. Roy Wilkens — 1
Office of Naval Research
Code 322 GG
800 North Quincy Street
Arlington, VA 22217-5660

39. Defense Technical Information Center — 2
8725 John J. Kingman Rd., STE 0944
Ft. Belvoir, VA 22060-6218

40. Dudley Knox Library, Code 013 — 2
Naval Postgraduate School
Monterey, CA 93943-5100

41. Research Office, Code 09 — 1
Naval Postgraduate School
Monterey, CA 93943-5138